

**ELECTRORETINOGRAPHIC MAPPING OF RETINAL
FUNCTION: EVALUATION AND CLINICAL APPLICATION**

by

Stuart William Parks

**Thesis submitted to the University of Glasgow
for the degree of Doctor of Philosophy.**

This research was conducted in the
Department of Clinical Physics & Bio-Engineering
and the Tennent Institute of Ophthalmology,
University of Glasgow, West Glasgow Hospitals
University NHS Trust, Glasgow.

January 1998

ProQuest Number: 13815391

All rights reserved

INFORMATION TO ALL USERS

The quality of this reproduction is dependent upon the quality of the copy submitted.

In the unlikely event that the author did not send a complete manuscript and there are missing pages, these will be noted. Also, if material had to be removed, a note will indicate the deletion.



ProQuest 13815391

Published by ProQuest LLC (2018). Copyright of the Dissertation is held by the Author.

All rights reserved.

This work is protected against unauthorized copying under Title 17, United States Code
Microform Edition © ProQuest LLC.

ProQuest LLC.
789 East Eisenhower Parkway
P.O. Box 1346
Ann Arbor, MI 48106 – 1346

GLASGOW UNIVERSITY
LIBRARY

11149 (copy 1)

GLASGOW
UNIVERSITY
LIBRARY

ABSTRACT

The conventional electroretinogram (ERG) is an electrophysiological examination that is used to assess the extent of retinal function within the eye. The test exploits the retina's ability to convert photons of light into electrical impulses. A flash stimulus is employed to evoke an electrical potential within the retinal cells (cones, rods and bipolar cells). These potentials, generated in the retina, are then recorded at the corneal surface of the eye using a contact lens or scleral electrode. The electrical potential generated possesses several distinct components that can be used to locate dysfunction from discrete layers of the retina. Although the ERG is used routinely in the diagnosis and monitoring of a wide range of retinal disorders its application is restricted because the diffuse stimulation of the retina evokes a global response thereby preventing the detection of localised abnormalities.

A new technique has recently been developed, the Visual Evoked Response Imaging System (VERIS), which overcomes some of the shortfalls of the conventional electroretinogram. This new method allows functional mapping of the retina by the ERG. The technique enables simultaneous recording from a large number of retinal areas. Each area is independently stimulated in a sequence employing Pseudo Random Binary Sequences (PRBS). The sequences of stimulation are uncorrelated (achieved by temporal modulation of the sequence for each area) therefore the individual responses from different areas of the retina can be extracted. This thesis describes the evaluation of this system with regards to its potential within routine clinical practice.

A number of investigations were performed to fulfil this evaluation. Possible factors that may influence the integrity of data obtained from the new technique were investigated and, where possible, minimised. These factors included quantifying the effects of filtering bandwidth, refractive errors, electrode type, response measurement method, luminance, contrast, dilation and the artefacts associated with poor patient shielding (from extraneous electromagnetic interference). The findings from these investigations were used to optimise the recovery of local ERG responses and established a protocol for future investigations. A custom software program was developed for analysis and interpretation of data. A study was undertaken to quantify the repeatability and reproducibility of the technique and to provide normative values. Finally these results were used to assess the techniques ability to objectively detect and quantify several retinal disorders. The investigations indicated that the system was of particular benefit in the assessment of local retinal pathology. However the system suffered a higher exclusion criteria than conventional electrophysiology and was unable, in the clinical setting, to identify retinal pathologies selectively affecting the ganglion cell layer. These factors limited the systems application within clinical practice.

Current developments are aimed at improving the technique and establishing a routine clinical test with improved sensitivity and specificity that can be successfully applied to a wider population group.

LIST OF CONTENTS

	Page
Title	1
Abstract	2
List of contents	3
List of illustrations	5
List of tables	10
Acknowledgement	12
Author's declaration	13
CHAPTER 1 INTRODUCTION	
1.1 The eye and the visual system	16
1.2 The visual field	26
1.3 Perimetry	27
1.4 Clinical electrophysiology of the visual system	30
1.5 Conclusions	37
CHAPTER 2 PSEUDO RANDOM BINARY SEQUENCES	
2.1 Introduction	40
2.2 Signal averaging	40
2.3 Pseudo Random Binary Sequences and VERIS	51
2.4 Conclusions	58
CHAPTER 3 VERIS™ SCIENTIFIC	
3.1 Introduction	60
3.2 System Specifications	60
3.3 Conclusions	79

List of Contents (cont.)

	Page
CHAPTER 4	FACTORS INFLUENCING THE MFERG
4.1	Introduction 80
4.2	Electrodes 81
4.3	Subject Variables 89
4.4	Recording Equipment Variables 103
4.5	Conclusions 118
CHAPTER 5	NORMATIVE STUDIES
5.1	The Normal Range 121
5.2	Comparison with Conventional Perimetry 136
5.3	Conclusions 142
CHAPTER 6	CLINICAL STUDIES
6.1	Introduction 145
6.2	The Hereditary Dystrophies 146
6.3	Diabetic Retinopathy 166
6.4	Glaucoma 174
6.5	Retinal Detachment 180
6.6	Conclusions 187
CHAPTER 7	CONCLUSIONS & FURTHER WORK
7.1	Recording System 189
7.2	Further Work 200
7.3	Conclusions 208
APPENDIX I	2×1.4MB HD Computer disks (back cover)
LIST OF REFERENCES	209

LIST OF ILLUSTRATIONS

	Page
1.1	Diagram and photograph of cross-sectional image of the eye. 17
1.2	Diagrams of the retinal layers. 19
1.3	Relative absorption spectrum of cone receptors. 20
1.4	Distribution of rods and cones along a horizontal line through the fovea. 21
1.5	Diagrammatic example of photoreceptor, bipolar and ganglion cell interaction to centre-surround stimulus. 23
1.6	Connections from the retina to the cerebral hemispheres 25
1.7	Image projection from the left visual field to the right occipital lobe. 26
1.8	Representative diagram illustrating visual field. 27
1.9	Diagram of five basic ERG responses defined by the ISCEV standard. 33
1.10	Typical pattern ERG response with components labelled. 35
2.1	A Typical system. 41
2.2	Basic modulo two PRBS generator. 50
2.3	Stimulus of four areas driven by shifted PRBS. 52
2.4	Non-linearity of the double impulse. 54
3.1	Stimulus paradigm (61 element geometrical array). 64
3.2	Spatial paradigm of local ERG responses 68
3.3	Effects of noise on MFERG features. 70
3.4	Scalar product plot with illustration of interpolation paradigm. 72
3.5	Trace array and scalar product plots of 'negativity'. 74
3.6	Screen shot from analysis program (FIDA). 75
3.7	Example of 'hard copy' of results provided for clinicians. 76

List of Illustrations (cont.)

	Page	
4.1	Common commercial electrodes.	81
4.2	Scalar product amplitude for each electrode with natural and dilated pupils.	87
4.3	Spatial grouping used for comparison of central and peripheral regions.	88
4.4	Plot of the variation of b-wave implicit time and b-wave amplitude for central and peripheral regions with induced defocus.	93
4.5	Variation in mean implicit time and amplitude.	97
4.6	Illustrations of marking used for eccentric fixation.	100
4.7	Correlation plot of fixation offset and effective D.C. saturation required.	101
4.8	Interference on MFERG response arising from imperfect CRT shielding.	104
4.9	The high-pass filtering circuit.	106
4.10	The frequency response curve of a high-pass filter and a differentiator.	107
4.11	High-pass filtering of simulated waveforms.	109
4.12	The effect of filter order on a normal and negative ERG.	110
4.13	A clinical ganzfeld ERG (upper branch vein occlusion) recorded by 1- and 10-Hz high-pass filtering.	112
4.14	Multifocal ERG waveforms (upper branch retinal vein occlusion) recorded by 1- and 10-Hz high-pass filtering.	113
4.15	Spatial luminance profile for multiscan monitor over stimulus paradigm.	114
4.16	Summed multifocal responses from all 61 areas to stimulus with different mean contrast.	115

List of Illustrations (cont.)

	Page	
4.17	Topographical difference in b-wave implicit time between 89% and 20% contrast.	116
4.18	Topographical difference in b-wave amplitude between 89% and 20% contrast.	117
4.19	Variation of multifocal response with mean luminance.	118
5.1	Topographical plot of a-wave and b-wave implicit time across the central 30 degrees of the retina.	123
5.2	Topographical change in mean b-wave implicit time between age groups.	124
5.3	Repeatability and reproducibility for b-wave implicit time with eccentricity.	125
5.4	Topographical variation of mean a-wave amplitude.	127
5.5	Topographical variation of mean b-wave amplitude.	127
5.6	Grouping paradigm for table 5.3	129
5.7	Normal topographical variation of mean scalar product value (left eye)	131
5.8	Plot of scalar product values as a function of age.	132
5.9	Comparison of b-wave normal range.	135
5.10	Illustration of custom (VERIS) Full Threshold Humphrey test chart and stimulus paradigm.	137
5.11	Mean sensitivity values and error of custom Humphrey test on right eye.	138
5.12	Repeatability and the normal range in the VERIS system and Humphrey perimeter.	139

List of Illustrations (cont.)

		Page
6.1	Custom Humphrey test chart of mild sector Retinitis Pigmentosa	150
6.2	Topographical plot of multifocal responses and Scalar Product values from patient with Retinitis Pigmentosa.	151
6.3	Scatter plot of photopic b-wave amplitude and implicit time in Retinitis Pigmentosa.	153
6.4	Confidence plots of b-wave amplitude and scalar product.	154
6.5	Confidence plots of b-wave latency and Humphrey custom field chart.	155
6.6	Topographical variation of b-wave implicit time in typical RP and control.	157
6.7	Custom Humphrey test chart of patient with cone dystrophy.	161
6.8	Signal response plot and derived scalar product plot of typical autosomal dominant cone dystrophy.	162
6.9	Confidence plots of b-wave amplitude and scalar product.	163
6.10	Confidence plots of b-wave Implicit time and Humphrey field result.	164
6.11	Custom Humphrey field test. Values indicate photopic sensitivity (dB	169
6.12	Signal response plot (a) and derived scalar product plot (b) of typical Diabetic Retinopathy.	170
6.13	Confidence plots of b-wave amplitude and scalar product.	172
6.14	Confidence plots of b-wave Implicit time and Humphrey field result.	173
6.15	Custom Humphrey field test in Primary Open Angle Glaucoma.	177
6.16	Mean second order luminance response for patient 5.	178
6.17	Mean multifocal pattern response for patient 5	179
6.18	Custom Humphrey field chart from patient 11 .	183

List of Illustrations (cont.)

	Page	
6.19	Signal response plot and derived scalar product plot of a subject with superior temporal retinal detachment.	184
6.20	Confidence plot overlaying response amplitude plot pre and post-operative retinal detachment.	185
7.1	Illustration of DLP system	202
7.2	Figure 7.2 One of motion stimulus	203
7.3	Screen-shot from Multifocal Visual Electrophysiology system.	207

LIST OF TABLES

	Page
2.1	Modulo-two sum digit table. 49
2.2	Second-order product of interactions. 58
3.1	Increase in noise required to induce a significant change in measure. 70
4.1	Statistical analysis of the effects of saturation. 88
4.2	The effects of defocus on signal response. 92
4.3	Fixation loss compared with saturation. 101
4.4	Mean amplitude and latency values related to stimulus contrast. 116
4.5	Mean amplitude and latency values related to stimulus luminance. 117
5.1	Number of controls tested in respective age groups. 121
5.2	Summary of mean age-related amplitude measures. 126
5.3	Summary of results from investigation into Photopic full field ERG. 128
5.4	Mean responses together with intra- and inter-subject repeatability. 130
5.5	Summary of results from investigation into Photopic full field ERG. 135
5.6	Intra- and inter-subject repeatability for custom full threshold Humphrey field test. 139
6.1	Results from scotopic ERG and Humphrey perimeter tests. 152
6.2	Results from assessment of responses to normative data. 156
6.3	Mean b-wave implicit times from central and peripheral regions before and after a one-year interval. 158
6.4	Results from photopic ERG and Humphrey perimeter tests. 160

List of Tables (cont.)

	Page
6.5	Results from assessment of responses to normative data. 165
6.6	Results from assessment of responses to normative data. 171
6.7	Mean 2 nd order luminance responses from regions. 179
6.8	Mean pattern reversal responses from regions defined by perimetry as normal and abnormal. 180
6.9	Test results and patient information pre- and post-operatively. 182
6.10	Test reliability. 188

ACKNOWLEDGEMENT

The author gratefully acknowledges the financial assistance of the Acute Healthcare Research Committee of the Chief Scientist Office, Home and Health Department, The Scottish Office, grant KMRS/50/C2336.

The author wishes to thank the following people:

Dr D Keating, supervisor (Department of Clinical Physics & Bio-Engineering, Ophthalmology) for his many contributions and advice in addition to his initial formulation of the research project.

Dr A L Evans (Department of Clinical Physics & Bio-Engineering, Instrumentation) for his help and advice throughout the research.

Professor A T Elliott, Department of Clinical Physics & Bio-Engineering West Glasgow Hospitals University NHS Trust, and Professor C M Kirkness, Tennent Institute of Ophthalmology, University of Glasgow for providing the facilities of their departments for the research.

Consultants and Senior Registrars from the Hospitals within greater Glasgow for referral of patients.

Mr D Smith from the Electronics Laboratory Department of Clinical Physics & Bio-Engineering for providing helpful advice and assistance and for the development of the amplifiers for use within the project.

Mr J McCormick, Tennent Institute of Ophthalmology of the West Glasgow Hospitals University NHSD Trust for providing photographic services.

Finally the author wishes to thank the many patients, colleagues and friends who acted as volunteer test subjects.

AUTHOR'S DECLARATION

The material presented in this thesis is the author's own work with the following exceptions:

Dr A L Evans and Mr D Smith designed and built the custom amplifiers discussed in chapter 3

Dr D Keating proposed the section on filtering artefacts of the MFERG.

PUBLICATIONS

Material contained in this thesis has been published in the following three papers:

Parks S, Keating D, Williamson TH, Evans AL, Elliott AT & Jay JL (1996)
Functional imaging of the retina using the multifocal electroretinograph: a control study.

Br J Ophthalmol. 80, 831-834

Parks S, Keating D, Evans AL, Williamson TH, Jay JL & Elliott AT (1997)
Comparison of repeatability of the multifocal electroretinogram and Humphrey perimeter.

Doc Ophthalmol 92, 281-289

Keating D, Parks S, Evans AL, Williamson TH, Jay JL & Elliott AT (1997)
The effect of filter bandwidth on the multifocal electroretinogram.

Doc Ophthalmol 92, 291-300

PRESENTATIONS

Material contained in this thesis has also been disseminated at local, national and international meetings including the following presentations:

Parks S, Keating D, Evans A L, Williamson T H, Elliot A T, Jay J L.
The response Topography of ERG b-wave amplitude densities with eccentricity using the m-sequence stimulation technique.

Vision Research 1995, Vol. 35, S238

Keating D, Parks S, Evans A L, Williamson T H, Elliot A T, Jay J L.
An objective method of assessing photoreceptor function in retinal detachment surgery.

Vision Research 1995, Vol. 35, S237

PRESENTATIONS (Cont.)

Parks S, Keating D, Evans A L, Williamson T H, Elliot A T, Jay J L.
Functional Perimetry
British and European Vitreal Retinal Surgeons (BEVRS) annual meeting, October 1995, Loch Lomond, Scotland

Keating D, Parks S, Evans A L, Williamson T H, Elliot A T, Jay J L.
Retinal Mapping; lessons to be learned
British and Eire Association of Vitreo Retinal Surgeons (BEAVRS) annual meeting, October 1995, Loch Lomond, Scotland

Parks S, Keating D, Evans A L, Williamson T H, Elliot A T, Jay J L.
The response Topography of ERG b-wave amplitude densities with eccentricity using the m-sequence stimulation technique.
Joint European Research Meeting in Ophthalmology and Vision (JERMOV), October 1995, Montpellier, France

Keating D, Parks S, Evans A L, Williamson T H, Elliot A T, Jay J L.
An objective method of assessing photoreceptor function in retinal detachment surgery.
Joint European Research Meeting in Ophthalmology and Vision (JERMOV), October 1995, Montpellier, France

Keating D, Parks S, Evans A L, Williamson T H, Elliot A T, Jay J L.
Functional Imaging of the Retina.
Scottish Ophthalmological Society (SOC) Meeting, November 1995, Aberdeen, Scotland

Parks S, Keating D, Evans A L, Williamson T H, Elliot A T, Jay J L.
Functional Imaging of the Retina.
British Ophthalmology & Photographic Association (BOPA), November 1995, Clydebank, Scotland

Keating D, Parks S, Evans A L, Williamson T H, Elliot A T, Jay J L.
Clinical Applications of Retinal Mapping
British Ophthalmology & Photographic Association (BOPA), November 1995, Clydebank, Scotland

Parks S, Keating D, Evans A L, Williamson T H, Elliot A T, Jay J L.
Identification of significant defects using the multifocal ERG
The Association for Research in Vision and Ophthalmology (ARVO), April 1996, Fort Lauderdale, USA

PRESENTATIONS (Cont.)

Keating D, Parks S, Evans A L, Williamson T H, Elliot A T, Jay J L.
Effect of pupil dilation, retinal blur and filter bandwidth on the multifocal ERG
The Association for Research in Vision and Ophthalmology (ARVO), April 1996,
Fort Lauderdale, USA

Parks S & Keating D
Effects of the dilation on the normal range in the Ganzfeld ERG.
The Association for Research in Vision and Ophthalmology (ARVO), May 1997,
Fort Lauderdale, USA

Chapter 1

INTRODUCTION

This chapter provides an introduction to the physiological structure of the primate visual system. In addition, a description is given of the main investigative procedures and techniques currently available to the clinician to assess the integrity of this system.

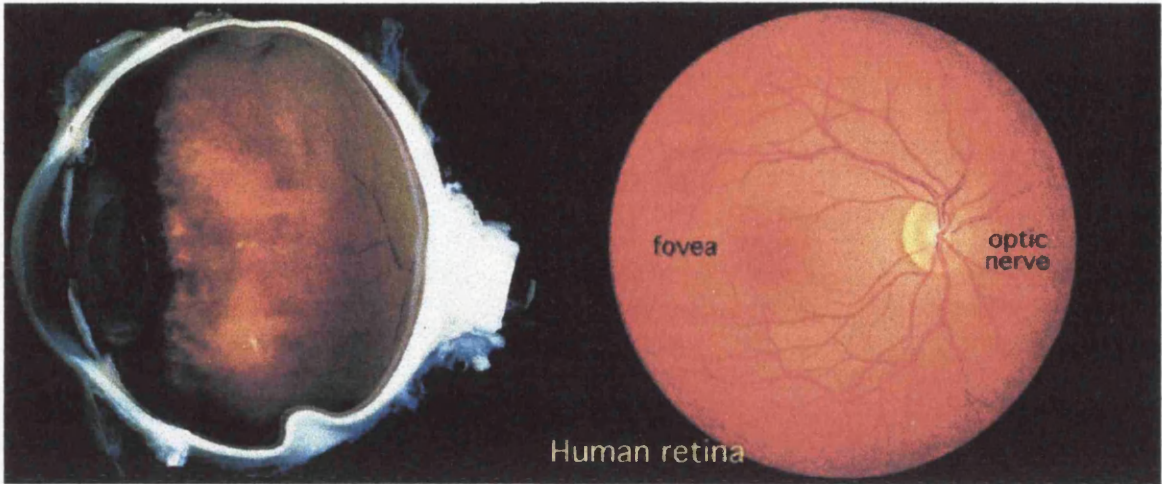
1.1. THE EYE AND THE VISUAL SYSTEM

The eye (see figure 1.1) has been compared in many instances to the camera. Although this analogy grossly underestimates the complex processes that occur within its boundaries, it helps to explain the optical features of the eye.

The eye broadly serves two main functions.

1. To deliver a clear image onto the surface of the retina.
2. To nourish and support the cells necessary for the photoreception, processing and transmission of images.

(a)



(b)

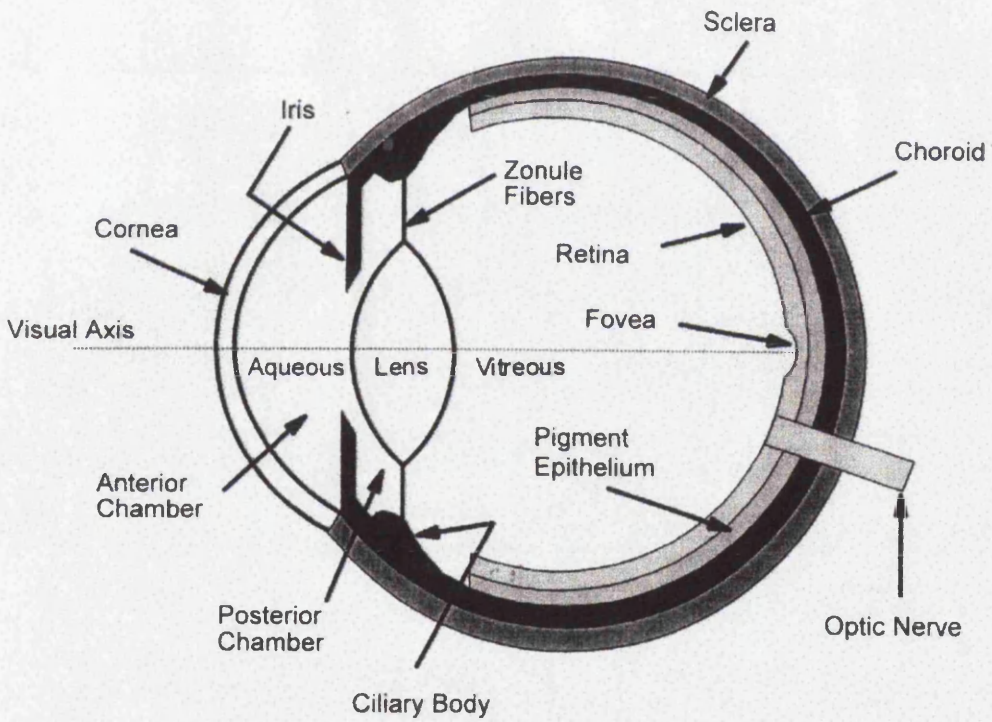


Figure 1.1 (a) Cross-sectional image from nucleated eye (courtesy of Prof. W Lee) and fundus view of retina (adapted from Kolb H, WebVision. <http://insight.med.utah.edu/webvision> 1997. (b) diagrammatic image of eye (adapted from *An introduction to the biology of Vision*, J.T. McIlwain, Cambridge University Press 1996)

The cornea, lens, iris and ciliary body constitute the eye's powerful focusing system. The cornea consists of a transparent ordered two-dimensional lattice of collagen fibres which provides a clear passage for the incident light. It constitutes the greatest refractive power within the system and its tough protective exterior serves as a shield against injury. The lens, although having only one-third of the focusing power of the cornea adjusts its refractive index (a process known as accommodation) to enable the desired image from the outside world to be formed on the retina. The iris is a circular disc analogous to the diaphragm of a camera. Its aperture regulates the amount of light entering the eye. The ciliary body assists in the elastic nature of the lens and is responsible for the shape of the lens and thus its refractive index.

The choroid, aqueous, vitreous and lacrimal apparatus fulfil the second of the eye's main functions to nourish the cells required for transmission and the initial processing of the visual signal. The choroid nourishes the outer layers of the retina, also the absorption of light by its melanin aids vision by preventing stray light from reflecting back into the retina. The aqueous, vitreous, and the lacrimal apparatus provide nutrients, oxygen and transportation of debris in those areas that have an absence of vasculature. In addition, the aqueous maintains the pressure inside the eye (~ 15 mm Hg) which is crucial to retain the eye's geometrical configuration thus ensuring the consistent formation of clear images by the optical pathway.

The visual process in its basic physiological form converts quanta of light through amplitude modulated chemical interaction to frequency modulated electrical impulses or action potentials. This process, known as phototransduction, starts in the receptive base of the eye, the retina.

1.1.1. THE RETINA

The retina is an extension of the brain separated early in development and isolated but for a bundle of neural fibres known collectively as the optic nerve. It measures 42 mm from ora to ora across the horizontal meridian (Van Buren 1963) and its

functional organisation serves to converge and process the information it receives through the formation of images on its surface. It consists of three layers of nerve-cell bodies separated by two layers containing synapses made by the axons and dendrites of these cells (see figure 1.2). The first layer of cell bodies, the photoreceptors, are located, surprisingly - given the passage of light, at the back of the retina against the pigment epithelium and choroid layers.

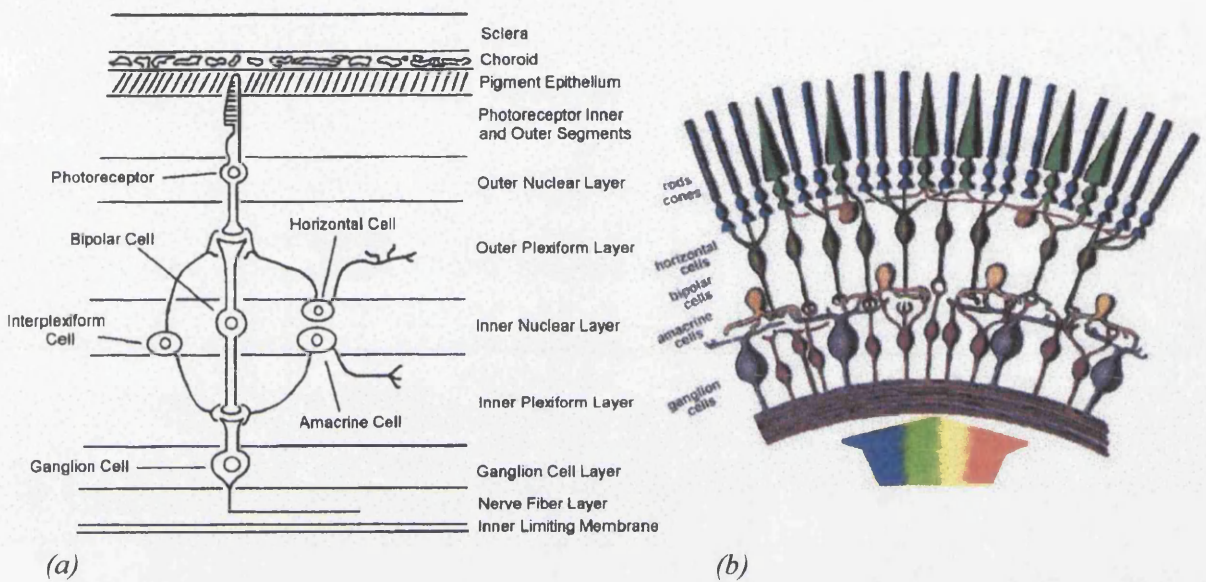


Figure 1.2 Diagrams of retinal layers illustrating the location of (a) principal types of cells (adapted from J T McIlwain, *An Introduction to the Biology of Vision*, Cambridge University Press 1996) and (b) the passage of light through the retinal layers (adapted from Kolb H, *WebVision*. <http://insight.med.utah.edu/webvision> 1997).

THE PHOTORECEPTORS

There exist two groups of photoreceptors in the human retina fulfilling separate but complementary functions (it is sometimes termed the *duplex* retina for this reason). These are the rods, responsible for vision in conditions of dim illumination and the cones which mediate daylight vision and colour sensation. The rods are most sensitive to blue-green light (~500nm) while the cones are

maximally sensitive to three wavelengths of light (430nm, 530nm, 560nm) although they have a broad bandwidth (see figure 1.3)

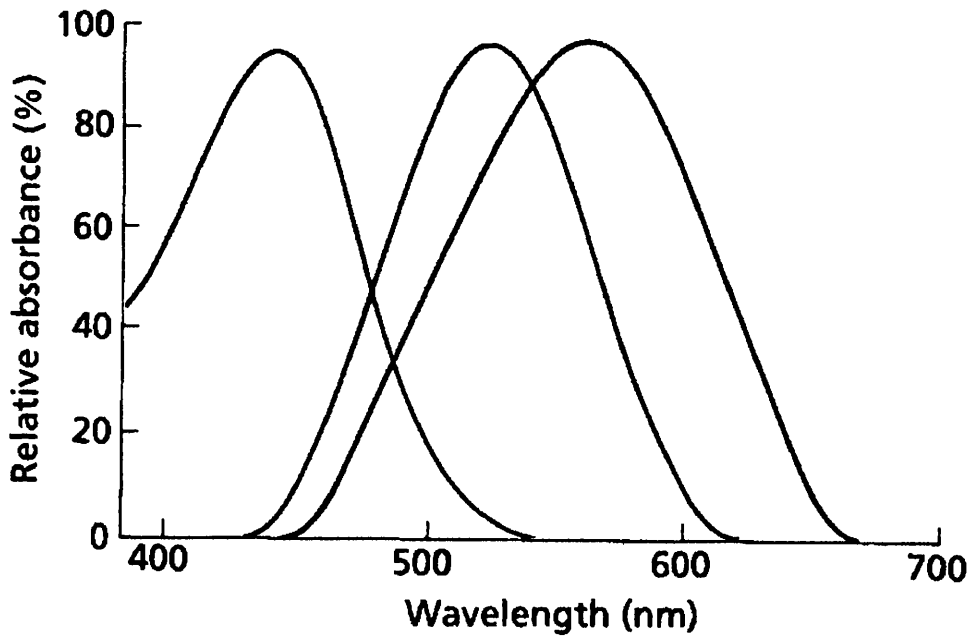


Figure 1.3 *Relative absorption spectrum of cone receptors (S Zeki, A Vision of the Brain, Blackwell Scientific Publications 1994).*

There is believed to be some 6 million cones and 115 million rods (Osterberg 1935, Curcio et al 1987) in the retina with a markedly varying topography (see figure 1.4 for photoreceptor topography across horizontal meridian of the retina).

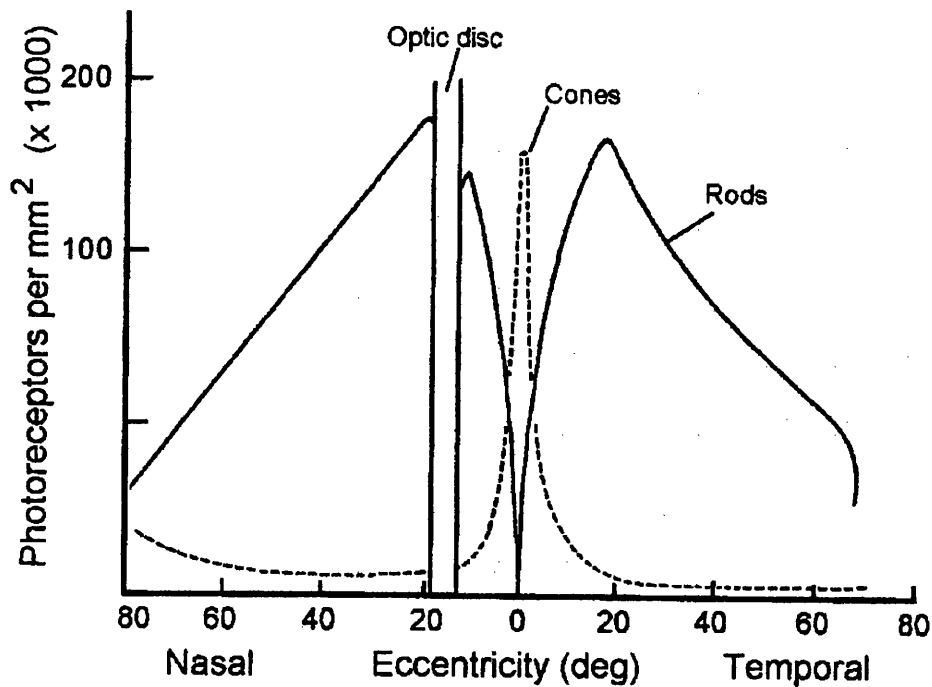


Figure 1.4 *Distribution of rods and cones along a horizontal line through the fovea (adapted from J.L. Brown, after Woodson: The structure of the visual system. In Vision and Visual Perception, ed C.H. Graham, pp. 39-59. New York: Wiley-Liss)*

The rod free zone, or fovea, accounts for only 1 degree of our central vision yet has the maximum cone density of between $147,000/\text{mm}^2$ and $161,900/\text{mm}^2$ (Osterberg 1935, Curcio et al 1987). This ensures the highest visual acuity at the central focusing point. Rods peak in density in a ring 18 degrees from the centre of the fovea where they reach a maximum concentration of around $160,000 \text{ rods}/\text{mm}^2$ (Curcio et al 1987). The optic nerve head is located 17 degrees nasal to the central fovea, measures $\sim 1.8\text{mm}$ (Jonas et al 1988) in diameter and has no photoreceptors.

The photochemical effect of phototransduction is a transient change in permeability and potential of the limiting membrane of the photoreceptor cell. The energy of a single photon (around $4 \times 10^{-19}\text{W}$) is amplified, by the process of transduction, some 10^5 times to produce an equivalent energy of $2 \times 10^{-14}\text{W}$ (Levick & Dvorak 1986). This increase in energy brings about a reduction in the

eye's axial standing potential of approximately 1 pA. Thus the movement of cations, which leads to the hyperpolarisation of the receptor cell, serves as a physiological photomultiplier. This cascade effect of the photoreceptor membrane potential, initiated by absorption of light, is passed to the next neuronal layer within the retina, the bipolar and horizontal cells.

THE BIPOLAR AND HORIZONTAL CELLS

The bipolar cells are the first processing stage of the evoked signal. They fall into two main categories, the on-bipolar which increase the polarity of their transmembrane potential (hyperpolarise) in response to the receptor membrane potential generated and the off-bipolar which decrease this transmembrane potential (depolarise) in response to the same signal (Hubel 1988).

The horizontal cells, as their name suggests, transmit information laterally across the retina. The horizontal cells serve to inhibit the transfer between photoreceptor and bipolar cells. This is believed to give rise to the initial stages of the receptive field organisation which selectively transmits signals on an antagonistic centre-surround stimulation basis. This inhibition and signal inversion is carried through to the third layer of cells, the retinal ganglion and amacrine cells.

THE GANGLION AND AMACRINE CELLS

The ganglion cell further processes the initial signal and enhances the antagonistic receptive field organisation initiated in the bipolar cells. Ganglion cells are categorised as on-centre, off-centre or on-off centre. Depending on their response to their respective bipolar connection they either produce signal inversion or transmission (see figure 1.5). They convert the amplitude modulated (analog) signal generated by the bipolar cells to a pulse frequency modulated signal or digital spike varying in the frequency of discharge in accordance with magnitude change of the stimulating signal.

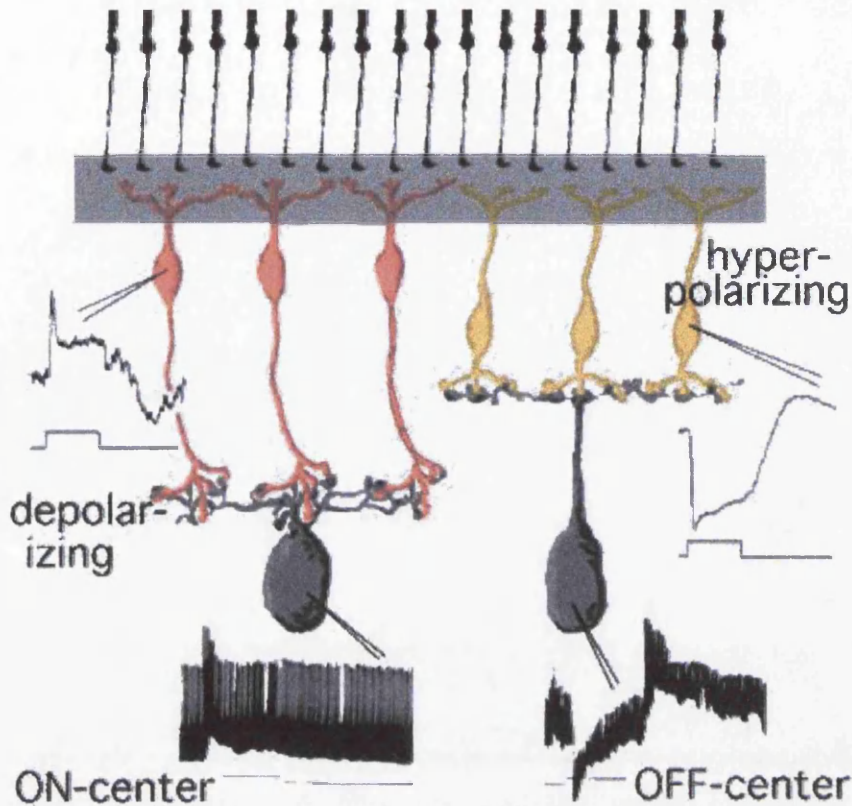


Figure 1.5 *Diagrammatic example of photoreceptor, bipolar and ganglion cell interaction to centre-surround stimulus (adapted from Kolb H, WebVision. <http://insight.med.utah.edu/webvision> (1997))*

The amacrine cells are also laterally transmitting cells analogous to horizontal cells. Unlike the bipolar horizontal relationship the electrical activity of the amacrine ganglion cell is not a constant potential, but rather a series of spike potentials of graded frequencies. The amacrine cells are considered inhibitory and are believed to be responsible for motion detection and complex receptive fields that respond only to the movement of the stimulus (Hubel 1988). The horizontal and amacrine cells thus add spatial and temporal aspects to the processing and convergence of transmitted signals.

The axons of the ganglion cells sweep across the inner surface of the retina to the optic nerve head. Since the ganglion cell fibres lie anterior to the receptors they undoubtedly cause a certain amount of scatter at the receptor layer. To avoid this scatter at the foveal region, where the eye's acuity reaches its highest level, the

ganglion cells travel in arcs around the fovea avoiding its centre and converging at the papilla or optic disc. Here the ganglion cell axons pass through the sclera and form the optic nerve.

1.1.2. THE PRIMARY VISUAL PATHWAY

The course taken by visual fibres from the retina through projections to the visual cortex is known as the primary visual pathway. The prominent features of that pathway are the Optic Chiasm and the Lateral Geniculate Nucleus.

THE OPTIC CHIASM

The axons of the ganglion cells leave the globe as the optic nerve. They maintain an orderly arrangement (in which fibres from the central retina occupy the central portion and fibres from the peripheral retina occupy a concentric position) as they project to the optic chiasm (see figure 1.6). At the optic chiasm there is a partial decussation (crossover) of fibres from the nasal halves of each retina. These fibres cross to the opposite side of the brain and project through the optic tracts, which contain nerve fibres from both retinae. From the optic tracts the fibres continue to several destinations in the brain. Most (approximately 90% (McIlwain 1996) terminate in the lateral geniculate bodies. The result of the partial decussation is that an object in the right-hand visual field produces effects in the left-hand side of the brain only.

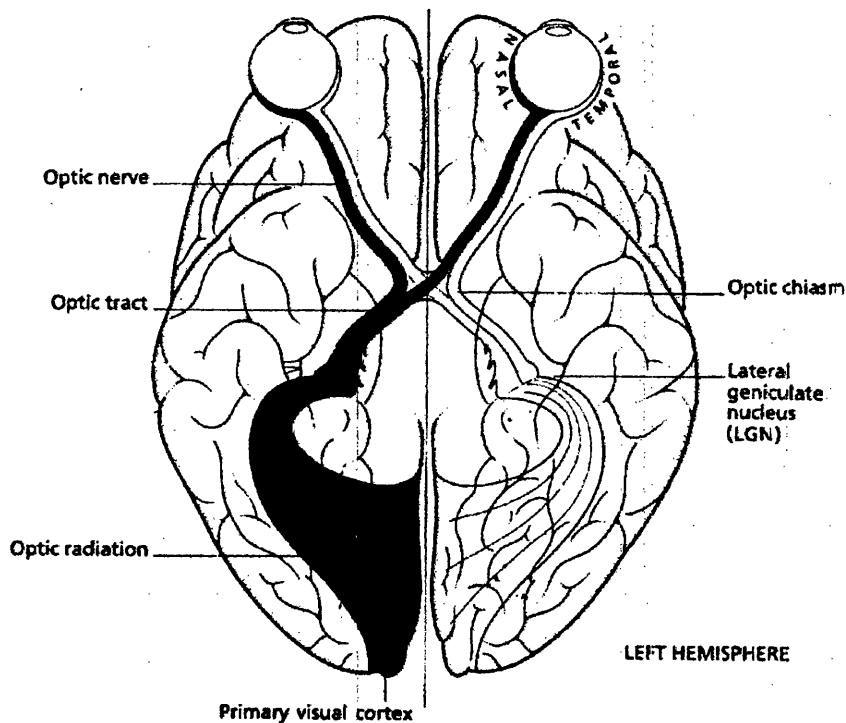


Figure 1.6 *Connections from the retina to the cerebral hemispheres (adapted from S Zeki, A Vision of the Brain, Blackwell Scientific Publications 1994 p25).*

THE LATERAL GENICULATE NUCLEUS (LGN)

The forebrain contains two lateral geniculate nuclei. Almost all of its one to one and a half million cells receive input directly from the optic-nerve fibres. The terminations of the optic tract fibres, in the LGN, are arranged according to their relative position within the retina, so that neighbouring retinal points are represented at neighbouring points in the LGN laminae. The inputs from both eyes are kept relatively separate in the LGN and this has given credence to the assumption that the LGN could play some part in the processes essential for binocular vision. Although some nerve fibres synapse locally and are believed to play some role in attention and arousal, most send axons on to the cerebral cortex (Hubel 1988).

Thus the lateral geniculate nucleus acts as a relay station for information on its projections to the primary visual cortex.

1.1.3. THE PRIMARY VISUAL CORTEX

The primary visual cortex or the striate cortex is the final stage for basic physiological processing and the start of more complex visual processing. It is believed to be responsible for colour, orientation, direction and possibly stereopsis. It retains the contralateral visual field developed in the LGN. A systematic study of gunshot wounds by Holmes in 1945 led to a definite picture of the projections of the retina on the visual cortex (see figure 1.7)

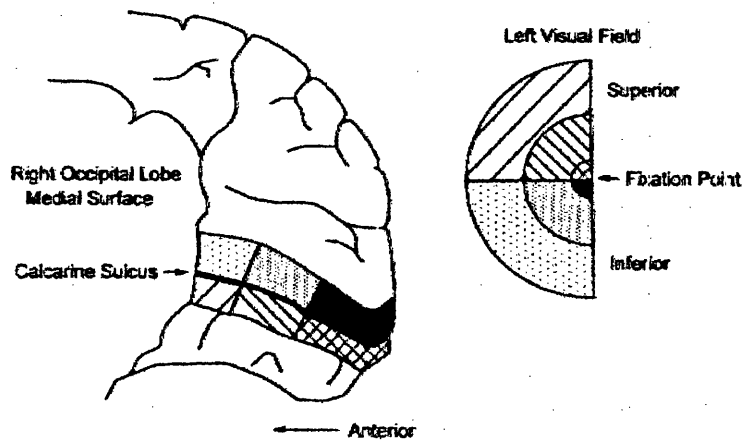


Figure 1.7 *Image projection from the left visual field to the right occipital lobe (J T McIlwain, An Introduction to the Biology of Vision, Cambridge University Press 1996 adapted from Holmes G. The organisation of the visual cortex in man)*

1.2. THE VISUAL FIELD

The visual field can be defined as an area of space that one eye can see at any given instant. The limits to this field are determined by the sensitivity and extent of the retina and the accessibility of light rays from the environment. The normal monocular extent of the visual field for a bright stimulus is 60 degrees superiorly, 75 degrees inferiorly, 100 degrees temporally and 60 degrees nasally (Henson

1993), although this can be affected by facial contours. The binocular field reduces the horizontal extent of this field to approximately 120 degrees (see figure 1.8).

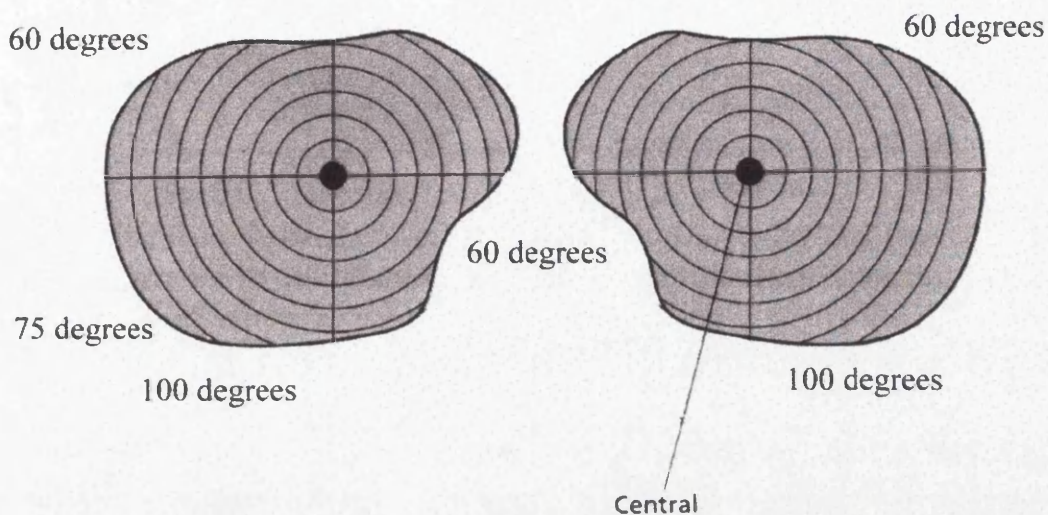


Figure 1.8 *Representative diagram illustrating visual field (adapted from S Zeki, A Vision of the Brain, Blackwell Scientific Publications 1994 p25).*

The non-uniform topography of photoreceptors and the selective convergence of signals in the visual pathways combine to produce a visual field of variable sensitivity. This complex variation is dependent on eccentricity, adaptation level and stimulus and is often described as an island, a concept attributed to Traquair (Harrington 1976). The island's gradient represents the eye's topographical sensitivity and only stimuli whose parameters place them within the island of vision can be seen.

The conventional method for clinical representation of retinal sensitivity is analogous to the contour lines used to illustrate the height and spatial extent of mountains. Isopters lines are used to represent points of equal sensitivity. The clinical recording of visual fields is called perimetry.

1.3. PERIMETRY

Perimetry allows the clinician to map the sensitivity and profile of the visual field to a predetermined resolution. A number of relevant texts give a thorough review

of the subject including (Bedwell 1982, Harrington & Drake 1990 & Henson 1993).

The current commercially available perimeters adopt two main examination strategies:

1. Kinetic strategies which involve moving stimuli.
2. Static strategies in which stationary targets are employed.

KINETIC PERIMETRY

In kinetic perimetry a stimulus of constant intensity and size is moved in different meridians from the periphery of the visual field toward the point of central fixation. The subject under test then indicates when and where they first observe the stimulus. This process is repeated for a series of stimuli of differing size and/or intensity. The results are then drawn as isopters on a chart linking points of equal intensity. Thus the kinetic strategy is useful at determining the size and shape of defects.

One major advantage of kinetic strategies is the full control the investigator has over the examination. This flexibility can be invaluable when assessing possible defects, concentrating on specific areas of the field or even accommodating less compliant subjects. The major disadvantage of a kinetic strategy is the time consuming protocols required for visual field assessment. This disincentive does not lend itself to the main function of perimetry as a quick screening tool. In addition the test is less sensitive when scotoma (localised areas of loss in the visual field) detection is required and the flexibility trumpeted as an advantage also brings its own problems. Differing test protocols between examiners can lead to varying results and so repeat measurements for the assessment of progression of disorders should be interpreted with some caution. Thus results are a qualitative assessment of visual impairment. To obtain a quantitative assessment static paradigms are used.

STATIC PERIMETRY

Static perimetry may use a large number of differing testing strategies. These have been developed for reasons of rapid assessment of the visual field or for greater sensitivity in assessment of depth and extent of visual field loss. Static strategies, as the name suggests, involve the presentation to a subject of 'static' stimuli of varying intensities and/or size across the visual field. Depending on whether these stimuli are presented at intensities slightly above the patient's threshold or are themselves an indication of the subject's full sensitivity they are termed suprathreshold or full threshold respectively. The strength of these static strategies is the repetitive controlled nature of the test. This lends itself well to computerisation and automation of the test and subsequently to the benefits then made available, such as instant statistical analysis, automatic patient archiving, repeatability and reduction of the investigator's influence on results. A disadvantage of static strategies is ironically the inflexible nature that makes it so repeatable. This inflexibility can be a disadvantage when confronted with a less co-operative or difficult subject.

Static perimetry has become a popular replacement for kinetic perimetry in many clinics. This is due to the incremental nature of the stimulus which can reveal the depth in addition to the profile of visual field loss.

1.3.1. ADVANCES IN PERIMETRY

Perimetry and conventional visual field analysers have, until recently, changed little in their style of assessment. However, the introduction of low-cost personal computers has brought with it, as with many fields in medicine, opportunities for the development of new and novel techniques for perimetric investigations of the visual field.

These new systems have been developed to address different goals. Some have targeted specific disorders such as glaucoma (Fitzke 1991) and others particular areas such as pediatrics (Johnson et al 1989b).

Certain new strategies have been developed which would have been difficult to achieve with previous modes of stimulus delivery. Multi-stimuli were developed for rapid field assessment (Mutlikan & Keating et al 1993). Dark stimuli were used on light backgrounds (Mutlikan et al 1992a, Mutlukan & Damato 1992b) which were shown to be effective in the identification of malfunctions arising from the off-pathways in the visual system.

Perimetry can have poor repeatability and sensitivity. It can only test the visual field monocularly and thus measurements from both eyes can be time consuming for both the operator and the subject under investigation. Moreover, one of its major disadvantages is its subjective nature. The test relies on patient recognition and so at best can only reflect abnormality perceived or otherwise from some part of the visual pathway. To give objective evaluation of visual dysfunction clinical electrophysiology is necessary.

1.4. CLINICAL ELECTROPHYSIOLOGY OF THE VISUAL SYSTEM

Clinical ocular electrophysiology exploits the electrical phenomena associated with the physiological process of the nervous system. It uses these processes as a measure of the integrity of the visual pathway. Rather than passively measuring responses, a variety of strategies are used to stimulate the retina and so evoke a response (this has given rise to the general name for ocular electrophysiology: Visual Evoked Response - VER). This response can be measured either from the retina (indirectly from the cornea) or from the visual cortex through the scalp. Clinical electrophysiology then serves to quantify, objectively, the integrity of the visual system.

There is a number of texts that review the subject comprehensively (Galloway 1981, Heckenlively & Arden 1991, Carr & Siegal 1990, Fishman & Sokol 1990) and guides to practice advocated by The International Society for Clinical Electrophysiology of Vision (ISCEV) (Marmor & Zrenner 1995, Marmor et al 1989, Marmor & Zrenner 1993, Harding & Odom et al 1995). The following

sections give a brief summary of the common strategies employed to assess visual loss.

1.4.1. THE ELECTRO-OCULOGRAM

The electro-oculogram (EOG) records, indirectly, the standing potential (0.4 to 1mV) that exists between the cornea (positive) and the posterior pole of the human eye (negative). There is considerable evidence to suggest that this potential arises in the retinal pigment epithelium (Heckenlively & Arden 1991). This standing potential, or dipole, is proportional to retinal illumination and its variance with incident light can be used to assess defects which selectively affect the retinal pigment epithelial layer.

To record the EOG, electrodes are placed on either side of each eye at the medial and lateral canthi. One ground electrode is placed usually on the forehead. The subject is asked to move his or her eyes through a fixed angle, usually determined by markers inside an evenly illuminated dome (Ganzfeld bowl), and the corresponding signal is recorded in conditions of light and dark adaptation. It has been observed that the standing potential falls in darkness and increases upon exposure to a bright steady light. This variation to light and dark is measured through a fixed time scale and plotted. The ratio of dark trough to light peak (the Arden Index (Arden & Fojas 1962)) or ratio of light peak to dark-adapted baseline is commonly used to assess normality or abnormality, although other measures have been employed such as the light rise time to peak or the fast oscillations of the response (Marmor & Zrenner 1993). While the electro-oculogram is abnormal in many retinal disorders this same information can be obtained quickly using the electroretinogram with some exceptions, notably Best's Macular Dystrophy and the assessment of retinal detachments in eyes with opaque media.

1.4.2. THE ELECTRORETINOGRAM

The electroretinogram (ERG) is one of the most common electrophysiological examinations performed to assess retinal function. It records the evoked potentials

produced within the retinal cells. If an electrode is placed on the cornea and another, indifferent electrode, is placed, for example, on the outer canthi, illumination of the retina is followed by a succession of electrical changes; the record of these changes is the electroretinogram or ERG. Modern analysis has shown that the electrode on the cornea records changes in potential occurring successively at different levels of the retina. The electrical changes occurring in the rods and cones - the receptor potentials - and those occurring in the bipolar cells are known to contribute in a different manner to the record of visual stimulation. Thus the possibility of recognising selective pathology of the mid and outer retinal layers (see section 1.1) becomes apparent. However, in general, the electrical changes caused by the different types of receptor and neural cells tend to overlap in time, so that the representation of cellular excitation in the electroretinogram is only a faint and attenuated index of the actual changes. Nevertheless, it has served not only as a valuable tool for the analysis of retinal mechanisms but more generally in the early diagnosis and assessment of a wide range of retinal pathologies.

THE FLASH ERG

The flash ERG is elicited from a diffuse flash stimulus and records hyperpolarising and depolarising activity from the outer and mid-retinal layers. The biphasic waveform produced possesses several distinct components such as the a-wave, a negative signal generated by the photoreceptors and off-bipolars and the b-wave, a positive signal generated by the on-bipolars (Bush & Sieving 1994, Bush & Sieving 1996)

The degree of influence specific cells have on the components in the response can be varied by means of stimulus illumination, background illumination and frequency of stimulation. Thus while the response to a flash of light under a steady background illumination (photopic response) will yield information predominantly from the outer and mid-retinal cone pathways, a dim flash of light

under dark adapted conditions (scotopic response) will yield information from the outer and mid-retinal rod pathways.

In 1989 and 1995 the International Standardisation Committee (Marmor et al 1989; Marmor & Zrenner 1995) recommended a basic protocol for the measurement of certain responses. This was to ensure that certain responses would be recorded comparably throughout the world. The five commonly obtained responses are;

1. The Rod Response to test the rod pathways (scotopic).
2. The Maximal Combined Response to test the rod dominated response (scotopic).
3. The Oscillatory Potentials to test the mid-retina (photopic).
4. The Single Flash Cone Response to test the cone dominated response (photopic).
5. The Flicker Response to test the cone pathway (photopic).

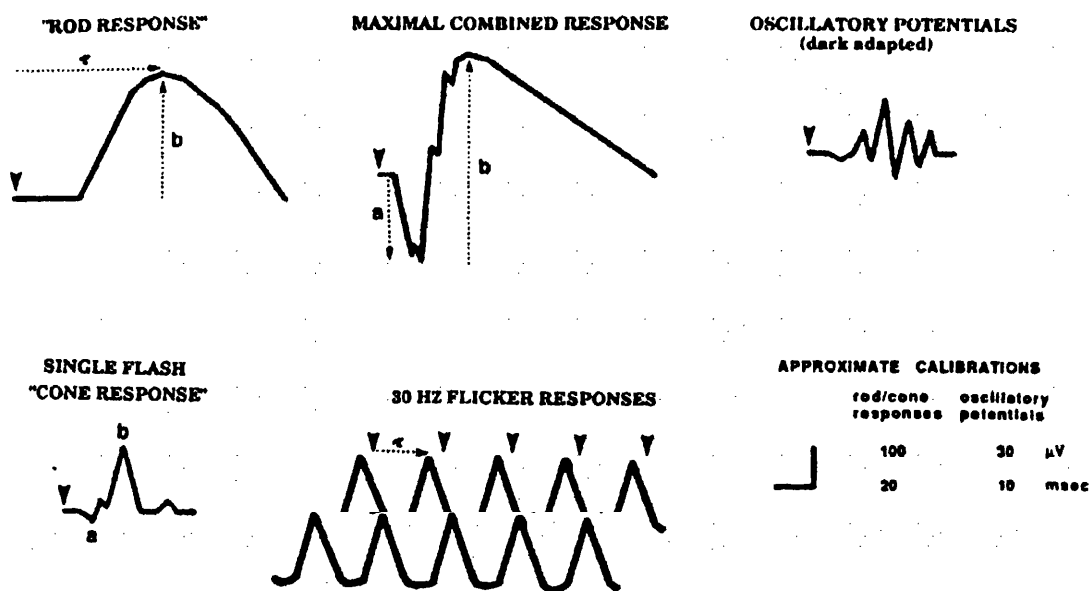


Figure 1.9 Diagram of five basic ERG responses defined by the ISCEV standard (M.F. Marmor & E. Zrenner., Standard for clinical electroretinography (1994 update), Documenta Ophthalmologica 89: 199-210, 1995)

The conventional method for reporting ERG results is to measure the cone, rod and maximal b-wave amplitude (measured from the trough of the a-wave to the peak of the b-wave) and the cone or flicker b-wave time to peak (see figure 1.9). The ERG amplitude and latency is dependent on stimulus intensity and adaptation level. The photopic response (single flash) at a background intensity of 25 cd/m^2 and flash intensity of $2.4 \text{ cd}\cdot\text{s/m}^2$ will yield a b-wave of amplitude $\sim 150\mu\text{V}$ and latency of 30ms. The scotopic response at a flash intensity of $2.4 \text{ cd}\cdot\text{s/m}^2$ attenuated by a 2.4 log filter will yield amplitude and latency values of $\sim 230\mu\text{V}$ and 80ms respectively (Jacobi et al 1993).

Although the ERG is used routinely in the diagnosis and monitoring of a wide range of retinal disorders its application is limited. Cones in the macula (central 10 degrees) account for only some 7% of the total cone population (Osteberg 1935, Curcio et al 1987). As a result, cone and rod responses from the macular region contribute less than 10% of the full field photopic ERG and so disease limited to the macular region typically is not detected with the standard diffuse response of the full field flash ERG. Since the macular region is the most important for visual acuity, this inability of the ERG to record local defects has encouraged the development of specialised techniques for objectively recording local responses to focal stimuli. The Focal Electroretinogram (FERG) was developed to address this limitation of the full field conventional ERG.

THE FOCAL ELECTRORETINOGRAM

The focal ERG is evoked by a small area of the retina (10 degrees or less) (Carr & Seigel 1990) and most commonly involves stimulation of the retina by a small flickering light with a steady background illumination contained within a modified ophthalmoscope (Carr & Seigel 1990). A static background illumination minimises the effects of reflected stimuli which evoke responses from areas of the retina not under investigation. Unfortunately the method suffers from prolonged recording times and varying signal to noise ratios.

It has long been believed that the diffuse and local flash electroretinogram are little influenced by the inner-retinal layers and as such are limited in their ability to detect abnormalities of the visual pathway at any level at and beyond the ganglion cells. Assessment of these sites is important in the detection of glaucoma and optic atrophy and evidence suggests that responses to pattern stimuli may reflect inner retinal activity (Mafei et al 1981; Marx et al 1988; Helligkeits et al 1985; Ambrosio et al 1988; Bach et al 1988; Bobak et al 1983).

THE PATTERN ELECTRORETINOGRAM

The pattern ERG is an evoked response generated by stimulation of the retina by patterned stimulus such as the checkerboard. Although the selective nature of this response was not known until recently (Maffie & Fiorentini 1981) the recording of the pattern ERG had been performed for sometime (Johnson et al 1966, Spekrijse et al 1975).

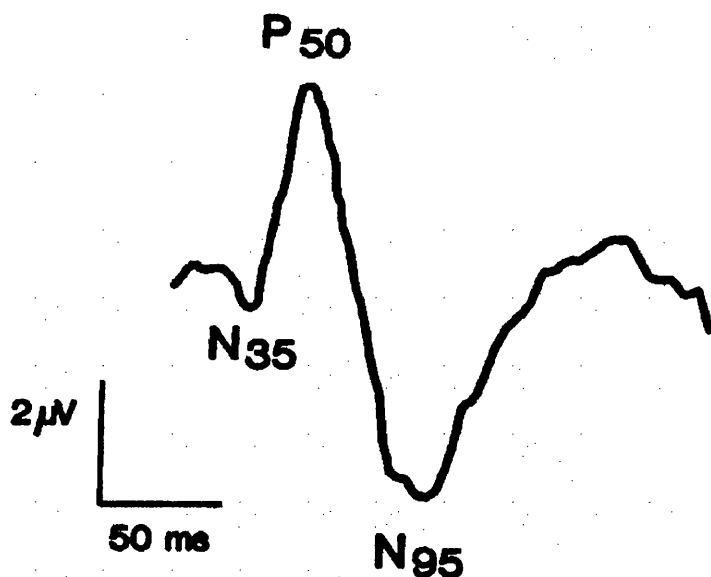


Figure 1.10 Typical pattern ERG response with components labelled (taken from Beringer T. Arden G.B. *The Pattern Electroretinogram* chapter 38 *Principles and Practice of Clinical Electrophysiology of Vision*. Mosby Year Book 1991).

The pattern ERG recording technique differs only slightly from that of the conventional electroretinogram. Similar electrodes are used, although lid electrodes have the advantage of not interfering unduly with the optics. The patient is not dilated and refractive errors are corrected for maximum acuity. The subject is then exposed to the pattern stimulus, usually displayed on a computer monitor. The ISCEV guidelines for pattern electroretinography (Marmor et al 1996) suggest the following stimulus parameters and reporting convention:

1. Field and check size. Field size $10^{\circ} \times 16^{\circ}$, and a check size of approximately $40'$.
2. Contrast. The contrast between black and white areas should be maximal (but not less than 80%)
3. Luminance. Maximum luminance should exceed 80cd/m^2
4. Transient or Steady State? Recordings should be transient (i.e. each stimulus frequency should be less than the response frequency).
5. Reversal rate. For transient responses this should not exceed 3Hz.
6. Reporting. Reports should contain measurements of P50 and N95 amplitude (see figure 1.10) and P50 latency.

In comparison to the flash ERG, the pattern ERG amplitude is of the order of a few microvolts and requires averaging to recover the signal. Although the pattern ERG has been shown to evoke responses from the cells entering the optic nerve, any lesion, atrophy or visual loss associated with the pathways beyond the optic nerve will have no effect on either the conventional electroretinogram or the pattern ERG. To assess, objectively, abnormalities distal to these sites the Visual Evoked Cortical Potential is required.

1.4.3. THE VISUAL EVOKED CORTICAL POTENTIAL (VECP)

The visual evoked cortical potential (VECP) is a measure of cortical responses to evoked retinal potentials. It is recorded from electrodes positioned on the back of the scalp over the occipital cortex and its origins lie in the central retinal ganglion

cell function. It is dependent on the integrity of the entire visual pathway and so is a measure of that function. The cortical magnification of central visual function present within the visual cortex restricts the VECF to a record of the macular response to the stimulus. Clinically the VECF shows latency changes in disorders of the macula, optic nerve and optic chiasma and is useful in identifying multiple sclerosis, malingering and for the objective measurement of visual acuity.

Electroperimetry has shown promise in the objective detection of local visual field defects. This method has included digital signal processing techniques to recover small visual evoked cortical potentials from the occipital cortex. One major disadvantage of this method is the time taken to recover signals from electroencephalographic activity and muscle noise, although improvements in SNR were achieved using adaptive noise cancelling (Bradnam 1994; Norcia et al 1985; Norcia et al 1989).

1.5. CONCLUSIONS

Although electrophysiology plays a prominent role within ophthalmology as a diagnostic tool, its ability to detect localised pathology leading to specific visual dysfunction is necessarily limited. A large number of retinal pathologies are manifest in small localised regions of the retina. Their progressive nature although a key indicator in severity is difficult to detect with conventional electrophysiology and so there remains a need for an objective measure of visual function of high resolution.

This chapter summarised the anatomy and physiology of the eye and the visual pathways within the brain. Sections dealt with the present methods of investigating the integrity of these pathways from the Electro-oculogram which reflects activity in the Retinal Pigment Epithelial layer to the Visual Evoked Cortical Potential which records responses generated within the visual cortex. Some conventional perimetric techniques were examined. These, although much more subjective in nature than conventional electrophysiology, provide a means to identify and quantify small localised areas of the field that may be abnormal.

The aim of this thesis is the evaluation of a new technique the Visual Evoked Response Imaging System (VERIS) for routine clinical use. This system promises to combine the spatial resolution of conventional perimetry with the objectivity of electrophysiology and, if this is true, it should provide a means of assessing localised retinal abnormalities. To provide a thorough evaluation a number of investigations are required:

1. Possible factors that may degrade the integrity of data obtained from the new technique should be investigated and their effect minimised where possible.
2. A quantitative assessment of repeatability and reproducibility of the technique should be undertaken.
3. The normal range of responses produced by the technique should be established from a wide control population.
4. An investigation of a selection of retinal disorders should be undertaken.

The next chapter introduces the concept of pseudo random binary stimulation using maximum length sequences and its application to this new technique.

Chapter2

PSEUDO RANDOM BINARY SEQUENCE

There has been a desire for some time to combine the objectivity of electrophysiology with the spatial resolution and depth of field present in visual field assessment. As mentioned previously the principal limitation that prevents this combination is the signal to noise ratio inherent in the recovery of focal electrophysiological responses. Conventional averaging techniques involve the serial averaging of responses synchronised in time. While this is adequate in the context of relatively large signals and fast responses, conventional serial averaging is not advantageous in the recovery of small signals as long recording periods are required to achieve signal to noise ratios of acceptable quality.

Electroperimetry was an attempt to objectively assess local visual disruption in a manner similar to conventional perimetry and in this context it made some advances (see previous chapter). However, the application of Pseudo Random Binary Sequences (PRBS) as an alternative to conventional averaging techniques has fuelled a recent resurgence in the field.

2.1. INTRODUCTION

This chapter presents the concept of Pseudo Random Binary Sequences (PRBS) and their application to signal averaging. It discusses the advantages of PRBS over conventional techniques and its application in the VERIS system.

2.2. SIGNAL AVERAGING

The technique of signal averaging led to the rapid development of electrophysiology as a viable clinical tool. It was Laplace in 1832 who predicted and Sabine in 1847 who demonstrated the recovery of responses to time-locked stimuli embedded in larger random variations (Regan & Spekreijse 1986). However, it was not until 1954 that Dawson applied this technique to electrophysiological signals.

Dawson's averaging technique synchronises the stimulus and the analysis sweep (Dawson 1954). The main advantage of this method is the ability to average consecutive time-locked responses. This superimposition of random variation of consecutive sweeps cancels as the time-locked responses add. The signal (s) to noise (n) ratio, which is a direct measure of the quality of the response, is proportional to the square root of the number of averages (see equation 2.1)

$$\frac{s}{n} \propto \sqrt{\text{Number of averages}} \quad (2.1)$$

Thus the recovery of a small transient electrophysiological visual evoked response is possible. The method, although the most common, requires that the time between consecutive stimuli be longer than the evoked response to a stimulus so that there is no overlap between a response and the next stimulus. Thus long recording periods are required for the recovery of small local responses which are always contaminated with some degree of random 'noise'. This limitation has been addressed by the introduction of Pseudo Random Binary Sequences to the averaging arsenal.

2.2.1. PRINCIPLES OF PSEUDO RANDOM BINARY SEQUENCES (PRBS)

A random signal $x(t)$ is applied as excitation to the input of the system under investigation, in this case local electrophysiological responses. The cross-correlation between this input and the resulting system output is then calculated, yielding an estimate of the system's impulse response function – an amplitude time curve which completely characterises the response.

To explain the theoretical basis of this method in more detail, it becomes necessary to define the following mathematical relationship. The Laplace Transform of a known function of time $x(t)$ for values $t > 0$, is defined by the integral equation:

$$X(s) = \ell[x(t)] = \int_0^{\infty} e^{-st} x(t) dt \quad (2.2)$$

Where s is the Laplace operator.

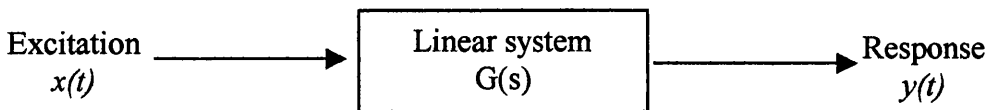


Figure 2.1 A Typical system

Similarly, the transfer function $G(s)$ of a system such as is illustrated in figure 2.1, may be defined as the ratio of the Laplace transforms of the output and input signals, i.e.

$$G(s) = \frac{\ell[y(t)]}{\ell[x(t)]} = \frac{Y(s)}{X(s)} \quad (2.3)$$

And the direct inverse Laplace transform of the transfer function is known as the system's impulse response function $g(t)$, i.e.

$$g(t) = \frac{1}{2\pi j} \int_{a-j\infty}^{a+j\infty} G(s) e^{st} ds \quad (2.4)$$

From equation 2.3, the transform $Y(s)$ is the product.

$$\begin{aligned}
 Y(s) &= G(s)X(s) \\
 &= \int_0^{\infty} e^{-su} g(u) du \int_0^{\infty} e^{-sv} x(v) dv
 \end{aligned} \tag{2.5}$$

where u and v are dummy variables of integration. This is equivalent to the double integral

$$Y(s) = \iint_S e^{-s(u+v)} g(u)x(v) du dv \tag{2.6}$$

Where S is the area of integration. Using the substitution

$$u + v = t$$

$$u = \tau$$

The region s in the u, v , plane is transformed into the corresponding region s' in the t, τ plane, and equation (2.6) is transformed to

$$Y(s) = \int \int_0^{\infty} e^{-s't} g(\tau)x(t-\tau) ds' \tag{2.7}$$

Integrating first with respect to τ yields

$$Y(s) = \int_0^{\infty} e^{-s't} \left\{ \int_0^t g(\tau)x(t-\tau) d\tau \right\} dt \tag{2.8}$$

So that by the definition (2.2)

$$y(t) = \int_0^t g(\tau)x(t-\tau) d\tau \tag{2.9}$$

Thus the output signal $y(t)$ may be expressed in terms of the impulse response function $g(t)$, and the input signal $x(t)$. This expression is called the Convolution Integral.

The average input signal, if considered over a large number of individual signals (k) is called the ensemble average and is defined as:

$$\bar{x}(T_1) = \frac{1}{k} \sum_{i=1}^k x_i(T_1) \quad (2.10)$$

If the statistical properties of these signals do not change with time, the process is called stationary, thus:

$$\bar{x}(T_1) = \bar{x}(T_2) = \dots \quad (2.11)$$

If each signal has the same statistical properties as every other signal the process is called *ergodic*. The average value is equal to the time average of any $x(t)$ over a sufficient length of time, thus:

$$\bar{x} = \lim_{T \rightarrow \infty} \frac{1}{2T} \int_{-T}^T x(t) dt \quad (2.12)$$

THE AUTOCORRELATION FUNCTION

Consider the present value of a signal $x(t)$ influences, in some degree, its value at a time τ in the future. That is $x(t + \tau)$ is in general dependent upon $x(t)$. The autocorrelation function is a statistical measure of this dependence i.e.

$$\phi_{xx} = \lim_{T \rightarrow \infty} \frac{1}{2T} \int_{-T}^T x(t)x(t + \tau) dt \quad (2.13)$$

White noise is a term given to random signals that contain constant power per unit bandwidth for all frequencies. The rate of change of such a signal is so great that its present value is completely independent of all past values. Thus, using equation (2.13) the autocorrelation function of white noise i.e. $\tau = 0$ since there are no periodic components is,

$$\phi_{xx}(0) = \overline{x^2(t)} = \sigma^2 \quad (2.14)$$

THE CROSS-CORRELATION FUNCTION

If one variable $x(t)$ influences the future value of another variable $y(t)$ there will be a connection or correlation between $x(t)$ and $y(t + \tau)$ where τ is the time shift. The cross-correlation of two time varying signals is thus,

$$\phi_{xy}(\tau) = \lim_{T \rightarrow \infty} \frac{1}{2T} \int_{-T}^T x(t)y(t + \tau)dt \quad (2.15)$$

Note that if $y(t) = x(t)$, the cross-correlation function reduces to the autocorrelation function.

THE POWER DENSITY SPECTRUM

The autocorrelation function can be both Laplace and Fourier transformed. The Fourier transform is defined as:

$$F(j\omega) = \int_{-\infty}^{\infty} f(t)e^{-j\omega t} dt \quad (2.16)$$

where $f(t)$ is the signal, $F(j\omega)$ is its Fourier transform, and ω is the angular frequency. The Fourier transform of the autocorrelation function of $x(t)$ is thus defined as

$$\begin{aligned} \Phi_{xx}(j\omega) &= \int_{-\infty}^{\infty} \phi_{xx}(\tau)e^{-j\omega\tau} d\tau \\ &= \int_{-\infty}^{\infty} \phi_{xx}(\tau)\cos(\omega\tau)d\tau \end{aligned} \quad (2.17)$$

The imaginary term is always zero because the autocorrelation function is always an even function. This is often written simply as $\Phi_{xx}(\omega)$ and is called the *power density spectrum*.

THE IMPULSE RESPONSE FUNCTION

The convolution integral (2.9) may be expressed in the form

$$y(t) = \int_{-\infty}^{\infty} g(s)x(t-s)ds \quad (2.18)$$

The impulse response must be zero before the input is applied i.e. $g(t) = 0$ for $t < 0$. The upper limit has been increased to infinity as the whole impulse response is of interest. Using this the cross-correlation function may be written as

$$\phi_{xy}(\tau) = \lim_{T \rightarrow \infty} \frac{1}{2T} \int_{-T}^T x(t) \int_{-\infty}^{\infty} g(s)x(t+\tau-s)dsdt \quad (2.19)$$

and by interchanging the order of integration

$$\phi_{xy}(\tau) = \int_{-\infty}^{\infty} g(s) \left\{ \lim_{T \rightarrow \infty} \frac{1}{2T} \int_{-T}^T x(t)x(t+\tau-s)dt \right\} ds \quad (2.20)$$

The term in brackets may be recognised as the autocorrelation function of the input signal $x(t)$ with argument $(\tau - s)$ so that

$$\phi_{xy}(\tau) = \int_{-\infty}^{\infty} g(s)\phi_{xx}(\tau-s)ds \quad (2.21)$$

Considering the Fourier transform of (2.21)

$$\begin{aligned} \Phi_{xy}(j\omega) &= G(j\omega)\Phi_{xx}(j\omega) \\ \Rightarrow G(j\omega) &= \frac{\Phi_{xy}(j\omega)}{\Phi_{xx}(j\omega)} \end{aligned} \quad (2.22)$$

EXCITATION USING A WHITE NOISE INPUT SIGNAL

If the input signal to the system is white noise, then as previously mentioned, its power density spectrum is flat, e.g.

$$\Phi_{xx} = 2\pi K \quad (2.23)$$

the relationship between the autocorrelation function and the power density spectrum is the Fourier transform, i.e

$$\phi_{xx}(\tau) = \frac{1}{2\pi} \int_{-\infty}^{\infty} \Phi_{xx}(w) e^{-jw\tau} dw \quad (2.24)$$

which becomes, for the white noise case

$$\phi_{xx}(\tau) = K \int_{-\infty}^{\infty} e^{-jw\tau} dw = K\delta(\tau) \quad (2.25)$$

where $\delta(\tau)$ is the Dirac delta function. The cross-correlation function (2.15) then becomes

$$\begin{aligned} \phi_{xy}(\tau) &= K \int_{-\infty}^{\infty} g(s) \delta(\tau - s) ds \\ &= Kg(\tau) \end{aligned} \quad (2.26)$$

That is, for a white noise input, the cross-correlation function of the input and output signals, is directly proportional to the impulse response function. This technique has one great advantage in that the measurements are immune from the extraneous effects of unwanted noise provided it is stochastically independent of (i.e. uncorrelated in any way with the input noise source, regardless of whether the unwanted noise originated internally or externally).

IDENTIFICATION USING PSEUDO RANDOM NOISE INPUT

One disadvantage of this method is the long time required for identification using a white noise input. This can be overcome by generating what could be called pseudo-random noise. This type of noise would require the same type of autocorrelation function as white noise except this would repeat over a period T.

That is the autocorrelation function would have the value of $\phi_{xx}(\tau) = \sigma^2$ (the mean square value) at $\tau = 0, T, 2T, 3T$, etc. and zero for any other value of τ .

The autocorrelation function of this type of pseudo-random noise input signal, again denoted $x(t)$ would be

$$\phi_{xx}(\tau) = \frac{1}{T} \int_0^T x(t)x(t+\tau)dt \quad (2.27)$$

because of its periodicity, or by taking an argument $(\tau - s)$

$$\phi_{xx}(\tau - s) = \frac{1}{T} \int_0^T x(t)x(t+\tau-s)dt \quad (2.28)$$

The cross-correlation function can thus be expressed as

$$\phi_{xy}(\tau) = \int_{-\infty}^{\infty} g(s) \left\{ \frac{1}{T} \int_0^T x(t)x(t+\tau-s)dt \right\} ds \quad (2.29)$$

Which by changing the order of integration becomes

$$\phi_{xy}(\tau) = \frac{1}{T} \int_0^T x(t) \left\{ \int_{-\infty}^{\infty} g(s)x(t+\tau-s)ds \right\} dt \quad (2.30)$$

$$= \frac{1}{T} \int_0^T x(t)y(t+\tau)dt \quad (2.31)$$

So that by using this pseudo-random noise, the cross correlation function may be obtained to its full accuracy by integration over one period of the noise only.

From equation (2.21), together with the assumption that the impulse response function $g(t)$ is zero for $t \leq 0$, and $x(t)$ is periodic with period T , the cross-correlation function may also be expressed in the form:

$$\phi_{xy}(\tau) = \int_0^T g(s)\phi_{xx}(\tau-s)ds + \int_T^{2T} g(s)\phi_{xx}(\tau-s)ds + \dots \quad (2.32)$$

So that from equation (2.26)

$$\phi_{xy}(\tau) = K \{g(\tau) + g(T + \tau) + g(2T + \tau) \dots\} \quad (2.33)$$

but if it is so arranged that the impulse response function has decayed to zero in a time less than T, equation (2.33) becomes

$$\phi_{xy}(\tau) = Kg(\tau) \quad (2.34)$$

as before.

THE GENERATION OF BINARY MAXIMUM LENGTH SEQUENCES

There are many algorithms that produce random sequences each with differing degrees of randomness associated with them. Most computer generated random sequences are known as uniform deviates and are simply random numbers that lie within a specified range.

It may appear contradictory that something as deterministic and precise as a computer program should produce 'random' numbers since by definition any output from a program is predictable, hence not truly 'random'. Nevertheless 'random number generators' are in common use. This entirely predictable nature of computer generated sequences gives rise to their description as *pseudo random sequences*.

System supplied random number generators are almost always linear congruential generators, which generate a sequence of integers I_1, I_2, I_3, \dots , each between 0 and $m - 1$ (a large number) by the recurrence relation

$$I_{j+1} = (aI_j + c) \bmod m \quad (2.35)$$

Here m is called the *modulus*, and a and c are positive integers called the multiplier and the increment, respectively. The recurrence will eventually repeat itself, with a period that is obviously no greater than m . If m , a , and c are properly chosen, then the period will be of maximal length, i.e., of length m . In this case, all possible integers between 0 and $m-1$ occur at some point, so any initial ‘seed’ choice of I_0 is as good as any other.

The linear congruential method has the advantage of being very fast, requiring only a few operations per call. However, as mentioned previously if the constants m , a and c are not *very* carefully chosen the sequences randomness can be compromised and repetition can appear.

One method of achieving the generation of single random bits, with 0 and 1 equally probable is an implementation based on ‘primitive polynomials modulo-two’. The theory of these polynomials is beyond the scope of this thesis but an introduction to their association with Pseudo Random Binary Sequences can be found in Kruth (1981) and in Davies (1970). A modulo-two gate produces a sum-digit table as shown in table 2.1. This is sometimes referred to as an ‘exclusive-or’ gate.

Input 1	Input 2	Modulo-two sum
0	0	0
0	1	1
1	0	1
1	1	0

Table 2.1 *Modulo-two sum digit table*

Every primitive polynomial modulo-two of order n defines a recurrence relation for obtaining a new random bit from n preceding ones. The recurrence relation is guaranteed to produce a sequence of maximal length (m -sequence), i.e., cycle through all possible sequences of n bits (except all zeros) before it repeats. Thus any excitation driven by a ‘primitive polynomial modulo-two’ m -sequence is

guaranteed to excite at all possible frequencies (no matter what seed is used) before repeating.

The primitive polynomials for an m-sequence of length 3 are $x^3 + x + 1$ (this gives 'tap' or feedback stages of 3 and 1). The derivation of m-sequence values for an m-sequence length of 2^3-1 (7) is given below. Here the contents of selected taps are combined addition modulo-two and the results shifted in from the right (see figure 2.2).

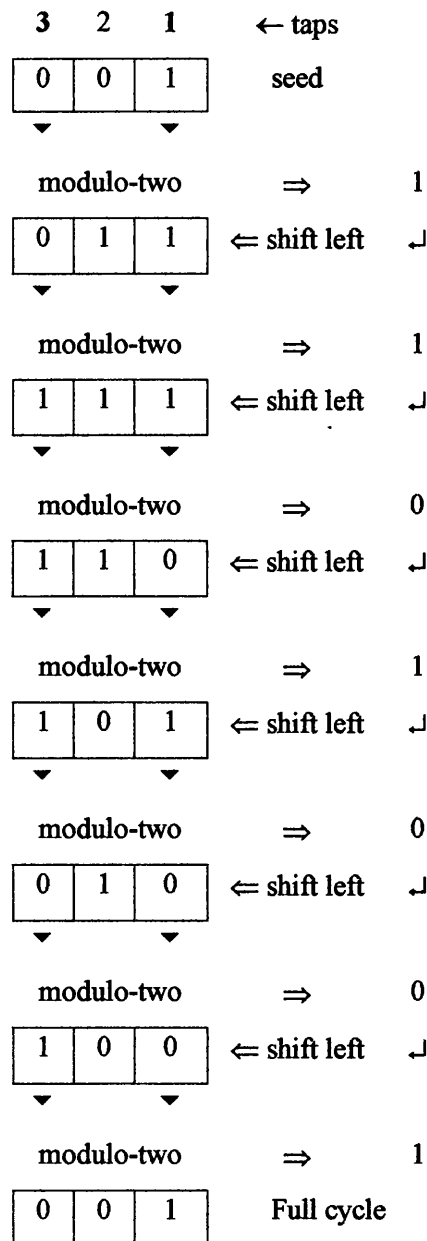


Figure 2.2 Basic modulo-two PRBS generator.

Thus the m-sequence generated will be of length 7 given as:

m-seq. 1 1 0 1 0 0 1

2.3 PSEUDO RANDOM BINARY SEQUENCES AND VERIS

The VERIS system displays two original features. It simultaneously stimulates multiple areas within the visual field by temporal modulation of a PRBS m-sequence for each stimulus element. In addition, by exploiting features of the fast Walsh-Fourier transform and the cross-correlation function it can provide rapid extraction of multiple ERG signals.

2.3.1 STIMULUS GENERATION

To provide an explanation of multifocal stimulation with PRBS a simple example is given.

Take a square stimulus consisting of 4 smaller squares of equal size. Each square can only display one of two colours (black or white). The determination of colour for this square is a sequence of 1's and -1's – a chain code. When the sequence has a value 1 the square is white, when the sequence is -1 the square is black. For future correlation each square requires a unique sequence that should be uncorrelated with respect to any other square. Due to the statistically random properties of m-sequences each shifted m-sequence will be uncorrelated with any other shifted cycle of the same sequence. Thus 4 shifted cycles of a Pseudo Random Binary Sequence could be used to drive the stimulus.

Take an m-sequence of length $2^4-1=15$ (with a substitution $0 \Rightarrow -1$). Use this to drive a stimulus consisting of 4 elements – see figure 2.3.

Sequence from left to right →

Area	1	2	3	4
	<i>1</i>	1	1	-1
	1	1	-1	-1
	1	-1	1	-1
	-1	-1	-1	<i>1</i>
	1	1	-1	1
	1	-1	-1	1
	-1	1	-1	-1
	-1	-1	<i>1</i>	1
	1	-1	1	1
	-1	-1	1	-1
	1	-1	-1	-1
	-1	<i>1</i>	1	1
	-1	1	1	-1
	-1	1	-1	1
	-1	-1	-1	-1

Figure 2.3 *Stimulus of four areas driven by a shifted Pseudo Random Binary Sequence. Note values in red indicate beginning of sequence.*

Figure 2.3 illustrates a pseudo random multi-input stimulus generated from a 4 bit m-sequence. If this stimulus was used as the excitation of a system (i.e. a physiological response from the eye) then from the previous section we are able to derive the response to individual elements independently by the use of cross-correlation. This is the method used by the VERIS system to stimulate multiple areas of the retina independently.

2.3.2 DERIVING THE MULTIFOCAL RESPONSE

The physiological response from the stimulus depicted in figure 2.3 would contain contributions from all areas stimulated. As defined in section 2.2 the cross-correlation of an input sequence with the output response will reveal the impulse

response generated by that unique sequence (any other contributions that are uncorrelated, i.e. neighbouring squares, will be discarded).

The cross-correlation of a *binary* sequence is a simplification of equation (2.31). This is because this two state sequence reduces the multiplication of sequence and response to a simple gating operation (i.e. addition of the response when elements of the sequence are 1 and subtraction when they are -1).

In a linear system this derived response would be considered a record of the impulse response to the input signal as discussed previously. However the electrophysiological response of the eye to a light stimulus, as with most other bio-potentials, is non-linear. Thus to reconcile the results obtained from this method a solution is required that will reflect the best linear predictor of the system as equation (2.34) has for the linear system.

A linear system is characterised entirely by its impulse response. This reveals the signal processing that occurs within the system, e.g integration, differentiation, delays etc. This can be achieved by calculating the convolution integral (equation 2.9) between the unit-impulse response and the input waveform. However the characteristics of a non-linear system have generally changed during this processing period. That is the response to one impulse in a sequence might be different from the response to another identical impulse. For example, the absorption of a fixed number of photons by a photoreceptor results in a receptor potential of a given amplitude. A second pulse of the same number of photons will evoke a smaller response, since the sensitivity of the cell has been reduced by the previous interaction (Larkin et al 1979). Thus we cannot predict a double impulse response for a non-linear system by adding single impulse responses. These systems do not obey the law of superposition. Volterra (1959) characterised a non-linear system as a series of functions rather than impulse responses; these he called kernels.

The zero order kernel, h_0 , is the mean value of the response. The first-order kernel of the system $h_1(\tau)$ is the best linear prediction of all the different impulse responses produced by the system (i.e. the closest match to the linear impulse response). If a double impulse response is constructed by superimposing two first-order kernels with the appropriate time separation (see figure 2.4) the difference between the calculated response and the measured double impulse response is one measure of the system's non-linearity. To describe this non-linearity completely the experiment would require to be repeated for all possible intervals.

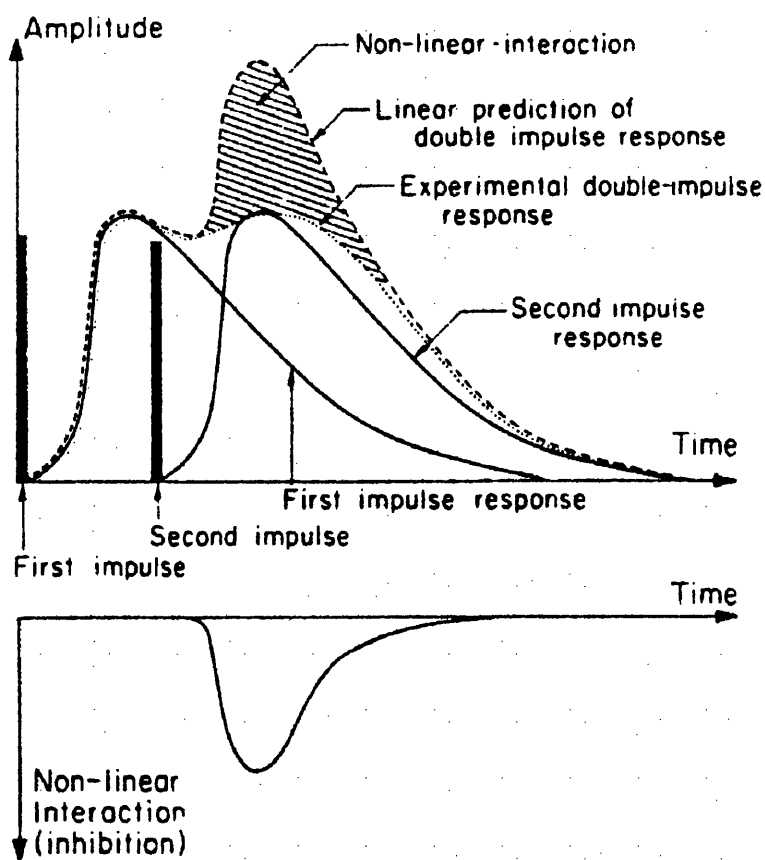


Figure 2.4 Shaded area indicates the nonlinearity (or inhibition) of the response for the time interval between impulses. (adapted from Larkin RM Klein S Ogden E & Fender DH (1979) *Nonlinear Kernels of the Human ERG. Biol. Cybernetics* 35, 143-160).

This, while possible, is impractical. The zero-, first- and second-order kernels can be thought of as the first three terms of an infinite expansion of functions that together describe the response of the system to the input. Wiener (1958) showed

that if the input $x(t)$ is a random signal with power density P , then the output can be obtained by combining various functions of the kernels as follows:

$$m^n = a_0, a_1, a_{\partial\partial 2}, \dots, a_{n-1} \quad (2.36)$$

where

$$\left. \begin{aligned} G_0(h_0) &= h_0 \\ G_1(h_1, x(t)) &= \int_0^{\infty} h_1(\tau) x(t-\tau) d\tau \\ G_2(h_2, x(t)) &= \int_0^{\infty} \int_0^{\infty} h_2(\tau_1, \tau_2) x(t-\tau_1) x(t-\tau_2) d\tau_1 d\tau_2 \\ &\quad - P \int_0^{\infty} h_2(\tau, \tau) d\tau \end{aligned} \right\} \quad (2.37)$$

Lee and Schetzen (1961) proposed a simpler calculation which only involves evaluating the cross-correlations between the random input $x(t)$ and the output $y(t)$, i.e.

$$\left. \begin{aligned} h_0 &= E\{y(t)\} \\ h_1 &= \frac{1}{P} E\{[y(t) - G_0(h_0)]x(t-\tau)\} \\ h_2(\tau_1, \tau_2) &= \frac{1}{2P^2} E\{[y(t) - G_0(h_0) - G_1(h_1, x(t))]x(t-\tau_1)x(t-\tau_2)\} \end{aligned} \right\} \quad (2.38)$$

where $E\{ \}$ signifies 'the expected value'. The linear portion of this can be written as:

$$y(t) = \sum_{\tau} h_1(\tau) x(t-\tau) \quad (2.39)$$

The first order kernel $h_1(\tau)$, can be determined by examining the cross-correlation $H_1(\tau)$, as follows:

$$H_1(\tau) = \frac{1}{T} \sum_{\tau} y(t) x(t-\tau) \quad (2.40)$$

where T is the total duration of the experiment. By substituting (2.39)

$$H_1(\tau) = \frac{1}{T} \sum_{\tau'} \left[\sum_{\tau} h_1(\tau) x(t-\tau') \right] x(t-\tau) \quad (2.41)$$

the autocorrelation function would be

$$\left. \begin{aligned} \frac{1}{T} \sum_{\tau} x(t-\tau)x(t-\tau') = \phi(\tau, \tau') &= \sigma^2 \text{ for } \tau = \tau' \\ &= 0 \text{ for } \tau \neq \tau' \end{aligned} \right\} \quad (2.42)$$

Inserting this in (2.40)

$$H_1(\tau) = \sum_{\tau'} \phi(\tau, \tau') h_1(\tau') = h_1(\tau) \sigma^2 \quad (2.43)$$

Thus the first order kernel $h_1(\tau)$, can be treated in a similar manner to the impulse response $g(\tau)$ in equation (2.34). Higher-order kernels can be derived using a similar method (Larkin et al 1979).

The second unique feature of the VERIS system is the rapid extraction of not only the first-order kernel but the simultaneous extraction of higher-order kernels. This is achieved by use of the fast m-transform.

The m-transform, M^T describes the transformation of a binary m-sequence m from a single sequence of length 2^{n-1} , into a 2^n dimensional symmetrical matrix. Let the elements of m be a_i for $i=0$ to $k-1$ where $k=2^{n-1}$

$$m = a_0, a_1, \dots, a_{k-1} \quad (2.44)$$

This matrix created by the transform consists of a zeroth element of 1 and 2^{n-1} columns of the m-sequence m in all its cyclical shifts (see 2.45).

$$M^T(m^n) = \begin{pmatrix} 1 & 1 & 1 & \dots & 1 \\ 1 & a_0 & a_1 & \dots & a_{k-1} \\ 1 & a_1 & a_2 & \dots & a_0 \\ \vdots & \vdots & \vdots & & \vdots \\ 1 & a_{k-1} & a_0 & \dots & a_{k-2} \end{pmatrix} \quad (2.45)$$

The purpose of this transformation is the creation of a 2^n dimensional symmetrical matrix with orthogonal elements. A matrix of this form is called a *Hadamard* matrix. The Hadamard matrix has many mathematical properties and features and lend themselves to the simplification of complex matrix transforms such as the fast Walsh-Fourier transform or the fast Walsh-Hadamard transform. These convert the computation required for large matrix multiplication to simple exclusive-or gates. Their derivation is beyond the scope of this thesis but further information can be found in (Shanks 1969, Lechner 1970, Henderson 1970, Fino & Algazi 1976, Schroeder 1987). In the VERIS system the fast m-transform (Sutter 1991) consists of two stages. The first is used to create a Hadamard matrix from a PRBS on which these Walsh transforms can be used (the m-transform previously defined). The second stage involves the creation of a symmetrical matrix from the full unprocessed response signal. This response is simply repeated 2^{n-1} times in identical columns of a response matrix, the zeroth row and column supplemented by 0's. Since the m-transformed matrix consists of all possible cycles of the PRBS the matrix multiplication between this and the response matrix will produce all possible correlations between response and sequence that exist and results in an array which consists of individual responses lagged along its length. While this is a fast method for providing rapid cross-correlation today's computational capabilities of computers reduce this transforms necessity. One interesting feature of this technique is that since all possible correlations of the response and sequence are extracted higher order non-linear responses are included.

There is however the possibility of higher-order cross-contamination with this method. To illustrate this consider the sequences generated for figure 2.3. The interaction of two consecutive responses (i.e the product of consecutive stimuli) is the second-order response. If we take area 1 then the second-order product would provide us with a new orthogonal sequence (see table 2.2). The cross-correlation

of this sequence with the full unprocessed response would yield the second-order response for area 1.

<i>Area 1</i>	1	1	1	-1	1	1	-1	-1	1	-1	1	-1	-1	-1	
<i>product</i>	1	1	-1	-1	1	-1	1	-1	-1	-1	-1	1	1	1	-1

Table 2.2 *Second-order product of interactions from area 1 from figure 2.3.*

However note that the m-sequence for area 2 is identical to the second order response from area 1. Thus in this case the cross-correlation of area 2 will result in a response that is contaminated with the second order response from area 1. Given the fact that in general higher order responses are small in comparison to first order responses this should have little influence on the first order response. However the converse is not true. The second order response from area 1 would predominately contain contamination from the first order response of area 2.

The VERIS system provides a facility of determining the final ‘tap’ of the sequence chosen. This, it claims, reduces the possibility of higher-order cross-contamination. However the means it uses to achieve this are undocumented and remain obscure.

The assessment of higher-order responses was minimal (see chapter 6). This was due not only to the lack of information on the separation of cross-contamination of higher-order kernels, discussed earlier, but that higher order responses were found to be difficult to recover. This would necessitate extensive lengthening of the recording protocol to obtain responses that could, if proven to be truly non-linear, provide a clinical benefit.

2.4 CONCLUSIONS

In this chapter the limitations of the conventional Dawson averaging technique were discussed. A new technique for multi-input excitation was introduced. This

new technique exploits the orthogonal nature of special Pseudo Random Binary Sequences called maximum length sequences or m-sequences.

The application of a PRBS to signal averaging overcomes the limitations inherent in conventional techniques as the recovery of the signal is no longer dependent on a time locked transient response. Thus many averages can be achieved in a short period of time. This method has been employed successfully in a number of electrophysiological studies as an alternative to simple (Dawson 1954) averaging (Fricker & Sanders 1974, Larkin et al 1979, Srebro et al 1980).

Also discussed in this chapter was the VERIS system's method of exploiting the features of PRBS in combination with special transforms. Although this technique provides a means of obtaining local ERG responses, some caution should be placed on the integrity of their derivation as higher-order cross-contamination of local responses can occur.

The following chapter provides an introduction to the VERIS system, its components and software features.

Chapter 3

VERIS SCIENTIFIC™

The Visual Evoked Response Imaging System (VERIS) is a new system that exploits PRBS (see previous chapter) in the recovery of local electrophysiological responses. The evaluation of this system in the context of routine electrophysiology forms the main aim of this thesis.

3.1. INTRODUCTION

This chapter presents a description of the instrumentation, recording techniques and protocols used to assess the VERIS system and its value in the routine clinical environment.

3.2. SYSTEM SPECIFICATIONS

The VERIS™ system is now commercially available from Electro-Diagnostic Imaging (EDI) Inc. and from the Tomey Corporation. The version under investigation was VERIS™ II Scientific. Additional components were required to fulfil a full electrophysiological system. For the recovery of responses, amplifiers were designed and added to the system. In addition, custom software was

developed to aid in the analysis and patient archiving of data. These additional components and the VERIS system are detailed in the following sections.

3.2.1. SYSTEM OVERVIEW

The system hardware is based on a standard Apple Macintosh 7100/66 computer with PowerPC processor. The computer contains 16MB of Random Access Memory (RAM) and has installed a digital signal processing card and an Electro-Diagnostic Imaging (EDI) Inc. dual VGA Card. Stimuli are presented on a 20" Microscan Monitor. A custom built four channel physiological amplifier is used to amplify and filter signals before they are digitised in the National Instruments NB-MIO-16 high performance multifunction analogue, digital and timing input/output board.

3.2.2. PHYSIOLOGICAL AMPLIFIER

The local potentials generated by the multifocal ERG stimulus are in general a thousandth the amplitude of conventional electrophysiological signals (of the order of a few hundred nanovolts). As with the conventional ERG, these signals therefore require substantial amplification to achieve an amplitude sufficiently large to be measured by the analogue to digital converter (ADC) which forms the initial processing stage of most electrophysiological equipment. However, the simple process of amplification is not sufficient to recover the true physiological signal as these potentials, as with all evoked potentials, are combinations of the true desired signal and extraneous unrelated potentials from a number of physiological and environmental sources. Thus an electrophysiological amplifier has to fulfil two main requirements. Firstly, to amplify the recorded signal to the desired operating range for analog to digital conversion and secondly, to filter extraneous artefactual noise to improve the signal to noise ratio (SNR).

PREAMPLIFIER

Part of the additional noise or random signal contained in the measured potential can be attributed to electrical interference picked up by connections and cables. The influence of such contributions can be minimised to some extent by pre-amplification.

A preamplifier was used to provide an initial amplification ($\times 100$). This preamplification has the advantage of reducing the amount of extraneous noise external to the unit. One major concern with any electrophysiological system, supplied by mains voltages, attached to patients is their safety. The preamplifier built for our equipment was electrically isolated using an opto-isolator chip to prevent any possible electrical feedback to patients. This has the additional advantage of an improvement in signal to noise ratio by interrupting ground loops and eliminating capacitance problems. The amplifiers were designed and built by the Department of Clinical Physics & Bioengineering's electronics workshop. A list of specifications for the amplifier is given below.

Common mode rejection ratio	125dB (pre-amp + amp) 170db (main amplifier)
(CMRR) balanced	
CMRR unbalanced	85dB (pre-amp + amp) 160dB (main amplifier)
Noise	1 μ V peak to peak (0.1Hz – 100Hz)
Bandwidth	DC – 700Hz (IA296@ 1KHz + signal 1KHz filter)
DC restoration	± 500 mV
Calibration pulse	15.25 μ V

3.2.3 ANALOGUE TO DIGITAL CONVERSION CARD

Analogue signal responses recorded by the amplifier are digitised using a sixteen channel NB-MIO-16 multifunction analogue, digital and timing input/output board (National Instruments). The NB-MIO-16 contains a 12-bit analogue to digital converter (ADC) and software programmable gain settings for analogue

input signals. The NB-MIO-16 is capable of data acquisition rates of up to 100kbytes/sec.

It is important when digitising analog signals that sampling rates are sufficient to prevent aliasing of frequency components in the input signal. To achieve this a sampling rate of at least double the greatest frequency component expected from the input signal is required. A sampling frequency of 675Hz was employed which is over twice the low pass filtering of 300 Hz. The maximum operating range for the NB-MIO-16 was ± 5.0 V.

3.2.4 EDI INC. DUAL VGA CARD

The Video Graphic Board was incorporated within the VERIS system to facilitate dual monitor control. Little information is available on the specifications of the Graphics board other than it uses a proprietary technique to control the stimulus display unit, facilitating palette animation for stimulus generation while permitting simultaneous control of a second monitor for the operator.

3.2.5 STIMULUS MONITOR

It is important that any stimulus system has a wide range of adjustable luminance levels and luminance uniformity. The stimulus monitored used during investigations was an Apple Macintosh 20" Multiscan Monitor. It had a maximum luminance of 116 cd/m² at a screen resolution and vertical refresh rate of 1024 × 768 and 75 Hz respectively.

LUMINANCE, INTENSITY, CONTRAST

Most visual stimulus generators suffer from both spatial and temporal luminance changes and the common VDU based system is no exception. The spatial characteristics of a Cathode Ray Tube (CRT) based display vary markedly across the screen. Variance can be as high as 30% measured from the central area of the

display to the periphery (Barber 1981; Bradnam 1994). Also the raster nature of a CRT based display produces obvious temporal luminance changes created by the analogue character of the stimulus. The influence of spatial and temporal variation in the VERIS stimulus required a quantitative analysis (see chapter 4).

3.2.6 SOFTWARE

The VERIS system comes with hardware specific software that is to some extent user configurable. The software allows the user to set a selection of stimulus patterns and to save the unprocessed data signal received from the ADC card to be archived for analysis. After data acquisition, the raw data signal can be processed to extract linear and non-linear components. These data signals can then be viewed using 3D topographical maps and exported in simple ASCII format. Further processing can be achieved by averaging signals or by extracting data from specific areas.

The software supplied with the VERIS system controls both the stimulus generation and data acquisition from the ADC card. The proprietary software can be broken down into three main sections.

RECORDING A DATA FILE

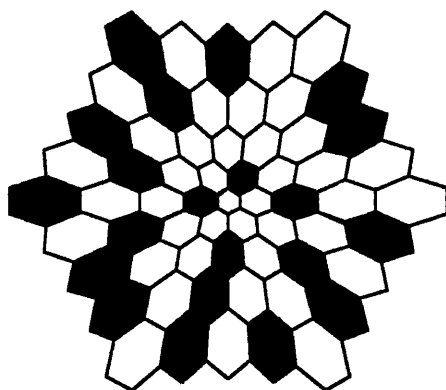


Figure 3.1 *Stimulus paradigm (61 element geometrical array).*

In recording a data set the user has a number of options. Stimulus resolution can be selected to be a geometrical array of 61, 103 or 241 elements. The selection of these will depend on the resolution and quality of signal required. Although a 241 element geometry within a 25 degree visual field gives high resolution functional topography, 61 areas will give a better signal to noise ratio due to the larger number of photoreceptors stimulated in a given area (see figure 3.1).

After selecting a stimulus, the user can then choose a “tap word” or length of m-sequence (see previous chapter). This will determine the duration of the recording period. The net recording time is primarily determined by the m-sequence length. Once a sequence length has been chosen an overlap test is required to avoid the possibility of kernel slices taking place in the same visual system memory. This would make separation numerically impossible. This overlap test is important because failure to select an appropriate m-sequence leads to cross-contamination of first order kernels from higher order kernels evoked from separate areas. The amplitude of signals from higher order kernels are small in comparison to first order kernels. The contamination of higher order kernels from lower order kernels would make them inappropriate as a means of quantifying non-linearities of the visual system. As yet it is unclear how the VERIS system achieves this identification of ‘good’ m-sequences and so the separation of cross-contamination.

All the areas in the stimulus array are modulated in time according to the same binary m-sequence cycle but a different starting point in the cycle is chosen for each area. The starting points are distributed periodically over the cycle. Once a tap word is selected the total recording period T is calculated as ...

$$T = \frac{(2^n - 1)}{f} \quad (3.1)$$

where n , is the length of the sequence and f is the frame rate of the stimulus.

Given the patient co-operation required for accurate test signals the duration of the recording period requires splicing or segmentation. The user can select the number of segments comprising each recording period. Thus if a patient can only comfortably fixate for a period of 30 seconds then 29 segments would be required for a tap word value of 16 and a 14 minute 30 second recording period. The segments are recorded slightly overlapping and are spliced in a way that forces a smooth transition. A linear splice is performed on the region of overlap beginning with 100% of the old segment, 0% of the new and increasing the percentage of the new until there is 100% of the new and 0% of the old. If low frequency noise is present, this technique avoids generating a step at the splice.

The system incorporates an artefact rejection technique which scans an individual segment for saturation. If saturation has occurred then the segment is discarded and two adjacent segments are combined and substituted for the saturated segment. This technique eliminates large potentials from the response that could distort the processed signal. However careful monitoring should be maintained during the recording period in order to identify periods of saturation. This method of artefact rejection has the disadvantage of shortening the m-sequence. This is because segments of the sequence are effectively eliminated and non-saturated segments are simply averaged. Thus the sequence increases its proportion of incorrectness and in addition does not truly represent a white noise sequence. Saturation of the signal can be used as an indicator of poor patient compliance or fixation and is discussed in chapter 4.

Any technique that samples multiple responses to a stimulus controlled by a raster action, as in the cathode ray tube used in standard computer visual display units (VDU), requires correction for scan delay. This is because multiple samples per frame will record responses dependent on the position of the cathode ray beam. No information is available on how the VERIS system accommodates scan delay during sampling but generally this would be achieved simply by synchronising each sample to a specific predefined raster line.

Once the patient is relaxed and all preparations are complete the patient is asked to fixate on a central cross. This is configurable in size and position and can be used to maintain fixation. The raw data signal is recorded over a 14 minute 20 second period (20 segments of 43 second duration) and so requires over 1MB of memory. One advantage of the program is that during the recording period the operator can pre-select a specific area of interest and watch this processed signal in real time. This is a useful visual indicator of signal quality in real time and also allows the examiner retrospective extraction of poor responses and re-examination. An additional tool to reduce noise contamination is the automatic artefact rejection algorithm discussed previously.

PROCESSING A DATA FILE

Processing of the data file is achieved by the method of cross correlation described previously. This method offers the advantages of limited processing requirements and fast extraction (Sutter 1991, Henderson 1970).

The extraction of local response contributions after the cross-correlation technique discussed produces a first order response component for all inputs distributed periodically along the cross-correlation cycle. These are found at intervals equal to the channel lag of $1/k$ th of the cycle length, where k is the number of areas stimulated. It is assumed that given the absence of significant nonlinearities, these first order kernels closely approximate the local impulse response.

ANALYSING A DATA FILE

There is some degree of flexibility with regards to analysis of signal responses. Each local ERG signal (or first order kernel) is displayed in an hexagonal array similar in topography to the stimulus array (see figure 3.2)

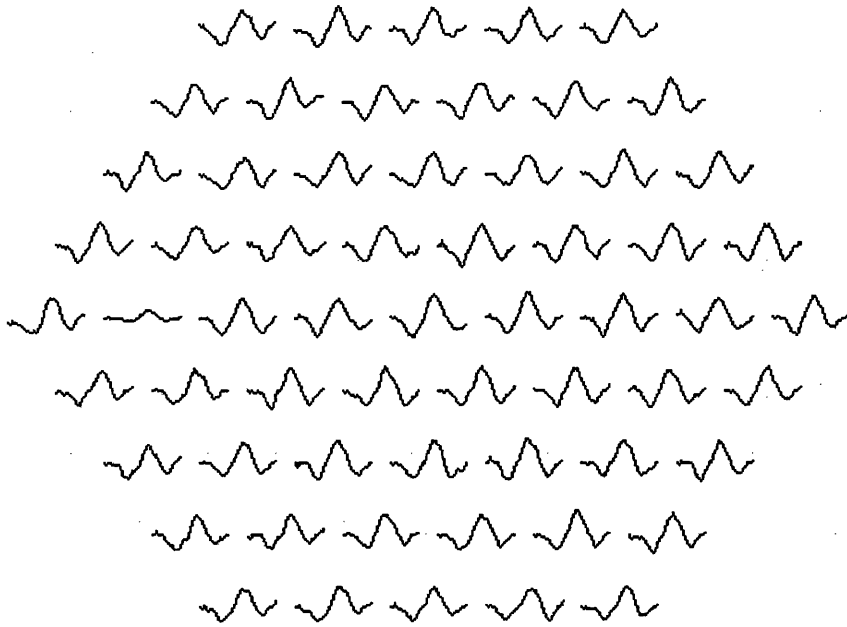


Figure 3.2 *Spatial paradigm of local ERG responses*

The software allows individual elements of these “trace arrays” to be grouped in any order and averaged with neighbouring elements.

There is a large volume of data produced from each recording session and a simple method is required to visualise signal responses on a topographical basis. To achieve this each waveform produced from local stimulation is reduced to a unique number which serves as a measure of either its response amplitude or latency.

Amplitude measures are usually taken from peak to peak values for the a- and b-waves (see chapter 1 section 1.4.2). Implicit time is usually measured from the time of stimulus onset to the peak of the b-wave amplitude. Peak-to-peak measurements are generally poor amplitude estimates since they are highly susceptible to noise contamination.

The conventional method for assessing the amplitude of a waveform $r = s \pm n$, where s is the true signal and n the noise in a time interval (a,b) , is the Root Mean Square (RMS) measure.

$$A = \sqrt{r \bullet r} = \frac{(s^2 - 2 \cdot sn + n^2)}{\sqrt{r \bullet r}} \quad (3.2)$$

However, this estimate suffers from a positive noise contribution ($+n^2$). A variation on this method employed by the VERIS system is the Scalar Product of a template t and the waveform to be measured.

$$A_s = \sqrt{t \bullet r} \quad (3.3)$$

The template consists of the normalised average of waveform to be measured (i.e. acts as a good approximation of signal without noise). Thus equation 3.3 becomes:

$$A_s = \sqrt{t \bullet r} = \sqrt{(s+n)s} = \sqrt{s^2 + sn} \quad (3.4)$$

Alternatively, if data from an adequate number of controls is available then a more accurate template can be used. This new template is no longer dependent on the waveform to be analysed. This new template is a direct measure of the Median normalised values from the control data and consists of 61 separate waveform templates.

There is no quantitative information available on how the accuracy of the method of measurement employed is affected by noise contamination. Given the low signal to noise ratio inherent in this system of measurement when compared to conventional electrophysiology a series of investigations was undertaken to assess a variety of measurement techniques and their dependence on signal quality.

Simulation software was written to enable the addition of a known amplitude of random noise to be added to a typical median waveform. The noise was variable from 0% to 100% of the signal amplitude. The standard template waveform from the control data study (see chapter 5) was used to form a scalar product with the noisy waveform. Amplitudes, implicit times and scalar products were calculated

for a range of added noise levels. The 95% confidence intervals were calculated in the normative study and these limits used to calculate the noise required to render a normal median waveform abnormal in terms of the confidence interval.

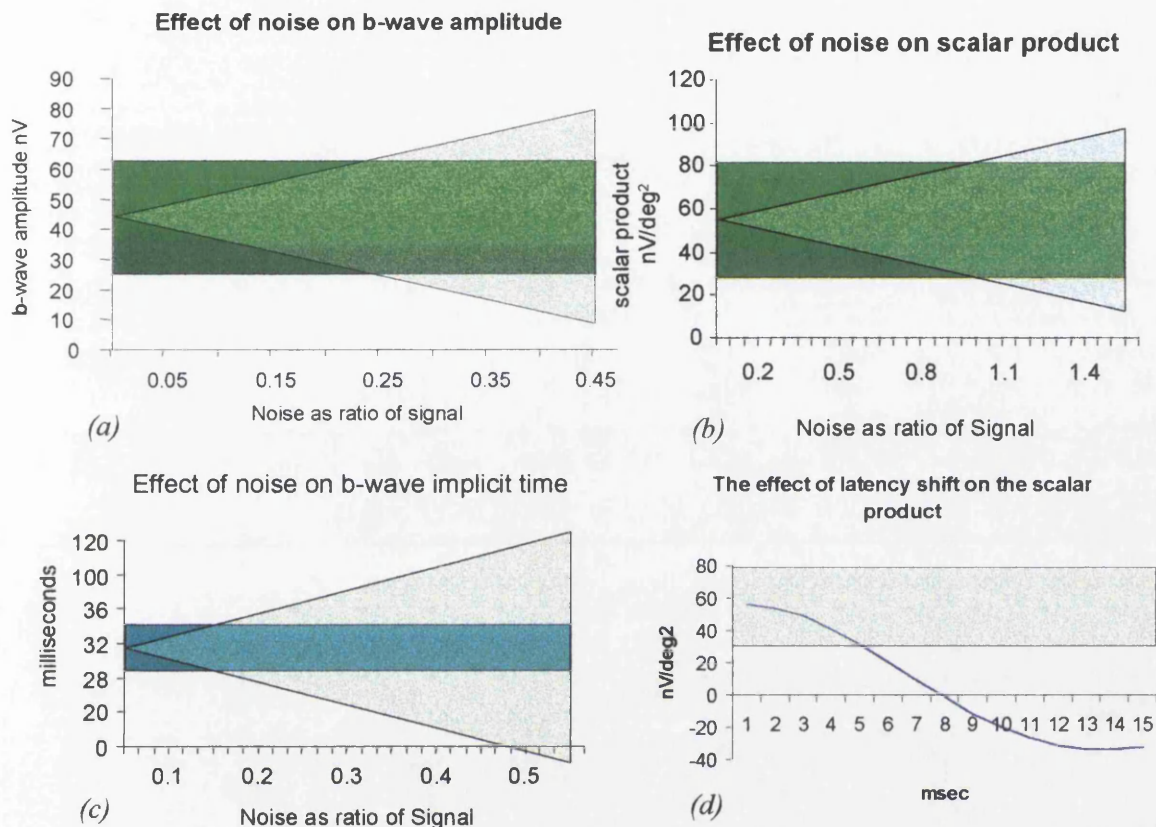


Figure 3.3 Effects of noise on b-wave (a) amplitude (b) scalar product and (c) implicit time measures. The effect of a latency shift on scalar product measure is indicated in (d). Horizontal bars indicate change required to be considered significant.

	Scalar product	Amplitude	Implicit time
Noise (%)	100	25	15

Table 3.1 Amount of noise required to induce a significant change in measure.

The results are illustrated in figure 3.3 and show that the addition of 100% noise is required to induce a significant change in scalar product (table 3.1). Only 25%

noise is required for a significant change in amplitude measurements and only 15% noise required for implicit time measures.

A further experiment was conducted to investigate the effect of implicit time changes on the scalar product measure. This was achieved by artificially introducing a latency shift in the recorded waveform and calculating the scalar product from the shifted waveform and the original median template waveform. The 95% confidence interval for implicit time measures indicate that a median waveform would require a 3 ms shift to be significant (see figure 3.3c). However the scalar product measure would require a latency shift of more than 5 ms for a significant effect to be detected.

The relatively high noise immunity of the scalar product estimate is related to its sensitivity to changes in wave shape. Theoretically, the scalar product measure is a robust measure of ERG waveform shape at low signal to noise ratios. However, care must be taken when more subtle changes such as latency shifts are present. The scalar product can detect a change in implicit time but is less sensitive than the implicit time measure itself. This decrease in sensitivity is more important at high signal to noise ratios.

The local response estimated by means of the above technique is generated by stimulus elements of different sizes. They have no direct physiological meaning unless they are converted to response densities by normalising to a unit retinal area. This is achieved simply by dividing each scalar product value by the area subtended by the stimulus element that generated it.

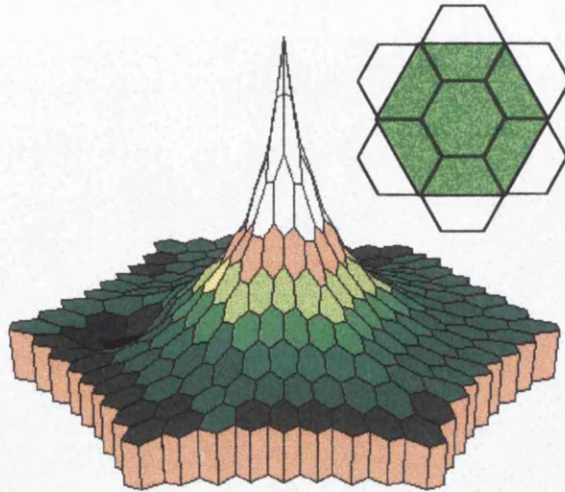


Figure 3.4 *Scalar product plot together with illustration of interpolation paradigm.*

These resulting values can be displayed in a 3-dimensional response density plot (see figure 3.4). An interpolation procedure is employed to derive a pattern of finer resolution. This is achieved by subdividing stimulus elements. These new elements are assigned the mean value of the two hexagons they straddled.

To improve signal to noise ratios, each signal can be averaged with its neighbours.

Although the VERIS system provides some basic analysis features, described previously, these features were found to be limited and inflexible. To provide an improved flexibility in the analysis, interpretation and archiving of data a software package was developed specifically to address these limitations.

CUSTOM ENHANCEMENTS

The computer program developed consisted of several inter-related components (or units). These were specifically written for Microsoft's™ 32-bit operating system *Windows 95* and consisted of just under 9,000 lines of code (see Appendix I). The reason for writing specifically for this platform was the familiarity potential operators had with the interface and the processing superiority of a 32-bit

platform, this was important for analysing the potentially large volumes of data produced by the VERIS system.

The main goal for this custom software was to provide a simple mouse driven interface to enable the operator to visually analyse common features of the waveforms produced (i.e. implicit time, amplitude and scalar product measures). The interface produced could be used to compare features of the waveforms either topographically or individually against multiple recordings. Specifically, as no information is available on the topography of waveform components, this was to provide information on retinal cell latency and deviation from normative values as this information would be required for the subsequent analysis of selected retinal disorders (see chapter 6). In addition results from the analysis of a control population (see chapter 5) were incorporated within the software to provide an automated estimate of the measured response deviation from normative values.

Although the scalar product method is a highly efficient method of waveform shape analysis the response template used by the VERIS system cannot exploit the full potential of this method of analysis. Theoretically, to reduce noise contamination each response element is required to be analysed against an ideal template (see previous discussion). The VERIS system does not have access to an ideal template and so a compromise is made. The VERIS system simply adds the signals from all areas together and normalises the response. This response is then used as the ideal template.

However there are some major difficulties surrounding this method of analysis. It assumes that, topographically, all areas under investigation give the same electrophysiological response and thus the sum of all these areas will give an estimate, free from contamination, of the ideal template. This is incorrect given the topographical information on the variation of photoreceptor densities and distribution available (Curcio 1991, Osteberg 1935). Additionally this method is open to contamination by the commonality of an artefact. That is any abnormality or artefact common in all local responses will be present in the ideal template

derived from these local responses. Thus a scalar product derived from this ideal template and a local response will ignore this common contamination and misjudgement will arise. One example of this is a reduction in the b-wave amplitude associated with toxic amblyopia or ischaemia (this is conventionally termed 'negativity'). Negativity present in the response template will not be shown in the response density plot because it is common to all responses (see figure 3.5).

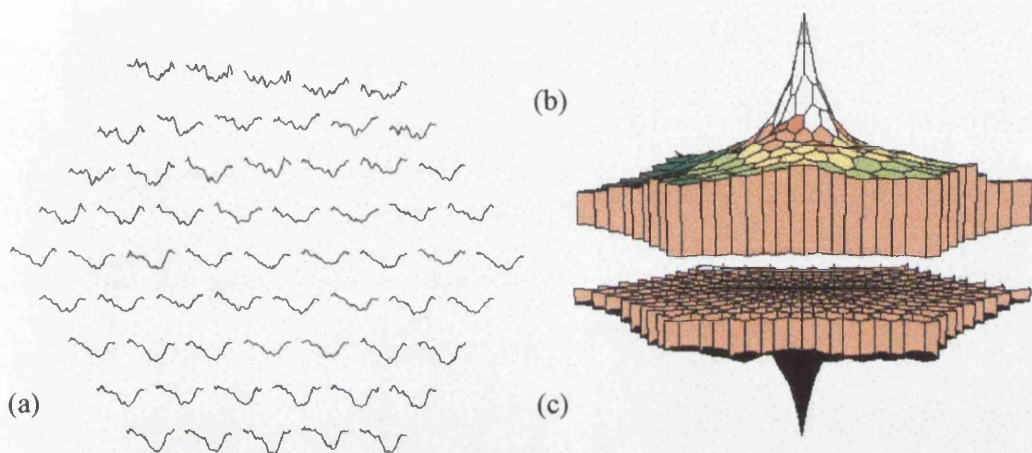


Figure 3.5 Trace array (a) illustrating 'negativity'. Standard scalar product response (b) derived from mass response. (c) true scalar product response derived from ideal template. Note the negative nature of the response is only reflected in the scalar product derived from an ideal template produced by the custom software.

It was decided that to exploit the obvious theoretical advantages of the scalar product method an ideal template should be created and incorporated within the analysis software. Chapter 5 CLINICAL STUDIES describes the investigation of seventy normal healthy volunteers who were tested to obtain a good approximation of an ideal template related to age.

Their waveforms were averaged and normalised in groups within the same decade. These values were then incorporated within a response amplitude algorithm that reduced each waveform through the ideal scalar product method to

a single value. These values were then used to establish limits of normality. The visual analysis of data included the response density plots of waveform features which would provide a statistical indication of deviation from the control population. Each area was colour coded to indicate whether that area fell within 95% confidence intervals, i.e. every area that fell outside the 95% confidence interval was colour coded blue, any area falling outside the 99% confidence interval was colour coded black and any normal area was colour coded green (see figure 3.6).

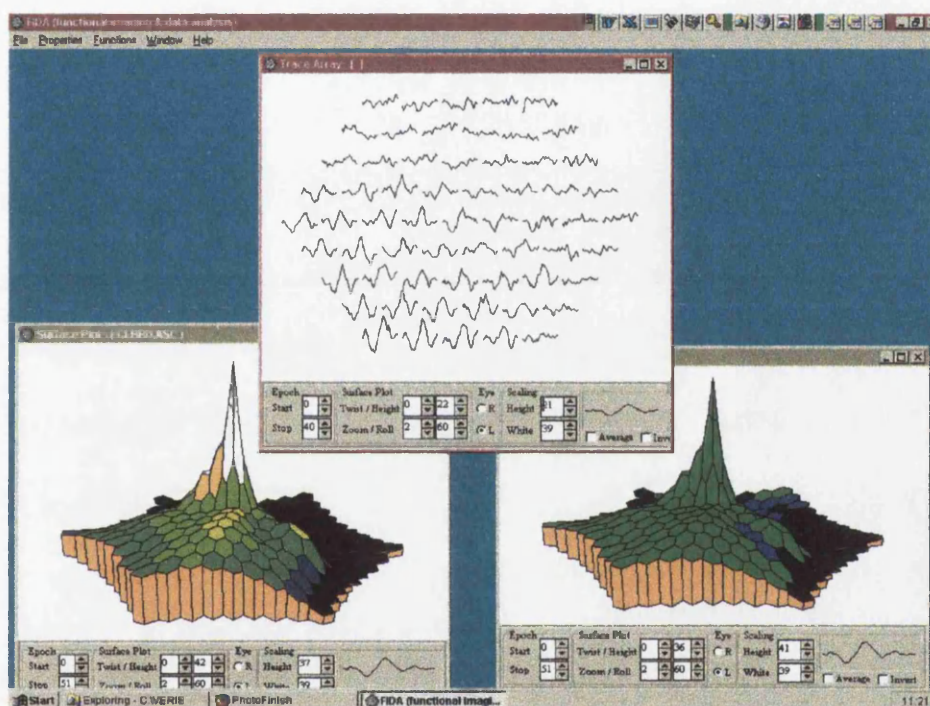


Figure 3.6 Screen shot from visual analysis program (FIDA - Functional Imaging & Data Analysis) illustrating incorporation of confidence plot – lower right.

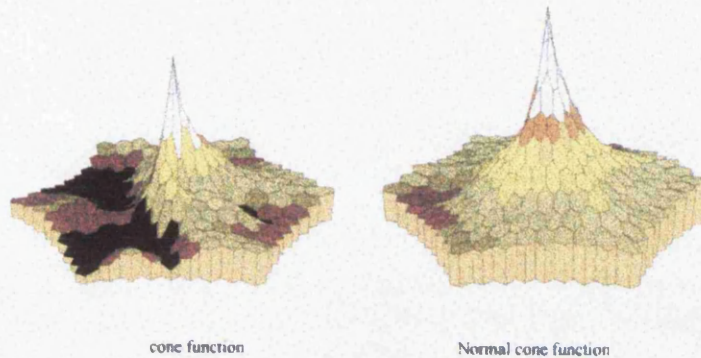
In addition to an ability for comparative analysis (i.e. subtract and isolated multiple features of one data set against another) a database was included to optimise search and archiving features and a facility for hard copy of results within the software for easy retrieval and dissemination of investigations. The report included hospital number, date of birth, reason for test etc. and an interpretation of results (see figure 3.7)

Tennent Institute
Department of Ophthalmology
University of Glasgow
Multifocal Electroretinogram

Name:
Hospital Number:
Eye: Left

Date of Birth:
Reason for Test: AZOOR?

Date of Test:



Interpretation:

Figure 3.7 Example of 'hard copy' of results provided for clinicians. Note these results were produced with an extensive annotation on their interpretation.

3.2.7 PATIENT PREPARATION

It is important when any patient is faced with a new and to them unknown test that they are assured and comforted. In recording data there is a requirement to establish a strict protocol (see following chapter). This was not only to relax the patient but additionally to minimise variation of results between patients due to poor compliance and operator variation. The equipment and techniques used including the test protocols are detailed in the following sections.

ELECTRODES

A differential amplifier, as previously described, is preferred when recording physiological signals as common mode rejection can be employed to increase signal to noise ratio. In order that this can be achieved, three electrodes are

required: a reference electrode, an active electrode and one ground (or indifferent) electrode. The active electrode used has to provide a stable signal and yet be comfortable for the patient (see chapter 4 section 4.2). The ground and reference electrode were made from the same material and consisted of disposable adhesive pads with a conductive jelly. The ground electrode should be placed on the forehead of the subject and reference electrodes placed on both outer canthi. Throughout the test the patient should be reassured and encouraged to relax. This improves signal quality by the reduction of extraneous potentials generated by muscle tension.

PUPIL SIZE

A period of patient adaptation is required to eliminate any change in pupil diameter that could influence signal amplitude. There is little doubt that pupil diameter could have a dramatic effect on signal size, although this variation is limited somewhat by the Stiles-Crawford effect (Stiles and Crawford demonstrated in 1933 that rays of light which enter the centre of the pupil are more effective as stimuli than those which enter near the edges. This is believed to arise from the directional sensitivity of the retinal mosaic). It was necessary therefore to estimate the effect of pupil diameter not only on the amplitude of response but additionally on its morphological features (see chapter 4).

REFRACTIVE ERROR

Refractive error is important not only to the signal quality but also the confidence with which an operator can determine the location of an abnormality. If the stimulus is not focused accurately on the retina, due to the arrangement of the optics, then the physiological responses to this stimulus will reflect this. Gross defocus would result in misalignment of stimulus areas to derived signals and produce erroneous results.

Although refractive error is important for the reasons stated some quantitative estimate of the variation of refractive error on signal integrity is required.

3.2.8 TEST PROTOCOL

In any determination of optimum preparation and procedure for the investigation of physiological measurements patient comfort and compliance are the main requirements. If patients are uncomfortable or unwilling to participate then results can be heavily contaminated. Problems with electrophysiology and its limited use within the field of ophthalmology can in some part be attributed to the inconvenience and preparation times experienced by patients. It was paramount in this study to maximise the efficiency of the protocol to reduce patient discomfort and balance this with reliable signal recovery.

STIMULUS

The electrophysiological response generated by the photoreceptors depends upon the intensity of retinal illumination. Thus the stimulus presented on a 20" multiscan monitor was set at its highest intensity. This was measured at 116 cd/m². In addition, to maximise signal strength but retain as much local information as possible, a 61 element hexagonal array stimulus was used (see figure 3.1). The geometry of the stimulus pattern was scaled with eccentricity to broadly reflect cone photoreceptor densities within the eye. This roughly equalises signal to noise ratios from individual areas.

TEST DURATION

As discussed previously the test duration is dependent on the length of m-sequence chosen. A 16 bit m-sequence ($2^{16}-1 = 65534$) would require a test duration of approximately 14 minutes. A 15 bit m-sequence (32767) would require approximately a 7 minute recording period. Obviously while an increase in m-sequence length will increase signal to noise ratios (by effectively doubling

the number of averages) and so improve signal quality, fatigue will arise from the prolonged recording time and will reduce the benefits of the improved signal to noise ratio.

3.3. CONCLUSIONS

An introduction to the new system under evaluation, the VERIS system, was given. This summarised the system's components, software features and method and mode of data analysis. Also discussed was the unique nature of the system to stimulate multiple locations of the retina simultaneously using the process of shifted m-sequences. Although the system has many advantages over conventional ERG recovery techniques it was found that the analysis features of the software were limited. Some additional software was developed that would improve and quantify the derived signals and address the archiving limitations of the software. The initial proposals for investigation and optimisations of the system for evaluation within the routine clinical environment were given. These proposals will be addressed in the following chapters.

The next chapter presents the results of an investigation into the factors that influence the multifocal ERG technique and particularly the VERIS system. These factors once quantified are used to optimise the recording of local signals.

Chapter 4

FACTORS INFLUENCING THE MULTIFOCAL ERG

4.1. INTRODUCTION

All electrophysiological recordings have associated artefacts. One of the main objectives in clinical electrophysiology is to minimise the influence of these artefacts on the real signal. Artefacts in evoked electrophysiological testing are defined as any electrical signal generated that does not represent the subject's response to the stimulus. The recording equipment, the environment or the subject may be sources of extraneous electrical signals. Artefacts can distort or obscure evoked responses to a degree that renders the recording of little diagnostic value.

This chapter examines a range of factors that can influence the results of the Multifocal ERG. A protocol is then established to minimise the influence of these factors and thus optimise the recording process.

4.2. ELECTRODES

Electrodes are possibly the most important single factor to influence the recording quality of the clinical ERG. The recording quality of any evoked response is determined primarily by the quality of the contact between the subject and the electrode, termed the electrode impedance.

However, recording quality should not be the only criterion that determines electrode choice. Other factors require consideration. These include:

1. Patient comfort, risk of injury (given the prolonged recording times).
2. Reliability and consistency in signal recovery
3. Optical quality.

There are many types of electrodes commercially available for visual electrophysiology. These electrodes fall into two main groups, the corneal contact lens electrodes (Burian Allen and JET) and the scleral lid electrodes (C-Glide, Gold Foil, DTL and more recently the Hawlina-Konec (HK) Loop (Hawlina & Konec 1992)) see figure 4.1. A brief summary of some commonly used electrodes and their construction is given below.



Figure 4.1 *Common commercial electrodes. From left to right Medicotest's Neuroline Neurology electrode (used for ground and references purposes), H-K loop, Carbon fibre, DTL fibre, Gold foil, JET and Burian Allen corneal electrodes.*

BURIAN ALLEN

The International Society for Clinical Electrophysiology of Vision recommends the Burian Allen electrode for flash ERG's in adults. The standard states that electrodes should make contact with the cornea, have a large optical opening and hold the lids apart (Marmor et al 1989). Most of the small numbers of investigators, now using the VERIS system, also use this contact lens electrode for MFERG recording (Hood et al 1997a, Hood et al 1997b, Bearnse & Sutter 1996c, Kondo et al 1995). This is most probably due to its reputation as an electrode that gives a larger amplitude signal, maintains a stable baseline recording and consequently produces a high quality signal.

The Burian Allen in its bipolar form consists of an active corneal contact lens and a reference speculum portion coated with a conducting material. Thus no reference electrode is required. Although the electrode is reported as having the largest signal amplitude (Hennessy & Vaegan 1995) it has some major limitations. When using the bipolar version there is a greater variability in ERG amplitude. This is mainly due to shorting between the lids and cornea as a result of tears in the wetting solution bridging the contacts. In addition the electrode can be uncomfortable (see later in this section) if worn for any period of time.

GOLD FOIL

Foil electrodes were initially described with silver coatings and then a polyethylene film (Mylar) strip coated on one side with aluminium and bent into a j shape (Chase et al 1976). Unfortunately, at low levels of alternating current the aluminium coating was less than adequate. The Mylar surface frequently became detached from the aluminium coating (Arden et al 1979, Borda et al 1978). A gold coated Mylar electrode was first described in which the gold surface did not unplate and in which 'sizeable' ERG's were obtained (Arden et al 1979). A number of reports have confirmed initial findings that waveforms and amplitudes of the ERG's obtained with Arden Gold Foil electrodes were smaller than with

Burian Allen electrodes, but with a similar morphological frequency response (Arden et al 1979, Hennessy & Vaegan 1995). The signal was estimated as approximately 80% of the Burian Allen amplitude (Hennessy & Vaegan 1995). The Gold foil does not secure the lids and is therefore more prone to blink artefacts. Breaks in the fragile foil can occur, which decrease the signal and increase the noise produced. While the Gold Foil electrode is associated with a lower risk of corneal injury than the rigid corneal contact electrodes, short lived corneal changes have been demonstrated with particular risk associated with the age of the patient and the application of topical anaesthetic prior to use (McAllan et al 1989).

DTL

The Dawson Trick & Litzkow (DTL) fibre electrode (Dawson Trick & Litzkow 1979) is commonly used when long recording periods are required. This is due to the lower risk of corneal injury associated with this style of electrode. It is constructed by impregnating nylon fibres (approximately 12 microns in diameter) with metallic silver. Manufacturers recommendations suggest at least three to six fibres be connected to an insulated electrical wire. The largest signals can be obtained when the electrode fibres are positioned in the tear film on the surface of the cornea. However, in this position, responses obtained are highly contaminated by signal disturbances which can arise from blinks, movements of the eye or the displacement of the fibre contact. Alternatively, and this is generally the case, the fibre is located in the lower conjunctival fornix. This site is much more stable than a position on the surface of the cornea, but the site has the disadvantage that much smaller amplitude signals are recovered.

In such a position the DTL does not interfere with the optics of vision and hence is useful where optical clarity is important, as in the Pattern Electroretinogram and MFERG.

C-GLIDE CARBON FIBRE

The C-glide (Barber & Tolia 1985, Papakostopoulos & Barber et al 1993) is a carbon fibre laminated between polypropylene / polythene film. A micro-thin saline pad is used for contact with sclera, and the carbon fibre connects this to a miniature socket. This material is of a more rigid construction than Gold Foil electrodes. Thus the reduction in signal to noise ratios due to the fragility of the Gold Foil and DTL electrodes is diminished. The advantage that carbon offers to conventional electrophysiology is the absence of a photovoltaic artefact produced by the liberation of photoelectrons from the noble metal by the interaction of the stimulus light. In addition, the electrode is disposable and thus the risk of cross infection is minimised.

H-K LOOP

The Hawlina-Konec (HK) loop is a new noncorneal electrode that has recently been developed (Hawlina & Konec 1992). The electrode is formed from a thin stranded or monofilament noble metal (silver, gold or platinum) wire, looped and soldered at the ends. The wire is insulated by a thin Teflon coating except the central region, where three windows 3mm in length are formed on one side, this is the site that contacts the sclera. The loop created is elastically deformable and self supporting in any position to which it is shaped. This has the advantage that the electrode does not move during the recording procedure. Previous studies have found that this can have a dramatic effect on the amplitude of the ERG signal (McAllan et al 1989). The effects of fragility, instability and delicacy upon recording quality with Gold Foil and DTL non-corneal electrodes are reduced.

Medicotests Neuroline Neurology EEG electrodes were chosen for reference and indifferent connections because they are disposable, gave a lower impedance than current standard Ag/AgCl electrodes and produce a stable signal.

Initial investigations on control subjects were performed with the Burian Allen electrode for its reported higher signal to noise ratio. However this was quickly abandoned after subjects complained of severe discomfort both during testing and after the removal of the contact lens. After investigation all subjects were found to have sustained mild corneal abrasions. Although these initial difficulties were probably in part the results of inexperience in the handling of this style of electrode the risk of corneal abrasion, however small, excluded the Burian Allen's further use within the trial.

Although there are a growing number of reports in the literature on the comparison of scleral noncorneal electrodes these reports only apply to full field ERG and PERG recordings. To find a suitable electrode for Multifocal ERG recording it was necessary to investigate the performance of a selection of noncorneal electrodes currently in use.

A study was undertaken to determine the comparative responses recorded from the four main electrode configurations: the Gold Foil Electrode, the C-Glide carbon fibre electrode, the DTL fibre electrode and the HK-loop electrode.

PROTOCOL

Three subjects had reference and indifferent electrodes (Neuroline Neurology Electrodes) positioned on the outer canthus and the central forehead respectively. Preparation of the site prior to the placement of the electrode included the application of a mild abrasive (Omniprep) followed by site cleansing using an alcohol swab.

Scleral electrodes were inserted after the application of a mild anaesthetic (0.5% Benoxinate). Responses were obtained both after the pupils were maximally dilated with a mydriatic (1% tropicamide) and on a separate occasion with natural pupils. This was to assess the effect of pupil dilation on the recordings for these commercially available electrodes.

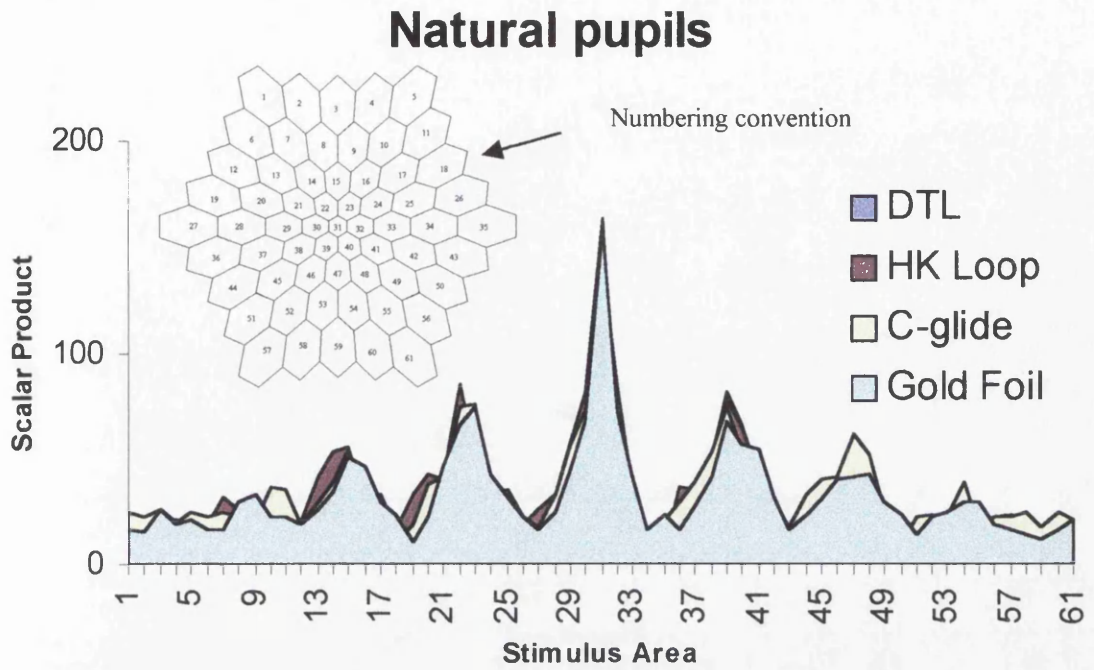
DTL electrodes were placed in the lower conjunctival fornix. The loose end of the fibre was attached to the skin of the medial canthus and the opposite end held in a conducting clasp anchored to the skin of the outer canthus.

The lowest resolution stimulus (61 scaled hexagonal areas) and the maximum m-sequence length ($m = 16$) were chosen to maximise the quality of the recorded response. The stimulus was displayed on an Apple Macintosh™ Multiscan monitor. The high luminance was set at the monitor maximum (I_{max}) of 116 cd/m² (measured using a Minolta LS-100 Photometer) and the low luminance at the monitor minimum (I_{min}) of 6.8 cd/m². These give stimuli contrast, or mean screen luminance of

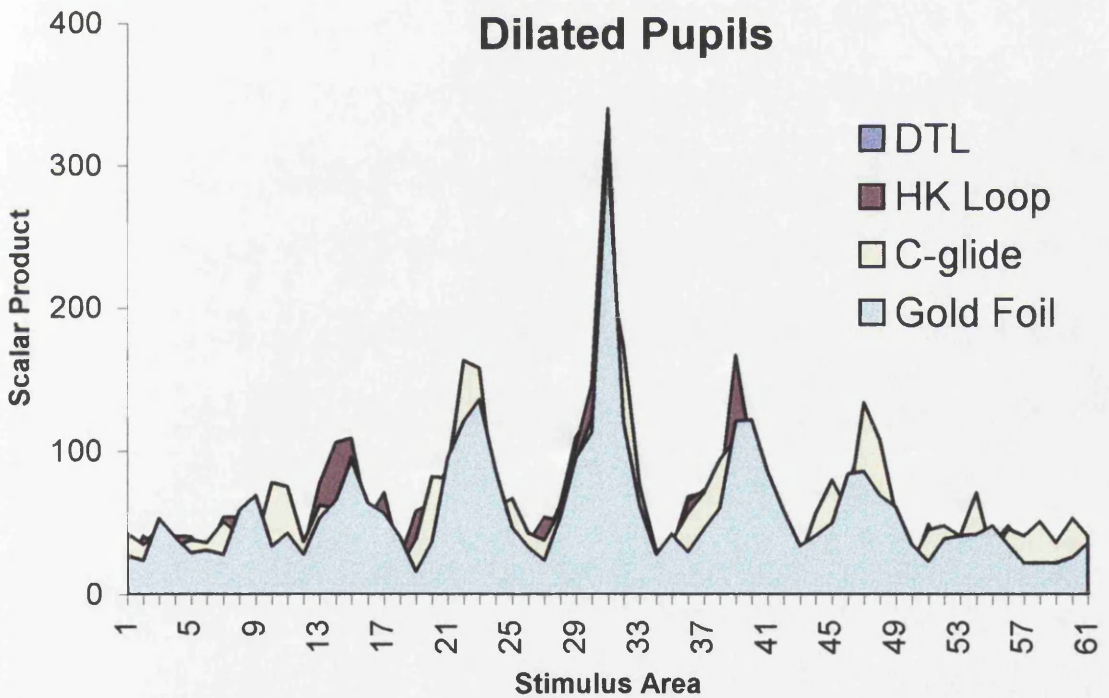
$$contrast = \frac{I_{max} - I_{min}}{I_{max} + I_{min}} = 89\% \quad (4.1)$$

With a stimulus frame rate maintained at 75 Hz and an m-sequence length of $2^{16} - 1 = 65535$ a recording period of 14 minutes 20 seconds duration was produced. The viewing distance for each subject was 32 cm producing a stimulus field of approximately 30 degrees. The signal amplification was set to 160,000 which consisted of a front end D.C. pre-amplifier stage of 100, main amplifier gain of 200 in the physiological amplifier stage followed by a further gain of 8 on the National Instruments' data acquisition card. The custom built amplifiers were discussed more fully in the previous chapter.

The mean scalar product values for each area stimulated were calculated for each configuration of the protocol. Results are plotted for each area stimulated in figure 4.2 (a) and figure 4.2 (b).



(a)



(b)

Figure 4.2 *Scalar product amplitude ($nV/degree^2$) for each electrode with natural (a) and dilated (b) pupils together with numbering convention.*

To determine if there was any statistically significant variation between electrodes the non-parametric Wilcoxon test was performed between mean waveform data obtained for each electrode. This data was grouped in a symmetrical basis between central 10 degrees and the periphery. The spatial grouping of these regions is illustrated in figure 4.3.

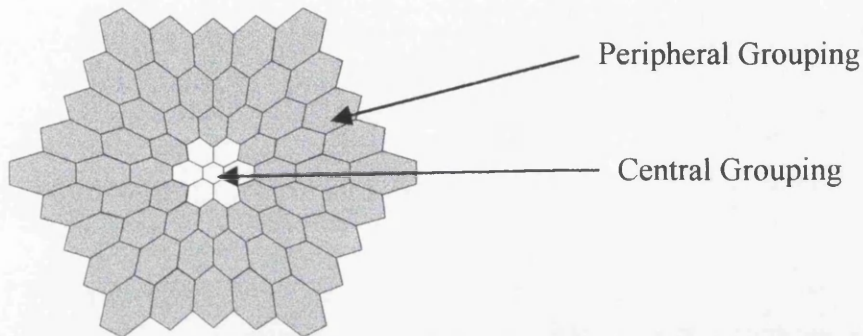


Figure 4.3 Spatial grouping used for comparison of central and peripheral regions.

Wilcoxon test		GF-HK	GF-CF	GF-DTL	HK-CF	HK-DTL	CF-DTL
Dilation	Central	0.74	0.82	0.95	0.84	0.57	0.6
	Peripheral	0.06	0.28	0.72	0.66	0.16	0.03(sig)
Non-Dilation	Central	0.14	0.47	0.06	0.84	0.26	0.08
	Peripheral	0.58	0.09	0.45	.059	0.15	0.08

(sig) = Significant

(a) Wilcoxon results

	Test Number	No. of repeated segments						Total
		1	2	3	4	5	6	
GF	Gold Foil	1	1	0	1	1	2	6
CF	Carbon Fibre	1	0	1	1	1	1	5
DTL	Dawson Trick & Litskow	1	1	0	0	2	1	5
HK	Hawlina Konec Loop	0	1	0	1	0	1	3

(b) Number of repeated segments

Table 4.1 Wilcoxon test results (a) and number of repeated segments (b) due to saturation.

Results indicate that in general (with the exclusion of DTL and carbon fibre after dilation) all noncorneal electrodes used in this protocol were comparable in the quality of their recovered signal. However, during the recording period, the H-K

loop was found to be less influenced by the D.C. baseline wander associated with rapid random eye movements (see EYE MOVEMENT ARTEFACTS in section 4.3). This leads to shorter recording periods because fewer segments are contaminated by baseline wander and have to be repeated. Thus after these preliminary findings the H-K Loop was chosen for all future evaluations of the VERIS system.

4.3. SUBJECT VARIABLES

The subjects under investigation can themselves generate noise from a number of sources.

1. Muscle artefacts
2. Eye movement artefacts
3. EEG artefacts

MUSCLE ARTEFACTS

Tension in muscles can generate significant electrical activity. The high frequency 'noise' produced combines with the baseline signal and can lead to variations as large as $\pm 50\mu\text{V}$. Such distortion of the signal to this level can severely mask the true evoked signal. Distortion of signals can be produced by subjects who tense their jaw muscles, tense their eyelids or even blink excessively.

To minimise muscle artefacts the patient should be as relaxed as possible and should be told of the consequences of blinking i.e. it will make the examination last longer. Additionally, because invariably the frequency content of this noise exceeds 300Hz, this distortion can be considerably reduced by low pass filtering.

EYE MOVEMENT ARTEFACTS

As previously discussed in section (1.4.1) the Electro-Oculogram (EOG) records the standing potential that exists between the cornea and the retina. Although this

dipole is usefully exploited to assess defects selectively affecting the retinal pigment epithelial layer, in the conventional electroretinogram it can give rise to substantial baseline shift or complete saturation of the signal. There are a number of artefacts produced by eye movements.

1. Slow eye movements generated from a patient's inability to concentrate can lead to saturation of amplifiers and a misrepresentation of ERG topography in local ERG measurements.
2. Small rapid eye movements can lead to some baseline wander in the recorded signal (see previous section on ELECTRODES). Recordings for patients with severe involuntary eye movements (Nystagmus) generally are of poor quality and this should be considered when determining a patient's suitability for the procedure.
3. Photomyoclonic reflex (PMR) is a reflex contraction of the orbicularis muscle in response to strobe flash. Although PMR can sometimes interfere with the interpretation of the b-wave in conventional ERG recordings (Johnson 1982) its effect is minimal in the fairly constant illumination produced by the MFERG stimulus.

One feature of the VERIS system is its ability to reject poor recording segments. Thus when excessive saturation occurs (a good indicator of poor fixation) the contaminated segments may be rejected (see chapter on VERIS SCIENTIFIC). Improper fixation can be effectively minimised by encouraging the subject to relax and to fixate centrally. Constant reiteration of this is required for good patient compliance.

The effects of baseline offset (associated with small rapid eye movements) can be minimised by the incorporation of D.C. restoration at the pre-amplifier stage and an appropriate choice of electrodes (see previous section). In addition, it is possible to reduce the low frequency artefacts associated with small eye

movements by setting the high pass cut off to 1Hz. However, it is not advisable to increase the high-pass cut off because it creates additional signal distortion which can lead to the misrepresentation of results (see section on FILTERING ARTEFACTS or (Keating & Parks 1997)).

EEG ARTEFACTS

Although not as serious as the previous subject based artefacts, EEG activity can lead to random fluctuations in the signal response. This is more of a problem in VECF recordings. As with the simple Dawson averaging used in VECF recordings, the effects of this random EEG 'noise' on MFERG responses are minimised by the averaging properties of PRBS cross correlation.

4.3.1. REFRACTIVE ERROR

As discussed previously (section 1.4.2) the conventional electroretinogram is elicited by a flash stimulus evoking a global response from the retina. Thus optical correction is not required, in fact, the optimum stimulus is diffuse and so defocus can enhance the uniform stimulation of cells. Recent interest in the Pattern ERG (PERG) has required greater care in optical correction and the removal of refractive errors. However correction of refractive errors is not without complication. Correction often involves lenses which themselves can produce artefacts. Conventional trial case lenses can produce lens rim artefacts at an eccentricity of 25-30 degrees. These artefacts are usually more prominent in the elderly (Zalta 1989), this may be due to their deep-set eyes which makes it difficult to place the lens near the eye. The effect of defocus is to spread the target's retinal image over a larger area creating an overlap of focal responses. This alters the luminance gradients at the edge of the target and, for small stimuli, reduces the luminance at the centre of the target. The smaller the stimuli the larger the influence of defocus. In addition, because of the topography of receptors within the retina, the effect of defocus is dependent on the location of

stimulation. Thus the more peripheral the target, the less influence defocusing has on the retinal image.

Defocusing can also be the result of a reduction in the accommodation potential (or flexibility) of the lens of the eye due to the normal ageing process (presbyopia).

To investigate the effects of refraction on the MFERG, three healthy volunteers (two emetropic, one hypermetropic) were tested with various lenses to induce defocus.

Each volunteer underwent seven MFERG recordings with induced defocus ranging from $-8D$ to $+8D$ in steps of $2D$. Monocular recordings were obtained in order to maintain the volunteer's ability to accommodate (and so fixate) using the contralateral eye. This had the advantage that the involuntary response of accommodation would be suppressed in the eye under investigation and so responses would reflect the true degree of defocus induced.

A wilcoxon test was performed between the mean waveform data obtained during defocus and that obtained with a zero dioptre lens. Results are provided in Table 4.2

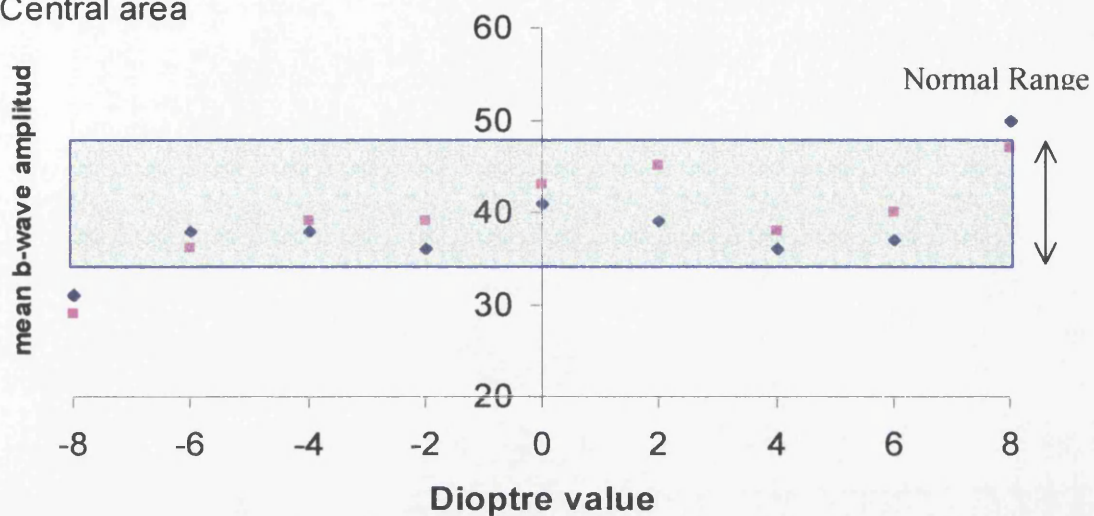
Dioptre defocus	-8	-6	-4	-2	0	2	4	6	8
Central area	0.00(sig)	0.03(sig)	0.04(sig)	0.23	-	0.19	0.01(sig)	0.01(sig)	0.00(sig)
Peripheral ring	0.02(sig)	0.03(sig)	0.05	0.07	-	0.3	0.08	0.04(sig)	0.00(sig)
Mean implicit time (ms)	33	34	33	33	32	33	33	34	33

(sig) Significant

Table 4.2 Non parametric statistics (Wilcoxon) relating significant change in signal response after induced defocus.

Induced Defocus (amplitude)

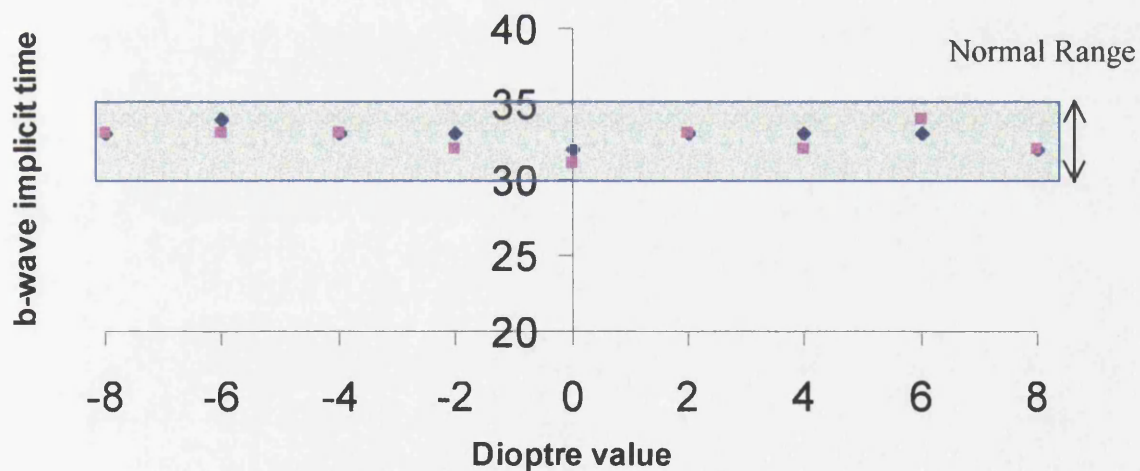
- ◆ Peripheral ring
- Central area



(a)

Induced defocus (implicit time)

- ◆ Peripheral ring
- Central areas



(b)

Figure 4.4 Plot of the variation of (a) b-wave implicit time and (b) b-wave amplitude for central and peripheral regions with induced defocus.

Implicit time of the local ERG recordings did not show a significant change with induced defocus, although a slight increase was observed with increasing defocus from 0 to 6 dioptre. Figure 4.4 (a) and (b) is a plot of mean implicit time and amplitude for peripheral and central regions at different values of lens power.

The amplitude measures displayed a marked variation that was related to defocus. The concave lenses (-8 to -2 dioptre) lead to a reduction in the mean amplitude of the b-wave in the central and peripheral regions. The convex lenses however (2 to 8 dioptre) produced an initial increase in response amplitude. Topographic analysis of amplitude displayed a mild inverse symmetrical relation to defocus with eccentricity, although only at the centre does this have any significant effect below a four dioptre change in refraction.

These findings are not surprising given the nature and scaling of the VERIS stimulus and effects of the optics. A convex lens will increase the stimulus area projected onto the retina and thus produce an increase in signal response. The affect of this increase will be inhibited as induced defocus leads to a loss of contrast of the image. Although this increased amplitude will reflect some influence from neighbouring areas. This has the greatest effect at the centre as this has the smallest area of stimulation and thus neighbouring areas will account for an increased percentage of the recorded response. A concave lens (-dioptre) will however reduce the size of the stimulus projected onto the retina and so lead to a reduction in the overall response. This decrease in stimulus size generated by a concave lens will produce a reduction in luminance of the stimulus again affecting predominately the central area, although to a lesser degree.

4.3.2. AGE AND THE MFERG

It is believed that a number of factors account for the observed reduction in retinal sensitivity as a function of the ageing process in normal subjects. The primary factors that have been reported to influence the ERG include, reduction of pupil

size (Weleber 1981; Johnson et al 1989a), transmission losses of the ocular media (particularly the lens) (Weale 1963; Pokorny et al 1987; van Norren & Vos 1974) and neuronal losses in the retina (Johnson et al 1989a; Devaney & Johnson 1980). Most studies believe this reduction in visual sensitivity to be linear with age (Drance et al 1967; Hass et al 1986; Weleber 1981) although recent evidence suggest an acceleration of this loss for individuals over the age of 50 (Johnson & Choy 1987). Although the sample sizes available are limited and most research reflects results obtained from subjective visual field testing, evidence suggests that only lenticular transmission losses become progressively greater for individuals over the age of 60 while all other factors show a linear relationship with age.

Although the effect of age on the amplitude of the conventional ERG has been documented (Weleber et al 1981) little information exists on the effects of local responses to the ageing process. In addition, to define the normal variation of a new technique there is a requirement to assess this in the context of age related samples. In the following chapter we investigate how the features of the MFERG change with age.

4.3.3. PUPIL SIZE

There is little doubt that pupil size has a direct influence on the quality and size of conventional full field ERG recordings. Since this aperture directly affects the amount of stimulus luminance reaching the retina it thus has a direct effect on the subsequent response of the retina to any stimulus.

To optimise the recovery of the full field flash ERG, ISCEV recommendations suggest that patients should be fully dilated with 1% tropicamide or its equivalent to maximise pupil size and therefore retinal illumination.

In the process of establishing a standard protocol, we conducted a preliminary trial to investigate the difference in signal response between the natural and

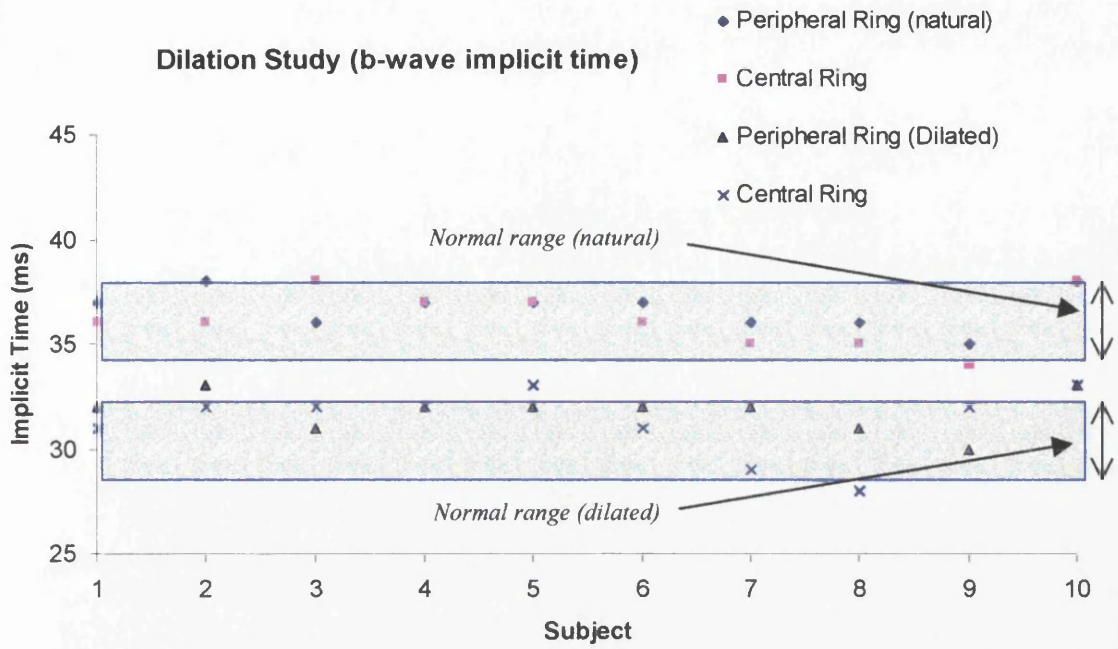
dilated pupil. This was particularly important to establish the influence of dilation on normative values.

Ten healthy volunteers underwent testing on two separate occasions. Tests were performed with natural pupils (non-dilated) and maximally dilated with 1% tropicamide (pupil diameters ranged in value from 8 to 10mm, measurements were taken at the beginning and end of each recording session). All subjects had refractive errors corrected.

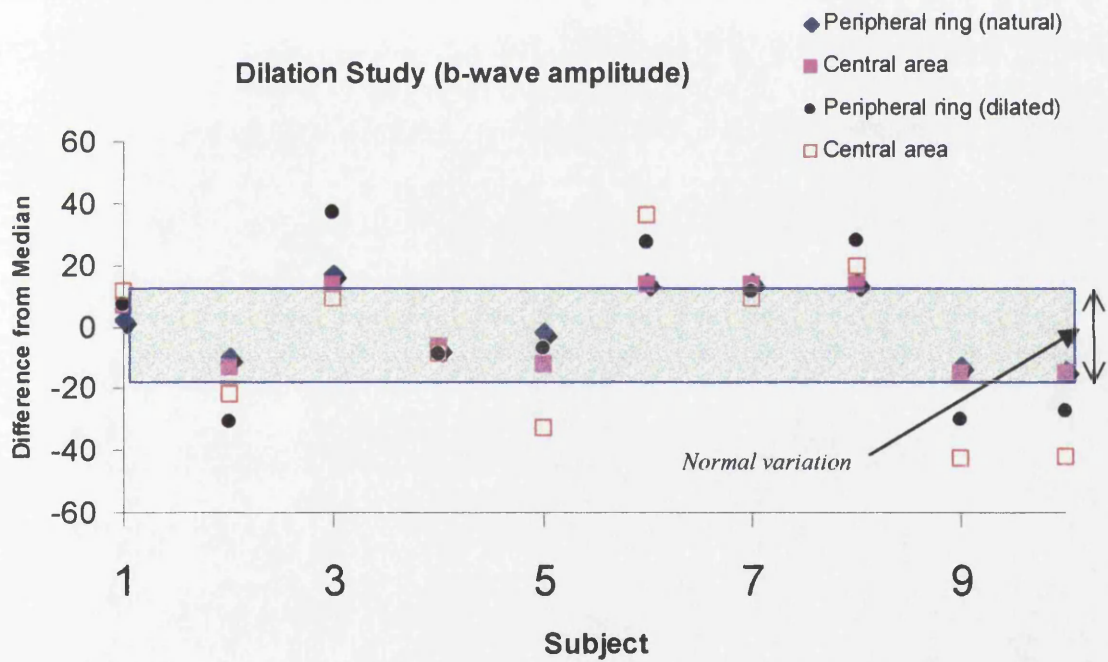
ERG recordings were taken following the protocol described in the previous sections.

Dilatation had a different effect on both the temporal and spatial characteristics of the ERG responses. Figure 4.5 illustrates the change in implicit time and amplitude for the central and peripheral regions before and after dilation.

Implicit time of the local ERG recordings decreased uniformly with dilation. The b-wave amplitude measures increased significantly with dilation and in one case amplitude measures doubled. Topographic analyses of this amplitude increase after dilation displayed a central bias where amplitudes roughly double the non-dilated recordings.



(a) Variation in mean implicit time measures for central and peripheral areas for natural and dilated pupils.



(b) Difference from median for mean amplitude measure.

Figure 4.5 Variation in mean implicit time (a) and amplitude (b) together with normal range.

Given the small number of volunteers tested this study is of limited value. However, figure 4.5 does indicate that dilation increases the variation of b-wave amplitude. Similar findings, on the spread of normative data, were found in a previous study – (Parks & Keating 1997a) - investigating dilation and the full field Ganzfeld ERG. This topographical variation could arise not only from greater amount of light stimulating the retina but from the physiological source of any evoked response. This is because evoked responses produced under conditions of dilation will represent a greater cone component (and possibly a reduced rod component – due to saturation) than those produced with natural pupils. Thus the physiological source of these evoked signals, and consequently their morphological features, would differ.

While it is not under dispute that signal amplitude is dependent on retinal illumination these preliminary results suggest that pupil dilation could have a significant effect on the normal range of the b-wave amplitude and possibly the topographical source of the response signal. This would adversely effect the ability of the test to detect and statistically quantify abnormalities. Standardising retinal illumination by dilation may, in fact, accentuate inherent physiological variation. This would reduce the potential of the MFERG to assess and identify retinal abnormalities and be disadvantageous to its role in the routine clinic.

Although a patient's pupil size is dependent mainly on mydriatics administered by the investigator, care should be taken when assessing a patient because common ophthalmic medications can also produce a marked variation in pupil diameters. Pilocarpine, which is frequently prescribed to patients in the treatment of glaucoma, causes marked miosis producing pupil diameters as small as 2 mm.

4.3.4. LENS & MEDIA OPACITIES

Lens and media opacities can affect the ERG in two ways:

1. They can act as a filter, reducing the luminance of light reaching the retina
2. They scatter the incoming light, thus altering the contrast of any stimuli.

In some way their effect is similar to that of defocus in their control of luminance and contrast.

Thus the influence of lens and media opacities can be simulated and so examined in a more controlled fashion by monitoring the effects of varying the luminance and contrast of the stimulus. The effects of luminance and contrast are addressed later in this chapter.

Patients with dense lens and media opacities which would filter and scatter the light beyond the resolution of the MFERG stimulus were excluded from this study. This was because any exhibited variation in response topography would not necessarily reflect underlying pathology.

4.3.5. FIXATION

Patient compliance and steady fixation are essential to the accurate estimation of retinal topography in the MFERG and, for that matter, in the recording of any visual field examination. However, in the context of this evaluation where the target environment is a routine clinic, any solution to the problem of fixation had to be simple, inexpensive and preferably non-invasive.

The VERIS system has a central fixation cross which can be varied in size and colour. This can be used to aid fixation. If only peripheral vision is present then

this cross can be extended giving the illusion of lines pointing towards the central area (see figure 4.6)

A number of methods have been employed to monitor fixation in the MFERG. These range from the conventional use (Barber et al 1996) of a video camera configuration mounted such that the operator could monitor fixation during the recording process to the painstaking technique (Kondo et al 1996) of projecting a

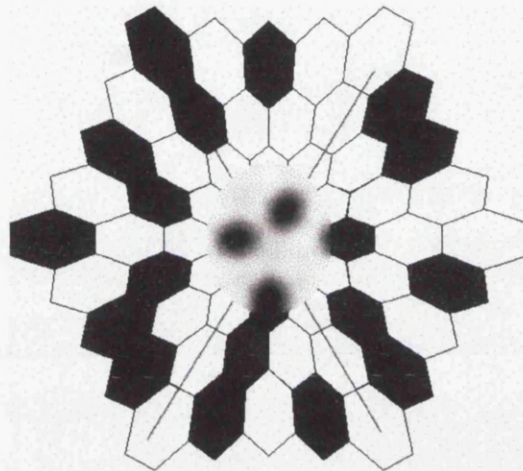


Figure 4.6 *Illustrations of marking used for eccentric fixation when central vision is compromised.*

small stimulus direct onto the fundus and examining its position using an ophthalmoscope. These methods are effective at monitoring fixation. However, this particular study was concerned with the evaluation of the system as it stood and any additional features have to simplify the recording and analysis process for the operator. The inclusion of a camera based fixation monitor would involve additional experience and data analysis for the operator and yet would still incorporate a subjective element. To address fixation a simple non-invasive technique was employed.

As was mentioned in the previous section (4.3) eye movement artefacts affecting fixation can be detected indirectly by monitoring the baseline shift observed during small eye movements.

To evaluate and quantify the resolution of this form of fixation monitoring one volunteer was asked to perform saccadic eye movements through predetermined fixed angles (created by positioning markers at fixed intervals on the monitor screen). These eye movements were then compared against the degree of D.C. offset produced. By increasing the amplifier gain, and so decreasing the level of D.C. offset required for saturation, it was possible to measure fixation loss.

Results from the small study performed are summarised in table 4.3 and illustrated in figure 4.7

Movement from fixation (degrees)	1	2	3	6	12	24
Gain required for saturation ($\times 1000$)	200	160	120	80	40	20
Effective D.C offset (μV)	50	62.5	83.3	125	250	500

Table 4.3 Fixation loss compared with saturation. Effective D.C. offset is calculated from ADC input range $\pm 5V$.

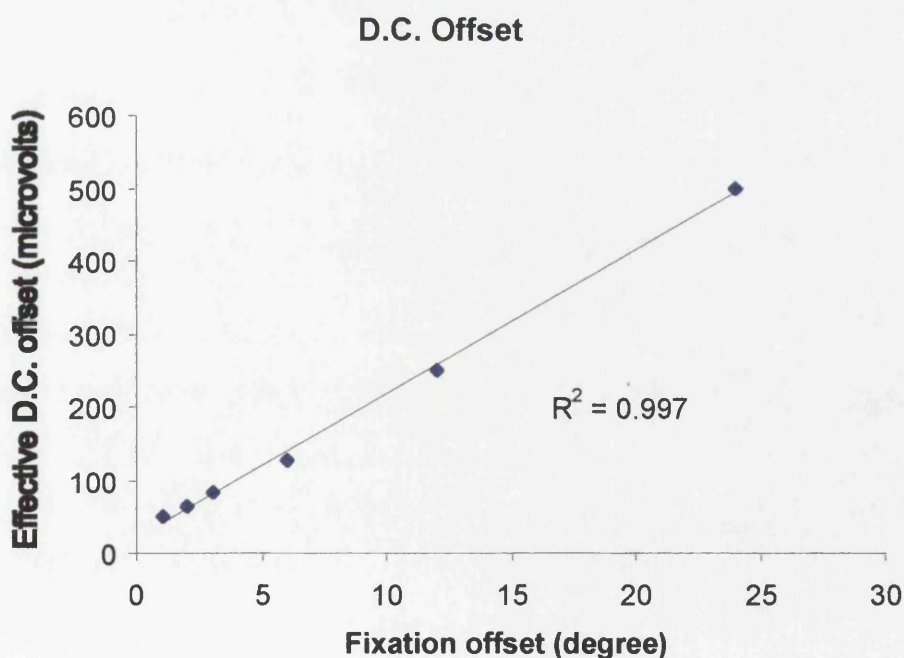


Figure 4.7 Correlation plot of fixation offset and effective D.C. saturation required. Plot indicates $\sim 30\mu V$ change in baseline per degree.

Although these results indicate that at least 2 degrees of eye movement would be required to produce saturation at the amplification currently used for MFERG recordings this resolution in fixation is adequate in the context of general clinical evaluation. It should be noted here that the saturation method for fixation monitoring is dependent on the filtering bandwidth employed (1-300Hz). This is necessary as a higher bandpass than 1Hz will mask the slow potential changes associated with fixation losses and thus disguise their occurrence. If a narrower filtering bandwidth was employed (e.g. 10-100Hz) then saturation would only occur at higher gains.

Saturation monitoring was the primary method used to monitor fixation and was a decisive factor in the exclusion of less compliant volunteers. If baseline wander and saturation of the raw signal was observed the current segment was discarded and the importance of fixation was reiterated to the patient. If the saturation persisted then the patient/volunteer was excluded from the trial. One disadvantage of this method was the lengthening of test times and the exclusion of patients with poor fixation or nystagmus (involuntary movement of the eye).

To retain the true objectivity of the MFERG technique automatic computerised eye tracking could be employed. However devices using this technique tend to be bulky, cumbersome and expensive. In addition the complex array of electronics used on the headsets would interfere with the recorded responses and so could further degrade the signal to noise ratio of the response signal. However, recently a number of new devices have become available in a form suitable for electrophysiology. With spatial resolutions of 0.01 degree and sampling rates in excess of 250 Hz these systems would be ideal for objective fixation monitoring (see CHAPTER 7 for discussion).

4.3.6. Fatigue

Since protocols for MFERG require greater patient compliance than conventional full field ERGs, patient fatigue can result in greater response fluctuations especially in the final stages of long recording sessions. It is difficult to minimise the effects of fatigue since they vary widely. However, the inclusion of segmented recording periods of 43 seconds duration was found to improve patients' compliance to a degree acceptable for MFERG recordings. During each segment the patient is reassured, relaxed and asked to maintain fixation. These segments are interspersed with variable breaks ranging from seconds to several minutes in some extreme cases. This segmentation of the recording period gives the investigator more control over the recording procedure. This flexibility for the investigator leads to a more patient-tailored recording session which generally was found to improve the quality of the recorded responses.

4.4. RECORDING EQUIPMENT VARIABLES

All electric circuits generate electrical noise due to molecular activity and other non-ideal aspects of signal amplification. This noise can be easily observed by short circuiting patient input terminals. This random noise should be of the order of a few microvolts and is usually dependent on the characteristics of the amplifier and bandwidth settings. It is generally minimised in the conventional averaging process.

4.4.1. ELECTRICAL INTERFERENCE

Electrical interference can be generated from a number of sources e.g. electrodes, amplifiers, the stimulus and even the environment. Equipment that commonly generates electrical interference includes fluorescent lights, motors and power transformers. These generate magnetic fields that couple 50 Hertz interference into the recordings. The patient should be isolated from these sources as much as

possible. Additionally, equipment can generate noise at very high frequencies (i.e. radio frequencies) although this can be eliminated by appropriate filtering. Care should be exercised to keep both recording equipment and the subject away from strong sources of radio frequency signals. It must be ensured that patient leads and amplifiers are not close to power lines or other electrical equipment. The electrode impedance should be low and the ground connection good.

The principal electrical interference that plagues multifocal recordings arises from the coils of the CRT used for the stimulus. The sampling frequency and the averaging sweep used to derive the local signals are synchronised to the refresh rate (and consequently the raster) of the CRT monitor. If this interference is not properly shielded then an artefact produced from the electromagnetic coils of the

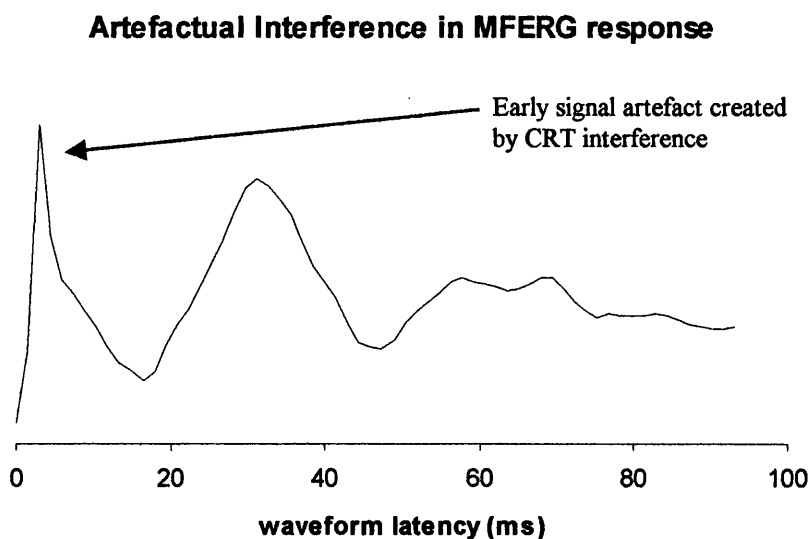


Figure 4.8 *Interference on MFERG response arising from imperfect CRT shielding.*

CRT will be averaged along with the required response. Examples of this can be seen in figure 4.8 and in Vaegan & Buckland (1995) where, due to poor shielding, the authors have mistakenly described this as an early receptor potential. In these cases the early portion of the 'signal' is no longer of equal amplitude with eccentricity but scales with the stimulus size. This is a classic indicator of artefact as any physiological response from the eye would reflect the topography of the

excited cells in relation to the stimulus pattern. To shield the patient from possible interference from the CRT coils, a simple conductive cone was made through which the patient would be placed. If this is properly grounded then effects of the CRT coils can be minimised.

Another important factor is the reduction of impedance between patient and electrode. To achieve low impedance care should be taken to clean the site of the electrode placement. A good ground connection must be made. Any unused channels in amplifiers should be shorted. Failure in this can lead to unwanted noise. Electrode leads should be as short as possible and not looped or in close proximity to power lines. Reduction can be achieved by twisting positive and negative electrode leads thus cancellation can be achieved due to magnetic induction.

As a rule if the interference on the MFERG response is directly proportional to the dimensions of the stimulus areas then electrical interference should be suspected.

4.4.2. Filtering Artefacts

As discussed previously high and low pass filtering is an effective and essential means of reducing unwanted electrical interference from the patients and their surroundings. However, the full consequences of filtering should be realised because filtering can have a major effect on the waveform shape. Stimulation rate and filter bandwidth both influence the shape of the multifocal electroretinogram. the former has been addressed by Hood et al (1997b) and by Usui and Nagasaka (1994). This section concentrates on filtering artefacts. It presents a theoretical argument, simulated waveform examples and clinical examples to investigate the important role that electronic filtering of signals plays in the recording process of the Multifocal ERG.

The conventional ERG is recorded with a wide bandwidth (0.3 - 300 Hz) (Marmor & Zrenner 1995). However, due to the high amplifier gains and low signal strength most published studies on multifocal ERG recording use a more constricted bandwidth with the high pass-filter setting set at 5Hz or higher (Sutter & Tran 1992; Kondo et al 1995; Kretschmann et al 1996). Low pass filtering presents less of a problem and is typically 100 Hz.

THE THEORETICAL ARGUMENT

The concern is the effect of high pass filtering on waveform shape. The high pass filter employed in the physiological amplifier consists of a single resistor-capacitor (RC) network as illustrated in figure 4.9

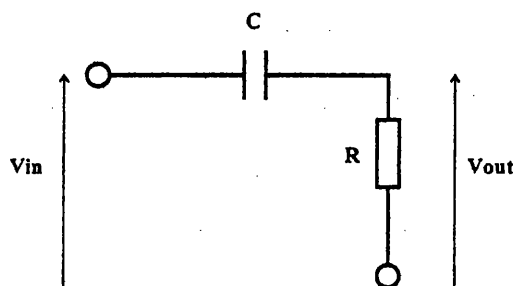


Figure 4.9 *The high-pass filtering circuit*

This RC network introduces a time constant into the circuit where the output voltage is related to the input voltage by equation (4.2).

$$V_{out} = \frac{R}{\sqrt{\left[R^2 + \left(\frac{1}{\omega^2 C^2} \right) \right]}} \cdot V_{in} \quad (4.2)$$

where $\omega = 2\pi f$ and f = frequency of input signal. Simple substitution shows that the output is approximately equal to the input at high frequencies ($\omega > 1/RC$) and tends to zero at low frequencies. The high pass filter cut-off value usually quoted

is the point on the frequency response graph where the gain has fallen from the band pass gain by 3 decibels (figure 4.10).

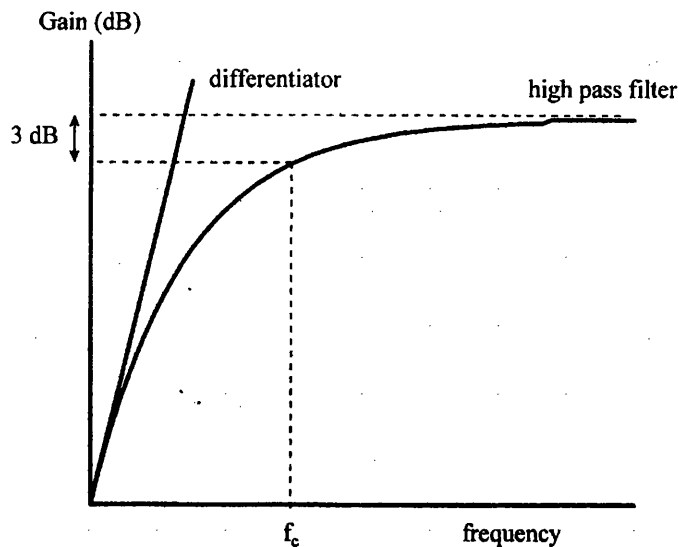


Figure 4.10 *The frequency response curve of a high-pass filter and a differentiator; f_c = critical frequency at which gain falls 3dB below bandpass gain (adapted from Keating, Parks, Evans, Williamson, Elliott & Jay. The effect of filter bandwidth on the multifocal electroretinogram. Documenta Ophthalmol 1997 92, 4, 291-300).*

At low frequencies, the high pass filter circuit behaves as a differentiator: D.C. voltages are blocked and higher frequencies passed without effect. The approximation to the differentiator is illustrated in the frequency response curve (figure 4.10) and can be represented by equation (4.3) relating the output voltage at time t to the differential of the input voltage multiplied by the circuit time constant (RC).

$$V_{\text{out}}(t) = RC \frac{d}{dt} V_{\text{in}}(t) \quad (4.3)$$

Physiological waveforms have components at various frequencies and therefore care must be taken to avoid distortion of the signals.

The high pass filter time constant determines how fast a changing signal has to be before the filter passes it. For example extremely low frequencies such as D.C. are blocked and fast step functions are passed. However, if a step function is applied the filter will pass the change in voltage and then quickly return to zero. This is in effect a differentiation where only changes in the signal are passed through the circuit.

SIMULATED EXAMPLES

The system used for the simulation experiment was a standard ERG recording system developed in our department (Bradnam et al 1994). This system contains, low noise amplifiers custom built for physiological measurements. The high pass filter is variable in steps, giving D.C., 0.1, 1, 5, 10 and 20 Hz cut-off values.

Filter order also influences signal shape and this was addressed by the option of a second order RC filter. The second order filter consists of two cascaded RC stages and has a steeper roll-off from the pass band than the frequency response curve of figure 4.10. An electronic simulator was built and waveforms generated by passing a digitised EPROM waveform through a Digital to Analog converter to our input amplifier. Three simulated waveforms of amplitude $30\mu\text{V}$ were used and the high pass filter varied for each of the quoted values. The simulated waveforms used were a square wave, a normal ERG waveform and a negative ERG waveform.

SIMULATED SIGNALS

The effect of filtering the simulated waveforms is illustrated in figure 4.11. The square wave illustrates the danger of signal distortion with high pass filtering showing subtle changes at low values through to differentiated spikes at the higher values (figure 4.11a). Of more interest is the effect on the ERG waveforms (see figures 4.11b and 4.11c). The normal ERG is not dramatically affected with the shape of a and b-waves preserved even with the 10Hz high pass filter. The

main difference is in a very slightly reduced amplitude and shift in implicit time with a fast return to the baseline following the b-wave.

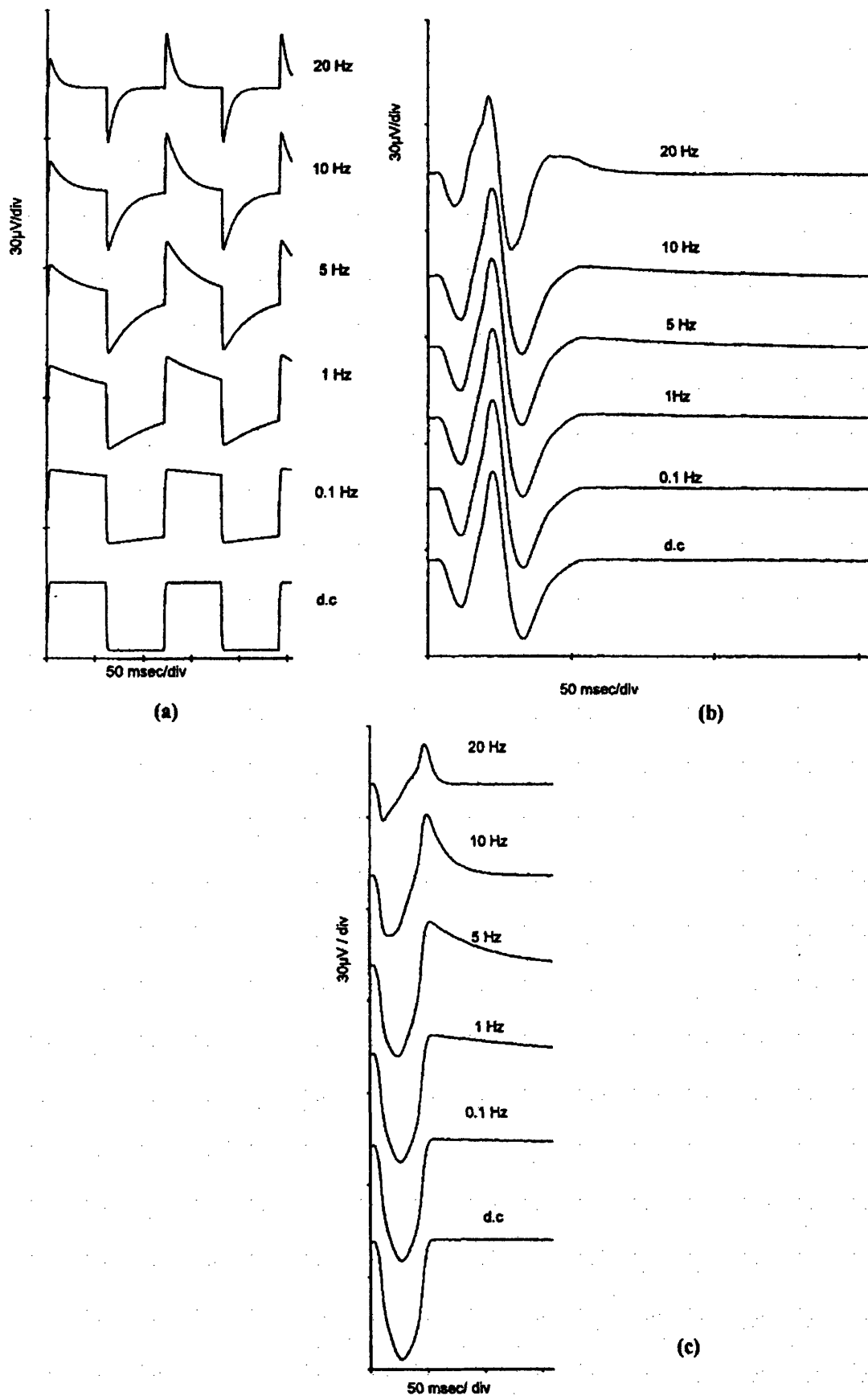


Figure 4.11 High-pass filtering of simulated waveforms. (a) Square wave. (b) Normal ERG. (c) Negative ERG (adapted from Keating, Parks, Evans, Williamson, Elliott & Jay. The effect of filter bandwidth on the multifocal electroretinogram. *Documenta Ophthalmol* 1997 92, 4, 291-300).

The negative ERG waveform shape can show major shape changes as the high pass filter value is increased. At low values, little effect is observed; however as the high pass filter is increased to 5 or 10 Hz, the effect of differentiation is evident. At these settings, an artificial positive component as large as the real

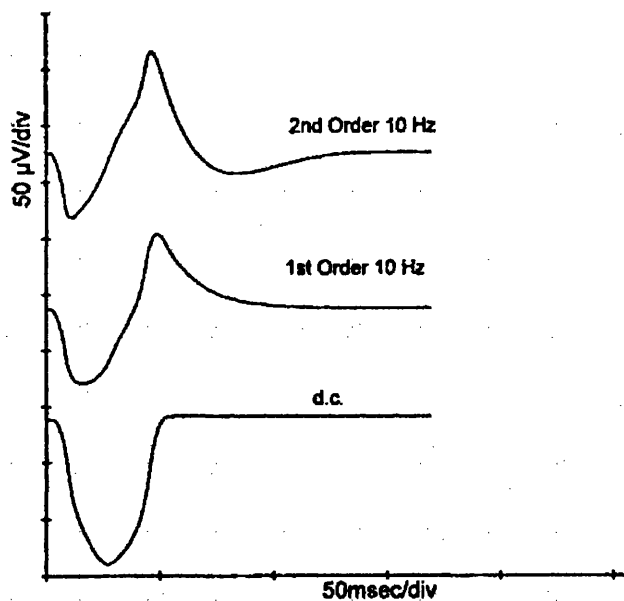
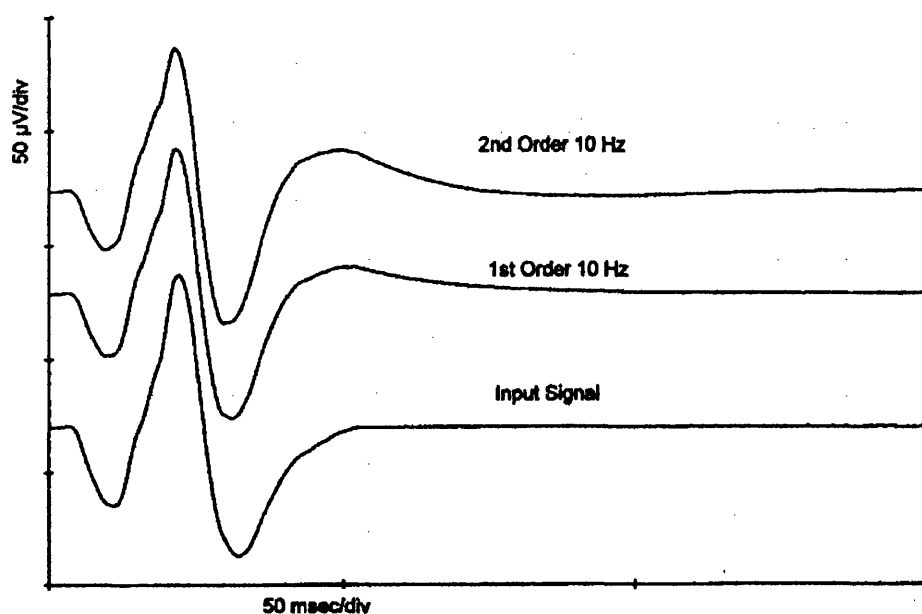


Figure 4.12 (a) the effect of filter order on a normal ERG. (b) The effect of filter order on a negative ERG (adapted from Keating, Parks, Evans, Williamson, Elliott & Jay. The effect of filter bandwidth on the multifocal electroretinogram. *Documenta Ophthalmol* 1997 92, 4, 291-300).

negative component is created. The second order 10 Hz filter increases signal distortion and this is illustrated in figure 4.12(a) for a normal ERG and in figure 4.12(b) for a negative ERG. The normal ERG shows small but increasing latency shifts as the filter order is increased and the positive artefact wave following the b-wave is emphasised by the higher order filter. The negative ERG illustrates the differentiation effect with the positive component more prominent with the higher order filter. It is important here to note that many commercial amplifiers that are used routinely for conventional electrophysiology incorporate second order RC filters. These will distort the waveform shape to a greater extent than first order RC filters.

CLINICAL RECORDING

MFERG recordings were made following the protocol previously established. Conventional Ganzfeld ERG's were recorded using our custom built system triggering a Ganzfeld stimulator (Medelec Instruments Ltd) The photopic ERG was recorded in accordance with the ISCEV protocol. Stimulus intensity was 2.62 cd/m² superimposed on a rod suppressing background of 22.6 cd/m². For the conventional ERG, pupils were dilated with 1% Tropicamide.

SUBJECTS

A clinical example of upper branch retinal vein occlusion was used to demonstrate the effect on negative ERG waveforms. Figure 4.13 illustrates the effect of 1 and 10 Hz filtering on a Ganzfeld ERG obtained from a patient with upper branch vein occlusion. The 1 Hz record shows a preserved negative ERG waveform whereas the 10 Hz record shows a large positive component. The trace arrays of the multifocal electroretinogram recordings from the same patient are shown in figure 4.14 The 10 - 300 Hz recordings show the differentiation effect creating a positive artefact component not present in the corresponding 1 - 300 Hz recording.

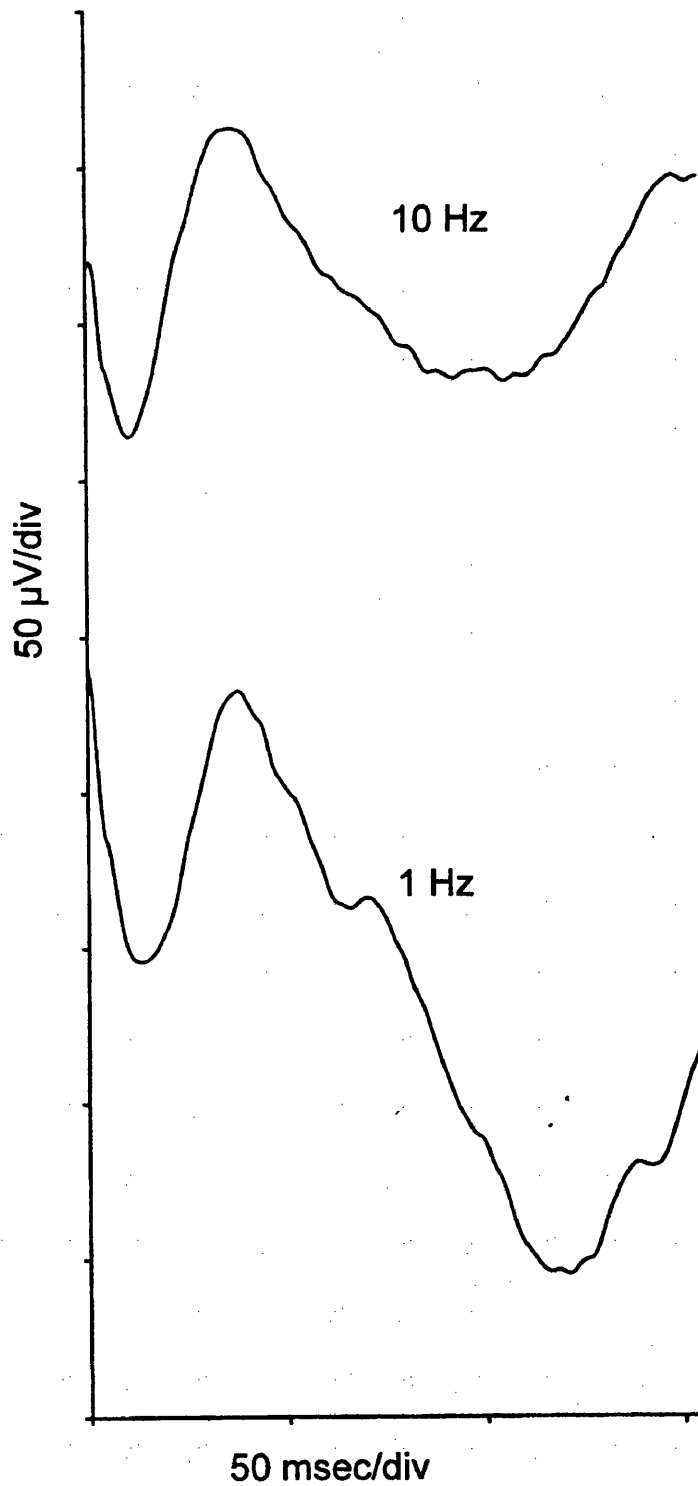
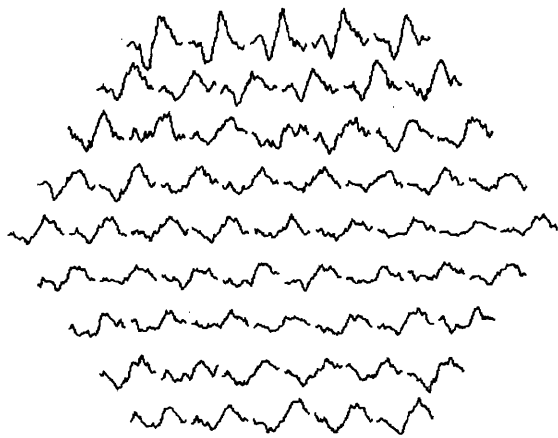
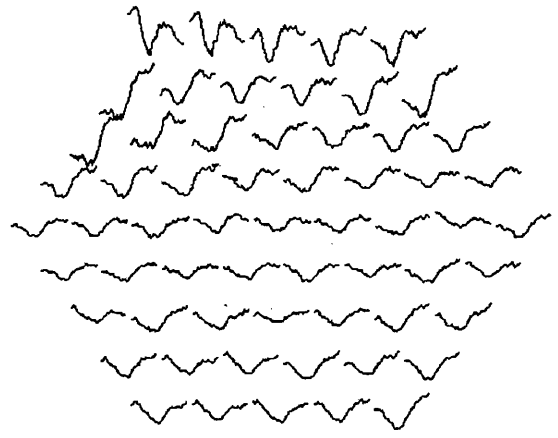


Figure 4.13 *A clinical ganzfeld ERG (upper branch vein occlusion) recorded by 1- and 10-Hz high-pass filtering (adapted from Keating, Parks, Evans, Williamson, Elliott & Jay. The effect of filter bandwidth on the multifocal electroretinogram. Documenta Ophthalmol 1997 92, 4, 291-300).*



10 Hz trace array



1 Hz trace array

Figure 4.14 *Multifocal ERG waveforms (upper branch retinal vein occlusion) recorded by 1- and 10-Hz high-pass filtering (adapted from Keating, Parks, Evans, Williamson, Elliott & Jay. The effect of filter bandwidth on the multifocal electroretinogram. Documenta Ophthalmol 1997 92, 4, 291-300).*

DISCUSSION

In practice, the low signal strength and high gains used mean limiting the bandwidth to cut-out baseline wander during long recording periods. This is still merited when one is simply looking for reductions in amplitude or scalar product measures. If however, waveform shape is important, as in the delay in implicit time observed in retinitis pigmentosa (see chapter 6 on clinical investigations) then a wide bandwidth should be employed.

In several papers, doubts have been raised on the origin of the multifocal ERG waveform components and it has been stated that they may not correspond to conventional ganzfeld ERG recordings (Kondo et al 1995; Usui & Nagasaka 1994). The author believes that these doubts are the direct consequence of excessive filtering in their investigations.

4.4.3. Stimulus Contrast and Luminance

It is well known that both contrast and luminance effect the pattern and conventional full field ERG respectively. As discussed in a previous section the monitor used in the evaluation was an Apple Macintosh Multiscan Monitor. Its maximum luminance was measured at 116 cd/m^2 using a Minolta LS-100 luminance meter and was found to vary markedly with eccentricity. To measure this degree of luminance and contrast, the maximum and minimum values of luminance were measured for each area of the stimulus (see figure 4.15). A more comprehensive study of stimulus luminance can be found by Barber (1981) and should be considered when interpreting local responses.

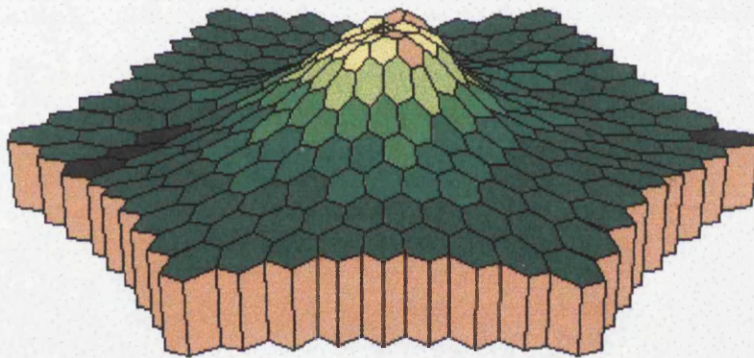


Figure 4.15 *Spatial luminance profile for multiscan monitor over stimulus paradigm. Central peak indicates a maximum luminance of 116 cd/m^2 (min. 92 cd/m^2)*

To study the influence of contrast and luminance on the MFERG a number of recordings were obtained from one volunteer under different conditions of contrast and luminance.

The recording protocol used for these examples was identical to those described previously with the exception of the use of a mydriatic. The volunteer was maximally dilated and corrected so as to obtain the maximum signal response.

This was to optimise the measure of subtle changes in signal response due to alteration of the stimulus contrast and luminance gratings.

CONTRAST

The contrast of the display was changed by altering the hue of the stimulus. This provided three stimuli of, 89% to 40% and 20% contrast. Full MFERG measurements were taken at each contrast level.

The results from these experiments were plotted (see figure 4.16). Contrast was found to affect both the temporal and spatial characteristics of the ERG.

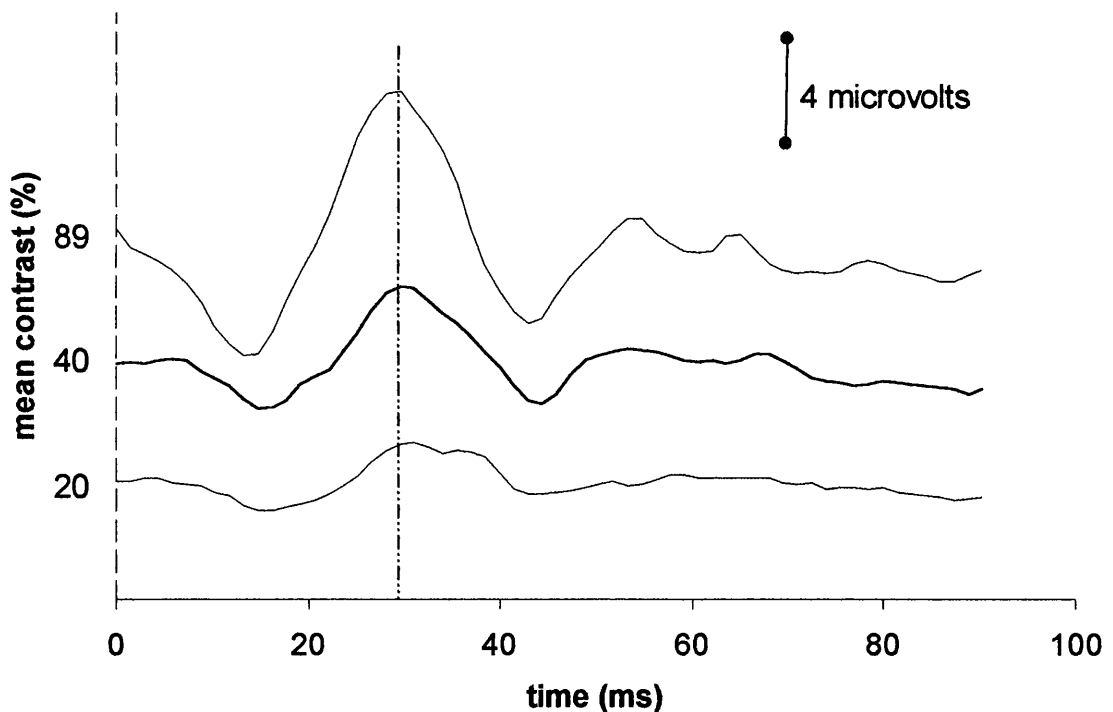


Figure 4.16 *Summed multifocal responses from all 61 areas to stimulus with different mean contrast.*

Implicit time of the local ERG recordings was more or less uniform with some increase in delay with decrease in contrast, both topographically and locally. They remained so throughout the study - although at 20% contrast, amplitudes were

markedly reduced and so their corresponding implicit times were difficult to detect. In addition note the double peak at 20% contrast; although amplitude values are low and definitive features difficult to identify this may reflect some reduction in the contribution from the centre-surround mechanisms of the bipolar cells. A topographic analysis of the change in latency from high to low contrast is illustrated in figure 4.17.

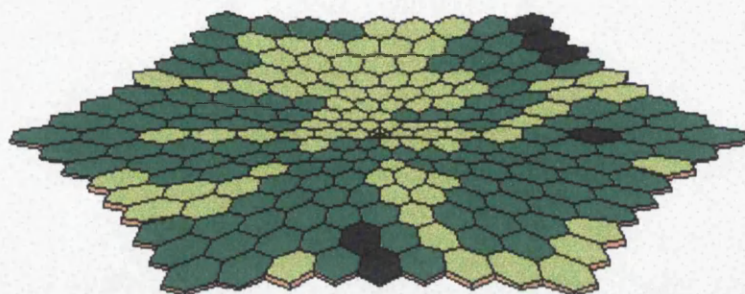


Figure 4.17 *Topographical difference in b-wave implicit time between 89% and 20% contrast.*

Mean contrast	Mean amplitude (nV)		Mean latency (ms)	
	Central area	Peripheral ring	Central area	Peripheral ring
89%	120(8)	134(18)	30(0)	30(1)
40%	75(9)	78(12)	33(3)	32(3)
20%	36(6)	43(11)	34(3)	33(4)

Table 4.4 *Mean amplitude and latency values related to stimulus contrast. Values in brackets indicate greatest deviation between individual areas.*

Unlike the implicit time the amplitude measures displayed a marked reduction that appeared directly proportional to a decrease in contrast. Topographic analysis of amplitude (high to low contrast – see figure 4.18 & Table 4.4) indicates a central bias in the reduction in amplitude.

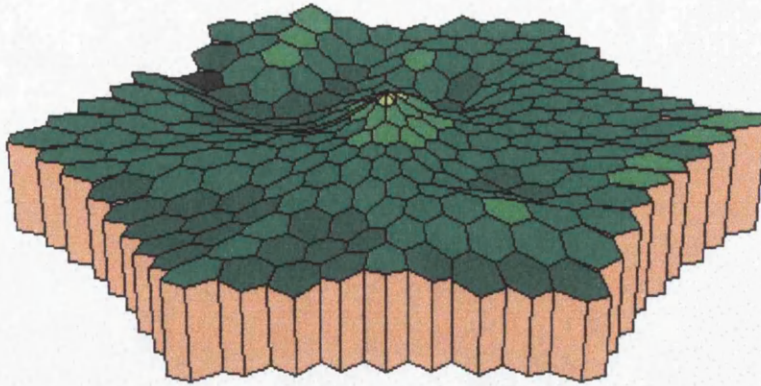


Figure 4.18 *Topographical difference in b-wave amplitude between 89% and 20% contrast.*

LUMINANCE

The mean luminance of the display was measured at 60 cd/m^2 ; the maximum luminance was changed from 116 to 58 and 29 cd/m^2 luminance while contrast was kept as close to 89% as possible. Again alteration of luminance gradient was found to affect the temporal and spatial characteristics of the ERG separately (see figure 4.19 and Table 4.5). Implicit time of the local ERG recordings again showed some increase in delay - although individual recordings at a luminance of 29 cd/m^2 were difficult to detect. The amplitude measures displayed a marked reduction that appeared directly proportional to a decrease in luminance. Topographic analysis of amplitude displayed an inverse symmetrical relation to luminance with eccentricity.

Mean luminance (cd/m^2)	Mean amplitude (nV)		Mean latency (ms)	
	Central area	Peripheral ring	Central area	Peripheral ring
116	120(8)	134(18)	30(0)	30(1)
58	50(5)	48(13)	34(3)	34(4)
29	25(9)	22(10)	36(7)	35(6)

Table 4.5 *Mean amplitude and latency values related to stimulus luminance. Values in brackets indicate greatest deviation between individual areas.*

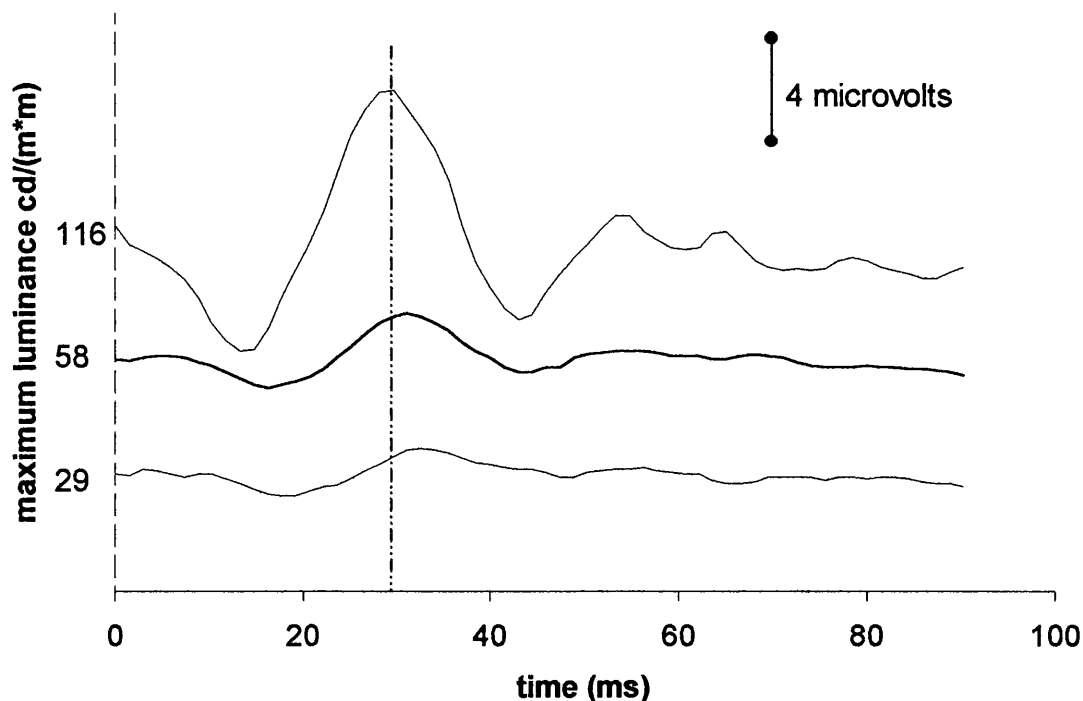


Figure 4.19 *Summed multifocal responses from all 61 areas of stimulus with different mean luminance.*

4.5. CONCLUSIONS

This chapter has examined the main factors that are believed to influence the MFERG. An investigation of non-corneal scleral electrodes concluded that the recently developed HK-loop electrode provides the most stable signal whilst retaining the amplitudes associated with the more commonly used non-corneal electrodes.

A limited investigation of pupil dilation and its effects on the multifocal ERG carried out on four volunteers concluded that signal amplitude was directly dependent on retinal illumination. This same improvement in signal strength had a significant effect on the normal range of the b-wave amplitude and the topographical source of the response signal. Standardising retinal illumination by dilation may, in fact, accentuate the inherent physiological variation between

normal individuals. These results led to the introduction of separate test protocols. Dilation was used only if a patient was undergoing repeat measurements.

The effects of luminance and contrast were examined both directly (by altering the monitor controls) and indirectly (by inducing refractive errors) in a cohort of volunteers. The observed changes were found to influence both the temporal and spatial features of the ERG waveforms. Contrast changes were found to affect the latency of local responses less severely than luminance changes although this could in part reflect a divergence in the centre-surround mechanisms of the bipolar cells since contrast plays an important role in defining the centre-surround boundaries.

Subject and environmental noise identified as extraneous to the evoked responses could be minimised by a combination of averaging and the use of high and low bandpass filters. This excludes the high and low frequency noise generated by patients and equipment. However, a detailed investigation of filtering artefacts concluded that care should be taken when employing bandpass filters as the morphological characteristics of the evoked responses would be affected. Optimum values for the high and low bandpass filter settings were found to be 1 and 300 Hz respectively.

The requirement for a simple method for fixation monitoring was investigated and found that saturation at bandpass filtering of 1-300Hz was a good indicator of fixation loss. This was the main method employed in the subsequent evaluation to monitor a patient's compliance.

The results were used to define a standard protocol. This protocol was employed in the following chapter in which a full clinical evaluation of the VERIS system was performed.

Chapter 5

NORMATIVE STUDIES

This chapter describes a number of investigations used to establish normative values for the VERIS system. The aim of this chapter was to determine the repeatability, reproducibility and inherent variation of this new technique over a broad control population. In addition, a cohort of these subjects was used to establish normative values for the conventional full field ERG and the custom Humphrey field test that will be used for comparison in the following chapter when a variety of retinal disorders are examined.

5.1. THE NORMAL RANGE

Before any new technique can be used in a clinical context a sound and scientific assessment of the system's variability within the normal population should be undertaken.

Normative values were obtained from 70 healthy volunteers following the protocol established in the previous chapter (grouping ratio is summarised in table 5.1).

Age group	20-30	31-40	41-50	51-60
No. of controls	22	18	15	15

Table 5.1 *Number of controls tested in respective age groups.*

This population ranged in age from 21 to 58 (mean age 38) and included 34 females and 36 males. To assess the repeatability and reproducibility of the system a small cohort of volunteers was re-tested. To measure reproducibility, 20 subjects were examined on two separate occasions. For repeatability, 10 repeat measurements were performed on three of the volunteers.

As with the conventional full field flash ERG there are a number of features of the MFERG waveform that may indicate discrete cellular pathology. In addition, there are a number of methods for reporting these measurements (Marmor et al 1989, Marmor & Zrenner 1995). The following sections detail the topography of these features and consider their repeatability and reproducibility individually. Analysis of the repeated measurements based on the definition of a repeatability coefficient adopted by the British Standards Institution (British Standards Institution 1979, Bland & Altman 1986) was performed on the results obtained. The coefficient of repeatability was defined as the standard deviation of the mean difference between pairs of repeated measurements divided by the average of the means of the two tests. The coefficient of reproducibility was defined as the

standard deviation of the difference from the mean of repeat measurements divided by their mean response.

Where it was deemed appropriate the mean results from areas were grouped to facilitate a clearer analysis of the data.

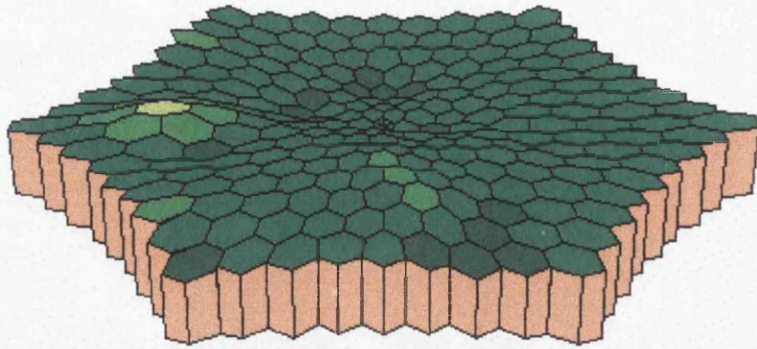
The study was approved by the local research ethics committee and informed consent was obtained for all participants.

5.1.1. IMPLICIT TIME

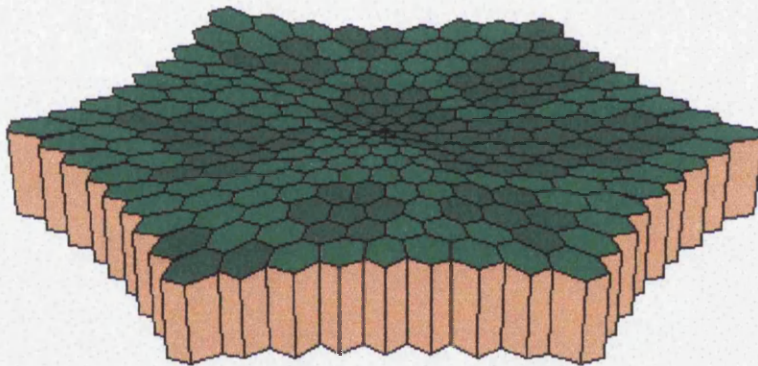
As described in Chapter 1 (section 1.4.2) the timing of ERG components can have diagnostic relevance. A delay in implicit time of the main components in the ERG can reflect photoreceptor and bipolar cell pathology (Berson et al 1969; Biersdorf 1982). This has been observed even in the early stages of the inherited retinal dystrophy Retinitis Pigmentosa (Berson 1993; Berson et al 1969a; Berson & Kantyars 1970). The following sections describe implicit times of ERG components obtained using the MFERG.

THE TOPOGRAPHY OF IMPLICIT TIME

The implicit time was not found to vary significantly over the central visual field of normal healthy volunteers (a nonparametric analysis of related samples was performed between the central five areas (for spatial grouping see figure 5.6 later in this chapter) and the remaining peripheral region). A summary of these results and those from separate features can be found in table 5.2. A plot of the latency topography of the a-wave and b-wave implicit time is shown in figure 5.1(a) and (b) respectively



(a) topographical plot of a-wave implicit time



(b) topographical plot of b-wave implicit time

Figure 5.1 *Topographical plot of (a) a-wave and (b) b-wave implicit time across the central 30 degrees of the retina. Plots indicate little variation within the 30-degree field examined.*

In this control population the implicit time of a-wave and b-wave waveform components (a-wave 17.76 ms SD 1.4 ms, b-wave 35.52 ms SD 1.2 ms) did not vary significantly over the retina. The ADC sampling rate used was 9 samples per refresh of the VDU which was driven at 75Hz. Thus the overall rate was 675Hz giving discrete intervals of 1.48 ms which is greater than the largest standard deviation.

AGE AND IMPLICIT TIME

As with the topography of MFERG implicit time, age was found to have little effect on implicit time. Latency values for a-wave and b-wave implicit time varied greatest, for the central 5 areas, between the first and last decades at 3 ms.

Figure 5.2 represents the mean topographical change in implicit time values between the first and last decades in the age matched groups.

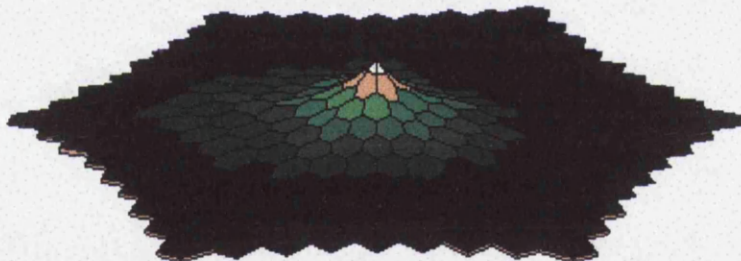
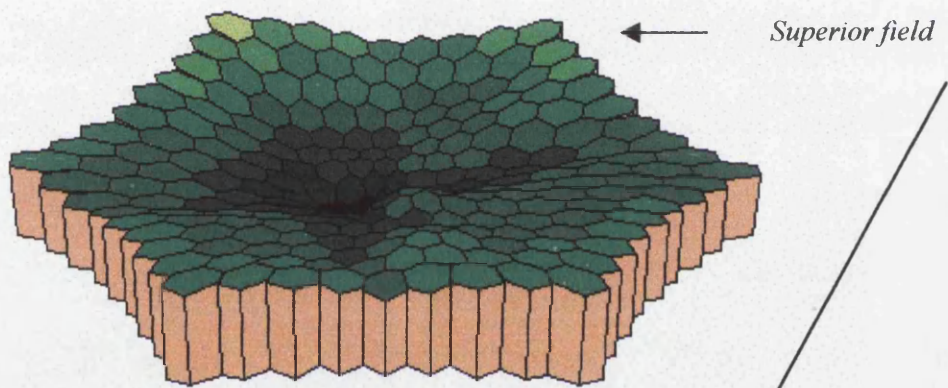


Figure 5.2 *Topographical change in mean b-wave implicit time between the 20-30s age group and the 50-60's age group. Peak indicates 3ms delay between groups.*

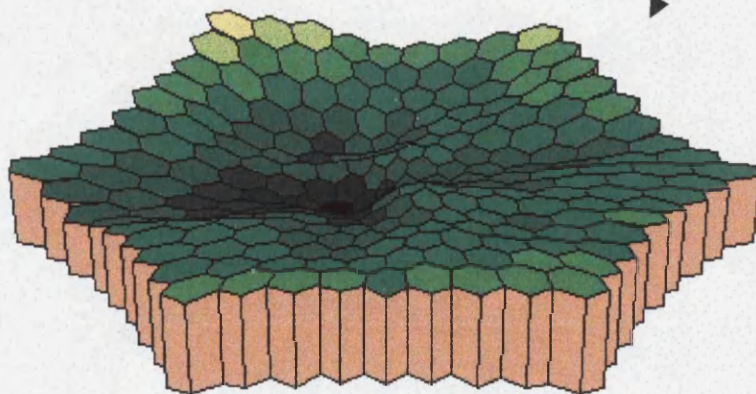
REPEATABILITY AND REPRODUCIBILITY OF IMPLICIT TIME

Repeatability and reproducibility of the a-wave implicit time of the MFERG was found to decrease with eccentricity. Coefficients of repeatability ranged from 10% in the central area to 13% in the peripheral areas. Inter-subject reproducibility ranged from 19% in the central area to 27% in the periphery. Repeatability displayed a concentric symmetry while inter-subject reproducibility displayed a marked superior inferior asymmetry

Repeatability and reproducibility for b-wave implicit time were also found to decrease with eccentricity. Coefficients of repeatability, obtained after 10 repeat measurements were performed on a cohort of the volunteers, ranged from 9% in the central area to 14% in the peripheral areas. Figure 5.3(a) and (b) illustrates the topographical variation in repeatability and reproducibility respectively. Inter-subject reproducibility, established after 20 volunteers underwent repeat investigations, ranged from 17% in the central area to 24% in the peripheral area. In a similar manner to the a-wave implicit time analysis, repeatability displayed a concentric symmetry while inter-subject reproducibility displayed a marked superior inferior asymmetry



(a) Topographical variation in mean b-wave implicit time repeatability



(b) Topographical variation in mean b-wave implicit time reproducibility

Figure 5.3 Repeatability (a) and reproducibility (b) for b-wave implicit time with eccentricity. Note the poorer repeatability in the superior field.

	Implicit Time		Amplitude		Scalar Prod.	Waveform
	a	b	a	b		
Cent. V Periph.	0.31(ns)	0.42(ns)	0.015(sig)	0.021(sig)	0.001(sig)	0.012(sig)
Cent. region 20 to 60	0.00(sig)	0.00(sig)	0.015(sig)	0.052(ns)	0.002(sig)	0.0063(sig)
Periph. region 20 to 60	0.051(ns)	0.05	0.048(sig)	0.072(ns)	0.04(sig)	0.035(sig)

Table 5.2 *Non-parametric wilcoxon test to identify significant variation between central and peripheral regions and between similar regions from the age groups of 20-30 and 50-60. Coding: (ns) not significant, (sig) significant.*

5.1.2. AMPLITUDE

As discussed, previously the b-wave amplitude is the most common measurement reported in the conventional full field flash ERG. The a-wave amplitude is much smaller and more difficult to measure thus care must be taken in the comparison of amplitudes. Despite this, analyses have been included even though these may have less diagnostic relevance than b-wave amplitudes.

The optic disc, as discussed in chapter 1, contains no photoreceptors and thus has no electrophysiological response. However, the optic disc is highly reflective and thus the light stimulus projected on this area will evoke a response from nearby areas of the retina due to the effects of scatter and reflection. When discussing statistical measurements in amplitude and implicit time the area of the optic disc has been excluded where appropriate. This was to minimise the statistical skew that would result from the false responses obtained from this area.

THE TOPOGRAPHICAL VARIATION OF AMPLITUDE

The topographical variation of a-wave amplitude is illustrated in figure 5.4.

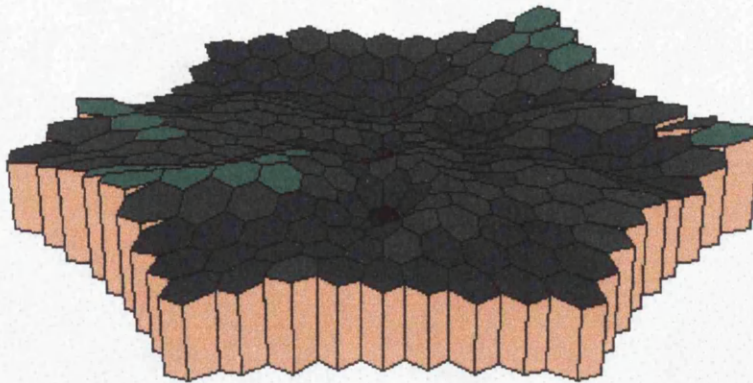


Figure 5.4 *Topographical variation of mean a-wave amplitude.*

The results indicate an asymmetrical variation between the superior and inferior regions, although the magnitude of this asymmetry should be considered along with this specific component's poorer performance in repeatability and reproducibility. The topography of b-wave amplitude is illustrated in figure 5.5

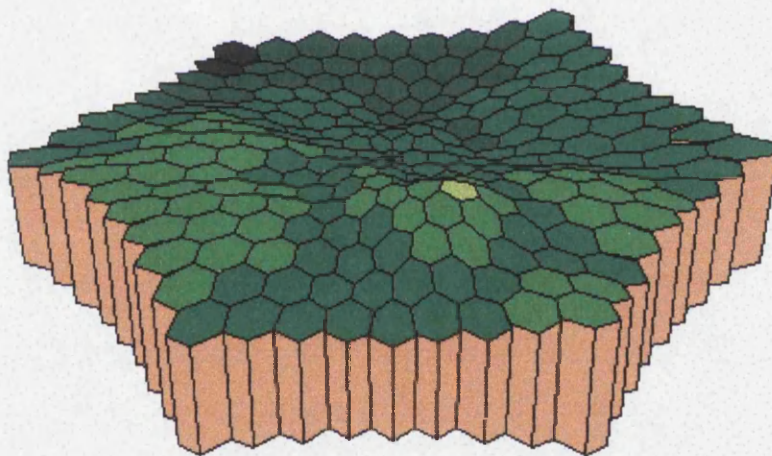


Figure 5.5 *Topographical variation of mean b-wave amplitude.*

In the same way as the a-wave amplitude, there is an asymmetrical variation between the superior and inferior regions of the field. The variation in magnitude ranged from 15nV in area 31 to 18nV in area 8. It should however be noted that these values, as with the a-wave amplitude, are dependent on the stimulus topography which is only roughly scaled with eccentricity.

AGE AND AMPLITUDE

The mean a-wave amplitude was found to vary significantly over the age groups tested. The mean value decreased slightly from the 20's to the 30's, stayed more or less constant to the 50's and then started a further decline (see table 5.3). This is also consistent with the limited data we have obtained from volunteers in their 60's, although as with a-wave implicit time the magnitude of variation is accentuated by the low signal to noise ratio.

Variation in MFERG amplitude with age			
Age group	Region	Mean a-wave amplitude (nV)	Mean b-wave amplitude (nV)
20-30	Central S/I	<i>18 / 18</i>	<i>47 / 47</i>
	Peripheral S/I	<i>14 / 16</i>	<i>34 / 38</i>
30-40	Central S/I	<i>15 / 16</i>	<i>44 / 45</i>
	Peripheral S/I	<i>13 / 15</i>	<i>32 / 38</i>
40-50	Central S/I	<i>15 / 16</i>	<i>46 / 45</i>
	Peripheral S/I	<i>12 / 14</i>	<i>31 / 37</i>
50-60	Central S/I	<i>13 / 13</i>	<i>43 / 42</i>
	Peripheral S/I	<i>12 / 13</i>	<i>30 / 32</i>

Table 5.3 *Summary of mean a-wave and b-wave amplitude measures as related to age. S/I indicates superior / inferior split in the field.*

The mean b-wave amplitude was also found to vary over the age groups tested (see table 5.3). In a similar manner to the a-wave amplitude variation, the mean value decreased slightly from the 20's to the 30's, stayed more or less constant to the 50's and then started a rapid decline. This rapid decrease can be attributed to a sensitivity loss related to age. Although we did find a nasal / temporal asymmetry in the values, this disparity is greatly exaggerated by the blind spot. Of greater interest is the superior / inferior asymmetry reported previously (Katz & Sommer 1986; Hass et al 1986; Brenton & Phelps 1986) using the results from static visual field tests. We found that a consistently lower response was obtained from the superior field

REPEATABILITY AND REPRODUCIBILITY OF AMPLITUDE

Repeatability and reproducibility of the a-wave amplitude was found to decrease with eccentricity. Coefficients of repeatability ranged from 9% in the central area to 18% in the peripheral areas (for values from grouped areas see table 5.4). Inter-subject reproducibility ranged from 14% in the central area to 26% in the peripheral area. In a similar way to a-wave implicit time variation, repeatability displayed a concentric symmetry while inter-subject reproducibility displayed a marked superior inferior asymmetry

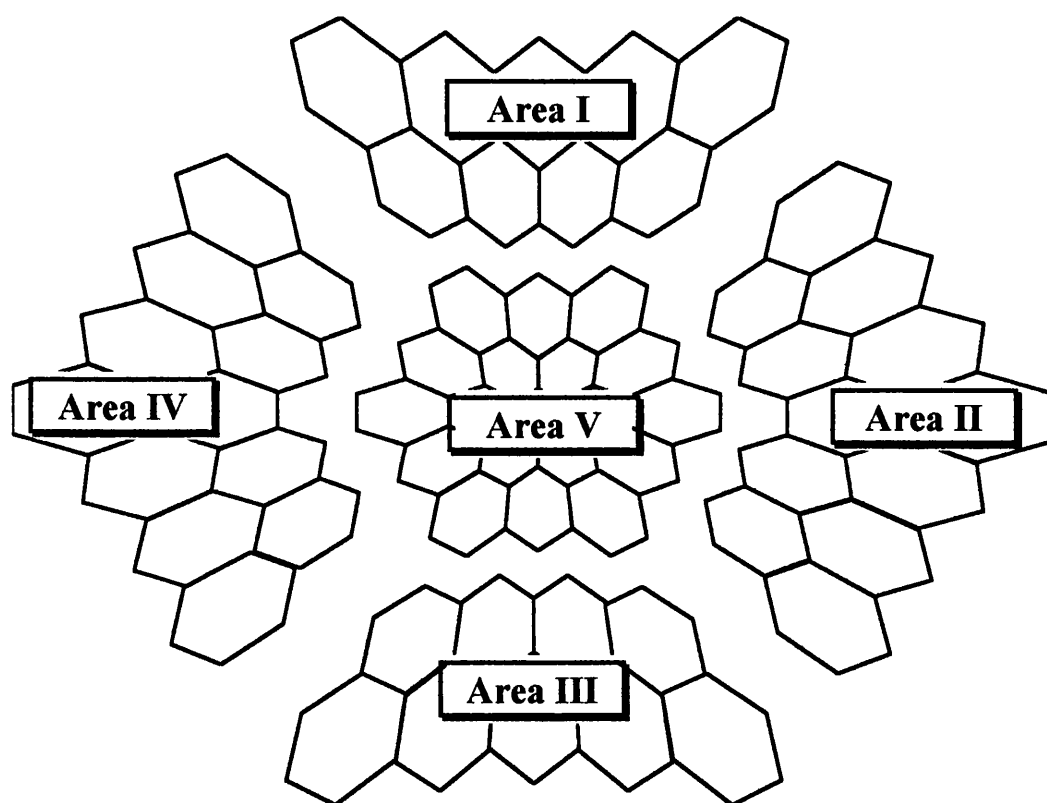


Figure 5.6 *Grouping paradigm for table 5.4*

Repeatability and reproducibility of the b-wave amplitude were also found to decrease with eccentricity. Coefficients of repeatability ranged from 12% in the central area to 17% in the peripheral areas. Inter-subject reproducibility ranged from 21% in the central area to 29% in the peripheral area. Similarly, b-wave amplitude repeatability displayed a concentric symmetry while inter-subject reproducibility displayed a marked superior inferior asymmetry

Group Area Number	I	II	III	IV	V
a-wave implicit time (ms)	17.76	17.76	16.28	17.76	16.28
<i>Intra-Subject Repeatability (%)</i>	12	12	13	13	11
<i>Inter-Subject Reproducibility (%)</i>	26	24	23	25	21
b-wave implicit time (ms)	34.04	32.56	32.56	32.56	31.08
<i>Intra-Subject Repeatability (%)</i>	13	12	9	14	14
<i>Inter-Subject Reproducibility (%)</i>	27	15	15	24	19
a-wave amplitude (nV)	14	17	16	14	14.5
<i>Intra-Subject Repeatability (%)</i>	17	15	15	14	10
<i>Inter-Subject Reproducibility (%)</i>	22	15	19	18	15
b-wave amplitude (nV)	35	42	38	33	36
<i>Intra-Subject Repeatability (%)</i>	15	14	14	15	14
<i>Inter-Subject Reproducibility (%)</i>	28	25	26	24	22
Scalar Product (nV/degree²)	13	14	17	18	35.5
<i>Intra-Subject Repeatability (%)</i>	13	14	14	12	9
<i>Inter-Subject Reproducibility (%)</i>	27	24	19	15	15

Table 5.4 Mean values for grouped areas and their respective intra- and inter-subject repeatability. Note ms are in increments of 1.48ms, this is due to the sampling resolution.

5.1.3. SCALAR PRODUCT

As discussed in Chapter 3 (section 3.2.6) the Scalar Product is a new method for combining features of the conventional ERG. It is dependent on an ideal template (recording) from which is derived an estimation of variance of each individual area from this ideal response. This, as discussed, provides a more accurate representation of each stimulated area's deviation from the normal population than the more direct features of the ERG components, latency and amplitude, discussed previously. All these measures have their advantages and disadvantages (see the end of this section). This section assesses the repeatability, reproducibility and variation of the scalar product with age.

THE TOPOGRAPHY OF THE SCALAR PRODUCT

The normal topographical variation of the scalar product is illustrated in figure 5.7.

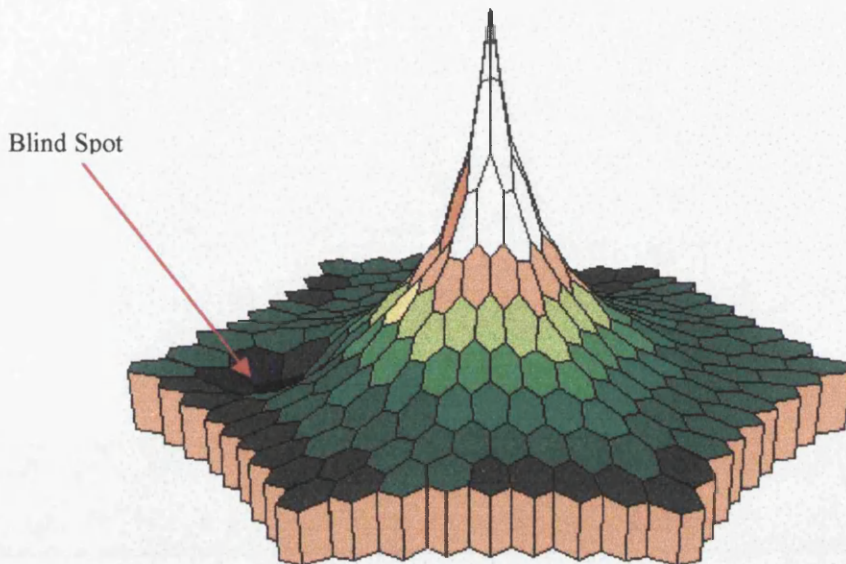


Figure 5.7 *Normal topographical variation of mean scalar product value (left eye)*

Results, as with our previous findings on amplitude variation, indicate a subtle asymmetrical variation both nasal/temporal and superior/inferior. The mean variation in magnitude ranged from $75\text{nV}/\text{degree}^2$ in area 31 (central peak) to $8\text{nV}/\text{degree}^2$ in the periphery. Although it should be noted that these values, unlike amplitude, are response densities (i.e. their values are divided by the size of the area of their respective stimulus elements) and thus are no longer dependent on the stimulus topography.

AGE AND THE SCALAR PRODUCT

The scalar product was found to vary significantly over the age groups as shown in figure 5.8.

Median Values

Scalar Product

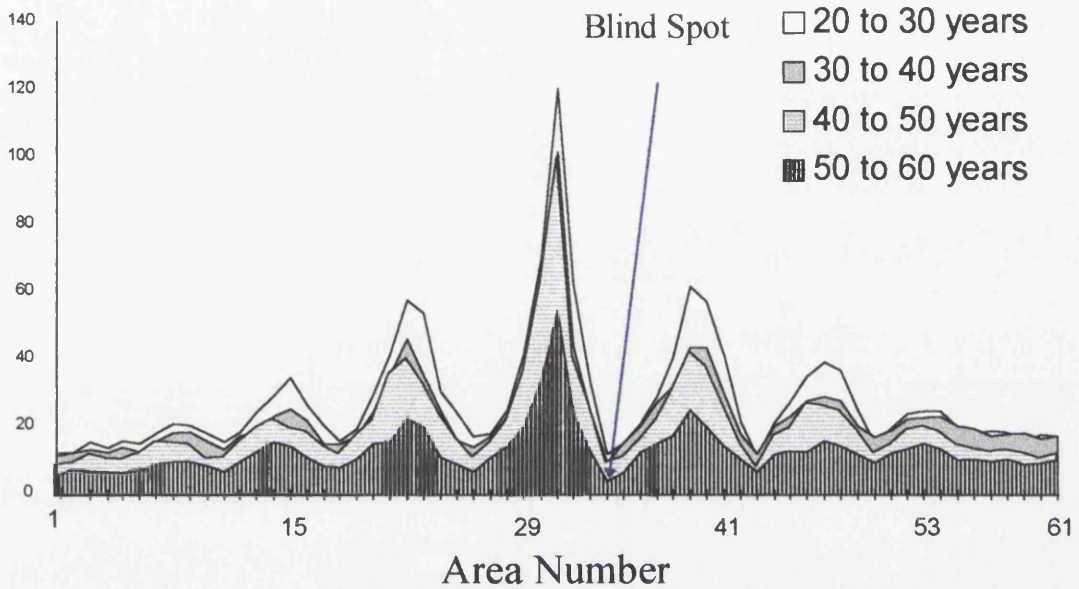


Figure 5.8 Plot of scalar product values (numbering convention defined previously – figure 4.2(a)) as a function of age. Central area 31 (fixation point) blind spot area 34. Largest age related decrease in scalar product value observed centrally. (From Parks, Keating, Evans, Williamson, Jay & Elliott; Comparison of repeatability of the multifocal ERG and Humphrey Perimeter. 1998 Documenta Ophthalmologica In Press)

In a similar manner to the variation of amplitude, the mean scalar product decreased slightly from the 20's to the 30's, stayed more or less constant to the 50's and then started a rapid decline. This rapid decrease would, due to its association with the more conventional amplitude measure, in some part be attributable to sensitivity loss as a variant with age. Although the superior / inferior asymmetry identified in the analysis of amplitude was of a greater extent, a consistently lower response was obtained from the superior field.

REPEATABILITY AND REPRODUCIBILITY OF THE SCALAR PRODUCT

Repeatability and reproducibility of the scalar product, not surprisingly since it is effectively derived from both latency and amplitude, were found also to decrease with eccentricity. Coefficients of repeatability ranged from 6.2% in the central area to 14.5% in the peripheral areas. Inter-subject reproducibility ranged from 8% in the central area to 28% in the peripheral area. As with implicit time and amplitude measures, repeatability displayed a concentric symmetry while inter-subject reproducibility displayed a marked superior inferior asymmetry. Comparison of the repeatability, both inter and intra-subject, of scalar product values with latency and amplitude variation illustrates the more consistent nature of this measurement as discussed in section 3.2.6.

The sharp fall in the median values of the scalar product in the over 50's is probably part physiological and part compliance in origin. The reduction in signal amplitude with age is consistent with previous findings on photoreceptor density and cone response as a function of age (Panda-Jonas et al 1995, Birch & Fish 1988). The inferior / superior asymmetry present in the inter-subject reproducibility can be explained in part by the consistently lower values obtained from the superior field and resulting reduction in signal to noise ratios. In addition, there appears to be a higher physiological response variation within this part of the field than is present within the lower field.

5.1.4. THE CONVENTIONAL FULL FIELD FLASH ERG

As discussed in chapter 1 the standard full field flash ERG is used routinely in the diagnosis and monitoring of retinal pathology. A full analysis of this variation within the normal population has been reported previously (Jacobi et al 1993). In order that a comparison could be made when encountering selected retinal disorders a cohort of volunteers was tested with the standard photopic flash ERG. It was decided that, given the light adapting nature of the MFERG stimulus, a photopic flash ERG would give the best comparison as the physiological site of the evoked responses from both methods would be similar. In a similar manner to

the MFERG protocol, tests were performed both dilated using a mydriatic and with natural pupils to allow a full comparison with the current International Society for Clinical Electrophysiology of Vision (ISCEV) standard (Marmor et al 1989 , Marmor & Zrenner 1995).

THE PROTOCOL

Volunteers were tested using the ISCEV protocol for full field Ganzfeld ERG's. Each subject underwent testing on four occasions. Two tests were performed with natural pupils (non-dilated) and two further tests were performed maximally dilated with 1% tropicamide (pupil diameters ranged in value from 8 to 10mm, measurements were taken at the beginning and end of each recording session).

Each subject was adapted, for a period of 10 minutes, to a background luminance of 22.6 cd/m^2 . ERG recordings were made, as with the MFERG protocol, with H-K loop electrodes. *Medicotest's* Neuroline Neurology electrodes were used for reference purposes. These electrodes were placed at the outer canthus and the indifferent electrode at the central forehead. Signals were amplified (gain 1,000; bandwidth 0.3-300 Hz). Light stimulation was generated by a xenon flash. The stimulus intensity was measured at $2.62 \text{ cd}\cdot\text{s/m}^2$.

THE NORMAL RANGE

The control range was established from 10 healthy volunteers (a cohort of the MFERG volunteers). For reproducibility, one repeat measurement was performed on all subjects. The amplitude measures obtained were then analysed.

RESULTS

The median, 5th and 95th percentiles of the photopic b-wave amplitudes and implicit times shown in table 5.5 illustrate the normal range of ERG response signals from dilated and natural pupils. Coefficients of reproducibility were measured at 10% for both protocols.

Comparison of b-wave normal range (amplitude measure)

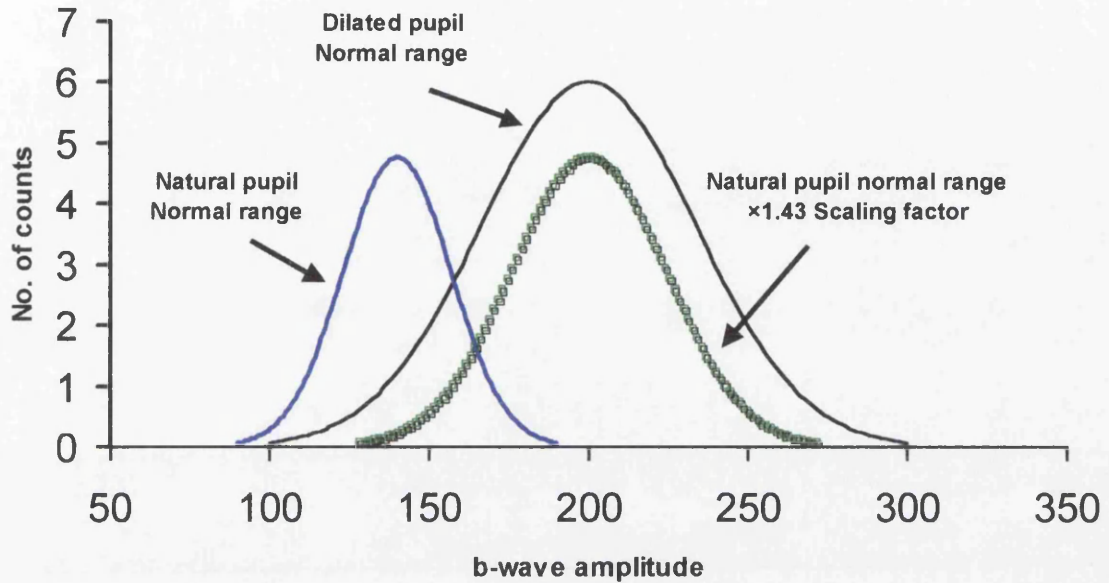


Figure 5.9 Comparison of b-wave normal range (b-wave amplitude measure). (Adapted from Parks & Keating. *Effects of dilation on the normal range in the Ganzfeld ERG. Invest Ophthalmol Vis Sci.* 1997; 38: 4094). Scaling factor (1.43) and Gaussian fit introduced for easier comparison of ranges.

	5 th	Median	95 th	Median b-wave implicit time
Dilated	143 μV	198 μV	254 μV	37ms
Natural	114 μV	146 μV	168 μV	39ms

Table 5.5 Summary of results from investigation into Photopic full field ERG.

DISCUSSION

The coefficients of reproducibility measured in this study were significantly lower than in more in-depth studies previously reported (Jacobi et al 1993). It is believed that this is probably in part due to the compliance and experience of this cohort of subjects who are familiar with these investigations. Pupil dilation led to an

increase in the spread of the normal range of the b-wave amplitude (see figure 5.9).

While these results indicate that signal amplitude is dependent on retinal illumination the findings (as to a lesser extent the previous results from experiments with pupil dilation in the MFERG) suggest that pupil dilation could have a significant effect on the normal range of the b-wave amplitude. Standardising retinal illumination by dilation, and so altering the balance of the rod/cone receptor contribution to the evoked response, may in fact accentuate inherent physiological variation and so reduce the benefits of dilation in the context of routine clinical assessment.

5.2. COMPARISON WITH CONVENTIONAL PERIMETRY

As discussed in Section 1.3 perimetry is the conventional method used to assess and quantify the depth of visual field defects. Thus any new technique must be compared to this conventional test. There are a number of publications that describe the variation of visual field data with age and population (Katz & Sommer 1986; Hass et al 1986; Brenton & Phelps 1986). However, for a scientific comparison a similar stimulus paradigm to the new technique would be required. No information is available on the conventional perimeter's repeatability and reproducibility in this context. This meant that a short study intended solely as a basis for a comparison with the new technique was necessary.

THE PROTOCOL

A custom Humphrey test chart (see figure 5.10) that stimulated 60 points corresponding to the centre of each hexagonal area within the VERIS stimulus was created. The fixation point corresponding to the additional central area stimulated in the VERIS system. The custom Humphrey test grid was designed to facilitate a simpler comparison with the stimulus topography of the MFERG. Eyes were tested monocularly with a background luminance of 31.5 Asb (10.02 cd/m^2) and stimulus intensity 3150 Abs (1002 cd/m^2). The test duration was approximately 12 minutes per eye.

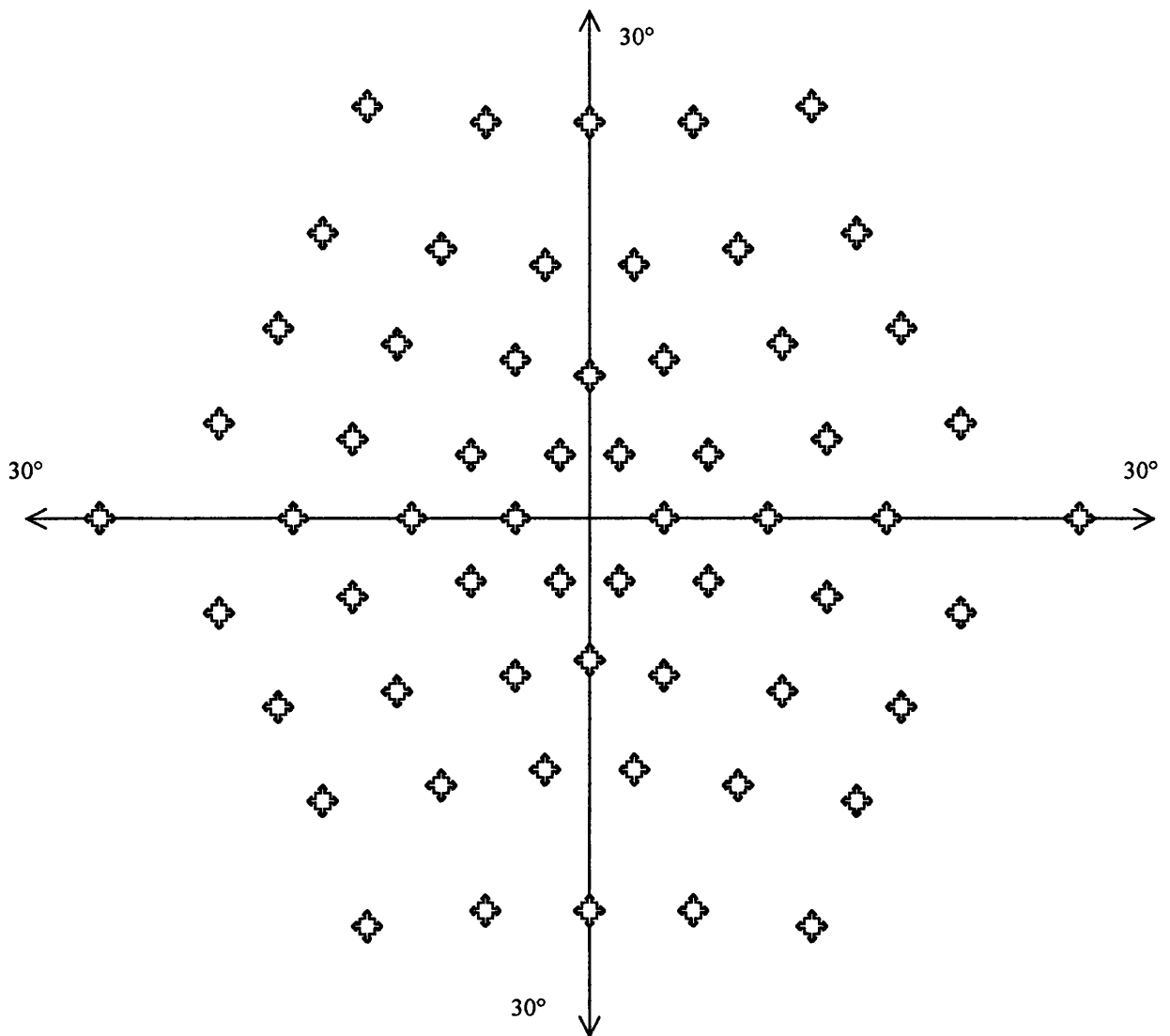


Figure 5.10 *Illustration of custom (VERIS) Full Threshold Humphrey test chart and stimulus paradigm which follows the VERIS stimulus layout.*

THE NORMAL RANGE

The control range was established from 20 healthy volunteers (a cohort of the MFERG volunteers) and included the same individuals tested previously with the full field conventional ERG. For reproducibility, repeat measurements were

performed on 10 subjects and for repeatability 10 repeat measurements were performed on four volunteers. The threshold values obtained were then analysed.

RESULTS

Mean threshold values and their corresponding confidence range are plotted in figure 5.11.

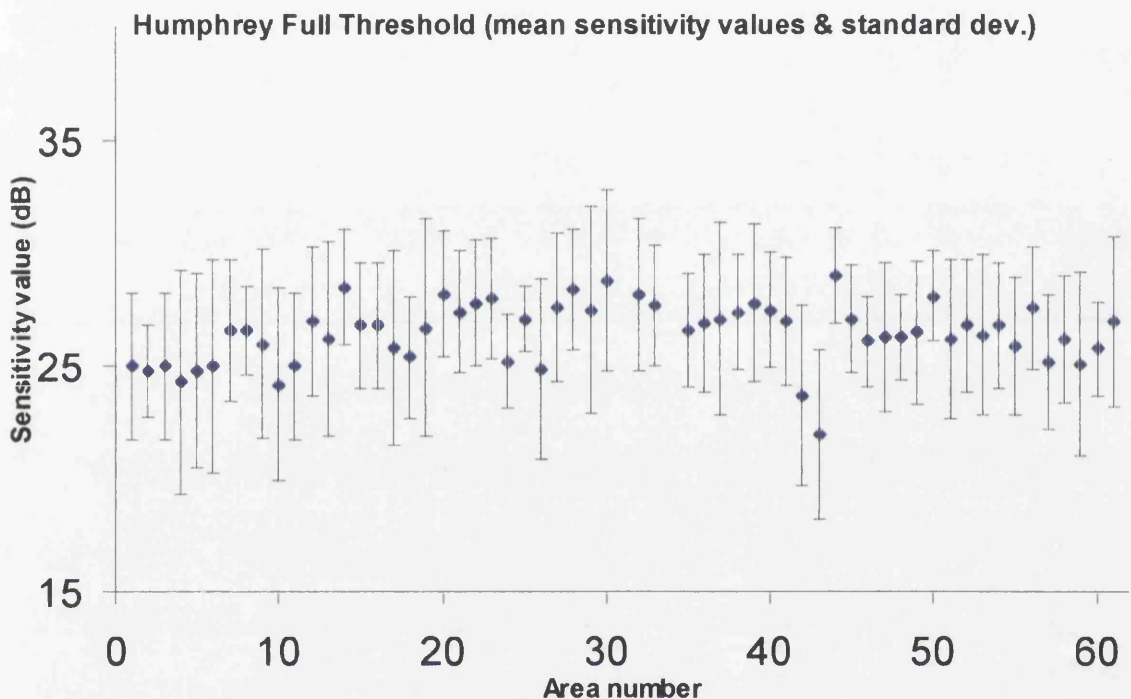


Figure 5.11 Mean sensitivity values and error (standard deviation) of custom Humphrey test on right eye (blind spot value 34 removed). Numbering convention defined previously – figure 4.2(a).

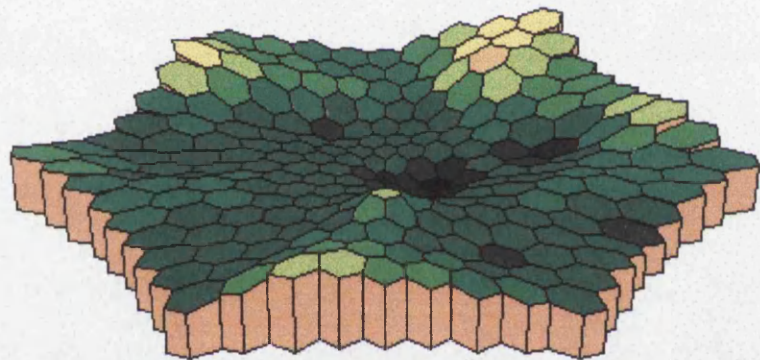
As with the multifocal technique, repeatability was found to decrease with eccentricity (coefficients of repeatability ranged from 4% in the central area to 8% in the periphery). Reproducibility exhibited a superior / inferior asymmetry and intra-subject repeatability displayed a concentric symmetry; table 5.6 summarises repeatability for grouped regions.

Group Area Number	I	II	III	IV	V
Intra-Subject Repeatability (%)	7	7	6	6	4
Inter-Subject Reproducibility (%)	16	11	7	8	6

Table 5.6 *Intra- and inter-subject repeatability for custom full threshold Humphrey field test. Grouped regions previously defined – figure 5.6.*

Figure 5.12 (a) and (b) is an interpolation plot of the topographical variation of Humphrey repeatability and reproducibility values across the visual field.

(a) Inter-subject repeatability



(b) Intra-subject reproducibility

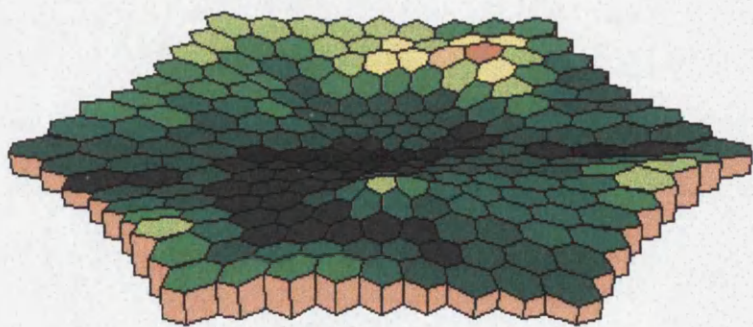


Figure 5.12 *Plots indicate topographical variation of (a) repeatability and (b) reproducibility of full threshold Humphrey perimeter test. Note central area (fixation light) is the mean of neighbouring areas.*

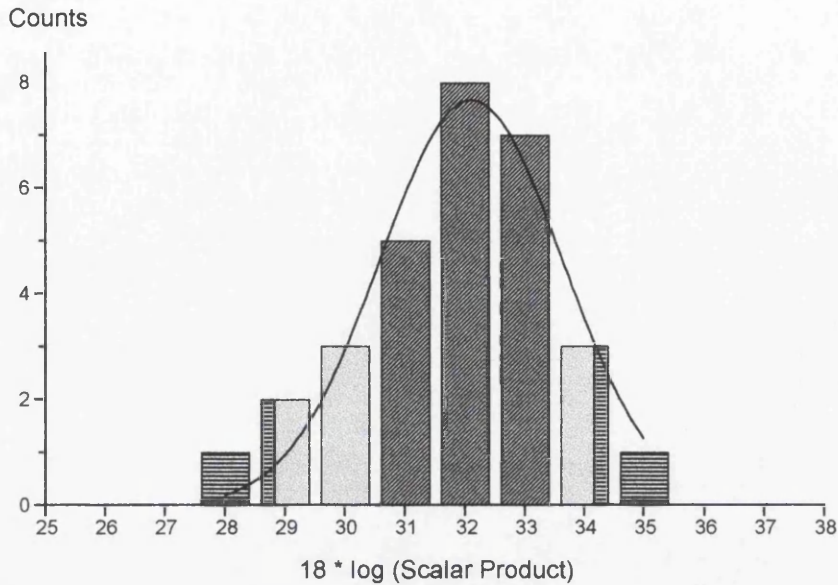
This is consistent with the limited data available on the repeatability of the perimetric field tests (Katz & Sommer 1986; Hass et al 1986; Brenton & Phelps 1986).

DISCUSSION

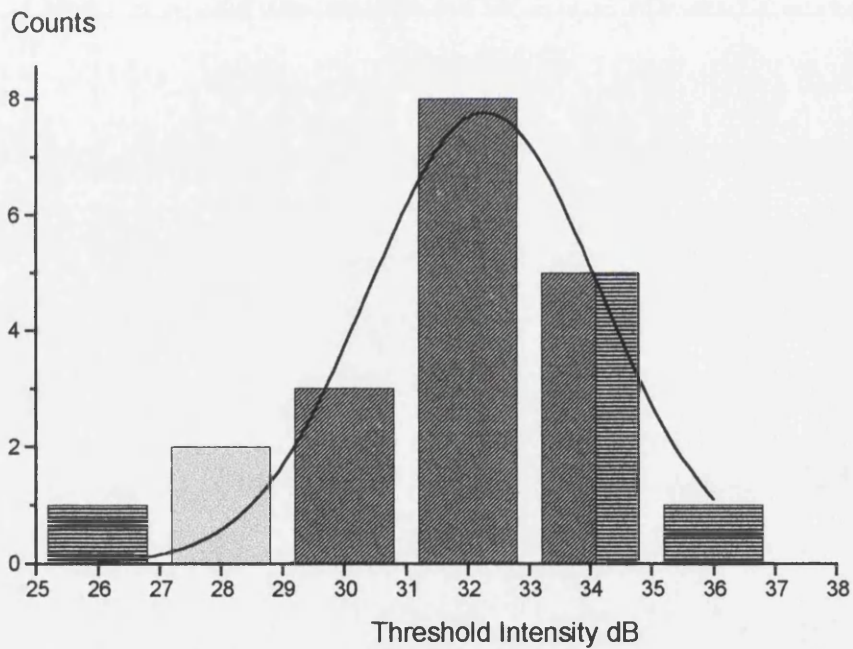
At first sight it would seem from this direct comparison of repeatability coefficients that Perimetry is more advantageous for routine population assessment of visual loss than the Multifocal Technique. However, it is important to consider these coefficients relative to the normal age matched range of values. The scalar product values are a continuous linear representation of ERG function over an area. The Humphrey Perimeter represents this visual function in a discrete logarithmic range measured at a specific retinal location. To allow a clearer analysis between these techniques it is necessary to compare their normal range on the same logarithmic scale. Figure 5.13 illustrates the normal range corresponding from a typical area (area 32) for both VERIS and the Humphrey Perimeter. Repeatability is also represented on the same diagrams. This repeatability analysis illustrates the change required in a measured result to be considered significant in both tests.

An examination of the relationship between repeatability and the normal range indicates how the variation of the system influences the population spread. The smaller the repeatability in comparison to the normal range, the less variation within the system is influencing the range. In addition, the spread of the normal range gives a direct indication of inter-individual response variation. Given the results shown in figure 5.13, the multifocal technique appears to have a smaller normal range and consequently a lower inter-individual response variation than Humphrey perimeter values. The normal range over discrete age groups and their respective confidence intervals were incorporated in the original software to enable the statistical qualification of localised retinal defects. This is the subject of the following section.

 5th, 95th Percentile
  Repeatability



(a)



(b)

Figure 5.13 *Repeatability and the normal range, including 5th and 95th percentiles in logarithmic scales, for area 32 in (a) the VERIS system. (b) the Humphrey perimeter (1dB increase indicates a 26% drop in intensity). (Adapted from Parks, Keating, Evans, Williamson, Jay & Elliott; Comparison of repeatability of the multifocal ERG and Humphrey Perimeter. 1998 Documenta Ophthalmologica In Press). Solid line indicates best Gaussian fit to histographic data.*

5.3. CONCLUSIONS

This chapter described normative studies in a clinical evaluation of the VERIS system. The investigations established the topography and variability of the main components of local ERG waveforms (implicit time and amplitude) and the new response measure (scalar product) across the 30 degree field.

Implicit times of the main components of the local ERG were found to vary little either across the retina or between age groups. Repeatability and reproducibility of implicit time did however vary across the retina with central areas less variable than peripheral regions. Repeatability (intra-subject) was on average half as variable as (inter-subject) reproducibility.

The amplitude of the main components of the local ERG are dependent on stimulus size and so vary in accordance with the area of stimulation. This is roughly scaled to reflect photoreceptor topography although some variation in amplitude between individuals was found. Repeatability and reproducibility were comparable to implicit time variation in the central regions although poorer in the peripheral regions.

The scalar product measure (derived from the waveform shape) reflects photoreceptor topography since it is considered in relation to the area of retinal stimulation. Scalar product repeatability was the lowest of all measures of response variation although this was not reflected in reproducibility which was comparable to other measures.

For comparison in the future clinical investigation of the technique on retinal disorders a control range was established for the conventional full field ERG and for the current standard for visual field assessment (static perimetry).

Repeatability for the full field ERG was low in comparison to the VERIS system although this could be partially attributed to the experience of the subjects. If previous, more extensive, studies on the normative values of the full-field ERG

were taken then repeatability would be comparable between the techniques. The influence of dilation on the normal range of the full field ERG conflicted with the International Standards recommendations that pupils should be maximally dilated prior to testing. Although, due to dilation, a similar increase was found in the normal range of the MFERG this increase was not as great.

Investigations on the repeatability and reproducibility of the custom Humphrey field test indicated that the variation of MFERG responses was comparable if not superior to this custom field test.

The normative data obtained from these investigations was incorporated into custom software which was then used in the second stage of clinical evaluation to assess multifocal responses to a group of retinal disorders.

Chapter 6

CLINICAL STUDIES

This chapter describes the clinical evaluation of the VERIS system for the objective analysis of ocular electrophysiological responses. The aim of this chapter is to assess a variety of retinal disorders using the new technique. These selected retinal pathologies were chosen to examine the system's effectiveness at identifying discrete cellular abnormalities. The hereditary conditions Retinitis Pigmentosa and Autosomal Dominant Cone Dystrophy were chosen to monitor the system responses to outer retinal abnormalities (specifically photoreceptor cell dysfunction). A cohort of patients with Diabetic Retinopathy, a complication of diabetes, was tested for random localised abnormalities specifically mid retinal in origin and a second cohort with Glaucoma for inner retinal / ganglion cell dysfunction. In addition, a cohort of retinal detachment patients was tested to measure gross retinal loss in localised areas.

6.1. INTRODUCTION

The electroretinogram, as discussed in chapter 1 (section 1.4.2) represents a combination of responses from discrete cellular layers within the retina. In addition to the test's objectivity, this ability to crudely identify the physiological site of an abnormality, has been the main clinical advantage of the standard ERG over subjective perimetry and has greatly improved diagnostic accuracy in clinical practice.

It would be desirable if any new technique, such as the MFERG, that aims to improve the spatial resolution of the electroretinogram (in an attempt to provide a topographical record of cellular sensitivity) retained this ability of conventional electrophysiology to detect retinal pathology from discrete cellular sites.

In order to test VERIS and its potential within the clinical setting, several retinal disorders were investigated. These retinal abnormalities were chosen specifically for the selective cellular site of their pathology.

REPORTING CONVENTION

As discussed in the previous section the MFERG generates a large volume of data. This is due to both the selective physiological basis of individual ERG components and the enhanced spatial resolution which separates the MFERG from conventional electrophysiology.

To facilitate a clearer analysis of the results a variety of paradigms were employed.

Confidence plots are used to illustrate deviation from normative values. These confidence plots are created from data previously established in the assessment of age grouped controls.

In conditions known to have a diffuse quasi-symmetrical retinal pathology (such as Retinitis Pigmentosa and Cone Dystrophy) the mean values for areas with concentric symmetry were calculated for central and peripheral regions. This follows the spatial grouping previously defined in chapter 4 (see figure 4.3)

An exclusion criteria was employed to reduce the occurrence of false negatives as the recording procedure is dependent on an adequate signal to noise ratio. There will always be overlap between noise and noise + signal; thus any reporting convention will be a trade off between the number of false negatives (no identification of signal) and false positives. The following selected diseased states were not only chosen for their specific cellular pathology but additionally because of the localised nature of their pathology. Thus identification of an area of retina passing the exclusion criteria would confirm the true physiological abnormality of areas with reduced signals that failed this criteria. After the analysis of responses from the normal population a value of 30nV (32nV was the lowest recorded normal response outside the blind spot area) was chosen as an appropriate cut-off value. That is if no area in the response array was found to have a b-wave amplitude measure greater than 30nV from a normal area of the retina then this indicated that the results could not be relied upon and these measurements were not incorporated within the study. Where appropriate the number of subjects who failed this selection have been documented.

The amplitudes, implicit times, and scalar products of the individual multi-focal responses were also measured and analysed using the custom software previously written (see chapter 3).

6.2 THE HEREDITARY DYSTROPHIES

Retinitis Pigmentosa and Cone Dystrophy are subgroups of the disorders known generally as retinal dystrophies. Although their commonality includes gradual photoreceptor dysfunction their pathologies and consequently their individual electrophysiological responses are distinct.

6.2.1. RETINITIS PIGMENTOSA

Retinitis Pigmentosa (RP) is the most common hereditary disorder of the retina with an incidence of 1:5,000 in the UK (Bundey & Crews 1984). It is a generic name for a group of inherited diseases. These disorders are usually characterised by night blindness and constricted visual fields. The clinical features of RP not only vary between individuals but even among family members with the disease. Typically RP is a diffuse, usually bilaterally symmetrical, retinal dystrophy. Although both cones and rods are involved, damage to the rod system is predominant. The clinical features of RP consist of a triad of symptoms: retinal pigmentation, arteriolar attenuation and a waxy disc pallor. Retinal pigmentary changes are typically perivascular and have bone-spicule appearance. Small irregular pigment spots are also frequently seen. The age of onset, the rate of progression, the amount of eventual visual loss and the presence or absence of associated ocular features are frequently related to the mode of inheritance. Although numerous subsets of the condition have been identified these, in general, can be subdivided into three main groups.

Autosomal recessive, as suggestive of the title, is the most common mode of inheritance. Of all the sporadic cases presented at specialist clinics most are probably of the recessive type. Unfortunately it is a severe form of RP with the early development and rapid progression of photoreceptor pathology, night blindness and cataract.

Autosomal dominant is the next most frequent mode of inheritance. This form of RP is usually less aggressive than its recessive cousin and so the hallmark photoreceptor pathology and consequent night blindness may not develop until adult life. Cataract may not even be a problem until the sixth decade of life.

X-linked recessive is commonly considered the most aggressive form of RP, although it is the least common mode of inheritance. The severity and the rapid progression of this disorder are similar to, and in some instances worse than, the recessive type.

The scotopic full-field ERG is the main objective clinical investigation in the diagnosis and assessment of Retinitis Pigmentosa (Berson 1993). In RP the main feature of the scotopic ERG response is a marked and significant reduction in b-wave amplitude. However, since the late sixties, reports have indicated that patients with Retinitis Pigmentosa show full-field, cone ERG's with delayed timings and reduced b-wave amplitudes (Berson et al 1969a; Berson et al 1969b; Massof et al 1986; Hood & Birch 1996a). This loss in photopic response was previously reported in conventional visual field assessments (Arden et al 1983; Yagasaki et al 1988; Massof et al 1984; Nusinowitz & Birch 1993) where photopic static visual field tests were shown to indicate losses in sensitivity among patients with RP. In addition to the information obtained from full field electrophysiology there is a requirement to establish and quantify the areas of field loss. This is usually achieved by field examinations. Thus to assess the performance of the MFERG in identifying functional change due to Retinitis Pigmentosa, it should be compared against these conventional tests.

PROTOCOL

Twenty-four patients with Retinitis Pigmentosa (12 Autosomal Recessive, 11 Autosomal Dominant and 1 X-linked recessive) were tested to investigate the MFERG responses in a condition with diffuse rod photoreceptor loss. Patients ranged in age from 26 to 68 and had no other ocular or systemic abnormalities. An additional requirement was stipulated together with the existing exclusion criteria: all participants should have normal visual fields of greater than 10 degrees. It is generally accepted that patients with a more constricted visual field than this show no significant response in the conventional electroretinogram and therefore, to provide a clearer comparison, these subjects were excluded. Furthermore, all patients had conventional full field ERG's performed and custom Humphrey (static visual fields) responses documented. MFERG examinations were repeated on 5 of the patients after a one year interval. This was to determine if the MFERG technique could detect any progression of photoreceptor loss in the more aggressive forms of this disorder.

RESULTS

Humphrey static perimetry demonstrated the hallmark constricted visual fields evident in patients with progressive Retinitis Pigmentosa (except in three patients whose field charts indicated early or mild sector Retinitis pigmentosa). Typical examples of a Humphrey visual field and a MFERG responses are shown in figure 6.1 and 6.2 respectively.

Of the twenty-four patients who underwent investigations, four were excluded because of consistent saturation (due to excessive blinking, poor fixation). A further five were not reported because of a failure to meet the previously identified exclusion criteria concerning the integrity of data (see previous section) and in one subject the system failed to save the data at the end of the recording period. Table 6.1 summarises Humphrey and full field scotopic / photopic ERG results for all patients who underwent MFERG examinations.

VERIS THRESHOLD TEST

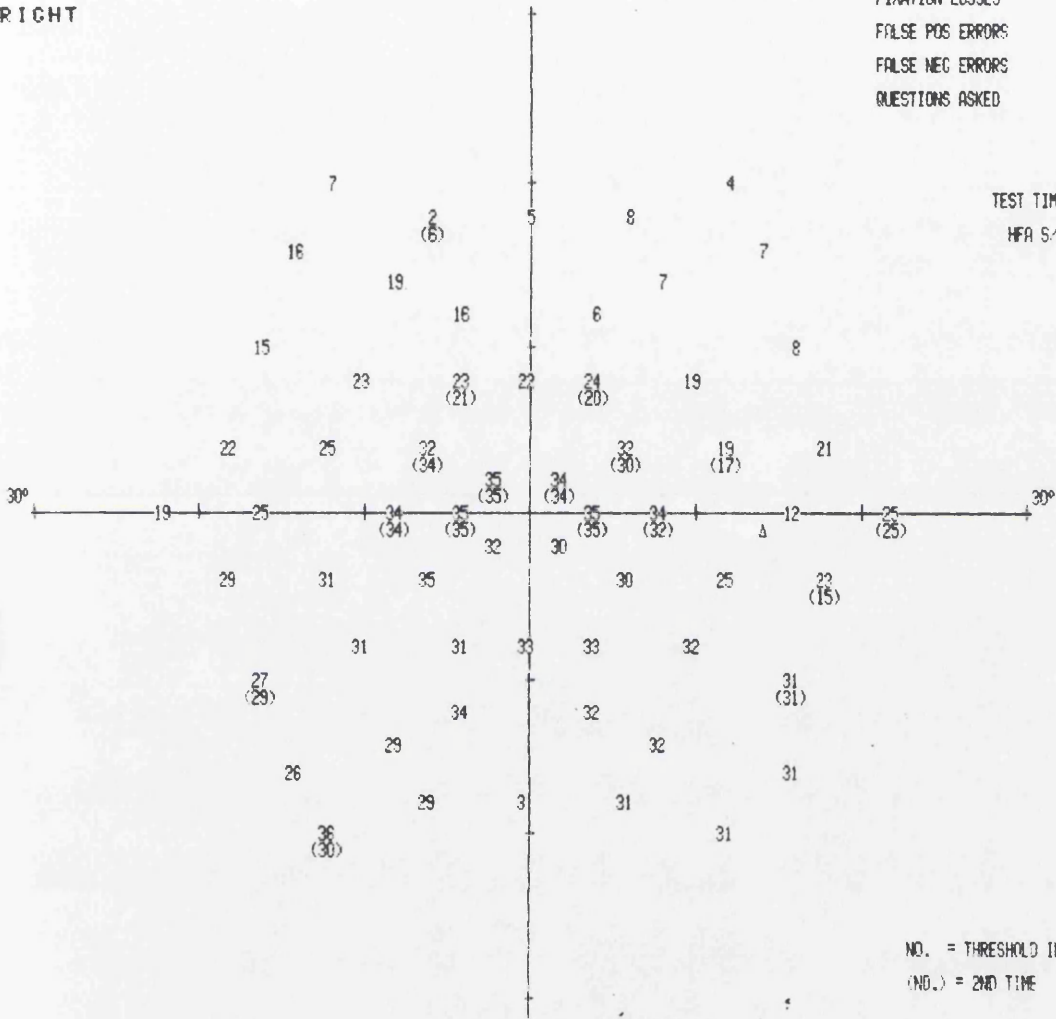
STIMULUS III, WHITE, BCKGND 31.5 ASB NAME
 BLIND SPOT CHECK SIZE III SPACING 2° ID 1
 FIXATION TARGET CENTRAL DATE
 STRATEGY FULL THRESHOLD PUPIL DIAMETER VA
 RX USED DS DCK DEG

BIRTHDATE
 TIME

RIGHT

FIXATION LOSSES 5/23 xx
 FALSE POS ERRORS 2/15
 FALSE NEG ERRORS 0/10
 QUESTIONS ASKED 454

TEST TIME 00:14:51
 HFA S/N 640-2423



NO. = THRESHOLD IN DB
 (NO.) = 2ND TIME

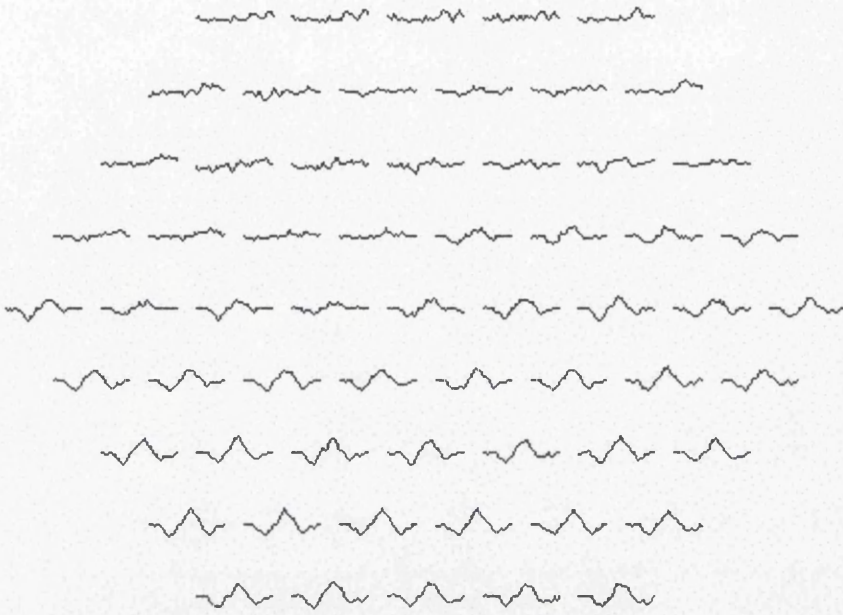
GRAYTONE SYMBOLS REV 5.3

SYM										
ASB	0.8 t _c .1	2.5 t _c 1	8 t _c 3.2	25 t _c 10	79 t _c 32	251 t _c 100	794 t _c 318	2512 t _c 1000	7943 t _c 3162	2 t _c 10000
DB	41 t _c 50	36 t _c 40	31 t _c 35	26 t _c 30	21 t _c 25	16 t _c 20	11 t _c 15	6 t _c 10	1 t _c 5	50

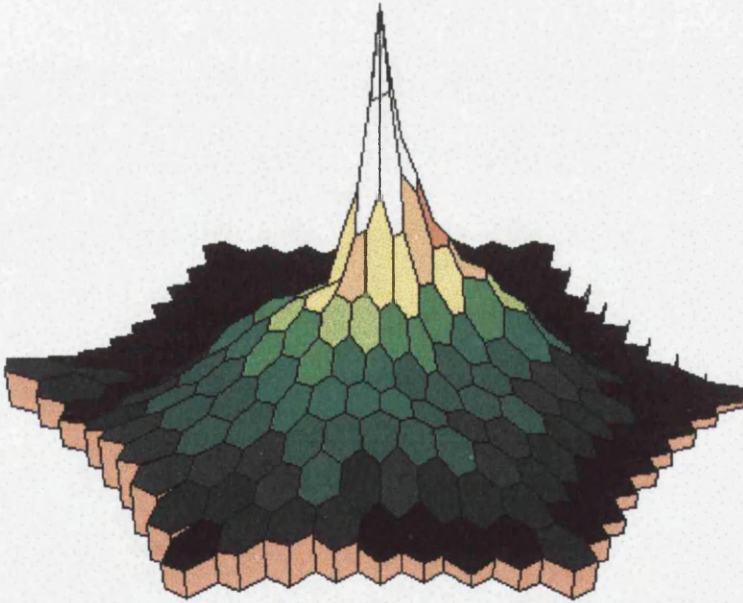
TENNENT INSTITUTE,
 C.O. WESTERN INFIRMARY
 GLASGOW
 0141-211-1769

ALLERGAN
 HUMPHREY

Figure 6.1 Custom Humphrey test chart of mild sector Retinitis Pigmentosa. Values indicate (dB) sensitivity, 0dB=3183 cd/m² 35dB=1cd/m². Values in brackets indicate second measure.



(a)



(b)

Figure 6.2 *Topographical plot of (a) multifocal responses and (b) Scalar Product values from patient with Retinitis Pigmentosa.*

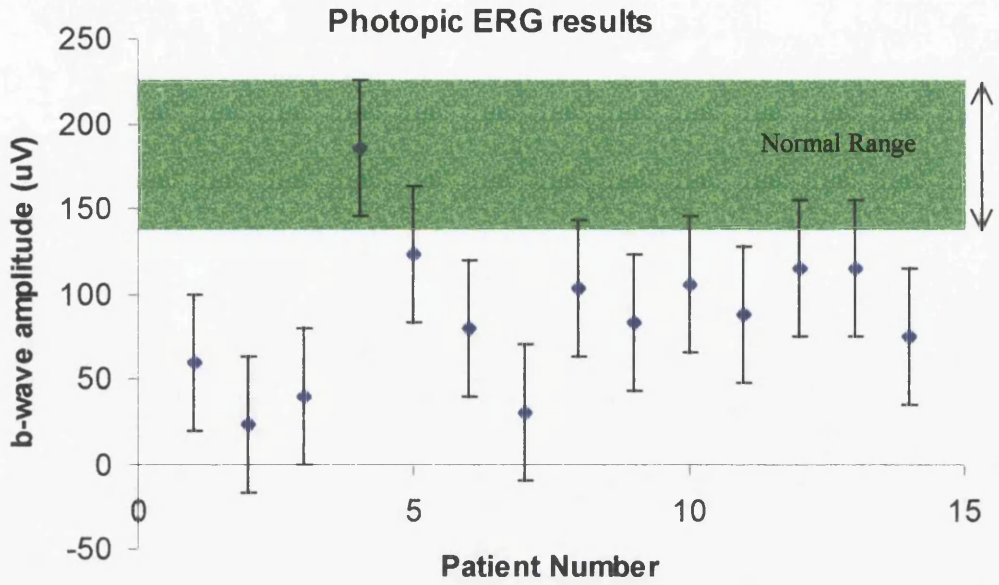
Patient	Age	Mode of Inheritance	ERG				Humphrey No. of abnormal areas
			Photopic		Scotopic		
			Amp. (μ V)	Lat. (ms)	Amp. (μ V)	Lat. (ms)	
No.1	35	AD	60	55	92.5	46	24
No.2	31	AD	22.5	59	22.5	58	38
No.3	29	AR	40	48	200	30	35
No.4	29	AD	185	45	200	32	16
No.5	30	AR	122.5	51	330	31	15
No.6	41	AD	80	53	92.5	52	17
No.7	26	AR	102.5	47	175	35	18
No.8	38	AR	30	58	105	37	29
No.9	52	AD	82.5	59	82.5	41	19
No.10	47	AD	105	41	140	36	21
No.11	59	AR	87.5	62	92.5	53	20
No.12	68	AD	115	38	550	29	21
No.13	60	AR	115	41	575	32	18
No.14	51	AD	75	49	157.5	42	34

Table 6.1 *results from scotopic ERG and Humphrey perimeter tests. Humphrey results indicate number of areas falling outside the limits determined in the previous section. AD, AR = Autosomal Dominant or Recessive.*

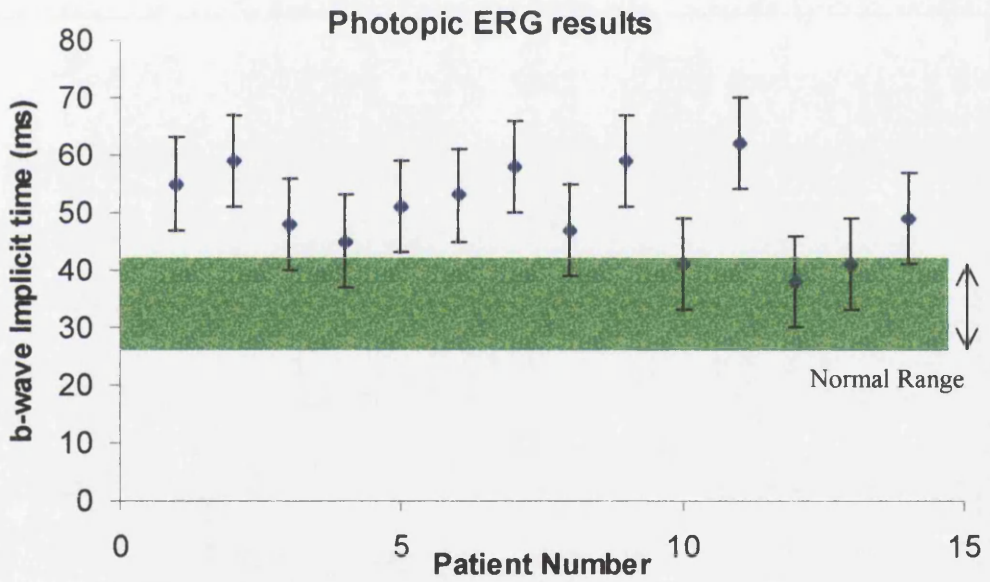
Results from all full field scotopic ERG's performed are illustrated in figure 6.3 (a) and (b). These plots illustrate the b-wave amplitude and time to peak together with their respective normal limits.

MFERG COMPARISON

As discussed previously, to evaluate the new technique in conditions of retinal pathology a quantitative comparison against existing techniques is essential. Thus results for implicit time, amplitude and scalar product measures were compared against the age matched normal range established previously. In addition custom Humphrey field results were also compared against normative data. The results from a typical example (Patient 4) are represented in confidence style plots (see figure 6.4 and 6.5 (a) and (b)). The number of areas identified as abnormal (outside a 95% confidence threshold) for each feature of the MFERG was counted and a summary of this data for all subjects is shown in table 6.2.

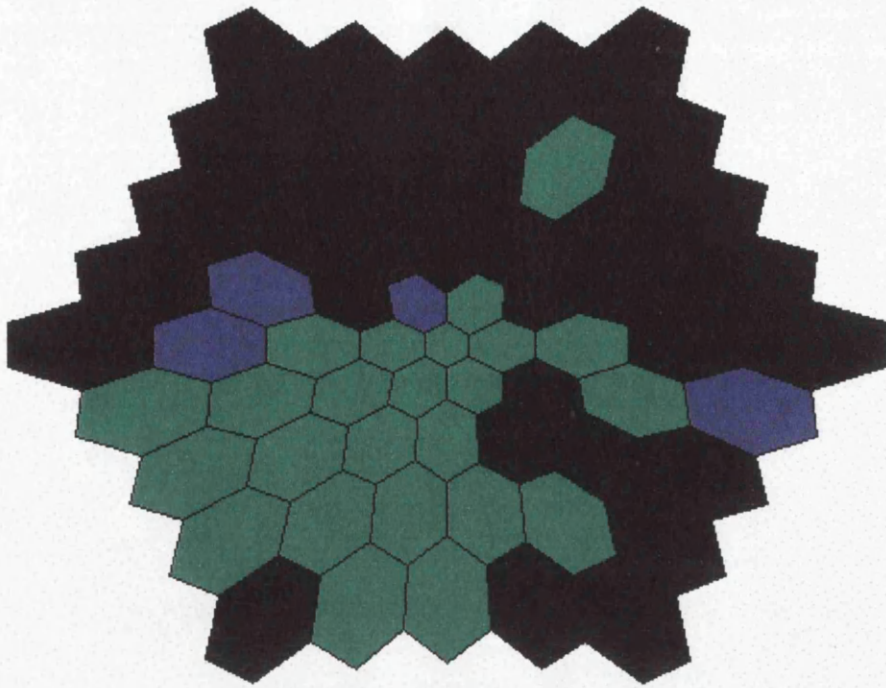


(a) Photopic b-wave amplitude and normal range in Retinitis Pigmentosa

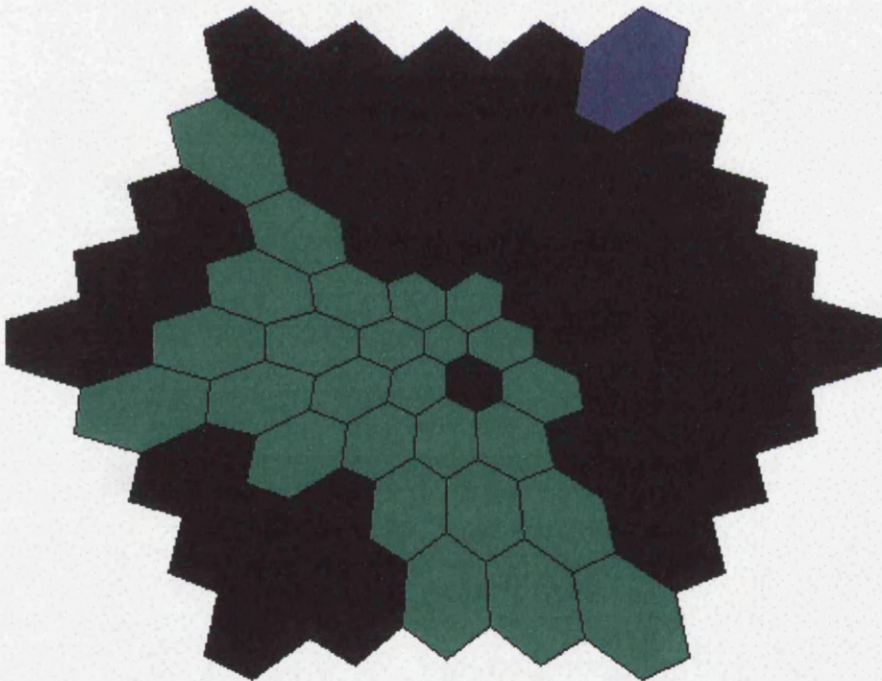


(b) Photopic b-wave Implicit time and normal range in Retinitis Pigmentosa

Figure 6.3 Scatter plot of photopic b-wave amplitude (a) and implicit time (b) in Retinitis Pigmentosa.

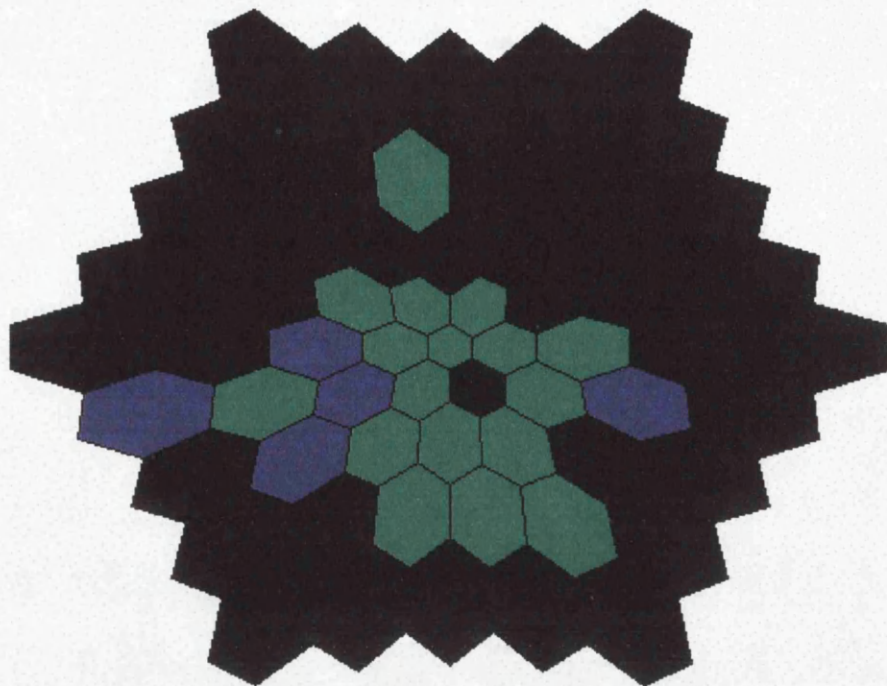


(a) *b-wave amplitude confidence plot.*

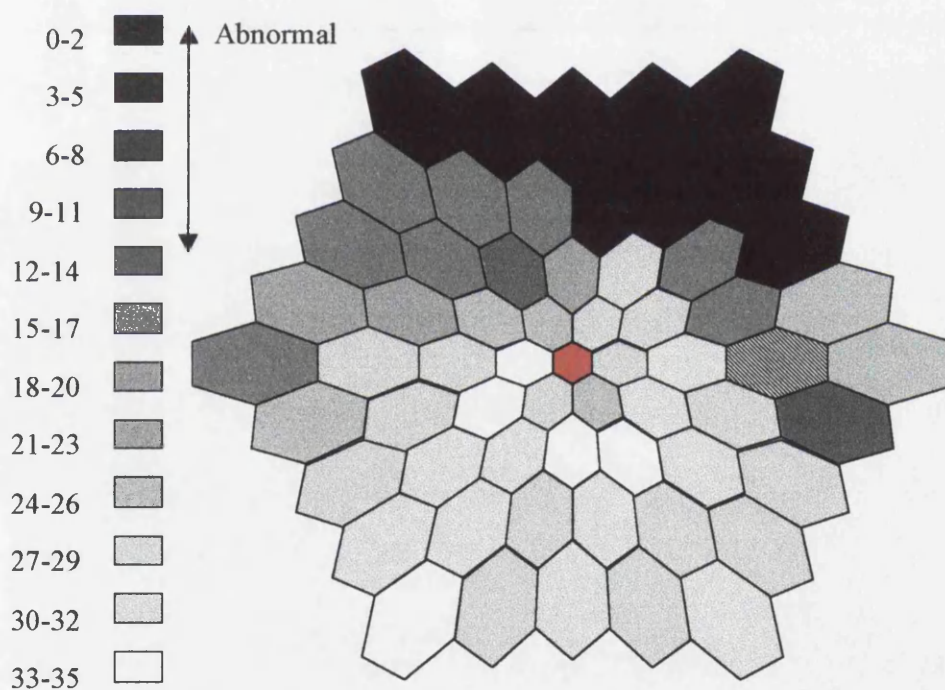


(b) *scalar product confidence plot*

Figure 6.4 *Confidence plots of (a) b-wave amplitude and (b) scalar product. Colour coding; green-normal, blue-outside 95% confidence, black-outside 99% confidence level as derived from age matched controls.*



(a) *b*-wave latency confidence plot



(b) *Custom Humphrey confidence plot*

Figure 6.5 Confidence plots of (a) *b*-wave latency and (b) Humphrey custom field chart. Colour coding for (a); green-normal, blue-outside 95% confidence, black-outside 99% confidence level as derived from age matched controls. Colour coding for (b) as indicated, hatched – blind spot, red – fixation target.

Patient	Number of abnormal areas			Humphrey
	implicit time	amplitude	scalar product	
No.1	28	35	31	24
No.2	47	51	49	38
No.3	52	48	51	35
No.4	44	37	35	16
No.5	38	29	30	15
No.6	42	25	27	17
No.7	41	38	39	29
No.8	37	42	38	18
No.9	40	35	37	19
No.10	32	28	34	21
No.11	31	35	34	20
No.12	43	34	39	21
No.13	47	38	41	18
No.14	45	41	45	34

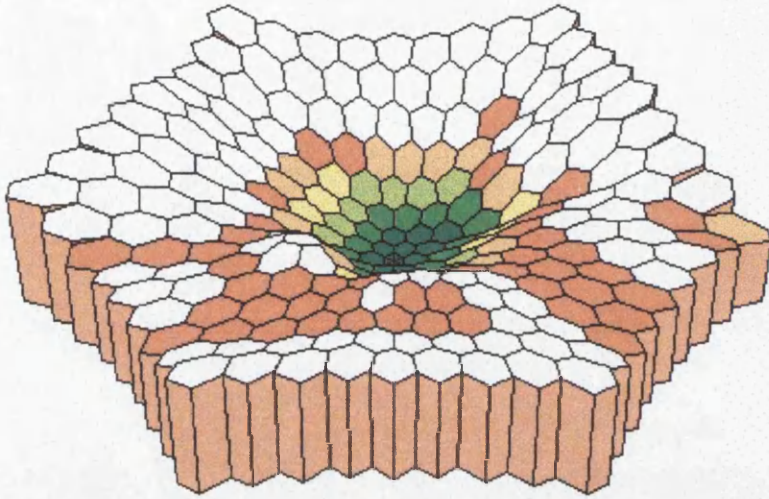
Table 6.2 *Results from assessment of responses to normative data. The values indicate the number of areas tested that fell outside the normal range.*

All plots displayed significant correlation of abnormal areas (Wilcoxon $p < 0.05$) between Humphrey field test and MFERG responses. However the number of b-wave implicit time recordings that fell outside the normal range was, on average, greater than that of other features. Figure 6.6 clearly illustrates the topographical variation of b-wave implicit time of a typical RP case (Patient 4) together with a plot of normative values. These results indicate a gross delay in implicit time of the responses.

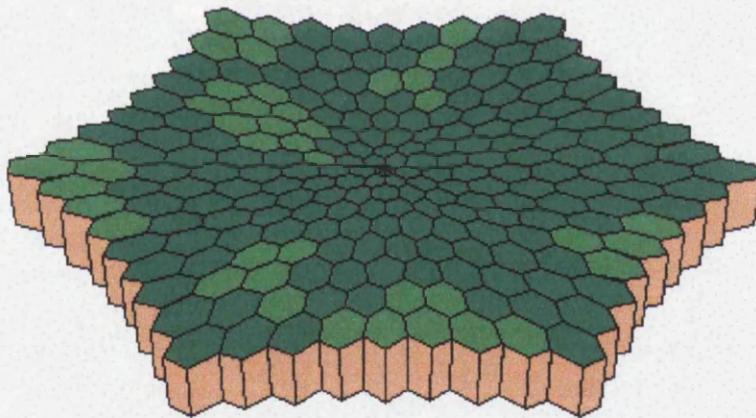
Recent research (Hood 1997b) supports these findings that gross delays in ERG timing are found in patients with RP. Given the exclusion criteria used for the selection of suitable RP patients for the trial (i.e. normal fields of at least 10 degrees) topographical monitoring of implicit time could be used to assess the progression of the condition.

To investigate the ability of temporal aspects of MFERG responses to reflect functional change within patients with retinitis pigmentosa, repeat measurements

were obtained from 5 individuals after a one-year interval. A summary of these results is shown (Table 6.3).



(a) *b-wave implicit time in typical RP.*



(b) *b-wave implicit time in control*

Figure 6.6 *Topographical variation of b-wave implicit time in (a) typical RP and (b) control. Plot (a) indicates increasing delay with eccentricity. Area coloured green represents normal values.*

Patient	First measurement		Second measurement (1 year)	
	Central area	Peripheral region	Central area	Peripheral region
No. 4	31.08	34.04	32.56	38.48
No. 7	31.08	34.04	31.08	37.00
No. 8	34.04	33.54	34.04	34.04
No. 11	32.56	33.54	34.04	34.04
No.12	32.56	32.56	34.04	34.04

Table 6.3 *Mean b-wave implicit times from central and peripheral regions before and after a one-year interval. Due to the sampling rate (1.48ms) results are in increments of these units.*

DISCUSSION

Comparison of Humphrey results and MFERG responses indicate that amplitude, implicit time and scalar product measures are all good indicators of retinal dysfunction in RP although implicit time appears to be the most sensitive measure of abnormality.

The protocol established in chapter 4 indicated that if repeat measures were to be taken then patients should be maximally dilated. However, at the onset of this study, it was not envisaged that repeat investigations would be required therefore all measurements were performed without pupil dilation.

Of the five repeat measurements taken after a one year interval four of the five showed an increase in the b-wave implicit time for peripheral areas. Of these four, two were significant (greater than two standard deviations). Over this same period little change in either response amplitude or Humphrey sensitivity values could be detected. Although these findings are from a limited data set they suggest that implicit time could be an important measure not only of the extent of retinal dysfunction but possibly an early indicator of the progression of the disorder.

It could be argued that this delay in implicit time is attributable to a change in sensitivity to light and does not reflect the underlying pathogenesis of the

disorder. However, section 4.4.3 illustrates that a delay of this magnitude cannot be achieved by a reduction in luminance alone. Thus any change in implicit time could not be attributed solely to sensitivity losses. These findings are consistent with previous studies in the full-field ERG (Berson et al 1969a; Massof et al 1986; Seiple et al 1993; Hodd & Birch 1996a) that suggest that implicit time may be a more robust measure of the retinal dysfunction associated with retinitis pigmentosa.

It should be noted that the measure of implicit time is dependent on a definitive plateau in the ERG waveform (see section 1.4.2 and section 3.2.6) and thus its measure must depend on some residual function being present. Thus implicit time could be an accurate measure of early dysfunction while amplitude reduction would be reflective of the more advanced stages of the disease.

6.2.2. CONE DYSTROPHY

In contrast to Retinitis Pigmentosa, in Cone Dystrophy inheritance is usually autosomal dominant although recessive cases have also been described. Patients with Cone Dystrophy usually present between the first and third decades of life with impairment of central vision, decreased vision in good illumination, defective colour vision, and occasionally nystagmus.

As with Retinitis Pigmentosa, Cone dystrophy primarily affects the inner retinal photoreceptors. However, unlike RP, its pathogenesis is restricted, initially, to the cone photoreceptors.

PROTOCOL

Twelve patients with autosomal dominant cone dystrophy were tested to investigate the MFERG responses in a condition with diffuse cone photoreceptor loss. Patients ranged in age from 23 to 63 and had no other ocular or systemic abnormalities. In addition, all patients had conventional full field ERG's performed and custom Humphrey full threshold (static visual fields) responses obtained.

RESULTS

Cone Dystrophy presents with marked deterioration in central acuity due to the degeneration of cone photoreceptors; this affects the accuracy of field examinations as central fixation is difficult to maintain.

The results from the static visual field tests reflected this diffuse loss of cone photoreceptors with marked losses in sensitivity of central function. A typical example of a Humphrey visual field chart of a patient with Cone Dystrophy is shown in Figure 6.7 and the MFERG responses for same subject in figure 6.8 (a) and (b). Poor fixation / nystagmus led to the exclusion of four patients from the trial. Table 6.4 summarises Humphrey and full field photopic ERG results for all patients who successfully completed the MFERG examinations.

Patient	Age	Mode of Inheritance	Photopic		Humphrey
			Amp. (uV)	Lat. (ms)	No. of abnormal areas
No.1	57	AD	131	37	11
No.2	41	-	210	36	7
No.3	35	-	175	37	5
No.4	23	-	168	36	9
No.5	29	-	195	38	4
No.6	46	-	240	39	7
No.7	63	-	158	39	5
No.8	61	-	187	38	8

Table 6.4 Results from photopic ERG and Humphrey perimeter tests. Humphrey results indicate number of areas falling outside the normal range. AD = Autosomal Dominant

MFERG Comparison

In a similar manner to the RP analysis confidence plots were obtained for features of the ERG waveform and for Humphrey field test results. A typical example of these results (Patient 1) is represented in confidence style plots (see figure 6.9 and 6.10 (a) and (b)). As with the Humphrey field chart data the number of areas identified as abnormal (outside a 95% confidence threshold) for each feature of the MFERG were counted and a summary of this data for all subjects is shown in

table 6.5. Note that only one out of the eight patients successfully tested had abnormal full field Ganzfeld ERG's.

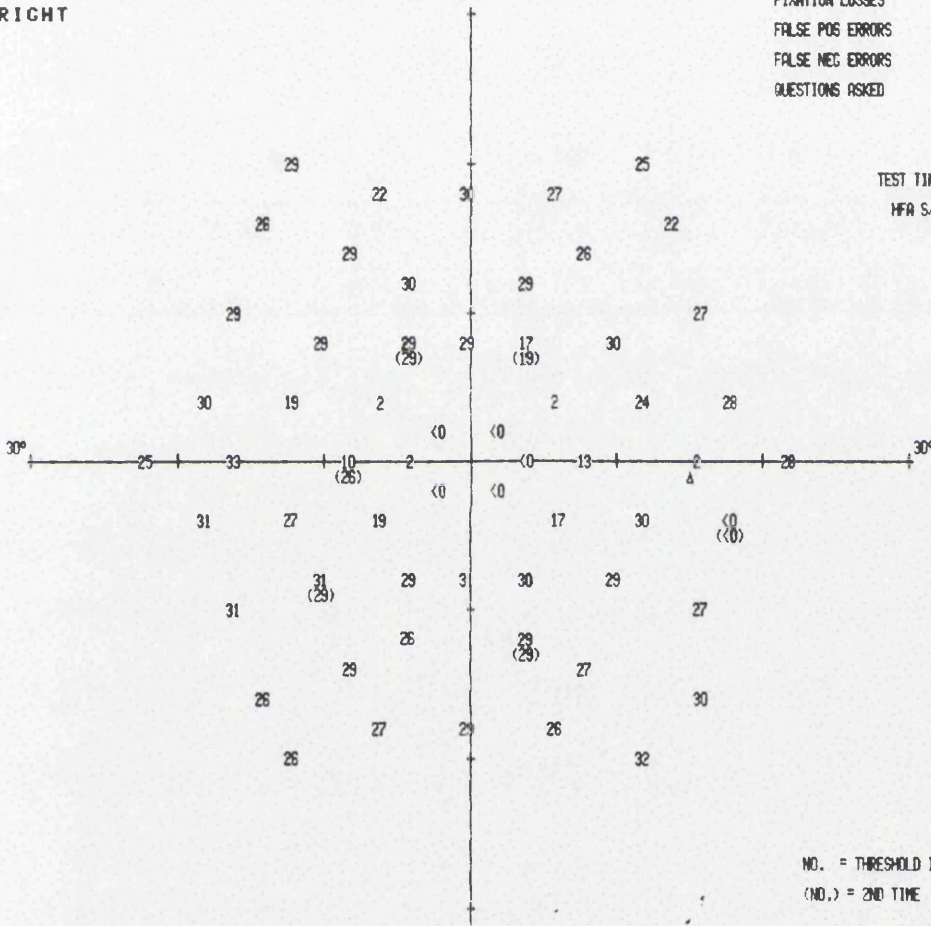
VERIS THRESHOLD TEST

STIMULUS III, WHITE, BCKGND 31.5 ASB NAME
 BLIND SPOT CHECK SIZE III SPACING 2° ID 217727
 FIXATION TARGET CENTRAL DATE TIME
 STRATEGY FULL THRESHOLD PUPIL DIAMETER VA
 RX USED DS OCK DEG

RIGHT

FIXATION LOSSES 3/19
 FALSE POS ERRORS 0/9
 FALSE NEG ERRORS 1/9
 QUESTIONS ASKED 340

TEST TIME 00:11:31
 HFA S/N 640-2423



NO. = THRESHOLD IN DB
 (NO.) = 2ND TIME

GRAYTONE SYMBOLS

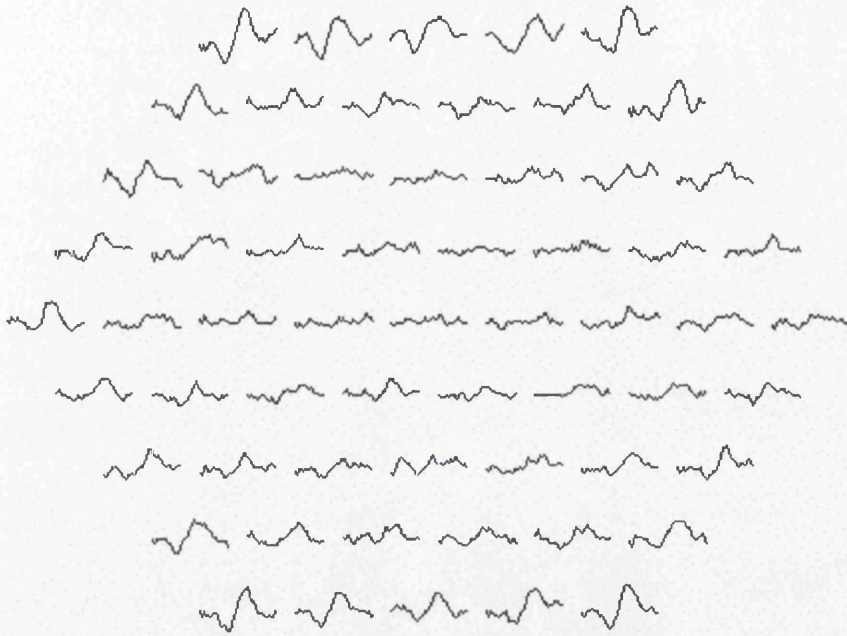
REV 5.3

SYM										
ASB	.8	2.5	8	25	79	251	794	2512	7943	2
DB	41	36	31	26	21	16	11	6	1	50

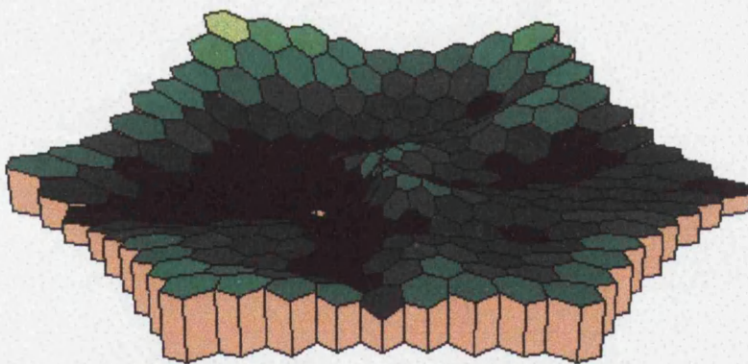
TENNENT INSTITUTE
 C.O. WESTERN INFIRMARY
 GLASGOW
 041 339 8822

ALLERGAN
 HUMPHREY

Figure 6.7 Custom Humphrey test chart of patient with cone dystrophy. Values indicate sensitivity (dB)

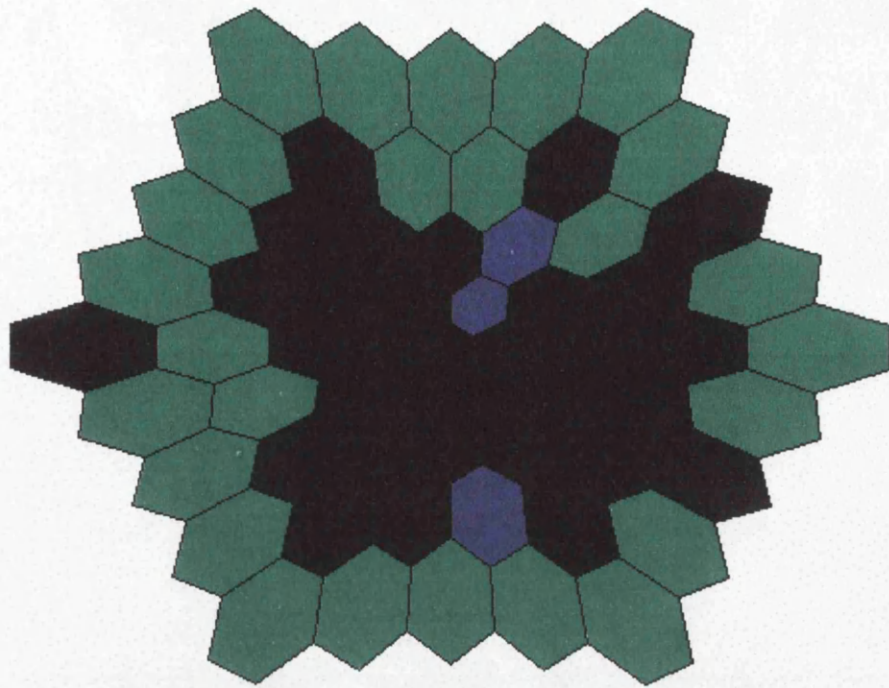


(a) MFERG waveforms from typical autosomal dominant cone dystrophy.

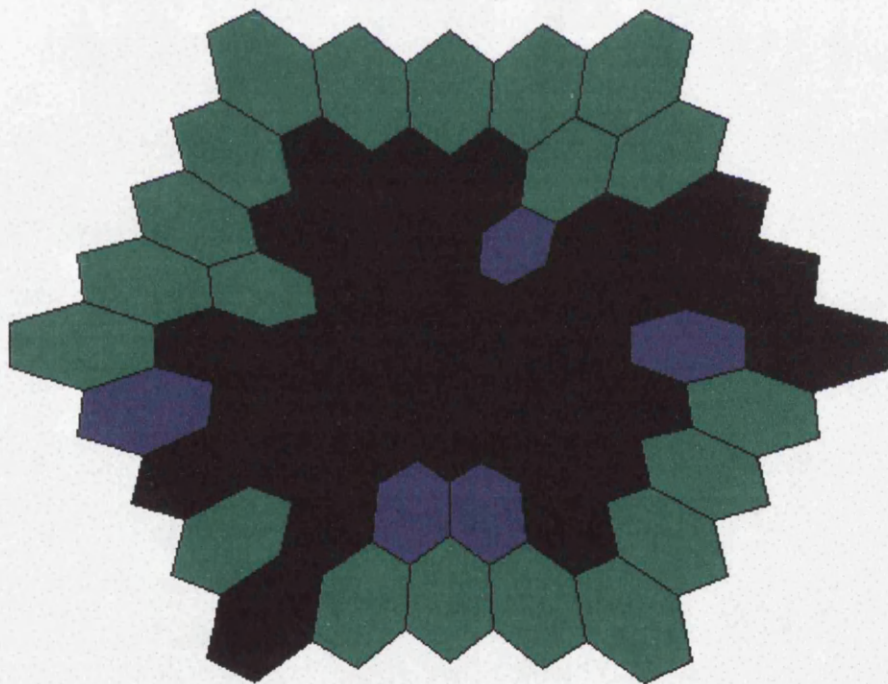


(b) MFERG Scalar product plot derived from waveform responses.

Figure 6.8 *Signal response plot (a) and derived scalar product plot (b) of typical autosomal dominant cone dystrophy.*

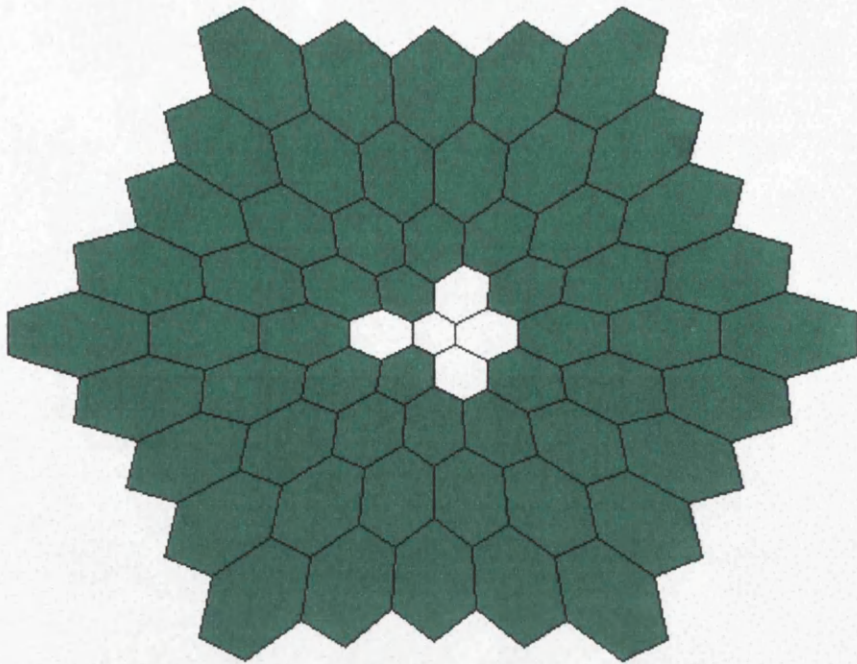


(a) *b*-wave amplitude confidence plot (cone dystrophy).

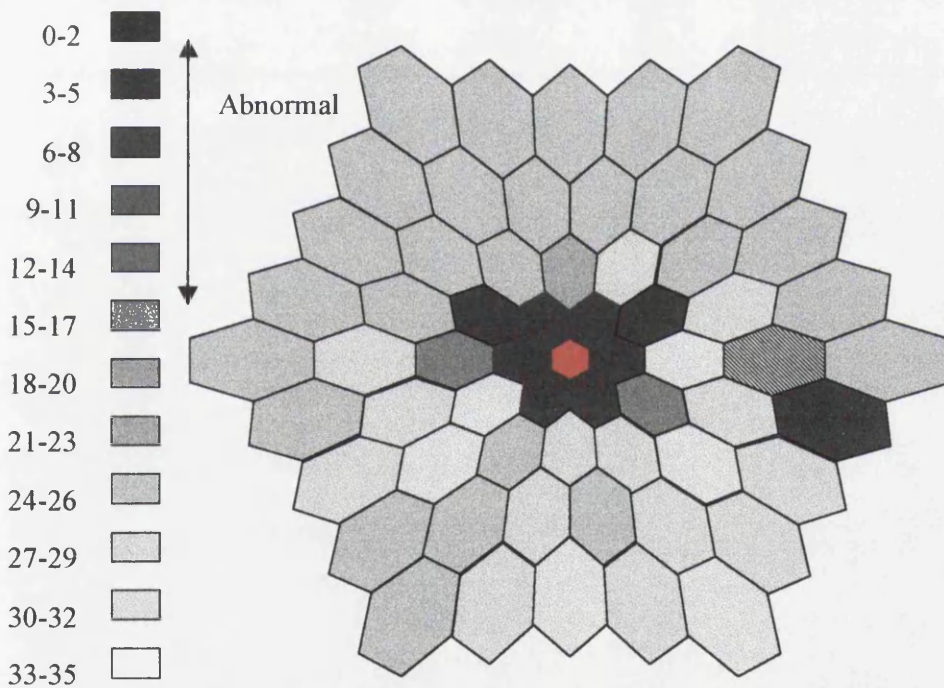


(b) *Scalar Product* confidence plot (cone dystrophy)

Figure 6.9 Confidence plots of (a) *b*-wave amplitude and (b) scalar product. Colour coding; green-normal, blue-outside 95% confidence, black-outside 99% confidence level as derived from age matched controls.



(a) *b*-wave Implicit time Confidence plot (Cone dystrophy).



(b) Humphrey visual field confidence plot (Cone dystrophy)

Figure 6.10 Confidence plots of (a) *b*-wave Implicit time and (b) Humphrey field result. Colour coding (a); white-no significant response, green-normal, blue-outside 95% confidence, black-outside 99% confidence level as derived from age matched controls. Colour coding (b) as indicated, hatched- blind spot, red fixation target.

Patient	Number. of abnormal areas			
	implicit time	amplitude	Scalar product	Humphrey
No.1	0*	31	42	14
No.2	0*	35	41	13
No.3	0*	22	24	9
No.4	1	27	28	12
No.5	0*	11	14	11
No.6	0*	14	18	15
No.7	1*	19	18	7
No.8	0*	31	41	18

Table 6.5 *Results from assessment of responses to normative data. The values indicate the number of areas tested that fell outside the normative range. *amplitude too low in central region to accurately determine latency of peak.*

The sensitivity losses apparent from the visual field charts indicate central dysfunction, which would be expected in a condition that selectively effects the cone system.

The amplitude of the MFERG waveforms was found to be markedly reduced in the central region and increased with eccentricity. The comparison with Humphrey field test sensitivity scores indicates a good correlation with areas of sensitivity loss. Scalar product values were also reflective of this central sensitivity loss.

Implicit time values were difficult to measure in the central region, because the amplitudes were low. However in the outer regions, where measurements could be made, little deviation from normal was found.

DISCUSSION

In contrast to results from the previous investigation of retinitis pigmentosa, amplitude and implicit time gave different indications on the abnormality of a local region. This is probably in part due to the selective nature of the stimulus in the MFERG. The stimulus topography, intensity and rate of stimulation all equip

the VERIS system to reflect cone dominated responses. It should be no surprise that cone dysfunction is reflected in the amplitude of evoked responses. However, it is unclear why implicit time values in cone dystrophy patients should be unaffected in contrast to those of retinitis pigmentosa sufferers. This may be due to the difference in pathogenesis of these dystrophies. If the pathology of cone dystrophy is diffuse, as is believed, then this contrast in the timing of ERG components in these conditions indicates that rod function has a greater influence on peripheral photopic ERG responses. This may not seem that incredible since our knowledge of the topographical variation of rod and cone density indicates a variation in ratios with eccentricity. Thus this difference in photoreceptor topography may be reflected indirectly by the lack of delay in cone dystrophy. Even if this is not the case the system remains a useful tool in the analysis of the topography of their pathology.

6.3. DIABETIC RETINOPATHY

Insulin Dependent Diabetes Mellitus (IDDM) affects about 2% of the population in developed countries and 3% of the world population. After disease duration of 15 years, 97.5% of IDDM patients (diagnosed under age 30 years) have retinopathy (Klein 1984a) 23% of non-IDDM patients have retinopathy within 2 years of diagnosis and after 15 years, prevalence rises to 58-85% (Klein 1984b). In the UK, various studies estimate the prevalence of sight-threatening retinopathy at 3.5% - 9% of the diabetic population (Buxton 1991; Foulds & MacCuish 1983; Grey 1986), with an annual incidence of 1.2% - 1.5%. Diabetic retinopathy is the commonest cause of blindness in the working age population.

Diabetic retinopathy is a generalised microvascular disease that also affects the kidneys and peripheral nerves. This will usually develop within five years of the onset of the disease. As the disease progresses the damage to local areas of the retina increases, eventually leading to sight threatening ischaemia. Retinopathy in diabetes can generally be subdivided into three major groups.

Background retinopathy. This is the early stage of the condition. Its main clinical features are microaneurysms (small weakened capillary walls), intraretinal

haemorrhages (patchy leakage of the vascular contents into the retina) and exudates (accumulation of lipids and lipoproteins).

Maculopathy. This is generally a special case or later stage of the previous group where background retinopathy affects the macular region. It is further characterised into focal maculopathy (a specified central area of microvascular leakage), oedematous maculopathy (diffuse leakage from macular capillaries) and ischaemic maculopathy (capillary non-perfusion within the macula).

Proliferative retinopathy. This is the most sight threatening stage of the condition where the development of new vessels in response to capillary shutdown compromises the natural flow of blood and nutrients throughout the retina.

Although diabetic retinopathy is the most common cause of blindness in the working age population it is preventable or treatable if detected at an early stage. Treatment consists of accurate localisation of leakage by fundus fluorescein angiography followed by application of laser treatment to destroy leaking vessels. Recent evidence suggests that care should be taken in the timing of laser photocoagulation after fluorescein angiography (Parks et al 1994) because changes in the light absorption characteristics of the retina occur after injection of fluorescein.

The conventional electroretinogram has been used for some time to study patients with diabetic retinopathy (Karpe et al 1958) where a reduction in b-wave amplitude (sometimes termed 'negativity' of the ERG) is a reliable indicator of ischaemia. In addition oscillatory potentials (OPs) are reduced in amplitude and timing in the earlier stages of the disease (Yonemura et al 1962; Li et al 1995). However the practical applications of electrophysiological testing in the management of diabetic retinopathy have not been widespread and are generally isolated to retinopathy with gross ischaemia. A study was undertaken on a group of diabetic patients with known ischaemia in order to investigate the possible improvement in detection and monitoring of the condition by the new focal nature of the MFERG

PROTOCOL

Twenty-six patients with diabetic retinopathy were tested using the system in order to assess the technique's ability to detect localised areas of ischaemia specifically affecting the b-wave amplitude. Patients ranged in age from 38 to 57 and had no other ocular abnormalities. In addition, all patients underwent custom Humphrey full threshold (static visual fields) investigations.

RESULTS

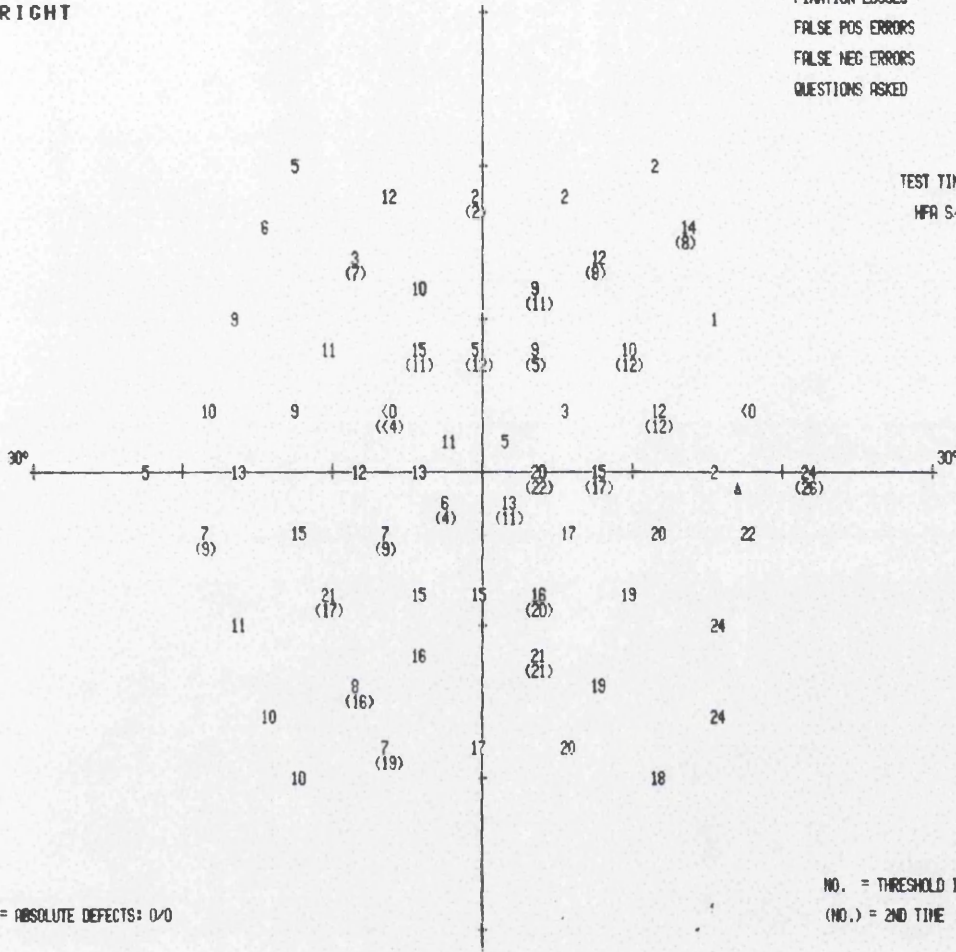
Humphrey static perimetry showed a generalised and scattered reduction in sensitivity with no defined pattern of loss between patients. A typical example of a Humphrey visual field and MFERG response is shown in figures 6.11 and 6.12 respectively. Due to the non-specific nature of retinal dysfunction the analysis of MFERG response was performed for each area individually. Of the twenty-six patients who underwent MFERG investigations, the majority (18) had their results discarded due to the poor quality of the recordings. This was mainly due to compliance problems, poor fixation, excessive blinking and general malaise.

VERIS THRESHOLD TEST

STIMULUS III, WHITE, BCKGND 31.5 ASB NAME
 BLIND SPOT CHECK SIZE III SPACING 2° ID 21181 BIRTHDATE
 FIXATION TARGET CENTRAL DATE 31-05-95 TIME 12:34:48
 STRATEGY FULL THRESHOLD PUPIL DIAMETER VA
 RX USED DS DCX DEG

FIXATION LOSSES 18/26 xx
 FALSE POS ERRORS 1/15
 FALSE NEG ERRORS 1/10
 QUESTIONS ASKED 484

RIGHT



TEST TIME 00:14:57
 HFA S/N 640-2423

■ = ABSOLUTE DEFECTS: 0/0

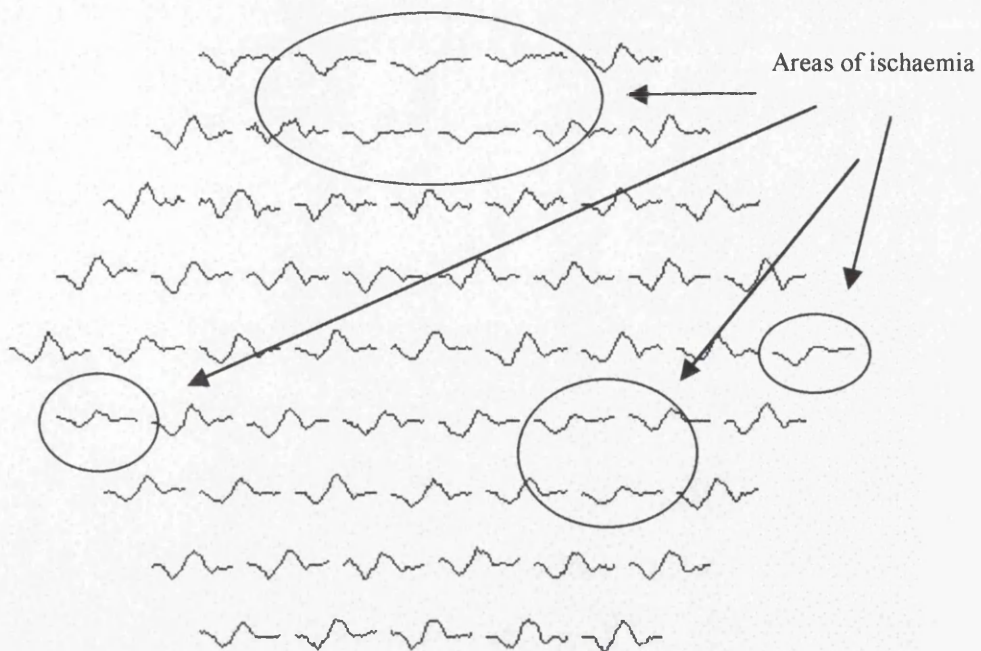
NO. = THRESHOLD IN DB
 (NO.) = 2ND TIME

	GRAYTONE SYMBOLS									REV 5.3
SYM										
ASB	.8 1	2.5 1	8 3.2	25 10	79 32	251 100	794 316	2512 1000	7943 3162	2 10000
DB	41 50	36 40	31 35	26 30	21 25	16 20	11 15	8 10	5 5	1 50

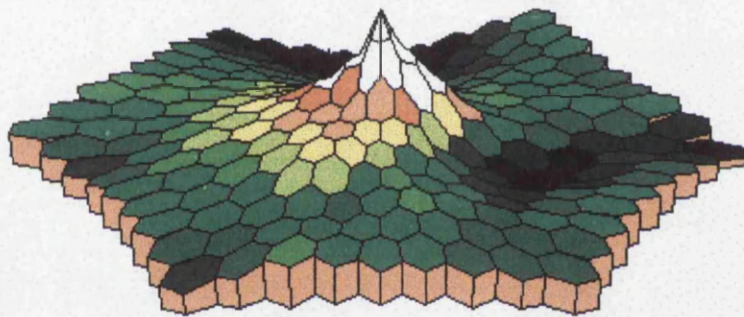
TENNENT INSTITUTE
 C.O. WESTERN INFIRMARY
 GLASGOW
 041 339 8822

ALLERGAN
HUMPHREY

Figure 6.11 Custom Humphrey field test. Values indicate photopic sensitivity (dB)



(a) Typical example of MFERG waveforms in Diabetic Retinopathy.



(b) MFERG Scalar product plot derived from waveform responses.

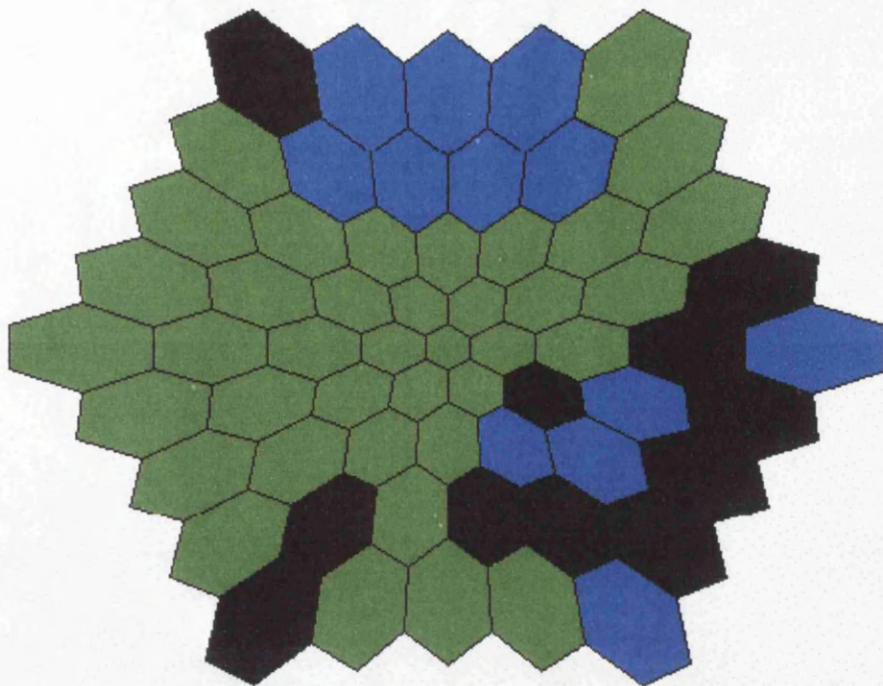
Figure 6.12 Signal response plot (a) and derived scalar product plot (b) of typical Diabetic Retinopathy. Areas of 'negativity' ischaemia indicated in (a).

A typical example of these results (Patient 3) is represented in a confidence style plots (see figure 6.13 and 6.14 (a) and (b)). As with the Humphrey field chart data the number of areas identified as abnormal (outside a 95% confidence threshold) for each feature of the MFERG were counted and a summary of this data for all subjects is shown in table 6.6.

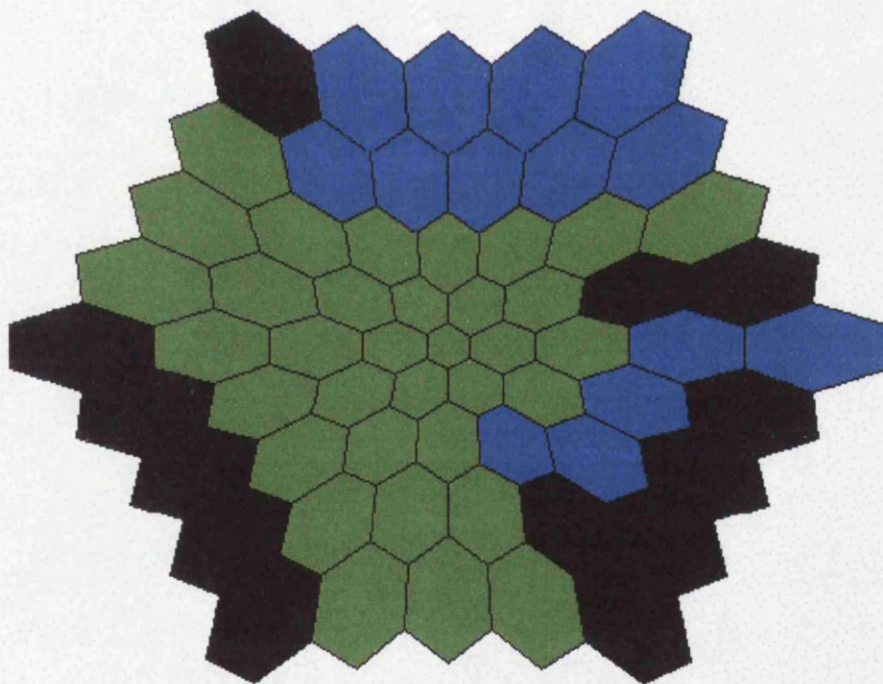
Patient	Number. of abnormal areas			
	implicit time	Amplitude	Scalar product	Humphrey
<i>No.1</i>	16	15	11	17
<i>No.2</i>	21	16	21	14
<i>No.3</i>	15	12	14	18
<i>No.4</i>	17	14	19	13
<i>No.5</i>	11	12	10	7
<i>No.6</i>	18	14	16	9
<i>No.7</i>	23	21	19	13
<i>No.8</i>	17	19	21	21

Table 6.6 *Results from assessment of responses to normative data. The values indicate the number of areas tested that fell outside the normal range.*

The amplitude of the local ERG waveforms reflected the scattered nature of the sensitivity losses indicated from Humphrey field perimetry. Areas of localised negativity (reduction in b-wave amplitude) correlated well (Wilcoxon $p < 0.05$) with reduced sensitivity scores from perimetry.

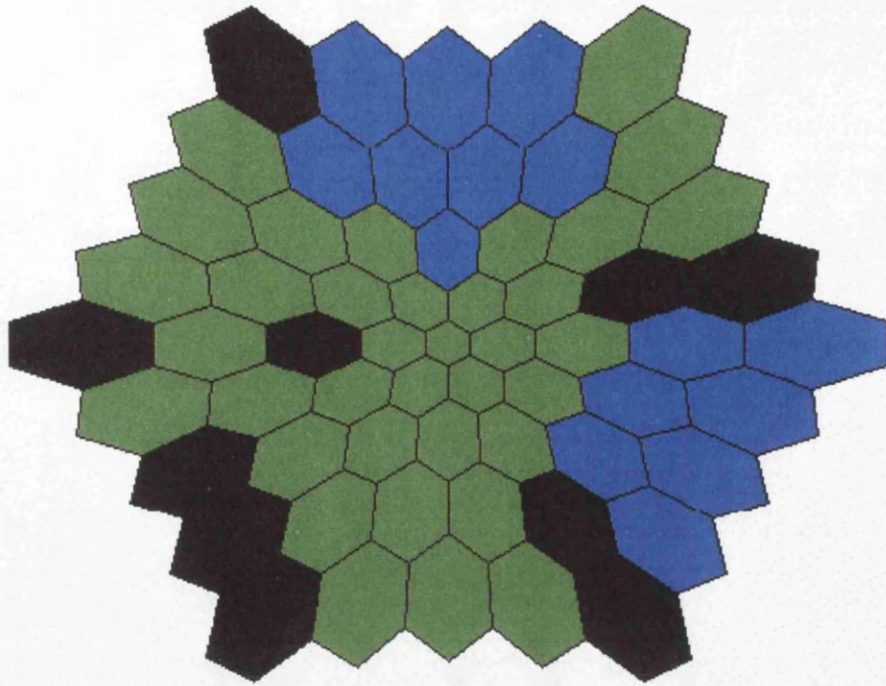


(a) *b-wave amplitude confidence plot (diabetic Retinopathy).*

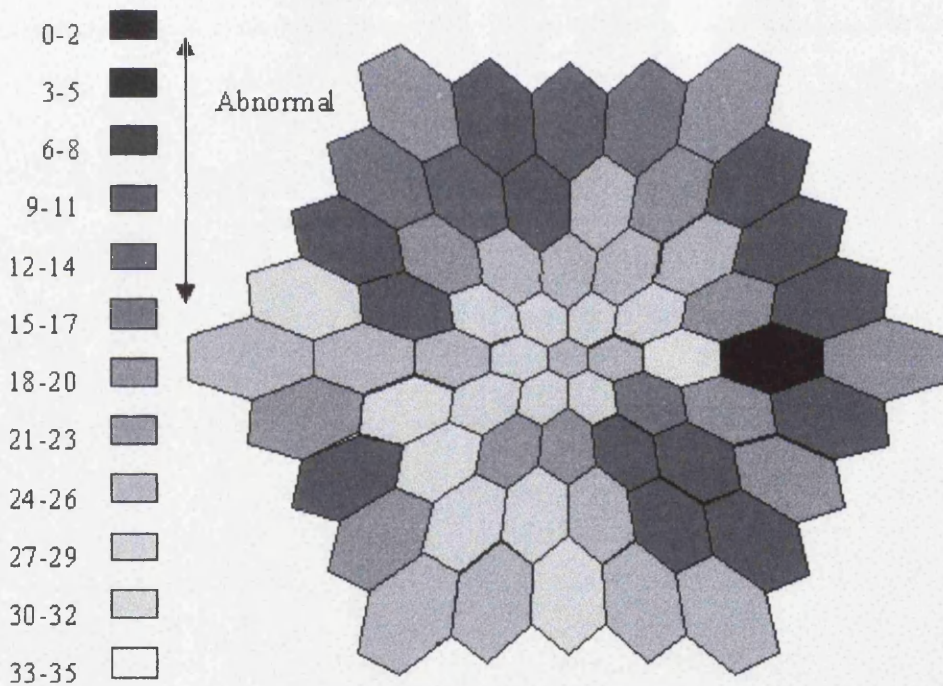


(b) *Scalar Product confidence plot (Diabetic Retinopathy)*

Figure 6.13 *Confidence plots of (a) b-wave amplitude and (b) scalar product. Colour coding; green-normal, blue-outside 95% confidence, black-outside 99% confidence level as derived from age matched controls.*



(a) *b-wave implicit time confidence plot (diabetic Retinopathy).*



(b) *Humphrey visual field confidence plot (Diabetic Retinopathy)*

Figure 6.14 *Confidence plots of (a) b-wave Implicit time and (b) Humphrey field result. Colour coding; white-no significant response, green-normal, blue-outside 95% confidence, black-outside 99% confidence level as derived from age matched controls.*

With the gross negativity associated with areas of ischaemia (see figure 6.12(a)) there was difficulty interpreting b-wave implicit times. Although b-wave amplitude values were above the exclusion criterion set the b-wave peak was markedly reduced and so implicit time measures of this feature were difficult to derive.

DISCUSSION

Ischaemia is known to affect the mid retinal layers of the retina. The negative b-wave present is quite marked in areas of localised ischaemia and thus the system would be an effective tool in the assessment and monitoring for Diabetic Retinopathy.

It is important to note here that the previous study on filter settings and their effect on MFERG responses (see chapter 4 and Keating Parks & Evans et al 1997) has a marked relevance to this pathology. Had filter settings been at the recommended 10-100 Hz these areas of ischaemia would not have been identified.

6.4. GLAUCOMA

Glaucoma is one of the most common causes of blindness in Scotland accounting for some 12% of registered blindness (Ghafoor et al 1983). Its main clinical feature apart from variably raised intraocular pressure is optic atrophy accompanied by glaucomatous cupping of the optic disc and progressive visual field loss. It is asymptomatic until advanced and, as glaucomatous damage of the optic nerve is permanent, irrecoverable loss of vision is common before the condition is diagnosed. Glaucomatous damage of the axons of the retinal ganglion cells in the optic nerve head leads to loss of these cells in the retina (Quigley et al 1989). In glaucoma, many ganglion cells have to be lost before there is an identifiable visual loss on clinical testing.

The VERIS system as discussed in chapter 3 has two modes of stimulation at its disposal to evoke responses from the inner retinal layer. Both methods of

stimulation reflect non-linearities of the derived response and both are presumed to contribute to the standard pattern ERG (PERG), discussed earlier. Although the different components of the flash ERG are now reasonably well understood, the origins of the separate components that form the PERG are still surrounded by controversy. It is believed that there are two main non-linear mechanisms reflected within the PERG, those induced by the local luminance response and non-linear mechanisms of lateral interaction, termed the pattern dependent component (Odom et al 1982; Hess & Baker 1984).

The VERIS system is well suited to separate these non-linear mechanisms because, if orthogonality is preserved, the isolation of evoked responses by cross-correlation using the m-transform should permit the extraction of higher order responses. Recent reports have suggested that these higher order components contain substantial contributions from the inner retina and have been selectively affected in optic atrophy and in early glaucoma. (Sutter 1987; Bearnse et al 1995a; Bearnse et al 1995b; Bearnse et al 1996a; Bearnse et al 1996b)

To investigate the potential for objective detection of glaucoma using the MFERG, patients previously diagnosed with Primary Open Angle Glaucoma had standard luminance MFERG and pattern reversal MFERGs performed.

PROTOCOL

Twenty patients with Primary Open Angle Glaucoma and marked field defects were tested. Eleven patients were tested with the standard luminance MFERG and eleven were tested with the pattern reversal MFERG (patients 3 and 5 had both tests performed on different occasions). Patients ranged in age from 62 to 81 and were chosen for their stable field defects and controlled intra-ocular pressure. In addition patients had custom Humphrey field tests performed.

RESULTS

Only fourteen of the twenty-two tests performed were completed successfully (8 luminance and 6 pattern). Visual field charts produced after performing

Humphrey static perimetry established the arcuate or altitudinal shape of the visual defects that had been the defining symptom for their diagnosis. A typical example of an altitudinal defect from patient 5 is shown in figure 6.15

Full-field photopic ERGs were not performed on these patients because it is well known that the inner retinal pathology associated with these defects would not be reflected in the photoreceptor dominated response from the full field ERG test.

SECOND ORDER LUMINANCE RESPONSE

The second order component from the standard multifocal luminance response was extracted. It should be noted here that, due to the reduced amplitude of higher order responses, these signals are generally of poor quality. In an attempt to improve the interpretation of these signals, areas previously identified by the Humphrey field test as abnormal were grouped together. An example of this spatial averaging from patient 5 together with a normal second order response is illustrated in figure 6.16(a) and (b).

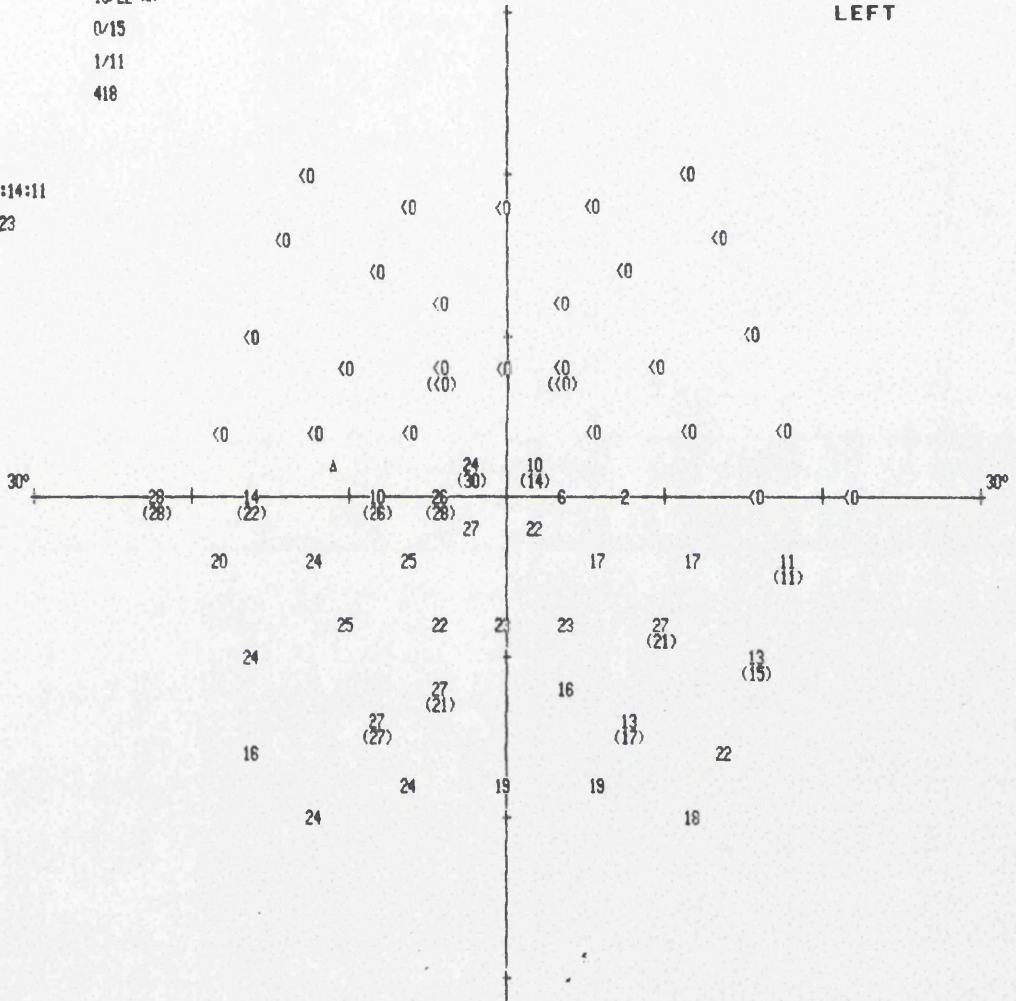
VERIS THRESHOLD TEST

STIMULUS III, WHITE, BCKGND 31.5 ASB NAME
 BLIND SPOT CHECK SIZE III SPACING 2° ID 8768 BIRTHDATE
 FIXATION TARGET CENTRAL DATE 09-06-95 TIME 11:35:52
 STRATEGY FULL THRESHOLD PUPIL DIAMETER VA
 RX USED DS DCX DEG

FIXATION LOSSES 15/22 xx
 FALSE POS ERRORS 0/15
 FALSE NEG ERRORS 1/11
 QUESTIONS ASKED 418

TEST TIME 00:14:11
 HFA S/N 640-2423

LEFT



NO. = THRESHOLD IN DB
 (NO.) = 2ND TIME

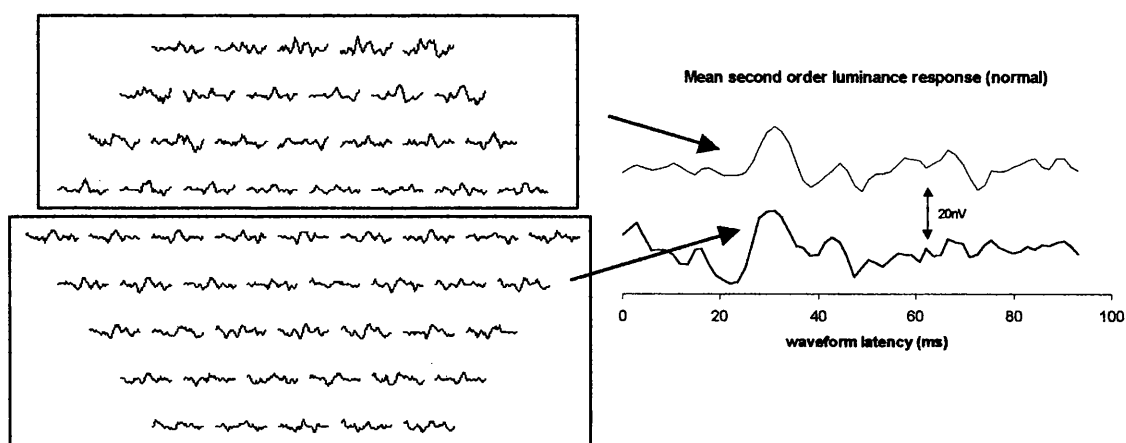
GRAYTONE SYMBOLS REV 5.3

SYM										
ASB	.8 +/- .1	2.5 +/- 1	8 +/- 3.2	25 +/- 10	79 +/- 32	251 +/- 100	794 +/- 316	2512 +/- 1000	7943 +/- 3162	2 +/- 10000
DB	41 50	36 40	31 35	26 30	21 25	16 20	11 15	8 10	5 5	1 ≤0

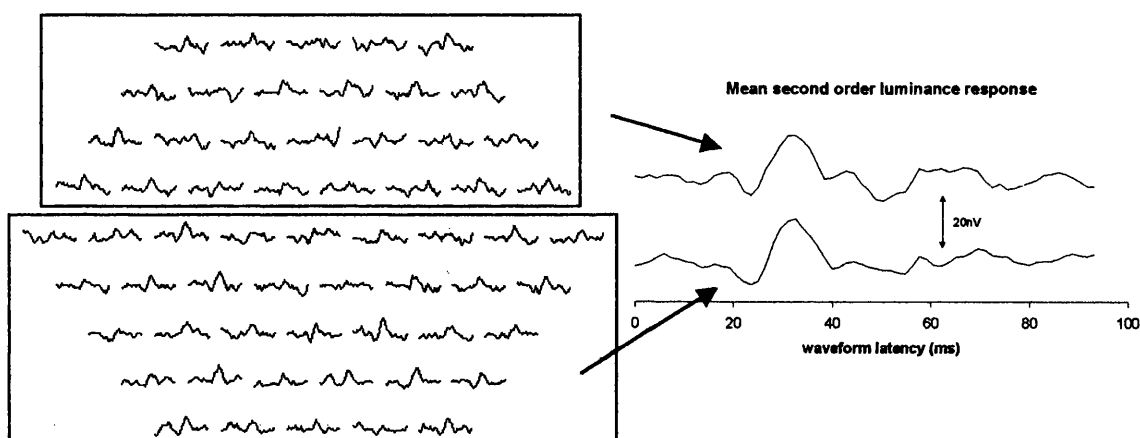
TENNENT INSTITUTE
 C.O. WESTERN INFIRMARY
 GLASGOW
 041 339 8822



Figure 6.15 Custom Humphrey field test in Primary Open Angle Glaucoma. Values indicate photopic sensitivity (dB) (patient 5)



(a) Normal multifocal second order response



(b) Multifocal second order response from patient 5.

Figure 6.16 Mean second order luminance response from superior and inferior field (a) normal control and (b) patient 5 (Primary Open Angle Glaucoma).

PATTERN DEPENDENT COMPONENT

The first order component from the multifocal pattern reversal stimulus was extracted. As little information exists for this mode of stimulation, areas established by perimetry as abnormal were grouped and compared to normal areas of retina. As with the second order luminance response signals were generally of poor quality. An example of this from patient 5, shown previously is illustrated in figure 6.17.

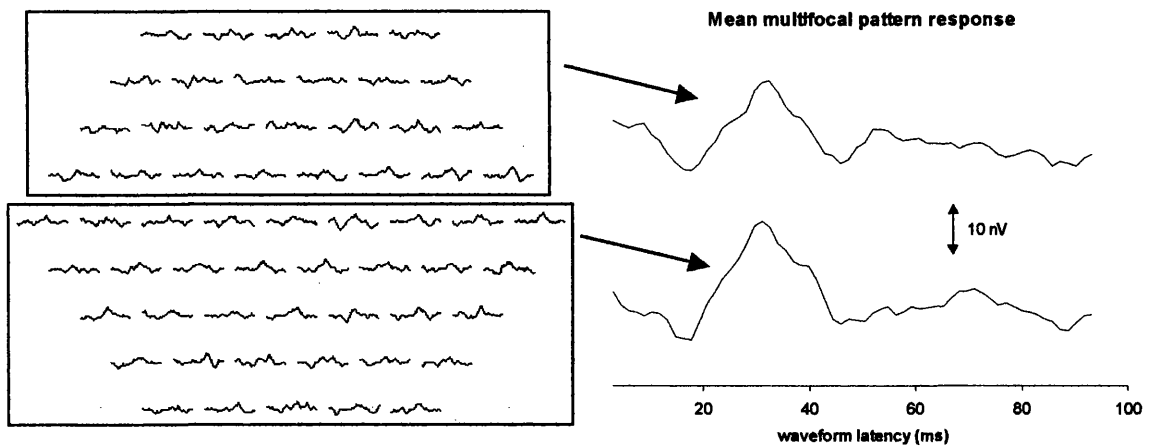


Figure 6.17 Mean multifocal pattern response for patient 5 (Primary Open Angle Glaucoma) from superior and inferior field.

COMPARISON WITH HUMPHREY PERIMETER

No correlation could be found between the sensitivity losses established by the custom test grid used on the conventional perimetry and the second order luminance or first order pattern responses. In addition, comparison of normal and abnormal areas defined by perimetry for pattern and luminance components revealed no appreciable difference (see tables 6.7 and 6.8).

Patient	2 nd Order lum. response (normal)		2 nd Order lum. response (abnormal)		Humphrey (mean sensitivity dB)	
	Amp. (nV)	Imp. (ms)	Amp. (nV)	Imp. (ms)	Normal	Abnormal
1	35	33	29	33	25	3
2	22	33	20	34	27	7
3	25	32	22	33	31	6
4	37	32	29	33	25	2
5	28	33	20	33	23	1
6	25	33	24	33	23	4
7	28	33	27	33	29	1
8	31	33	22	34	26	1

Table 6.7 Mean 2nd order luminance responses from regions defined by perimetry as normal and abnormal

Patient	Pattern Rev. response (normal)		Pattern Rev. response (abnormal)		Humphrey (mean sensitivity)	
	Amp. (nV)	Imp. (ms)	Amp. (nV)	Imp. (ms)	Normal	Abnormal
1	24	30	14	31	28	3
2	19	31	17	31	26	4
3	31	30	13	31	31	6
4	35	29	19	31	27	1
5	25	30	18	31	23	1
6	28	30	21	30	29	2

Table 6.8 *Mean pattern reversal responses from regions defined by perimetry as normal and abnormal*

DISCUSSION

Due to the nature of the stimulus, VERIS evokes predominantly a cone response and so little indication of rod function or ganglion cell function can be derived. The suggestion that the second order response which can be derived from data signals or the pattern reversal components could, in part, reflect ganglion cell function (Sutter 1987; Bearse et al 1995a; Bearse et al 1995b; Bearse et al 1996a; Bearse et al 1996b) has been investigated. No correlation between field loss identified by perimetry and temporal or spatial changes in the MFERG second order luminance or pattern reversal components could be found. At this stage the findings would suggest that these methods for identifying dysfunction due to ganglion cell loss are unsuitable for clinical practice.

6.5. RETINAL DETACHMENT

Loss of visual function following retinal detachment is conventionally assessed subjectively by perimetry and visual acuity (Gundry & Davies 1974; Foulds et al 1974). More recently, focal electroretinography (FERG) and visual evoked cortical potentials (VECP) have been employed as an objective method of assessing central retinal visual function in retinal detachment (Ueda & Adachi-Usami 1992). However, to assess the extent of spatial retinal dysfunction and

depth of field loss then full threshold perimetry or FERG must be used. Although both these methods can be used to monitor spatial retinal function, loss of visual function at visual cortex, optic nerve or ganglion cell level will influence perimetry results. Thus only FERG can be used as a direct objective measure of photoreceptor function.

The electroretinogram, it would appear then is an ideal test for assessing retinal detachment as the evoked response is a direct measure of photoreceptor and bipolar cell function (Bush & Sieving 1994; Bush & Sieving 1996).

The aim of this preliminary study was to assess and record the multifocal responses obtained in a condition with known gross retinal dysfunction that was localised in nature.

PROTOCOL

Twenty-five patients with unilateral rhegmatogenous retinal detachment were examined pre-operatively using VERIS. Repeat measurements were performed at 10 weeks post-operatively. The 15 male and 10 female patients ranged in age from 17 to 70 years (mean age 35.4 years) and had no other ocular or systemic abnormalities. Since repeat measurements were to be performed patients were maximally dilated with 1% tropicamide. In addition, all patients underwent conventional full field photopic ERGs and Custom Humphrey full threshold static visual fields. The duration of pre-operative detachment ranged from 1 to 156 weeks (it is assumed here that retinal detachment occurred at the onset of visual loss). Eleven of the patients were not included in the final analysis (six did not attend repeat appointments and five failed the exclusion criteria previously set).

RESULTS

Significance maps of the contralateral eye from all fourteen patients, who successfully completed the test, fell within the normal range of our control population on all occasions. A typical example Custom Humphrey field chart is

shown in figure 6.18. MFERG responses and a scalar product plot are shown from the same subject in figure 6.19 (a) and (b) respectively.

Patient	Age	Duration (weeks)	Macular Involvement	Pre-op VA	Post-op VA	Increase in Normal areas	
						MFERG	Humphrey
No.1	39	>26	yes	CF	CF	11	13
No.2	62	>26	partial	1/60	1/60	9	10
No.3	25	8	yes	CF	1/60	22	31
No.4	69	24	yes	HM	6/18	6	7
No.5	49	>156	yes	HM	CF	7	16
No.6	37	>1	yes	6/36	6/24	2	15
No.7	30	>1	no	6/9	6/9	35	42
No.8	24	26	yes	CF	CF	26	23
No.9	33	26	no	6/9	6/9	18	27
No.10	17	6	no	6/9	6/9	8	17
No.11	26	2	partial	6/36	6/24	23	32
No.12	65	unknown	no	6/6	6/6	35	44
No.13	25	1	yes	HM	CF	5	7
No.14	30	>20	yes	CF	CF	3	4

Table 6.9 Test results and patient information pre- and post-operatively. HM: Hand movements, CF: counting fingers.

Significance maps obtained from the affected eye revealed areas of loss, as indicated by the number of areas falling outside the normal range. In each case a postoperative improvement in visual function was exhibited both by the multifocal ERG system and by the threshold response obtained using the custom Humphrey test grid. Paired sample t-test of change in abnormal areas between Humphrey results and MFERG responses gave good correlation (mean $p=0.932$). Table 6.9 shows the change in abnormal areas for each of the fourteen patients pre and postoperatively. A typical example of recovery (patient No.11) is shown in figure 6.20

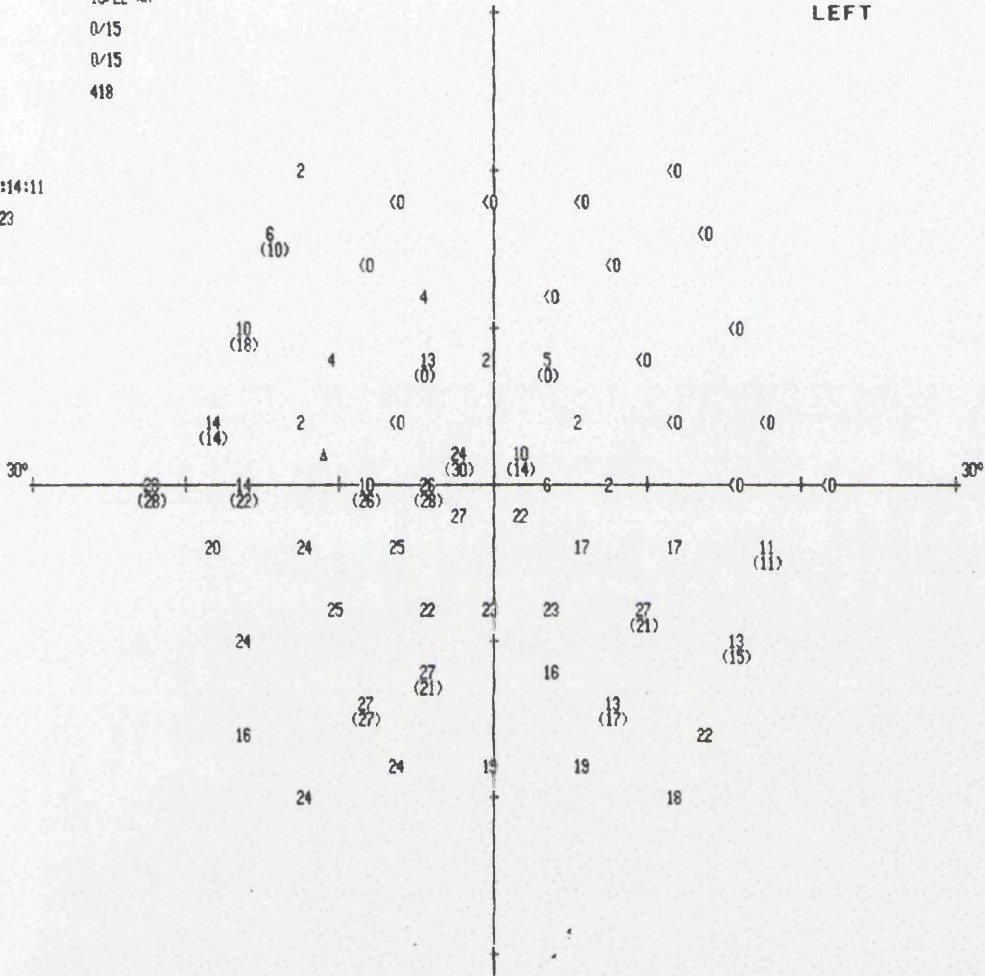
VERIS THRESHOLD TEST

STIMULUS III, WHITE, BCKGND 31.5 ASB NAME
 BLIND SPOT CHECK SIZE III SPACING 2° ID 8788 BIRTHDATE
 FIXATION TARGET CENTRAL DATE TIME
 STRATEGY FULL THRESHOLD PUPIL DIAMETER VA
 RX USED DS OCX DEG

FIXATION LOSSES 15/22 xx
 FALSE POS ERRORS 0/15
 FALSE NEG ERRORS 0/15
 QUESTIONS ASKED 418

TEST TIME 00:14:11
 HFA S/N 640-2423

LEFT



NO. = THRESHOLD IN DB
 (NO.) = 2ND TIME

GRAYTONE SYMBOLS

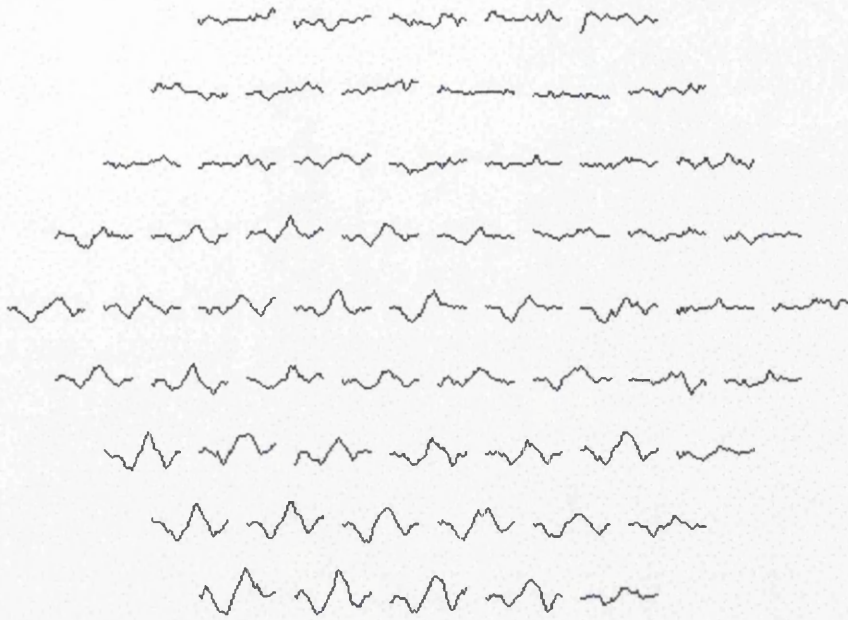
REV 5.3

SYM										
ASB	.8 to .1	2.5 to 1	8 to 3.2	25 to 10	79 to 32	251 to 100	794 to 316	2512 to 1000	7943 to 3162	?
DB	41 to 50	36 to 40	31 to 35	26 to 30	21 to 25	16 to 20	11 to 15	6 to 10	1 to 5	50

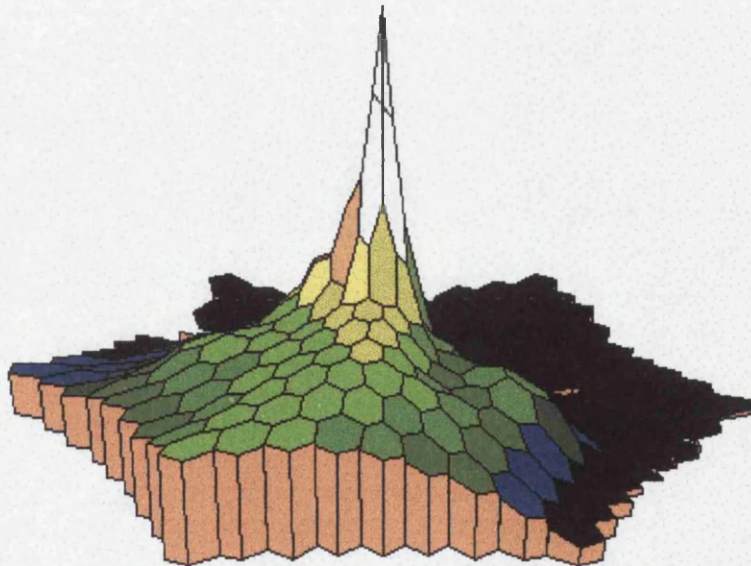
TENNENT INSTITUTE
 C.O. WESTERN INFIRMARY
 GLASGOW
 041 339 8822

**JALLERGAN
 HUMPHREY**

Figure 6.18 Custom Humphrey field chart from patient 11 with inferior temporal retinal detachment.

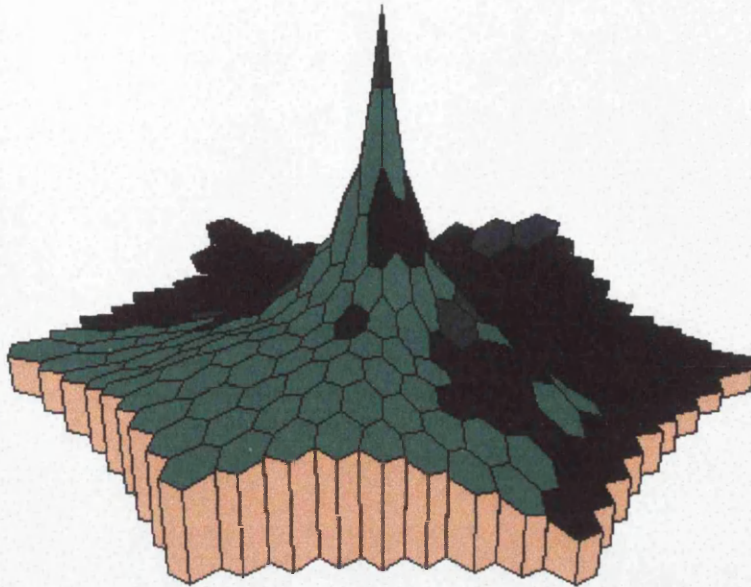


(a) MFERG waveforms from Superior temporal retinal detachment.

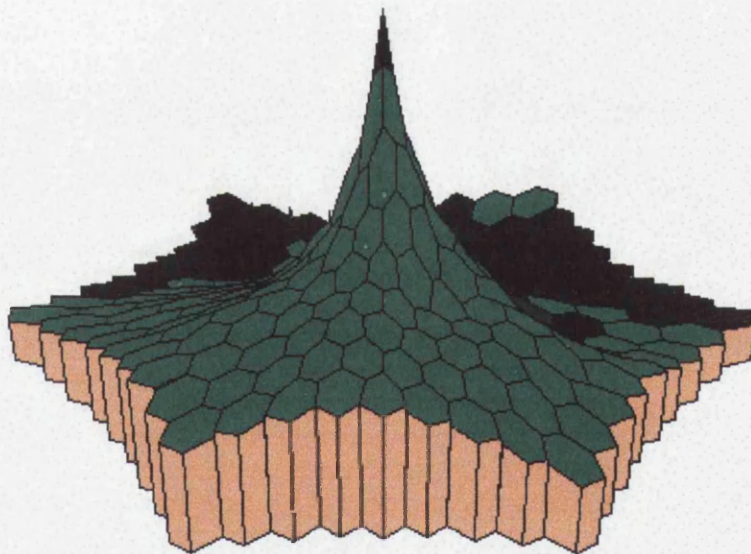


(b) MFERG Scalar product plot derived from waveform responses.

Figure 6.19 Signal response plot (a) and derived scalar product plot (b) of a subject with superior temporal retinal detachment.



(a) Confidence plot of retinal function pre-operative.



(b) Confidence plot of retinal function (10 weeks) post operative

Figure 6.20 *Confidence plot overlaying response amplitude plot pre (a) and post-operative (b) retinal detachment. Green, normal function, blue outside 5th percentile and black outside 1st percentile.*

Unlike the previous investigations of retinal dysfunction, where a localised discrete cellular layer was the site and source of the dysfunction, retinal detachment is accompanied by gross cellular destruction at the photoreceptor level. Thus it becomes difficult to assess features of the waveforms such as implicit time where some residual function is required.

COMPARISON WITH HUMPHREY PERIMETER

The nature of the measurement system in the static threshold responses precludes accurate estimation of field defect. Since the test administered requires monocular fixation, macular detachments are difficult to investigate as peripheral fixation is required if at all possible. Where macular involvement was not involved a good correlation of sensitivity losses and reduction in amplitude was evident.

DISCUSSION

In the fourteen post-operative cases studied to date, an improvement in retinal function was found even in some long standing detachments with macular involvement. However, in patients with macular involvement improvement was limited to the peripheral areas.

In conclusion multifocal ERG mapping of retinal function in retinal detachment may be an important objective monitoring tool. Anatomical success is not always accompanied by functional success (Foulds et al 1974). This tool enables detailed studies to be carried out to assess the influence of parameters such as length of detachment, site and size of detachment on the efficacy of treatment. It is possible that ERG mapping could prove to be a useful prognostic indicator in corrective surgery.

6.6. CONCLUSIONS

This chapter described the clinical evaluation of the VERIS system. A number of retinal pathologies were investigated. These retinal pathologies were chosen to examine the system's effectiveness at identifying discrete cellular abnormalities.

The hereditary conditions retinitis pigmentosa and autosomal dominant cone dystrophy were examined to investigate the system's responses to outer retinal abnormalities (specifically photoreceptor cell dysfunction).

The studies show that while cone dystrophy resulted in an amplitude reduction of MFERG responses, retinitis pigmentosa had a greater affect on the temporal features of these responses. Implicit time was the most accurate measure of visual dysfunction. This was further corroborated with the findings from repeat measurements after a one year interval where significant shifts in implicit time were evident. This ability to objectively quantify the progression of retinitis pigmentosa could be a valuable tool in the assessment of new treatments for the condition.

In the assessment of diabetic retinopathy to quantify mid retinal change the MFERG was successful in the delineation of localised areas of ischaemia. This 'ischaemia' was clearly identified by a reduction in the b-wave amplitude (or increase in negativity). This will be useful in future studies which could assess the efficacy of treatment for laser photocoagulation in the prevention of complications of retinopathy. Although, out of all the groups of retinal pathologies tested patients with diabetic retinopathy were in general less compliant than other groups. Only 31% of subjects tested produced 'reliable' results as opposed to a general average of 61% (see table 6.10). This is probably in part to do with the large number of investigations these patients undergo on a routine basis. This examination 'fatigue' produces, understandably, a less accommodating subject which ultimately leads to a higher exclusion ratio and a less repeatable response.

Disorder	RP	CD	DR	Glaucoma	RD
Number tested	24	12	26	22	25
Failed exclusion criteria	9	4	18	8	5
Reliability %	63	67	31	64	80

Table 6.10 *Test reliability. (RP: retinitis pigmentosa, CD: cone dystrophy, DR: diabetic retinopathy, RD: retinal detachment).*

The investigation of inner retinal pathology in the form of Primary Open Angle Glaucoma illustrated the system's limitations. Attempts at retrieving inner retinal responses were unsuccessful. Pattern reversal stimuli were used to evoke outer retinal responses but the amplitude of these measures required mass summation of areas to obtain waveforms with common identifiable features. The investigation of second order responses also uncovered little evidence of outer retinal responses. Although in defence of recent reports (Bears et al 1996b) the author's investigations included the summation of serial measurements over several recording periods. In addition, Burian Allen contact lens electrodes were used (although excluded from this evaluation) which yield an improved signal to noise ratio (see chapter 4).

The study on patients with Retinal Detachment pre- and post-operatively yielded promising results. Bearing in mind the MFERG technique's objectivity, these results indicate that this technique could be used to assess the efficacy of current surgical practices in retinal re-attachment surgery. This at present is the subject of a more detailed examination of retinal detachment surgery and surgical outcomes. This will involve serial measurements on a cohort of individuals over a longer period of time pre- and post-operatively.

CHAPTER 7

CONCLUSIONS & FURTHER WORK

This thesis describes the evaluation of a new objective method (The Visual Evoked Response Imaging System - VERIS) for imaging localised retinal abnormalities. The purpose of the research was the evaluation of this new system within the context of a routine clinical setting. In chapter 1 (section 1.5) a proposed framework of research was devised to quantitatively assess this new technique. The conclusions from this research are discussed in the following four sections (7.1 to 7.4).

7.1 RECORDING SYSTEM

The Visual Evoked Response Imaging System (VERIS) employs novel recording techniques to achieve its high resolution visual evoked retinal response. Each area of the stimulated field alternates states driven by a Pseudo Random Binary Maximum Length Sequence. The cross-correlation of this binary sequence with the recorded mass response from the subject results in the recovery of impulse responses from localised retinal areas.

The system offers flexibility in the stimulus resolution and length of sequence (recording period) although the generation of stimuli is limited to fixed pattern and flash paradigms.

The stimulus used (20 inch monitor), is not ideal. It has a small field of view (~30 degrees) of variable intensity which is low in comparison to conventional electrophysiology. Although this could be addressed by the use of alternative stimulus techniques. These would require high resolution, a larger field of stimulation and refresh or excitation rates comparable to existing CRT technology. There are a number of alternative stimulus systems available that provide some if not all of these features.

1. The Laser Scanning Ophthalmoscope. This has a high refresh rates and can reach intensities far greater than standard VDU's. However it lacks the resolution flexibility of the current stimulus.
2. Active matrix projection systems offer the flexibility of standard CRT and can be manipulated optically. However, these liquid crystal display systems have lower switching rates than current CRT's and so would require longer recording periods to complete a full m-sequence.
3. Micro-mirror devices offer projection systems of comparable resolution, higher luminance and faster refresh rates than the current stimulus(see further work) and would provide an improvement in signal quality.

The current system however cannot be used with these technologies at present as the sampling rates and stimulation sequences expect a raster based stimulus (CRT) or fixed resolution and incorporation of any non-raster based stimulus would interfere with the cross-correlation of responses.

With the stimulus resolution set at the smallest number of areas (61) and a recording period set at the maximum (~14 minutes) to recover the largest responses possible, some 40% of the examinations were unsuccessful, due to poor signal response (a combination of fixation losses, poor compliance and signal quality). Poor fixation is the single most important factor in the exclusion of responses. This cannot be addressed by passive monitoring alone. It requires

the subject under investigation to actively fixate, whether that be at a stationary point or a moving stimulus the systems poor success ratio could be dramatically improved by using active dynamic fixation (e.g. letters appearing at intervals to spell out a word), see section on further work.

An improvement in the integrity of responses could be achieved by grouping neighbouring areas together, this would improve signal to noise ratio and thus the reliability of the results. However, this would reduce the resolution of the response topography and may mask the subtle changes in latency found in some disorders. A reduction in saturation would be achieved by employing the recommended narrower bandpass filter 10-100Hz this would decrease the failure rate and consequently the accuracy of the system. By employing this filtering the operator would mask poor fixation and thus reduce the sensitivity of the test. A further option would be to return to the corneal electrode and benefit from its superior signal to noise ratio, although this improvement in signal quality would bring with it a greater incidence of corneal abrasion.

In the final optimised protocols implemented, both dilation and non-dilation were employed. Dilation was used where serial measurements were necessary, such as in monitoring the progression of an identified field loss. When only one measurement was required to assess dysfunction, no improvement in the identification of abnormal evoked responses was achieved with dilation.

Due to the small evoked signals and high amplifications required custom built amplifiers were developed (Department of Clinical Physics & Bio-Engineering Electronics Laboratory) to improve signal recovery. These units included a pre-amplifier stage to minimise electrical interference produced by connecting cables and surrounding potentials. In addition, the unit had the facility for D.C. restoration; this was found to reduce the occurrence of saturation which plagues signal amplification at this level due to shifts in the D.C standing potential.

The ability to remove or minimise this low frequency D.C. component in the signal allowed the use of a wider bandpass filter which was crucial when investigations included conditions that selectively affected ERG responses (such

as ischaemia). The use of a narrower bandpass will alter the features of the local responses (e.g. amplitude and latency). This will lead to errors in the reporting of latency and amplitude values (see later in this section).

The analysis software supplied with the VERIS system allowed the comparison of local responses. In addition, regions could be grouped to improve signal quality. However the system did not provide the facility to compare responses either between individuals or with normative data. In addition, operators were unable to evaluate the most commonly documented features of the ERG response (implicit time and b-wave amplitude). Moreover the incorporation of a new method of signal analysis (the scalar product) was flawed. Although the mathematical derivation of this method for assessing the amplitude of a response is sound, it is dependent on the quality of the template from which it is derived. The template with which the VERIS system derives its signal is simply the sum of all responses from the patient under investigation. This will compromise the validity of the results if a defect common to all responses from a subject exists. The need for greater flexibility and improved analysis led to the development of a separate analysis package (Functional Imaging & Data Analysis – FIDA – Appendix I). This provided a quick means of visually assessing topographical information on the common features of the response (amplitude and latency). This ability to view and compare these features from multiple investigations both locally and globally led directly to the discovery of delays in retinitis pigmentosa. The derivation of the scalar product was corrected by incorporating normative data within its calculation. A theoretical study on the comparative benefits of the three main features of the responses, implicit time, amplitude and scalar product identified their benefits and weaknesses. Implicit time and amplitude measures were accurate if signal quality was good, however scalar product was found to be the best estimate of dysfunction and is a robust measure of local ERG waveform shape at low signal to noise ratios when signal quality was poor. However care must be taken when viewing scalar product measures when more subtle changes such as latency shifts are present.

In addition this software was also used to archive patient results (in a database format) and provide hard copy for clinicians (see figure 3.7 in chapter 3).

7.2 SYSTEM VARIABLES

A number of investigations were used to assess how different factors influenced the integrity of the results obtained from the VERIS system. While the signal amplitude from commonly used non-corneal electrodes was found to be comparable, the Hawlina-Konec (HK)-loop had the advantage of reducing the number of repeat segments produced by excessive saturation. This is important for the cross-correlation process where large temporal variations produced by excessive time lapses between segments will influence the quality of the derived signal.

The recommendations for standard full field electrophysiology were closely followed although a possible restriction resulting from the existing recommendations was uncovered. Dilation, in the full field Ganzfeld ERG, was found to increase the normal range of the response (i.e. inter-individual) but to improve the repeat measure. Moreover the inclusion of dilation in the protocol was found to lengthen the examination time considerably, involved greater discomfort for the patients and increased their sensitivity and intolerance to light (photophobia). These factors combined to produce a less accommodating subject and led to the creation of two protocols: one for the identification of defects (non-dilation) on a single visit and one for serial measurements (dilation) where the progression or improvement of the disorder (e.g. retinal detachment) was to be measured.

The effects of luminance and contrast were investigated both directly by altering the monitor controls and indirectly by inducing refractive errors in a cohort of volunteers. The observed changes were found to influence both the temporal and spatial features of the ERG waveforms. At low contrast there may be a separation of components which are not evident in conditions of low illumination. This could reflect changes in the centre-surround mechanisms from the bipolar contribution to the evoked response because these cells would contain a contrast dependent component.

Subject and environmental variables identified as extraneous to the evoked responses could be minimised by a combination of averaging and the use of high and low bandpass filters. This excludes the high and low frequency noise generated by patients and equipment. A detailed investigation of filtering artefacts concluded that care should be taken when employing bandpass settings that had been recommended (10-100Hz) because the spatial and temporal characteristics of the evoked responses would be adversely effected. It is no surprise that these settings are recommended. The subtle D.C. offset shifts and saturation associated with poor fixation will combine to produce a high exclusion ratio. This would limit the application of the system and its attractiveness to users. Other workers in the field do not report a high exclusion ratio but neither do they employ a wide bandwidth. It is important to emphasise that without this wide bandwidth the sensitivity of the system is reduced and the integrity of the results compromised. This trade off between exclusion ratio and filter bandwidth is difficult to reconcile. Before the current system could be used routinely in clinical practice the consequences of filtering would have to be recognised and considered during each investigation. Optimum values for the high and low bandpass filter settings should be 1 and 300Hz respectively to ensure the identification and elimination of poor fixation and the accurate analysis of results.

Fixation monitoring was essential for the identification of accurately localised field defects. Poor fixation leads to erroneous responses from areas of dysfunction. However the restriction placed on any enhancements of the system (additional costs, training and access to system software) led to the requirement for a simple, inexpensive and effective method for minimising the consequences of poor fixation. Initial investigations which led to the widening of the bandpass filter settings (see previously) had increased the incidence of saturation from D.C. offset. A study was performed to evaluate the amplification and fixation loss required to saturate the amplifiers at a bandpass filter setting of 1-300Hz. This was found to identify fixation losses of greater than 2 degrees which was sufficient to enable accurate assessment of responses. This was the main method employed in the evaluation and exclusion of results with regard to fixation monitoring and poor patient compliance respectively.

The findings were used to define a standard protocol. This protocol was employed to perform a full clinical evaluation of the VERIS system.

7.3 CLINICAL EVALUATION I (THE NORMAL RANGE)

In order to estimate the variability of the VERIS system, seventy age matched controls were tested to obtain normative values. The results indicated that the system's response variability was concentric while the waveform features were fairly uniform across the field. Variation of the system was compared to the conventional method for field assessment (static perimetry). It was necessary for accurate comparison that a custom perimetric field chart was created to stimulate the same areas as the VERIS system. Results on repeatability and reproducibility indicated that the system is comparable to conventional perimetry for a field no greater than 30 degrees.

Perimetry and electrophysiology show that sensitivity and response amplitude decrease with age. Therefore a study was undertaken to assess the variation of response features with age. Results indicated a modest reduction in signal quality and response amplitude with age which accelerates in the over 50's.

The normative data obtained from the investigations were incorporated within custom software (FIDA) that was then employed in the second stage of clinical evaluation to assess a selection of retinal disorders. These retinal pathologies were chosen to examine the system's effectiveness at identifying discrete cellular abnormalities that had been identified by conventional methods.

7.4 CLINICAL EVALUATION II (RETINAL DISORDERS)

A variety of retinal disorders were tested with the system to establish its ability to detect pathologies that were known to affect the discrete receptor/neuronal layers of the retina.

The hereditary conditions retinitis pigmentosa and autosomal dominant cone dystrophy were examined to investigate the system's responses to outer retinal abnormalities (specifically photoreceptor cell dysfunction). Results indicated that while cone dystrophy resulted in a marked reduction in amplitude of MFERG responses, retinitis pigmentosa affected responses in a much more subtle fashion. Temporal changes in waveform responses were a more sensitive indication of retinal dysfunction in retinitis pigmentosa. This was further corroborated with the findings from repeat measurements taken after a one year interval. In the small cohort of patients with retinitis pigmentosa who were retested 4 had an identifiable shift in temporal responses and in 2 this shift was statistically significant yet little change in response amplitude or Humphrey sensitivity values could be detected.

The subtle changes in implicit time evident in retinitis pigmentosa could become an identifying feature of early dysfunction in the disease. This would have important implications for prospective therapies for the condition and is the subject of a more detailed investigation currently underway into the short term progression of retinitis pigmentosa in the recently diagnosed.

In cone dystrophy amplitude responses were markedly reduced, or absent, within the central 5 degrees. However, in contrast with RP, this was not reflected in any temporal changes in the responses. It is important to note that although this technique has not revealed the subtle temporal changes reflected in RP it has established gross central retinal dysfunction which is in contrast to the normal full field ERG's obtained from all but one patient. The clear discrimination of this technique between these hereditary disorders indicates the potential this

technique has for the objective assessment of retinal dystrophies and their prospective therapies.

The assessment of diabetic retinopathy to quantify mid retinal change was successful in the identification of localised areas of ischaemia. This resulted in a reduction in the b-wave amplitude (or increase in negativity). Of all the groups of retinal pathologies tested, patients with diabetic retinopathy were less compliant than other groups. This led to a higher exclusion ratio than other disorders and thus a reduced reproducibility and signal to noise ratio of results. If the high exclusion ratio could be addressed then this technique would be useful in future studies which could assess the efficacy of treatment for laser photocoagulation in the prevention of complications of retinopathy.

The investigation of inner retinal pathology in primary open angle glaucoma demonstrated one of the system's limitations. Attempts at retrieving ganglion cell responses were unsuccessful. Pattern reversal stimuli were used to evoke outer retinal responses but the amplitudes required mass summation to show any common features. The investigation of second order responses also uncovered little evidence of outer retinal responses. The second order response included an N1 (25 ms) and a P1 (33 ms) component. Although reports have suggested that these components contain a ganglion cell contribution their timing is close to that of the photoreceptor/bipolar cell response and since the signal must be transmitted through these cells first, it raises doubts as to their origins. A recent report (Bears et al 1996b) suggests that these inner retinal responses can be recorded but the responses must be summed over repeated measurements with undocumented iterative subtraction algorithms employed to derive these inner retinal components. This would require three 14 minute recording periods which, even if successful, would be impractical for routine clinical practice.

Retinal detachment was by far the most successful group mainly due to the complete devastation of retinal cells and thus the ablation of any localised response from areas of detachment. In addition, patients with retinal detachment had the lowest exclusion percentage. This could be attributed to the sudden onset of the condition and an initial, understandable, anxiety and desire in the patient

for a speedy resolve. These factors combine to produce a far more compliant and accommodating subject. These investigations of patients with retinal detachment are continuing and will be the subject of a more detailed examination of the efficacy of retinal re-attachment surgery.

Although offering great potential for the investigation of retinal dysfunction, these investigations have identified limitations which would require fundamental changes to the present system:

1. The field of view stimulated by the system while adequate in the context of central visual function lacks the spatial extent of existing subjective methods of visual assessment (perimetry). This recording of the depth and extent of peripheral responses is one of the requirements of field examinations used for the detection and monitoring of retinal disorders. At present VERIS's stimulation of retinal cells only covers some 30% of the visual field.
2. The mode of stimulation employed primarily evokes responses from the outer retinal portion of the cone pathway. Thus the early detection of disorders relies on cone dysfunction which account for only 10% of retinal diseases. The system cannot detect disorders located in the inner retina (i.e. the ganglion cells). Thus the present system has not shown itself to be useful for the detection of glaucoma or other optic nerve diseases in the clinical setting.
3. Again due to the mode of stimulation (standard VDU) only relatively low luminance levels are obtainable. Since ERG signal amplitude is directly proportional to stimulus luminance levels, repeatability and reproducibility are adversely effected by this low stimulation luminance. This limits the accuracy of the system and its practical use in the electrophysiology clinic.
4. More generally the system suffers a higher exclusion criteria and a greater requirement for patient compliance than other methods of field assessment. While this is largely the consequence of a wider bandpass filter and a higher sensitivity than conventional investigations, the distortion of responses

produced by a narrower bandpass filter, the author believes, prevent their use in clinical practice.

The improvement of limitations (1-4) individually and in combination could lead to a significant increase in the signal to noise ratio of responses and routine application of the technique. This would ultimately improve the system's repeatability and accuracy in detecting localised pathology.

The main aim of this research was to evaluate the VERIS system for use in routine clinical assessments. The investigations performed suggest that the system has potential within the conventional electrophysiology arsenal, although its high exclusion criteria limit its use to selected retinal disorders. However the potential it offers in these selected disorders is promising. In conditions such as retinitis pigmentosa treatments are not available. This is not because of failure of research but mainly due to the difficulty in making a quantitative estimate of progression. Without an accurate estimate of progression within manageable time scales possible treatments are difficult to evaluate. VERIS and the multifocal technique offer a true advance not only in monitoring of the disease process but additionally in understanding their pathogenesis. This may ultimately lead to improved treatment for the conditions.

In conclusion, the VERIS system and more generally the technique is a major advance in the field of electrophysiology. It provides the tools for rapid accurate assessment of photoreceptor based disorders and could be applied to the main retinal pathologies with the promise of improved diagnostic accuracy. The system offers both the objectivity associated with electrophysiology together with the spatial resolution inherent in perimetry.

Since the inception of this research an additional aim was to develop or modify the technique to improve its reliability, diagnostic accuracy and lower its failure rate. The work has acted as a foundation on which to address recognised and previously undiscovered limitations of the technique. The following sections describe current research that attempts to address these limitations.

7.5 FURTHER WORK

Although our analysis and assessment of the VERIS system in the previous chapters has shown it to be a formidable tool in the early detection and monitoring of retinal pathology, our investigations have also uncovered the systems main limitations. These were:

1. A reduced field of stimulation.
2. An inflexible stimulus, limited to the assessment of outer retinal responses.
3. Low stimulus intensity and consequently signal amplitude.
4. High exclusion ratio.

This chapter details current and further research that addresses these restrictions and in so doing attempts to create a more robust system that would achieve the primary objective of the research: to provide a reliable accurate means of establishing topographic retinal function in the context of existing routine electrophysiology practices.

The following section introduces the concept of a new prototype stimulation system, Digital Light Processing (DLP), and a variety of stimulation techniques. These in combination offer the potential of addressing the limitations inherent in the VERIS system.

The preliminary electrodiagnostic system which is described exploits the projection nature of DLP and the stimulus dimensions achievable in perimetry to achieve fields of stimulation greater than is currently available. In addition a new mode of stimulation is discussed that is designed to evoke potentials from the inner retina and could thus be useful in the early detection of glaucoma.

7.5.1 BACKGROUND

New advances in micro-engineering led Texas instruments in late 1993 to announce a new projection technology designed and developed to achieve fast

refresh rates at high luminance. These features are comparable, and in most cases superior, to existing Cathode Ray Tube (CRT) techniques. The technique is called Digital Light Processing (DLP) and promises a flexibility not before seen in projection systems. Projection systems had existed in the form of Liquid Crystal Display (LCD) units but they could neither achieve the fast refresh rates or luminance required to challenge CRT based systems.

7.5.2 DIGITAL LIGHT PROCESSING

The uniqueness of DLP revolves around silicone based micro-electronics. At the core of the DLP solution is a micro-mechanical silicon chip, the Digital Micromirror Device (DMD™). Light is shone onto the DMD's reflective aluminium surface, and reflected by its 800×600 pixel array surface. The standard resolution device measures 0.594 × 0.501 inches (15 mm × 13 mm) producing a pixel dimension of around 16 × 21 microns. Positioned at the bottom corner of each mirror is a Dynamic Random Access Memory cell (DRAM). When a voltage is applied, computer controlled electrostatic charges cause each mirror to switch into either of two rotational angles (+10 or -10 degrees). When the voltage is switched off the mirror returns to its original state and thus acts as a bistable switch. Each mirror, when switched 'on', reflects the incident light into or out of the aperture of the projection lens. When switched 'off' this incident light is reflected onto an absorber.— see figure 7.1. The projected image of the surface of the DMD produces a digital greyscale image of the input image. The digital speed of the DMD controls the intensity of greyscale images through pulse width modulation (PWM) of the on-versus-off time in a video frame rate. Using this technique, the observer's eye integrates the light from each pixel and builds recognisable greyscale images. In a single chip system, PWM implements 8-bits of greyscale allowing for 256 levels from black to white. Colour is added by placing a colour filter system in the path of the incident light. Sequential colour (red/green/blue) rotating in time to the PWM can produce up to 16.7 million colours every three 'frames'. The DLP subsystem can alternate more than 1,000 times per second to build the digital bit frames into film-like video images of consecutive primary colours with dramatically reduced flicker levels.

The system's ability to accomplish this switching in excess of a thousand times per second enables refresh rates comparable and in most cases superior to existing CRT based systems. In addition, since the technique relies on reflection rather than transmission of stimulus the system can achieve high intensities in excess of 1000 lumens in monochrome mode.

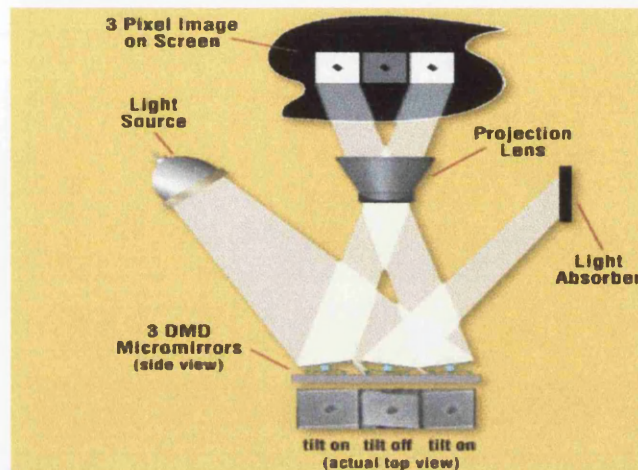


Figure 7.1 *Incident light is reflected off the pixelated surface. This reflected light is either turned 'on' and reflected to the projection lens or turned 'off' and reflected to the light absorber. Thus by tilting the aluminium mirrors through a fixed angle a pixelated image can be produced on the projection screen.*

One additional advantage that this method of stimulation offers in contrast to the standard VDU CRT based system is a completely digital interface. Any raster based stimuli will create complications in the accurate timing of ADC sampled evoked signals. This is because an ON state determined by the stimulation sequence will be displayed by the raster system as a decaying pulse, the features of which will depend on the decay rate of the phosphor and the current line position (or frame rate) of the raster. Thus sampling needs to allow for latency delays due to the specific raster position at the time of the sample and responses to this raster may have an unknown effect on the theoretical non-linearities of the evoked response. This is the main reason why the current VERIS system could not be used with DLP technology. The digital technology of DLP no longer requires this compensation and will reflect, in simple black and white mode, a

true response to a digital ON and OFF state thus providing the facility to investigate these non-linearities of the visual system.

Thus given the high intensities and fast refresh rates achievable within a DLP subsystem it would appear an ideal alternative to the conventional monitor based system.

7.5.3 MOTION STIMULI

As discussed previously the signal in conventional electroretinography (ERG) is derived mainly from the retinal receptors and bipolar cells in the mid-retina with selective contributions (see following section) from ganglion cell activity. Potential changes originating in the ganglion cells can however be recorded by the use of patterned (Trick 1991) and motion (Hubel 1995; Clarke 1973) stimuli. Since it was known that the neuro-retina processes the fundamental elements of vision such as motion with special ganglion and amacrine cells. Responses to these stimuli have also been identified cortically (Kuba & Kabova 1992; Zeki et al 1991) and have been reported abnormal in patients with Glaucoma (Kohl & Korth 1997).



Figure 7.2 *Illustrates motion onset stimulus paradigm. Each of the 17 segments is independently driven by a shifted 13-bit m-sequence. Each region has concentric bars that move centrally for a predefined duration.*

A multifocal motion stimuli has been developed. It consists of an annulus stimulus field divided into 13 sections. Each section is driven by a 13-bit m-sequence and involves the annulus rings moving centrally at a user defined speed (this can be a maximum of 1 pixel per frame $\sim 0.08\text{m/s}$) and duration (see figure 7.2).

7.5.4 COLOUR STIMULI

Recent research suggests that there is a retinal ganglion and amacrine cell contribution to the photopic and scotopic flash ERG (Viswanthan et al 1997; Frishman et al 1997). A negative component some 60 ms after flash onset was the main feature of this inner retinal contribution. The negative deflecting component was found to be maximally evoked in controls using a high intensity red flash upon a (3.6 log scotopic trolands) blue background. To investigate this, macaque monkeys, with previously recorded negative components and normally functioning inner retinal responses, were treated with intra-vitreous injections of Tetrodotoxin (TTX). This compound is known to block ganglion and amacrine spiking potentials. In addition N-methyl-DL-aspartate (NMDA) was used to suppress all inner retinal responses. In a separate group of macaque monkeys, monocular experimental glaucoma was induced by laser trabeculectomy. With activity of the inner retinal layer suppressed these components were either significantly reduced or absent. Thus the authors concluded that this negative component must originate either from ganglion cells directly or from their axons.

At present our group are developing stimuli to investigate this inner retinal component within the multifocal context. This would be incorporated into the projection system to enable it to assess inner retinal function which is not at present possible.

7.5.5 SEQUENCE STIMULATION

As discussed in previous chapters m-sequence stimulation is a proficient method for recovering a large number of averages within a short time period. VERIS adds to this exploitation of m-sequences by the inclusion of its m-transform which facilitates the extraction of partial values by the method of cross

correlation of the data set. Recently, the sequencing potential has been further exploited by the use of the corrected m-sequence (Kutschbach 1997). These are m-sequences that have been altered to allow for the inherent incorrectness induced by the non-even nature of the m-sequence length. This produces short, self-contained m-sequences of an even length. However the author has failed to address its main disadvantage i.e. the higher probability of cross-contamination from kernels of higher order between stimulated regions.

All stimuli driven by these sequences are binary and as such have an on or off state. However, with the inclusion of a third intermediary state a ternary sequence is produced which, with the advent of DLP, could enable the inclusion of segmentation of stimulus luminance. This would give an added dimension to the m-sequence impulse response and include in its derivation a direct intensity dependent response. This would require a more complex cross-correlation algorithm but nevertheless would be useful in the separation of rod and cone receptors and their associated pathways.

To provide active dynamic fixation a cycling fixation mark can be presented that, when linked to the stimulus sequence can provide improved fixation during the examination sequence. This dynamic control of fixation reduces the incidence of saturation and ultimately lead to a lower exclusion ratio.

7.5.6 THE SYSTEM

It is the group's intention to exploit the high intensity and fast refresh rates obtainable using the DLP and combine this with the field of stimulation presently available to perimeters. The dimensions of a hemispherical bowl used in most perimeter systems is ideal as a projection screen for the DLP output, as these have been designed to retain an equidistant field of view. However, unlike conventional projection systems which would project an image onto a surface, back projection is employed. This nature of projection has one main advantage. The projection unit produces some degree of excess noise (both auditory and electrical) and thus its position should be at some distance from the subject. However if forward projection is used then the system would have to be some

distance from the screen and thus produce a reduction in luminance. By utilising back projection it is possible to retain an adequate stimulus luminance but still isolates, to some degree, the subject from the DLP system and its associated noise. An optical system is being designed to achieve this projection with minimum image aberration.

7.5.7 THE STIMULUS

The findings from previous chapters indicated that the amplitude of the ERG signal is related to the stimulus luminance. As the VERIS stimulator uses a conventional computer monitor, we are therefore limited to a maximum screen luminance of approximately 120cd/m^2 (although specialist monochrome monitors, notably the Dotronix 500 and Richardson Electronics new Ultra-Brite can both achieve luminance's in excess of 400cd/m^2). This would produce multifocal flash ERGs with b-wave amplitudes greater than 150nV for each of the 61 stimulated areas. This increase in response amplitude achieved by brighter stimulation should improve signal to noise ratio and thus produce a more repeatable response.

It has been known for sometime that although the pattern ERG evokes an inner retinal response (believed to emanate from the ganglion cells) this is macular dominated and so contributions from peripheral neurones to any recorded response is small if not absent.

It is proposed to utilise a combination of motion onset, pattern onset and high intensity colour stimulus (see following) to provide a foundation on which responses from outer retinal neurones could be recorded.

7.5.8 THE FIELD OF VIEW

As discussed in chapter 2 the VERIS system employs a shifted Pseudo Random Binary Maximum Length Sequence to stimulate multiple retinal areas simultaneously. One consequence of this form of stimulation is that at any one

time an area has approximately 50% chance of changing state (i.e. a previously white – on – hexagonal area becomes black – off – when a change in the sequence is encountered). Thus only half of the field under examination is stimulated at any one time. As we are restricted, in the VERIS system, to at most a 30 degree field of stimulation this leads to only 10% of the retinal cells generating a response at any one time (Curcio et al 1991).

However by extending the stimulus to cover a field of view to say, 150 degrees by using back projection, approximately 45% of the cells will be stimulated at any one time. This will yield improved signal to noise ratios and significantly shorten test protocols.

7.5.9 THE SOFTWARE

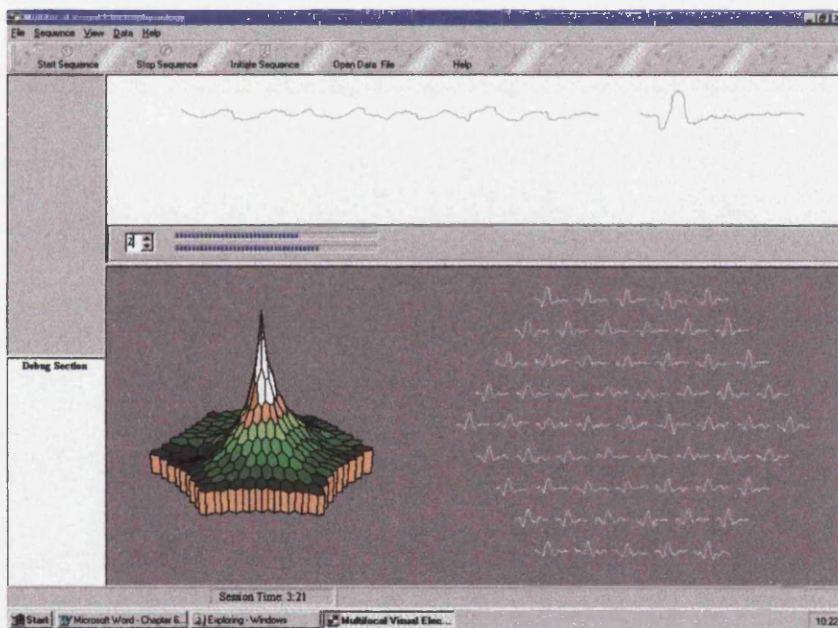


Figure 7.3 Screen-shot from Multifocal Visual Electrophysiology system. Top panel; (left) incoming signal from amplifier (right) cross-correlated response from chosen area. Lower panel; (left) scalar product response (right) cross-correlated response from all stimulated areas. This session represents a 2^{15} m-sequence using real time cross-correlation. The stimulus is driven at 90Hz and thus one full session lasts only just over 6 minutes. Screen shot was taken after 3 minutes 21 seconds.

At present all components of the system are being developed in parallel. This is so that we may optimise stimulus paradigms before incorporation of the DLP technology. A preliminary (beta) software program has been developed which in addition to real time cross-correlation of multifocal luminance responses has produced both multifocal motion and pattern ERG's. A screen shot from the system software is shown in figure 7.3.

7.6 CONCLUSIONS

This chapter reviewed current research to advance the technique of multifocal electroretinography. This, it is believed, would improve the technique's accuracy in the clinical setting. A new system is being constructed that will exploit current micro-mirror technology to project custom stimuli onto a large hemispherical surface. This will enable not only a higher intensity stimulation – which would improve signal recovery – but additionally would achieve a greater field of stimulation and thus improve the detection of peripheral pathologies. Also discussed were the attempts to optimise the stimulus to increase diagnostic accuracy by targeting specific neural layers. This would revolutionise the detection and monitoring of sight threatening disease specifically affecting the inner retinal neurones such as in glaucoma.

At present the Scottish Office Home & Health Department is funding research into the design, development and evaluation of this new instrument for the early objective detection of Glaucoma. This three year plan of investigation aims to answer the following questions:

1. How well can the instrument objectively map glaucomatous ganglion cell death at an early stage of the disease process?
2. Can the instruments' repeatability and reproducibility be optimised to enable objective assessment of new and existing treatments?
3. Can we extend the field of stimulation to investigate peripheral retinal disorders?

REFERENCES

- Ambrosio G Arienzo G Aurilia P Colasanti A & Fusco R (1988)
Pattern electroretinograms in ocular hypertension.
Documenta Ophthalmologica, 69, 161-163
- Arden GB & Fojas MR (1962)
Electrophysiological abnormalities in pigmentary degenerations of the retina.
Archives of Ophthalmology, 68, 369-389
- Arden GB Carter RM Hogg C Siegel IM & Margolis S (1979)
A gold-foil electrode: extending the horizons for clinical electroretinography.
Invest. Ophthalmol. Vis. Sci. 18, 421-426
- Arden GB & Vaegan (1983)
Electroretinograms evoked in man by local uniform pattern stimulation.
J. Physiol 341, 85-104
- Bach M Hiss P & Rover J (1988)
Check size specific changes of pattern electroretinograms in patients with early open-angle glaucoma.
Documenta Ophthalmologica, 69, 315-322
- Barber C (1981)
Inherent characteristics of visual stimulus systems and their effect on the visual evoked potential.
Clin Phys. Physiol Meas 1981.2: 2 135-146
- Barber C Tolia J (1985)
The Carbon Glide electrode for pattern and flash electroretinography
Presented at the 23rd ISCEV Symposium, Mie, Japan
- Barber C Anderson S Galloway NR (1996)
The effect of pupil size on the multi-focal ERG and VEP.
Presented at the International Society for Clinical Electrophysiology of Vision XXXIV symposium, Tübingen, Germany
- Bearse MA Sutter EE (1995a)
Extraction of a ganglion cell component from the corneal response.
Vision Science and Its Applications 318-321
- Bearse MA Sutter EE Smith DN & Stamper R (1995b)
Ganglion cell components of the human multi-focal ERG are abnormal in optic nerve atrophy and glaucoma.
ARVO abstracts. Invest. Ophthalmol. Vis. Sci. 36, S445
- Bearse MA Sim D Sutter EE Stamper R & Lieberman M (1996a)
Application of the multifocal ERG in glaucoma.
ARVO Abstracts. Invest. Ophthalmol. Vis. Sci. 37, S511

- Bearse MA Sutter EE Sim D & Stamper (1996b)
Glucomatous dysfunction revealed in higher order components of the electroretinogram.
Vision Science and Its Applications. Technical Digest Series. Vol 1
Washington DC. Optical Society of America 104-107
- Bearse MAJ & Sutter EE. (1996c)
Imaging localised retinal dysfunction with the multifocal electroretinogram.
J Opt Soc Amer. 13, 634-640
- Bedwell CH (1982).
Visual fields: a basis for efficient investigation.
Butterworths, London
- Berson E Gouras P & Hoff M (1969a)
Temporal aspects of the electroretinogram.
Archives of Ophthalmology, 81, 207-214.
- Berson EL Gouras P Gunkel RD & Myrianthopoulos NC (1969b)
Rod and cone responses in sex-linked retinitis pigmentosa.
Archives of Ophthalmology, 81, 215-2225
- Berson EL & Kantyars L (1970)
Cone and rod responses in a family with recessively inherited retinitis pigmentosa.
Archives of Ophthalmology, 84, 288-297
- Berson EL (1993)
Retinitis pigmentosa: the Friendwald lecture.
Investigative Ophthalmology & Visual Science, 34, 1659-1676
- Biersdorf WR (1982)
Temporal factors in the foveal ERG.
Current Eye Research, 1, 717-722
- Birch DG & Fish GE (1988)
Focal cone electroretinograms: Ageing and macular disease
Doc Ophthalmol 69, 211-220.
- Bland JM Altman DG (1986)
Statistical methods for assessing agreement between two methods of clinical measurement.
The Lancet, ii, 307-10
- Bobak P Bodis-Wollner L Harnois C Maffei L Mylin L Podos S & Thornton J (1983)
Pattern electroretinograms and visual evoked potentials in glaucoma and multiple sclerosis.
American journal of ophthalmology 96, 72-83

- Borda RP Gilliam RM Coates AC (1978)
Gold coated mylar (GCM) electrode for electroretinography.
Doc Ophthalmol Proc Series 15, 339-343
- Bradnam MS (1994a)
Visual field analysis using digital signal processing of visual evoked potentials.
Thesis
University of Glasgow
- Bradnam MS Evans AL Montgomery DMI Keating D Damato BE Cluckie A & Allan D. (1994b)
A personal computer based visual evoked potential stimulus and recording system.
Doc Ophthalmol 86, 81-93
- Brenton RS & Phelps CD (1986)
The Normal Visual Field on the Humphrey Field Analyzer.
Ophthalmologica 193, 56-74.
- British Standards Institution. (1979)
Precision of test methods I: Guide for the determination and reproducibility for a standard test method.
(BS 5497, part 1) London BSI
- Bullimore MA Wood JM & Swenson K (1993)
Motion perception in glaucoma.
Invest Ophthalmol Vis Sci. 34, 3526-3533
- Bunday S & Crews SJ (1984)
A study of retinitis pigmentosa in the city of Birmingham II. Clinical and genetic heterogeneity.
J Medical Genetics 21, 421-8
- Bush RA, Sieving PA. (1994)
A proximal retinal component in the primate photopic ERG a-wave.
Invest Ophthalmol Vis Sci. 35, 2, 635-645
- Bush RA & Sieving PA. (1996)
Inner retinal contributions to the primate photopic fast flicker electroretinogram.
J. Opt. Soc. Am. 12, 3, 557-565
- Buxton MJ (1991)
Screening for treatable diabetic retinopathy: a comparison of different methods..
Diabetic Med 8, 371-376
- Carr RE and Seigel IM (1990)
Electrodiagnostic testing of the visual system: a clinical guide.
F.A. David Company Philadelphia

Chase WW Fradkin NE & Tauda S (1976)
A new electrode for electroretinography.
Am. J. Optom. Physiol. Optics. 53, 668-671

Clarke PGH (1973)
Visual evoked potentials to changes in the motion of a patterned field.
Exp Brain Res 18, 145-155

Curcio CA Sloan KR Packer O Hendrickson AE & Kalina RE (1987)
Distribution of cones in human and monkey retina: individual variability and radial asymmetry.
Science 236, 579-582

Curcio CA Millican CL Allen KA & Kalina RE (1991)
Aging of the Human Photoreceptor Mosaic: Evidence for Selective Vulnerability of Rods in Central Retina
Invest Ophthalmol Vis Sci 34, 3278-3296

Davies WDT (1970)
The Principles of Random Signal Testing
System Identification for Self-Adaptive Control.
Wiley-Interscience, Chichester

Dawson GD (1954)
A summation technique for the detection of small evoked potentials.
Electroenceph Clin Neurophysiol 6, 65-84

Dawson WW Tricke GL & Litzkow CA (1982)
Improved electrode for electroretinography.
Invest Ophthalmol Vis Sci. 18, 988-991

Devaney KO & Johnson HA (1980)
Neuron loss in the aging visual cortex of man
J Gerontol 35 836-843

Drance SM Berry V & Hughes A (1967)
The effects of age on the central and peripheral isopters of the visual field in normal subjects.
Am J Ophthalmol 63, 1667

Fino BJ & Algazi VR (1976)
Unified Matrix Treatment of the Fast Walsh-Hadamard Transform.
IEEE Transactions on Computers. 1142-1146

Fishman GA and Sokol S (1990)
Electrophysiologic Testing of Disorders of the Retina, Optic Nerve and Visual Pathway.
American Academy of Ophthalmology, Monograph Series 2

Fitzke F (1991)

Desktop test catches glaucoma early.
New Scientist 16 March, 27.

Foulds WS Reid H & Chisholm IA (1974)

Factors influencing visual recovery after retinal detachment surgery.
Mod. Probl. Ophthalmol. 12, 49-57

Foulds WS & MacCuish AC (1983)

Diabetic retinopathy in the West of Scotland: its detection and prevalence and the cost-effectiveness of a proposed screening programme.
Health Bulletin 41, 318-325

Fricker SJ Sanders JJ (1974)

A new method of cone electroretinography: the rapid random flash response
Investigative Ophthalmology 14, 131-137.

Frishman LJ Shen FR (1997)

The scotopic electroretinogram of macaque after retinal ganglion cell loss from experimental glaucoma.
Invest Ophthalmol Vis Sci. 37, 125-141

Galloway NR (1981).

Ophthalmic electrodiagnosis 2nd edition.
Lloyd-Luke, London.

Ghafoor IM Allan D & Foulds WS (1983)

Common causes of blindness and visual handicap in the West of Scotland.
Brit. J. Ophthalmol. 67, 4, 209-213

Grey RHB (1986)

Ophthalmic survey of a diabetic clinic. I. Ocular findings.
Br. J. Ophthalmol. 70, 797-80

Gundry MF & Davies EN (1974)

Recovery of visual acuity after retinal detachment surgery.
Am. J. Ophthalmology 77, 310-314

Harding GFA Odom JV Spileers W & Spekreijse H (1995)

for the International Society for Clinical Electrophysiology of Vision.
Standard for Visual Evoked Potentials.
Vision Res 36, 21, 3567-3572

Harrington DO (1976)

The Visual Fields
Mosby Saint Louis

Harrington DO & Drake MV (1990).

The Visual Fields: Text and atlas of clinical perimetry (sixth edition)
CV Mosby, St Louis.

- Hass A Flammer J & Schneider U (1986)
Influence of age on the visual fields of normal subjects.
Am J Ophthalmol 101, 199
- Hawlina M Konec B (1992)
New noncorneal HK-loop electrode for clinical electroretinography.
Documenta Ophthalmology 81, 253-259
- Heckenlively J and Arden GB (Eds) (1991)
Principles and Practice of Clinical Electrophysiology of Vision.
Mosby Year Book, Saint Louis, MO.
- Helligkeits Wagner P & Persson HE (1985)
Pattern-reversal electroretinograms in ocular hypertension.
Documenta Ophthalmologica, 61(1), 27-31
- Henderson KW (1970)
Comment on computation of the fast Walsh-Fourier transform.
IEEE Trans. Computers, 19, 50-51
- Hennessy M Vaegan (1995)
Amplitude scaling relationship of Burian-Allen, gold foil and Dawson, Trick Litzkow electrodes.
Documenta Ophthalmologica 89, 235-248.
- Henson (1993)
Visual Fields
Oxford University Press New York
- Hess RF & Baker CL (1984)
Human pattern electroretinogram.
J Neurophysiol 51, 939-951
- Hood DC & Birch DG (1996a)
Abnormalities of the retinal cone system in retinitis pigmentosa.
Vision Research, 36 1699-1709
- Hood DC Seiple W Holpigan K Greenstein V & Carr RE. (1996b)
A comparison of the components of multi-focal and full field ERGs.
Proceedings XXXIV Symposium Tubingen, Germany
- Hood DC Seiple W Holopigan K & Greenstein VA (1997a)
Comparison of components of the multi-focal and full-field ERG's.
Vis Neuroscience 314, 533-544
- Hood DC Seiple W Holopigan K & Greenstein VA Li J Sutter EE & Carr RE (1997b)
Assessment of local retinal function in patients with retinitis pigmentosa using the multi-focal ERG technique.
Vision Research in press

Hubel DH (1988)
Eye, Brain and Vision
Scientific American, New York

Jacobi PC Miliczek D & Zrenner E (1993)
Experiences with the international standard for clinical electrophysiology: normative values for clinical practice, interindividual and intraindividual variations and possible extensions.
Documenta Ophthalmology 85, 95-114

Joffe KM Raymond JE Crichton A (1991)
Motion perimetry in glaucoma.
Invest Ophthalmol Vis Sci. 32, 1103

Johnson EP Riggs LA & Schick AML (1966)
Photopic retinal potentials evoked by phase alteration of a barred pattern
Clinical Electretinography, pp 75-91, Pergamn Press, Oxford

Johnson MA Masof RW (1982)
The photomyoclonic reflex: an artefact in the clinical electroretinogram.
Br. J. Ophthalmol. 66, 368-378

Johnson MA & Choy D (1987)
On the definition of age-related norms for visual function testing.
Applied Optics 26, 1449 1987

Johnson CA Adams AJ & Lewis RA (1989a)
Evidence for a neuronal basis of age-related visual filed loss in normal observers
Invest. Ophthalmol. Vis. Sci. 30, 2056-2064

Johnson SC Damato BE Evans AL & Allen D (1989b)
Computerised visual field test for children using multiple moving fixation targets.
Med Biol Eng Comput 27, 612-616

Jonas JB Gusek GC Guggenmoos-Holzmann I & Naumann GOH (1988)
Variability of the real dimensions of normal human optic discs.
Graef's Arch Clin Exp Ophthalmol 226, 332-336

Karpe G Kornerup T & Wulfing B (1958)
The clinical electroretinogram VIII. The electroretinogram in diabetic retinopathy.
Acta Ophthalmol 36, 281-291

Katz J & Sommer A (1986)
Asymmetry and Variation in the Normal Hill of Vision.
Arch Ophthalmol 104, 65-68

Keating D Parks S Williamson TH Evans AL Elliott AT & Jay JL (1997)
The effect of filter bandwidth on the multifocal electroretinogram.
Documenta Ophthalmologica 92, 291-300

Klien R (1984a)

The Wisconsin epidemiological study of diabetic retinopathy II. Prevalence and risk of diabetic retinopathy when age at diagnosis is less than 30 years.

Arch Ophthalmol 102, 520-526

Klien R (1984b)

The Wisconsin epidemiological study of diabetic retinopathy III. Prevalence and risk of diabetic retinopathy when age at diagnosis is less than 30 years.

Arch Ophthalmol 102: 527-532

Kohl S & Korth M (1997)

Motion VEPs in normals and Glaucoma patients,

Invest Ophthalmol Vis Sci. 38, 4632

Kondo M Miyake Y Horiguchi M Suzuki S & Tanikawa A (1995)

Clinical evaluation of multifocal electroretinogram

Invest Ophthalmol Vis Sci 36, 10, 2146-2150

Kondo M & Miyake Y (1996)

Recording multifocal electroretinograms with fundus monitoring.

Invest Ophthalmol Vis Sci. 38, 4 1475

Kretschmann UH Ruther KW & Zrenner E (1996)

Observations regarding the waveform of the ERG recorded with the m-sequence stimulation technique

Invest Ophthalmol Vis Sci 37(suppl.), 3, 346

Kruth DE (1981)

Semi-numerical Algorithms

The Art of Computer Programming

Reading MA, Addison-Wesley, 2nd ed., vol.2

Kuba M & Kubova Z (1992)

Visual evoked potentials specific for motion-onset.

Doc. Ophthalmol. 80, 83-89

Kubova Z Kuba M Hrochova J & Sverak J (1997)

Motion-onset visual evoked potentials improve the diagnosis of glaucoma.

Doc Ophthalmol 92 3, 211-221

Kubova Z & Kuba M (1992)

Clinical application of motion-onset visual evoked cortical potentials.

Doc. Ophthalmol. 81, 209-218

Kutschbach E (1997)

Method for the multifocal ERG using short length and corrected m-sequences

ISCEV 35th International Symposium July, Monterey Peninsula, California USA

Larkin RM Klein S Ogden E & Fender DH (1979)
Nonlinear Kernels of the Human ERG.
Biol. Cybernetics 35, 143-160

Lechner RJ (1970)
Comment on the Computation of the fast Walsh-Fourier transform.
IEEE Tans. Computers, 19, 174

Lee YW & Schetzen M (1961)
Measurement of the kernels of a non-linear system by cross-correlation. Quarterly
progress report no. 60
Research Labs of Electronics, Cambridge Mass, MIT Press

Levick WR & Dvorak DR (1986)
The retina -from molecules to networks.
Trends Neurosci. 9: 181-5

Li X Sun X & Hu Y (1995)
Electroretinographic oscillatory potentials in diabetic retinopathy; An analysis in the
domains of time and frequency.
Documenta Ophthalmologica 81, 173-179

Maffie L & Fiorentini A (1981).
Electroretinographic responses to alternating gratings before and after section of the
optic nerve.
Science 211, 953-955

Marmor MF Arden GB Nilsson SEG Zrenner, E (1989)
for the International Society for Clinical Electrophysiology of Vision.
Standard for Clinical Electroretinography.
Arch Ophthalmol Vol 107, 816-819

Marmor MF & Zrenner E (1993).
Standard for Clinical Electro-oculography.
Arch Ophthalmol 111, 601-604

Marmor MF & Zrenner E (1995)
for the International Society for Clinical Electrophysiology of Vision.
Standard for Clinical Electroretinography (1994 update)
Documenta Ophthalmol Vol 89, 199-210

Marmor M Holder GE Porciatti VP Trick GL & Zrenner E (1996)
for the International Society for Clinical Electrophysiology of Vision.
Guidelines for basic pattern electroretinography.
Documenta Ophthalmol 91: 291-298.

Marx MS Podos SM Bodis-Wollner I Lee PY Wang RF & Severin C (1988)
Signs of early damage in glaucomatous monkey eye. Low spatial frequency losses in
pattern ERG and VEP.
Experimental Eye Research, 346, 173

Massof RW Wu L & Finkelstein D (1984)
Properties of electroretinographic intensity-response functions in retinitis pigmentosa.
Doc Ophthalmol 57, 279-296

Massof RW Johnson M Sunness J Perry C & Finkelstein D (1986)
Flicker electroretinogram in retinitis pigmentosa.
Documenta Ophthalmologica, 62, 231-245

McAllan A Sinn J Aylward GW (1989)
The effect of gold foil electrode position on the electroretinogram in human subjects
Vision Research 29, 1085-1087

McIlwain JT (1996)
An Introduction to the Biology of Vision.
Cambridge University Press

Mutlukan E & Damato BE (1992a).
The dark perimetric stimulus.
Br J Ophthalmol 76, 264-267.

Mutlikan E Bradnam MS Keating D & Damato BE (1992b)
Visual evoked cortical potentials from transient dark and bright stimuli: selective 'on'
and 'off-pathway' testing?
Doc Ophthalmol 80, 171-181

Mutlikan E Keating D & Damato BE (1993)
A touch-screen multi-stimulus video campimeter.
Mills R. (ed) *Perimetry Update*, 92/93
Kugler Publications, Amstersam, New York, 589-595, 1993

Norcia AM Clarke M & Tyler CW (1985)
Digital filtering and robust regression techniques for estimating sensory thresholds
from the evoked potential.
IEEE Eng Med Biol Magazine, Decmeber, 26-32

Norcia AM Tyler CW Hamer RD & Wesemann W (1989)
Measurement of spatial contrast sensitivity with the swept contrast VEP
Vision Res 29, 627-637

Nusinowitz & Birch DG (1993)
The relationship between rod & cone function loss in retinitis pigmentosa and cone-
rod degeneration.
Invest Ophthalmol Vis Sci. 34, 1074

Odom JV Maida TM & Dawson WW (1982)
Pattern Evoked Retinal Responses (PERR) in human: Effects of spatial frequency,
luminance and defocus.
Current Eye Research, 2, 99-108

- Osterberg G (1935)
 Topography of the layer of rods and cones in the human retina.
 Acta Ophthalmol., suppl. 6, 1-103.
- Panda-Jonas S Jona JB & Jakobczyk-Zmija M (1995)
 Retinal Photoreceptor Density Decreases with Age.
 Ophthalmology 102, 1853-1859
- Papakostopoulos D Barber C & Dean-Hart JC (1993)
 The sampling properties of different types of ERG electrode.
 Clin Vision Sci 8, 5, 481-488
- Parks S Aitken D Keating D & Dutton GN (1994)
 Argon laser photocoagulation of fluorescein stained retina – an unrecognised hazard?
 Br J Ophthalmol 78 476-477
- Parks S, Keating D, Williamson TH, Evans AL, Elliott AT & Jay JL (1996)
 Functional imaging of the retina using the multifocal electroretinograph: a control study.
 Br J Ophthalmol. 80, 831-834
- Parks S & Keating D (1997a)
 Effects of the dilation on the normal range in the Ganzfeld ERG.
 Invest. Ophthalmol. & Vis. Sci. 38, 4, 4094
- Parks S, Keating D, Evans AL, Williamson TH, Jay JL & Elliott AT (1997b)
 Comparison of repeatability of the multifocal electroretinogram and Humphrey perimeter.
 Doc Ophthalmol 92, 281-289
- Pokorny J Smith VC Lutze M (1987)
 Aging of the human lens
 Applied optics 26, 1437-1440
- Quigley HA Dunkelberger GR & Green GR (1989)
 Retinal ganglion cell atrophy correlated with automated perimetry in human eyes with glaucoma.
 Am. J. Ophthalmol. 107, 5, 453-564
- Regan D & Spekreijse H (1986)
 Evoked potentials in vision research 1961-1986
 Vision Res 26, 1461-1480
- Schroeder MR (1987)
 kronecker Products
 Number theory in Science and Communication Fast Transformation
 Springer Series, Addison-Wesley, New York

- Schoessler JP Jones R (1975)
Improved electrode for electroretinography
Invest Ophthalmol Vis Sci, 18, 988-991
- Seiple W Holopigian K Greenstein V & Hood DC (1993)
Temporal frequency dependent adaptation at the level of the outer retina in humans.
Vision Research 32, 2043-2048
- Shanks JL (1969)
Computation of the fast Walsh-Fourier transform.
IEEE Trans. Computers 18, 457-459
- Silverman SE Trick GL Hart WM (1990)
Motion perception is abnormal in primary open angle glaucoma and ocular hypertension.
Invest Ophthalmol Vis Sci. 31, 722-729
- Spekreijse H Estevez O & Van den Tweel LH (1975)
Luminance responses to pattern reversal.
Documenta Ophthalmologica Proceedings Series 2. 205-211
- Srebro R Weldon W Wright (1980)
Visually Evoked Potentials to Pseudorandom Binary Sequence Stimulation
Arch Ophthalmol 98, 296-298.
- Sutter EE & Vaegan (1990)
Lateral interaction component and local luminance nonlinearities in the human pattern electroretinogram.
Vis Res. 30, 659-671
- Sutter EE (1991)
The fast m-transform: A fast computation of cross-correlations with binary m-sequences
Siam J Comput, 20, 686-694
- Sutter EE & Tran D (1992)
The Field Topography of ERG components in Man - I. The Photopic Luminance Response.
Vision Research 32, 3, 433-446
- Trick GL. (1991)
The Patterned electroretinogram in Glaucoma and Ocular hypertension. In principles and Practice of Clinical Electrophysiology of Vision
Mosby, St louis, 107, 766-772
- Ueda M & Adachi-Usami E (1992)
Assessment of central visual function after successful retinal detachment surgery by pattern visual evoked cortical potentials.
Br J Ophthalmol 76, 482-485

- Usui & Nagasaka E (1994)
 Spatial distribution of local flash electroretinogram by multi-input stimulation.
 Doc Ophthalmol 88, 57-63
- Vaegan & Buckland L (1995)
 Outer retinal changes in early Glaucoma detected with the 'VERIS' local luminance
 ERG field test.
 Presented at the International Society for Clinical Electrophysiology of Vision
 XXXIII symposium, Athens, Greece
- Van Buren JM (1963)
 The retinal ganglion cell layer.
 Charles C. Thomas, Springfield, Illinois
- van Norren D & Vos JJ (1974)
 Spectral transmission of the human ocular media.
 Vision Res 14, 1237-1242
- Viswanthan S Frishman LJ Robson JG & Harwerth RS (1996)
 Inner Retinal Contributions to the Photopic flash ERG of Macaque monkey:
 Suppression of responses by pharmacological agents and experimental Glaucoma. S.
 Invest Ophthalmol Vis Sci. 37, 1601
- Viswanthan S & Frishman LJ (1997)
 Negative potentials that originate from inner retina in the photopic electroretinograms
 of cats and primates.
 Invest Ophthalmol Vis Sci. 38, 4125
- Volterra V (1959)
 Theory of functionals and of the integral and integro-differential equations.
 New York, Dover Publ.
- Weale RA (1963)
 The aging eye.
 Lewis HK Pergamon Press, London
- Weleber RG (1981)
 The effect of age on human cone and rod ganzfeld electroretinograms
 Invest Ophthalmol Vis Sci 3, 20, 392-399
- Wiener N (1958)
 Nonlinear problems in random theory
 New York Wiley
- Yagasaki et al (1988)
 Rod and cone psychophysics and electroretinography: methods of comparison in
 retinal degenerations.
 Doc Ophthalmol 62, 119-130

Yonemura D Aoki T & Tsuzuki K (1962)
Electroretinogram in diabetic retinopathy.
Arch Ophthalmol 62, 19-24

Zalta AH (1989)
Lens rim artefacts in automated threshold perimetry.
Ophthalmology 96, 1302-1311

